PERFORMANCE CHARACTERISTICS OF ELECTROLESS PLATING BATHS FOR NICKEL–CERAMIC COMPOSITE MEMBRANE FABRICATION

Vijaya Kumar Bulasara

Chapter 1:

Introduction and literature review

Chapter 2:

Experimental

Chapter 3:

Performance characteristics of conventional electroless plating baths

Chapter 4:

Performance characteristics of agitated electroless plating baths

Chapter 5:

Performance characteristics of ultrasonic electroless plating baths

Chapter 6:

Performance characteristics of hydrothermal electroless plating baths

Chapter 7:

Conclusions and future work

References

Appendix

Publications

Performance Characteristics of Electroless Plating Baths For Nickel–Ceramic Composite Membrane Fabrication

Thesis submitted in partial fulfillment of the
requirements for the degree of

DOCTOR OF PHILOSOPHY

by

Vijaya Kumar Bulasara

Roll No.: 08610701

Department of Chemical Engineering
Indian Institute of Technology Guwahati
Guwahati – 781039, India
July 2011

Dedicated to

My Parents

Department of Chemical Engineering
Indian Institute of Technology Guwahati
Guwahati – 781039, India

CERTIFICATE

This is to certify that the thesis entitled **"Performance characteristics of electroless plating baths for nickel–ceramic composite membrane fabrication"** being submitted by ***Vijaya Kumar Bulasara*** for the award of Ph.D. degree has been carried out under my guidance and supervision. The work documented in this thesis has not been submitted to any other University or Institute for the award of any degree or diploma.

Dr. Ramgopal Uppaluri

Associate Professor
Department of Chemical Engineering
Indian Institute of Technology Guwahati
Guwahati – 781039, India
Email: ramgopalu@iitg.ernet.in
Phone: 0361 2582260; Fax: 0361 2582291

Acknowledgements

I would like to express my gratitude to all those who helped me in different ways in completing this research work within the time span of three years directly or indirectly. First and foremost, I would like to express my deep felt gratitude to my supervisor, **Dr. Ramgopal Uppaluri**, for providing me continuous inspiration and guidance throughout the entire course of my Ph.D. as well as M.Tech. I am indebted to him for his useful suggestions and constant encouragement throughout the entire period.

I am grateful to **Dr. Ramgopal Uppaluri** for his continuous support, interesting discussions and giving me freedom in handling different issues. I appreciate very much his expertise in analyzing the experimental data to model them suitably. His uncompromising approach to complete the experimental part, data analysis, writing manuscripts as well as thesis within the stipulated time period helped me a lot in completing my research work in this shorter span. The numerous brain storming sessions during the project meetings with him were very useful in enriching my analytical power. It has been an amazing experience working with him in two consultancy projects during my M.Tech, which has helped me a lot in completing any work within stipulated time without compromising upon the quality.

I would like to express my sincere gratitude to **Dr. Mihir Kumar Purkait** of the Department of Chemical Engineering for his valuable contribution in publishing my research work. I appreciate very much his flexibility and openness in dealing with the specific and general needs of this research work. He helped me in improving the quality of the articles and finding suitable journals for publishing my work. I thank him for his patience and helping nature. It has been a great privilege to work with him.

I thank **Dr. G. Pugazhenthi** of the Department of Chemical Engineering for helping me in several ways and supporting me to enroll into the Ph.D. program.

I must thank **Prof. A.K. Ghoshal** of the Department of Chemical Engineering for providing me valuable suggestions and insights while working in the consultancy projects of IOCL and BRPL. I am also thankful to him for his caring for me during my Ph.D.

I must also thank my doctoral committee members **Dr. Pallab Ghosh**, **Dr. B.P. Mandal** and **Dr. Chandan Das** of the Department of Chemical Engineering and **Dr. V.V. Dasu** of the Department of Biotechnology, for their valuable suggestions and contribution towards the improvement of my research work.

I am thankful to **Dr. Harjyoti Thakuria** of the Department of Chemistry for his assistance as an SRF, without whom I could not have completed this thesis in time. I also acknowledge the financial support provided by the **CSIR, New Delhi**.

I also thank all the faculty members of the Department of Chemical Engineering for their kind cooperation during my stay in the department. I am also thankful to all the staff members and scientific officers of the Chemical Engineering Department for their genuine help during my entire research period.

I am thankful to the **Central Instruments Facility** of IIT Guwahati for allowing me to carry out **FESEM** analysis on my own**,** which has been very important in this research work. In this regard, I should acknowledge the help of **Mr. K.K. Senapati**, Scientific Officer, Central Instruments Facility, IIT Guwahati. He taught me how to use the FESEM instrument and take images at various critical conditions of the sample. I am also thankful to the **Mr. B. Choudhury** of Central Workshop, IIT Guwahati for helping me in the fabrication of my experimental setup which was very much essential in my research work.

I was fortunate enough to get excellent batch mates like **Vijayakrishna, Sriharsha** and **China Malakondaiah** for their friendly support and timely assistance whenever needed. I am also thankful to **Chandrashekar**, **Mahesh**, **Abhimanyu** and **Pranav** for their friendly behavior and assistance. Special thanks to **Dr. B.K. Nandi**, **Bipul Das** and **Aparajita** for their help and co-operation in the initial stages of my research work.

Last but not the least; I would like to express my deepest sense of gratitude to my parents and family members. Their love, care, sacrifice and encouragement have made it possible for me to come so far. I appreciate the courage, understanding and dedicated support shown by all of them despite many testing times at their end.

Vijaya Kumar Bulasara

(Email: vk5050@gmail.com)

Abstract

Metal composite membranes made of palladium, silver and nickel have numerous applications in process industries. Amongst these, nickel composite membranes have several applications such as production of ultrapure gases, recovery of TiO_2 from waste water streams, new generation supports for dense palladium membranes etc. Electroless plating is one of the most versatile methods adopted for metal composite membrane fabrication. Despite possessing several advantages such as uniformity of coating and ease of scale-up, electroless plating suffers with the basic limitation of very slow deposition rate and hence mass transfer enhancements can be coupled for process efficacy.

As opposed to the conventional performance characteristics of electroless plating baths for metal–ceramic composite membrane fabrication, this work addresses systematic methodology for the assessment of electroless plating and mass transfer enhanced electroless plating processes for nickel–ceramic composite membrane fabrication. Combinatorial performance characteristics of the plating baths are expressed in terms of bath conversion, plating efficiency, selective conversion, nickel plating rate, metal film thickness, average pore size (based on air permeation data), effective porosity (based on air permeation data) and percent pore densification (PPD). Various mass transfer enhancements considered in this work include agitation, sonication and hydrothermal conditions (with and without sonication). Both hypophosphite and hydrazine based plating baths have been assessed for their performance characteristics with a major objective of achieving 100% pore densification using mass transfer coupling effects. A laboratory fabricated symmetric low cost ceramic membrane support having a nominal pore size of 275 nm and a porosity of 40% with wider pore size distribution is used as the support (substrate) to obtain deeper insights with respect to the deposition characteristics. The plating characteristics are investigated for wide range of nickel solution concentrations (0.04–0.16 mol/L), loading ratios (196–393 cm^2/L) and stirrer speeds (0–200 rpm). All nickel–ceramic composite membranes are fabricated for a total plating time of 8 hours that constitute eight sequential deposition steps of one hour each. Nickel concentration in the plating solution before and after plating was evaluated using the complexometric titration with standard EDTA solution using xylenol orange as indicator. Membrane thickness was estimated using the weight gain method. Of the two reducing agents, hydrazine shows better performance than hypophosphite as the latter suffers from the generation of hydrogen bubbles which induce shear effect leading to process inefficiency. Effect of loading ratio is found to be insignificant compared with the solution concentration. However, a higher loading ratio is always preferred in order to minimize the metal layer thickness and chemicals cost. In general, it is observed that mass transfer enhancements have been effective in the increasing order as follows:

Base case < Stirring < Sonication < Hydrothermal < Hydrothermal + Sonication (HTSO).

At a loading ratio of 393 cm^2/L, hypophosphite plating baths offer a selective conversion of 11.9–24.2% for the base case, 13.6–23.0% for stirring case, 31.8–50.8% for sonication case, 36.2–45.4% for hydrothermal case and 42.1–58.8% for hydrothermal coupled sonication (HTSO) case. The maximum nickel film thickness of the nickel membrane for the hypophosphite plating baths is 31.4 μm that corresponds to an average membrane pore size of 33 nm. The PPD values are highest for HTSO case followed by hydrothermal, sonication, stirring and base cases. The obtained membranes using hypophosphite baths have a characteristic wider pore size (128–33 nm) for relatively larger membrane thickness (1.6–31.4 μm). A striking feature of the hypophosphite baths is that 100% pore densification is not achievable despite using highest nickel solution concentration (0.16

mol/L) for the best mass transfer enhancement (HTSO) case. Besides these, the evaluated selective conversion values with a maximum of 58.8% are not satisfactory from industrial perspective. For all solution concentrations, mass transfer enhancements played a significant role in reducing the average nickel membrane pore size.

Hydrazine based nickel electroless plating baths provide better performance characteristics than hypophosphite baths. At a loading ratio of 393 cm^2/L, the base case with hydrazine as the reducing agent corresponds to a selective conversion of 17.5–44.6% and enhances to 41.8–72.4% for the HTSO case, which is satisfactory even from the industrial perspective. Mass transfer enhancements enable the reduction of average membrane pore size from 94–22 nm (base case) to 81–18 nm (stirring), 58–16 nm (sonication), 66–21 nm (hydrothermal) and 41–8 nm (hydrothermal + sonication). This corresponds to a variation in average nickel layer thickness from 2.3–23.8 µm to 2.7–24.6 µm (stirring), 4.5–35.8 µm (sonication), 5.2–32.5 µm (hydrothermal) and 5.6–31.4 µm (hydrothermal + sonication). An important observation of hydrazine based plating baths is that the mass transfer enhancements play a significant role only at lower nickel solution concentrations (0.04–0.08 mol/L). Also, mass transfer enhancements did not enable 100% PPD value due to large average pore size and wider pore distribution of the ceramic membrane support.

A suitable mass transfer model whose parameters are obtained from non-linear regression analysis provides valuable theoretical insights. For all cases, it is observed that the partition coefficient values are close to 1000 and this is indicative of the fact that mass transfer enhancements enabled larger transport of the nickel ions to the surface to undergo the autocatalytic reaction. Further, the values of the mass transfer coefficient enhanced significantly for sonication (194–809 s^{-1}), hydrothermal (251–810 s^{-1}) and HTSO (304–984 s^{-1}) cases as opposed to the base case (37–487 s^{-1}) and stirring (60–573 s^{-1}).

Finally, this work focuses towards introducing a conceptual process parameters and general rules of thumb so as to quantify the combinatorial performance of electroless plating baths for membrane fabrication. These guidelines are anticipated to provide substantial insights in this fascinating area of research in the near future. Further, the fundamental research work reported in this work is expected to catalyze research in the fields of nickel/γ-alumina membranes for hydrogen separation, dense Pd–Ni composite membranes, porous Ag–Ni composite membranes for bacteriostatic applications and performance characteristics of mass transfer enhanced Pd electroless plating baths for dense Pd membrane fabrication.

Contents

Title	**Page No.**

List of Tables

List of Figures

Nomenclature

Symbols

C_i	initial concentration of Ni^{+2} in the plating solution (mol/L)
C_f	concentration of Ni^{+2} in the solution after plating (mol/L)
x	conversion of Ni^{+2} to Ni in the plating bath
η	plating efficiency
w_0	amount of nickel originally available in the plating bath (kg)
w_1	dry weight of the membrane before plating (kg)
w_2	dry weight of the membrane after plating (kg)
d_i	average pore diameter of the substrate (m)
d_o	average pore diameter of the nickel–ceramic composite membrane (m)
δ	thickness of porous nickel film (m)
ρ_{Ni}	density of nickel metal (kg/m^3)
A_m	membrane surface area (m^2)
$(\varepsilon/q^2)_{film}$	effective porosity of the nickel–ceramic composite membrane skin layer
K	effective permeability factor (m/s)
$\bar{P}$	average trans-membrane pressure (Pa)
A	slope in equation 2.15 (m/(s.Pa))
B	intercept in equation 2.15 (m/s)
η_g	viscosity of gas (Pa.s)
v	molecular mean velocity of the gas (m/s)
Q	volumetric flow rate (m^3/s)
P_2	membrane pressure at permeate side (Pa)

S	effective membrane area (m^2)
ΔP	trans-membrane pressure drop (Pa)
$\bar{r}_{\text{model}}$	average reaction rate obtained from the model (mol/L.s)
$\bar{k}$	average mass transfer coefficient (s^{-1})
$\bar{C}_B$	average bulk concentration of nickel ions in the plating bath (mol/L)
$\bar{C}_S$	average nickel ions concentration at the liquid–substrate interface (mol/L)
$\bar{C}_M$	average metallic nickel concentration on the substrate (mol/L)
$\bar{\gamma}$	partition coefficient
M_{Ni}	atomic weight of nickel (= 58.71 g/mol)
$\bar{r}_e$	average reaction rate obtained experimentally (mol/L.s)
t	plating time (s)
θ	loading ratio (cm^2/L)
ω	membrane stirrng speed (rpm)

Abbreviations

PPD	percent pore densification (%)
HT	hydrothermal condition
HTSO	hydrothermal condition in combination with sonication

INTRODUCTION AND LITERATURE REVIEW

This chapter presents a brief summary of the metal membranes and their fabrication methods along with the basis of the problem chosen in this work. State-of-art on the preparation of metal–ceramic composite membranes and their potential applications has been elaborately discussed. Based on the state of art on the membrane preparations and their applications in gas separation and purification, the aim of the present work has been summarized. Finally, the organization of the thesis has been presented.

1.1 Introduction to metal membranes

Numerous commercial applications have been suggested for polymeric membranes. These include hydrogen separation from refinery process streams [1], desalination of sea-water using reverse osmosis [2], hemodialysis [3], concentration of proteins using ultra- and micro-filtration, ultrafiltration of fruit juice etc. Even though polymeric membranes are inexpensive, due to their adaptability for scale-up and large scale production, they have been suggested for industrial scale applications. However, polymeric membranes are not susceptible to high temperatures that are typically encountered in process engineering. These include reactive transformations and availability of high temperature intermediate process streams with corrosive components. For such applications, inorganic membranes have been suggested and few industrial applications are also at place [4, 5].

Metal composite membrane technology research is highly sophisticated. Typically, metals such as nickel, silver, palladium and its alloys, niobium, tantalum and vanadium are the target skin layer materials on a porous support fabricated using materials such as Vycor glass, alumina, titania, stainless steel etc.

1.1.1 Palladium membranes

In the past 10 years, metal composite membrane technology received considerable attention in terms of both academic and industrial research and development studies. Amongst several metal membranes, palladium membranes are the most commonly investigated membranes. Due to the high cost of palladium and relatively low mechanical strength, commercially available palladium foils and tubes are not suitable for large scale industrial/commercial applications. Composite membranes consisting of a thin palladium film supported on a porous substrate is a good alternative that provides both mechanical strength and a thin separation layer for high hydrogen flux and reduced cost. Therefore, palladium membrane technology addresses the fabrication of a dense palladium membrane with minimal palladium film thickness on a structured asymmetric support. Numerous applications for palladium membranes include removal of water-vapor from hydrogen generated in water electrolysis process [6], generation of high purity hydrogen in laboratory scale applications [7], membrane catalysis in reforming [8], membrane catalysis in high temperature gas phase dehydrogenation schemes [9] etc. Typically, these applications target very efficient separation and flux performance characteristics of the membranes at temperatures ranging from 400–600°C. One of the striking characteristics of palladium is its ability to atomize hydrogen at higher temperatures. However, it is well known that palladium embrittles at lower temperatures (up to 300°C). Therefore, palladium membrane technology is suggested to be supplemented with automated control system that disallows the contact of the membrane with hydrogen up to 300°C (heating in inert environment). It is well known that palladium is a rare-earth and its cost is equivalent to that of gold. Therefore, palladium membrane technology research involves the engineering of thin palladium films (up to a maximum of 5 microns in the existing state of the art) on a superiorly engineered asymmetric support to simultaneously reduce the cost of the membrane and enhance the membrane hydrogen flux without compromising upon the separation factor.

1.1.2 Silver and nickel membranes

Due to the high cost of palladium, silver and nickel membranes are also targeted. For both silver and nickel membranes, dense membrane fabrication has not been addressed. These membranes are porous in nature, and therefore applications not confirming to the dense membranes have been suggested. Silver being bacteriostatic is suggested to serve as a pathogen free water purifier in medical applications [10]. Other applications for silver membranes include XRD analyses media and analyses of dissolved organic carbons or coke oven emissions.

Nickel and nickel composite membranes are suggested for the separation of dust particles from gaseous streams to produce ultrapure gases, removal and recovery of TiO_2 from waste streams, hydrogen separation and asymmetric supports for dense palladium composite membranes.

Various corporate institutions specializing towards metal membrane technology along with suggested applications are presented in Table 1.1.

Table 1.1: A summary of companies that manufacture various metal membranes.

S. No.	Corporate institution	Membrane fabricated	Support used	Applications
1	Johnson Matthey [11]	Palladium composite membrane	Porous stainless steel	◆ Hydrogen generators ◆ Steam reforming ◆ Membrane reactors ◆ Fuel cell applications
2	ECN Netherlands [12]	Palladium composite membrane	Commercially available ceramic supports	
3	General Electric (GE) [13]	Porous silver membrane	Not available	◆ Water filters ◆ Treatment of contaminated water ◆ Elimination of bacteria from water ◆ Removal of turbidity ◆ Filtration of alcoholic beverages ◆ High temperature sterilization procedures
4	SPI-Pore [14]	Pure porous silver membrane	No support used	
5	SKC filters [15]	Porous silver composite membrane	Porous plastic support	
6	Sterlitech [16]	Pure porous silver membrane	No support used	
7	Wacorp Hyundai Private Limited [17]	Porous silver membrane	Not available	
8	Mott Corporation [18]	Pure porous nickel membrane	No support used	◆ Liquid filters ◆ Removal and recovery of TiO_2 from waste streams ◆ Separation of dust particles from air ◆ Supports for palladium membranes ◆ Hydrogen purification ◆ X-ray diffraction media
9	Mykrons [19]	Sintered porous nickel membrane	No support used	
10	Entegris [20]	Porous nickel composite membrane	Stainless steel	

1.2 Metal membrane fabrication methods

Various metal membrane fabrication methods that are deployed both in academic and industrial R&D include physical vapor deposition (PVD), thermal evaporation, chemical vapor deposition (CVD), magnetron sputtering, electro-deposition and electroless plating. A brief summary of these methods are presented as follows.

1.2.1 Physical vapor deposition

Physical Vapor deposition (PVD) is a less laborious technique, provides faster deposition rates and allows for better control of the film thickness. In contrast to CVD, the film can be obtained at relatively low temperatures, avoiding damaging the surface. PVD is the process of depositing solid material on a substrate from vapor phase. The source of the vapor phase is generally a solid "chunk" of the desired film material. This deposition technique has the advantage of depositing a desired film thickness, even in nanometer range, in the clean environment of high vacuum. The desired material is either heated until evaporation (thermal evaporation) or sputtered by ions (sputtering) on the target surface.

1.2.2 Thermal evaporation

The vacuum thermal evaporation includes heating a material under vacuum to a temperature where a large number of atoms or molecules leave the surface of the material and deposit on a substrate by condensation. The main parameters that control the growth and structure of evaporated films are the type of the substrate, substrate and evaporation temperature, the angle of incidence of evaporate and contamination. In thermal evaporation techniques the average energy of vapor atoms reaching the substrate surface is generally low which seriously affects the morphology of the films, often resulting in a porous and little adherent material. With respect to sputtering, evaporation results in larger grains and poorer adhesion.

1.2.3 Magnetron sputtering

During sputtering (Figure 1.1), a low pressure gas with large number of ions and free electrons, referred as plasma, is created via high energy field. Bombardment of solid (target) by high energy chemically inert (e.g. Ar) ions extracted from plasma causes ejection of atoms from the target which are then re-deposited on the surface of the substrate with the help of magnetic field generated by permanent magnets. The main advantage of this technique is that ultra thin nano-structured films with minimal impurity can be prepared with greater flexibility for synthesizing alloys. During deposition the substrate is already heated enhancing the inter diffusion of metal ions, which are in close contact, therefore no heat treatment or low annealing temperatures is needed for alloying. While sputtering an alloy film from a corresponding target, in the beginning there is a tendency to eject one atomic species in excess of the other species. But after sometime, the atoms are ejected in the same ratio as the original ratio in the target.

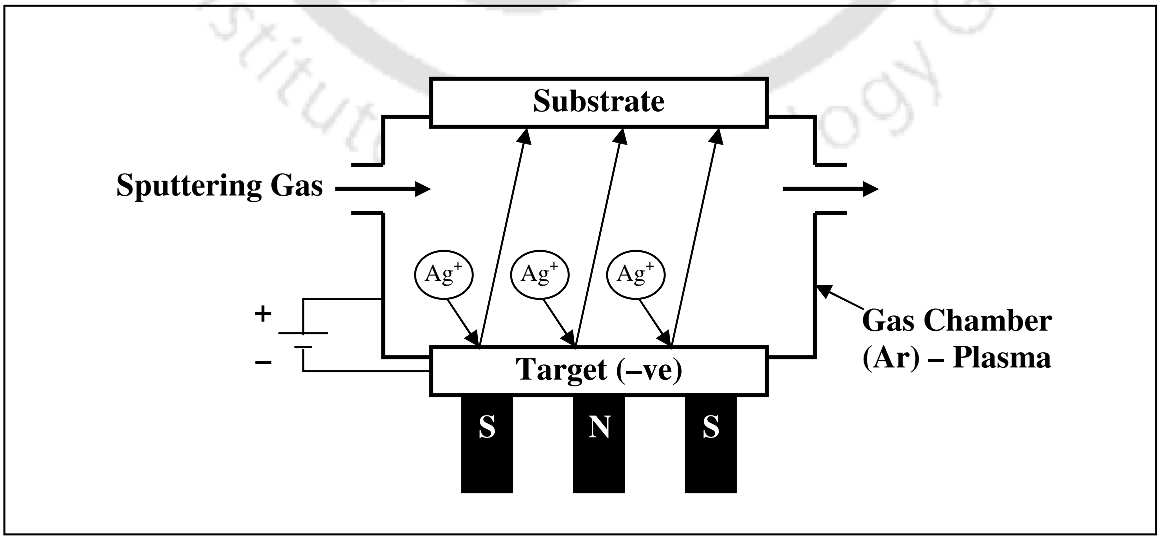

Figure 1.1: Schematic diagram of magnetron sputtering process.

1.2.4 Chemical vapor deposition

Chemical vapor deposition (CVD) is a chemical process used to produce high-purity, high-performance solid materials. The process (Figure 1.2) is often used in the semiconductor industry to produce thin films. In the chemical vapor deposition (CVD) process, the deposits are produced by a vapor-phase chemical reaction at a controlled temperature. Gaseous compounds of the materials to be deposited are transported to a substrate surface where a thermal reaction/deposition occurs. Reaction byproducts are then exhausted out of the system. The CVD process has the advantage of depositing metallic or dielectric coatings of low and high temperature melting materials and it is very easy to control the thickness in submicron scales. On the other hand, it is difficult to deposit alloys and it requires very high purity and strict deposition conditions, making it a very uneconomical process.

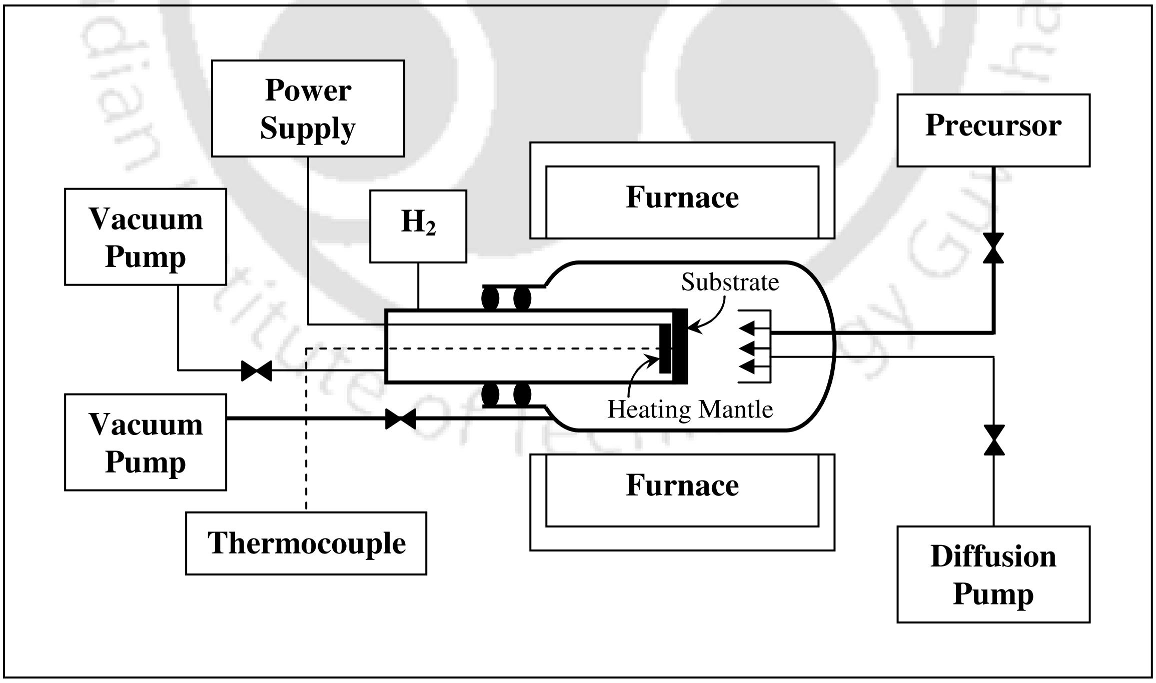

Figure 1.2: Schematic diagram of chemical vapor deposition process.

1.2.5 Electroplating

In electroplating (Figure 1.3), the electro-deposition of an adherent metallic coating takes place on a metallic coating electrode. Because of the electric field between the electrodes, metallic ions in the solution migrate to the cathode where they are neutralized and included into the metal lattice. The film is affected by several parameters, such as current density, temperature of the electrolyte, migration and diffusion velocity of ions, specific weight of ions, geometric form of cathode (distribution of current lines), and the bath composition.

1.2.6 Electroless plating

Electroless deposition (Figure 1.4) is a technique based on the controlled autocatalytic reduction of a dissolved metallic salt by reducing agents at a substrate interface. Among other techniques, electroless deposition provides strong advantages such as uniformity of deposits even on very complex shapes, very simple equipment and low cost. Unlike electrodeposition, non-conductive surfaces as well as conductive surfaces can be coated easily by using electroless deposition. The deposit follows exactly all the

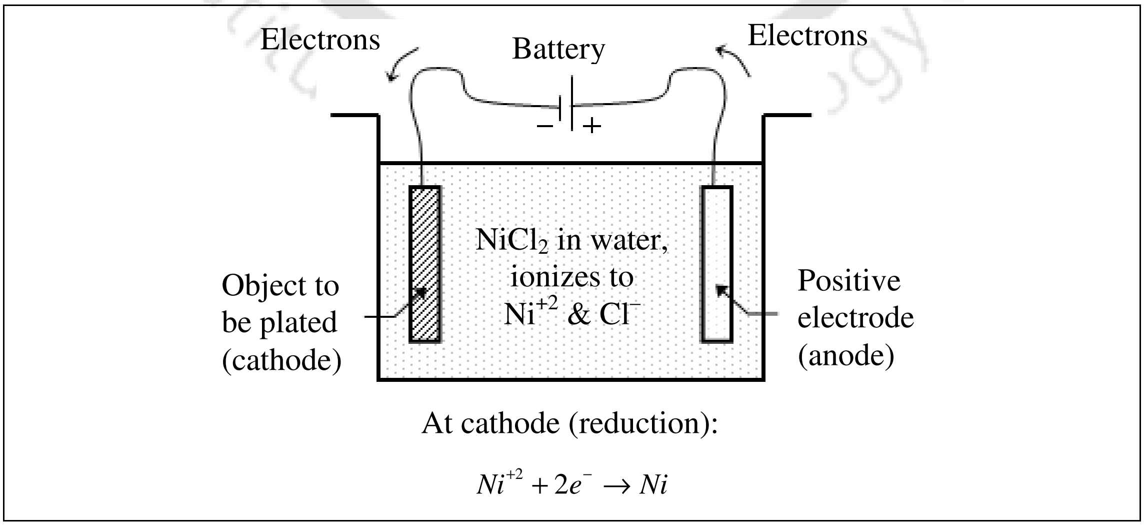

Figure 1.3: Schematic diagram of typical electroplating bath.

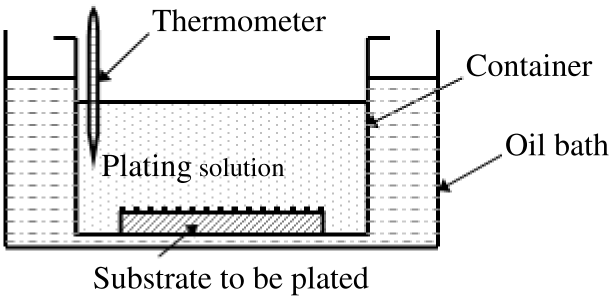

At catalyst surface (redox reaction):

$$Ni^{+2} + reducing\ agent \rightarrow Ni + oxidized\ salt$$

Figure 1.4: Schematic diagram of typical electroless plating bath.

contours of the work-piece without build-up at edges or corners.

Electroless plating is possibly the simplest means of composite membrane fabrication, although support quality, surface activation methods, electroless plating procedures and bath chemistry influence membrane selectivity, permeability and Pd/Pd-alloy film stability. Conventional electroless plating constitutes two hierarchical steps namely sensitization and surface activation, and metal deposition.

1.2.6.1 Sensitization and surface activation

The traditional activation process consists of successive dipping of the substrate in acidic solutions of Sn^{+2} and Pd^{+2} salts respectively with gentle rinsing in de-ionized water between two baths. Sn^{+2} is adsorbed on the substrate surface in hydrolytic form (sensitization step) and replaced by Pd^0 through the process described by Equation 1.1 (activation step). This procedure is repeated several times to produce enough Pd particles for catalyzing further deposition of palladium/nickel.

$$Sn^{+2} + Pd^{+2} \rightarrow Sn^{+4} + Pd^{0} \qquad (1.1)$$

1.2.6.2 Metal deposition

The electroless plating solution generally consists of a metallic salt, a complexing agent, a reducing agent, and a stabilizing agent. Electroless plating process occurs on the solid liquid interface between the support and the plating solution. It involves reduction of a metal salt on a catalytic surface. It is similar to electroplating except that a flow of electrons is not supplied by an external source. The reaction is initiated by the oxidation of reducing agent in the plating solution with simultaneous release of electrons, which reduce the metal ions on the target surface. The deposited metal catalyses the further oxidation-reduction process resulting in a uniform film on the surface, referred to as an autocatalytic reaction. An activation of the support prior to plating is necessary to initiate this autocatalytic plating process.

V, Cr, Fe, Co, Ni, Cu, Ru, Rh, Pd, Ag, Pt and Au are some of the metals that can be plated autocatalytically. Several reducing agents such as dialkyl amine borane, borohydride, hypophosphite, formaldehyde and hydrazine are available for the electroless plating process. Hypophosphite is commonly used, but deposits contain phosphorus, reducing the quality of the film. Formaldehyde is not a good reducing agent, especially in the case of Pd deposition since H_2 gas is released during plating and contributes to mechanical instability of the film. Also the reducing effect of formaldehyde is low. Hydrazine is the most commonly used reducing agent.

As described above, the traditional technique for preparing metal composite membranes by means of electroless plating consists of two steps; activation of the support and plating. After activation, the supports are immersed in the plating solution. During the plating process, metal and the reducing agents in the solutions are depleted and require replacement to continue the processing. The supports are plated until the activity of the supports diminishes. The supports are reactivated for further plating. These steps are repeated until the pores on the support are fully covered with the deposited metal. Agglomerates of crystals combine to form metal clusters on the surface. Many factors including the support quality, activation process and the bath chemistry, contribute to the thickness, stability and selectivity of the membranes. In addition, researchers are also trying to modify the plating procedures to make thinner membranes.

1.2.7 Summary

The well-known deposition methods summarized in sections 1.2.1–1.2.6 have several advantages as well as disadvantages. Firstly, amongst all fabrication methods, it is important to note that even though magnetron sputtering enables obtaining a metal film with superior characteristics, magnetron sputtering cannot be subjected to scale-up, as scale-up requires maintenance of vacuum in the sputtering chamber and it is highly expensive. Secondly, chemical vapor deposition technique is susceptible to scale up but requires a sophisticated control system to support the CVD set up. Thirdly, physical vapor deposition is a rather disadvantageous process due to its poor deposition characteristics. Though both electroplating and electroless plating are susceptible for scale up, the electroplating technique suffers with the disadvantages of current polarization, inability to deposit on non-conducting surfaces etc.

Further, an important issue for metal membrane fabrication is to allow maximum flexibility in fabrication variables so as to obtain metal films with desired characteristics. While temperatures play a key role in the CVD technique, vacuum (pressure) plays a greater role in the sputtering process. Similarly, electro-plated membranes are largely influenced by the current density and solution concentration. On the other hand, electroless plating provides maximum flexibility in terms of fabrication variables. These include concentration of metal precursors (palladium/nickel/silver ion concentration in the solution), selection and reducing agent concentrations, scheduling of reducing agent addition to the bath, loading ratio (defined as volume of solution used per unit area of membrane surface subjected to the plating), pH and temperature of the system.

Therefore, from fabrication perspective, it is herewith inferred that electroless plating process offers maximum advantages when compared to the other deposition processes. These include flexibility in various operational variables in addition to other advantages such as ease of deposition, simple experimental set up, ability to deposit on non-conducting surfaces and ability to ensure uniform deposition even on complex surfaces.

1.3 Performance characteristics of membrane fabrication methods

The primary objective of various fabrication methods is to yield metal membranes with good performance characteristics i.e., acceptable combinations of hydrogen flux and separation factor at desired temperature. In this section, we summarize various research findings that elaborated upon the potential of various fabrication methods based on membrane as well as process performance characteristics.

1.3.1 Chemical vapor deposition (CVD)

Itoh et al. [21] prepared palladium composite membranes using tubular α-alumina supports having an average pore size of 0.15 µm by a forced-flow CVD technique. The metal precursor used was palladium diacetate, $(CH_3COO)_2$–Pd. The palladium membranes thus obtained had a thickness of 2–4 µm and showed a good H_2/N_2 selectivity exceeding 5000 at 300°C with a hydrogen flux of 0.1–0.2 mol/m^2/s.

Cooper and Lin [22] modified γ-alumina (pore size 4 nm) membranes supported on α-alumina discs having an average pore size of 0.2 μm by a CVD technique. The metal precursor used was liquid trimethylaluminum (TMA). Aluminum oxide was deposited in the pores of the γ-alumina membrane by alternating additions of trimethylaluminum (TMA) and water vapor. The modified membrane exhibited the best separation properties with a water vapor permeance ranging from 1.5×10^{-6} to 3.0×10^{-7} mol/m^2 s Pa, an oxygen permeance ranging from 1.7×10^{-7} to 1.5×10^{-9} mol/m^2 s Pa, and a separation factor as high as 140 at room temperature.

Ha et al. [23] deposited thin films of TiO_2 on the inner surface of porous Vycor glass tubes (pore size 4 nm) by atmospheric pressure chemical vapor deposition (APCVD) at temperatures ranging from 200 to 400°C using titanium isopropoxide as a precursor. They observed that dense and hydrogen-permselective membranes were formed only in the temperature range between 230 and 300°C. A maximum H_2/N_2 selectivity of 57 was obtained at a deposition temperature of 250°C.

Gopalakrishnan and Costa [24] prepared high flux silica membranes by a counter diffusion CVD method using tetraethyl orthosilicate (TEOS) and O_2 as reactants. The single gas permeation of H_2 increased from 5.1×10^{-7} to 7.0×10^{-7} mol m^{-2} s^{-1} Pa^{-1} in the temperature range 100–400°C, and H_2/CO_2 and H_2/N_2 selectivities reached 36 and 57 at 400°C, respectively.

Gu and Oyama [25] deposited a selective top layer of SiO_2–TiO_2 on modified γ-alumina supports (pore size 5 nm) by chemical vapor deposition of titanium isopropoxide (TIP) and tetraethylorthosilicate (TEOS) at high temperature using an inert gas carrier. The membrane prepared at 873K using a molar ratio of TIP/TEOS = 0.10 had the best performance with a H_2 permeance of 2.3×10^{-7} mol m^{-2} s^{-1} Pa^{-1} and H_2 selectivities over CH_4 and CO_2 of 37 and 57, respectively at 873 K.

Tong et al. [26] prepared thin Pd membrane (6μm thickness) on CeO_2-modified porous stainless steel tubular support by combined method of electroless plating and chemical vapor deposition. The electrolessly prepared Pd membrane showed a high hydrogen flux of 0.235 mol/(m^2 s) at 773K with a pressure gradient of 100 kPa, but the separation factor (H_2/Ar) was only 14 due to the surface defects. After the CVD treatment, the separation factor increased greatly to 565 without decreasing the original hydrogen flux.

Huang and Dittmeyer [27] prepared thin palladium membranes on a porous stainless steel tubes coated with a porous layer of yttria-stabilized zirconia (YSZ) by three different techniques namely magnetron sputtering (MS), atmospheric plasma spraying (APS) and electroless plating (ELP). The YSZ layer served as a barrier against intermetallic diffusion between the palladium membrane and the metallic support. They observed that magnetron sputtering did not result in sufficiently dense films while atmospheric plasma spraying produced relatively thick continuous films, but with some residual open porosity. On the other hand, electroless plating gave the densest layers. Yet rather thick layers were required to limit the number of defects, which is associated with high cost and low hydrogen flux. The deposited palladium layer had a thickness of 2, 30 and 10 μm for MS, APS and ELP respectively.

Kikuchi et al. [28] prepared two types of supported precious metal membranes on the outer side of commercially available alumina tube with an average pore size of 200 nm for steam reforming of methane: one was an electroless-plating palladium membrane, and the others were CVD palladium, platinum, and ruthenium membranes. They observed that the CVD platinum membrane had a H_2/N_2 separation factor as high as 280 gave an excellent performance comparable to the electroless plated palladium membranes which had the highest H_2/N_2 selectivity (∞) than all the other membranes.

Wang and Hong [29] deposited carbon-based molecular sieve (CMS) films on porous Al_2O_3 disks using hexamethyldisiloxane by a remote inductively-coupled-plasma chemical vapor deposition (CVD) method. The H_2/N_2 selectivities of the as-deposited films were in the range of 5–10, higher than the Knudsen diffusion selectivity, 3.7. They observed that the permeance increased by one order of magnitude after pyrolysis of the as-deposited film at 873K with no significant change of the selectivity.

Jun and Lee [30] prepared thin Pd membranes by the metal-organic CVD method using a cold-wall technique on disk type mesoporous α-alumina support having a skin layer of γ-alumina with a pore size of 3–6 nm. The H_2 permeance of the Pd/Al_2O_3 was 1.5×10^{-2} $cm^3\ cm^{-2}\ cmHg^{-1}\ s^{-1}$ (723 K); the H_2/N_2 selectivity was >1000.

1.3.2 Magnetron sputtering

Ryi et al. [31] prepared Pd–Cu–Ni alloy membrane of 4 μm thickness on porous nickel support (33 nm) by multitarget sputtering and Cu-reflow technique. The weight composition of Pd:Cu:Ni from EDS analysis was 89:4.5:6.5. They observed that the nickel support was very stable and a very high H_2/N_2 separation factor (∞) was obtained.

Xiong et al. [32] fabricated $Nb_{40}Ti_{30}Ni_{30}$ membranes by magnetron sputtering on porous nickel support prepared by uniaxial compression of nickel powders for hydrogen separation and purification. They found that the $Pd/Nb_{40}Ti_{30}Ni_{30}/Pd$/porous nickel support composite membrane exhibited excellent permeation capability and satisfactory mechanical properties. The permeance of H_2 and the H_2/N_2 selectivity increased proportionally with permeation temperature. The H_2 permeance of the prepared membranes was 3.3–4.2×10^{-6} mol m^{-2} s^{-1} Pa^{-1} (723 K) and the H_2/N_2 selectivity was 2.3–3.6.

Ryi et al. [33] deposited Pd–Cu–Ni alloy of about 4 μm thickness deposited by sputtering and Cu-reflow on to a porous nickel support to study the effect of support resistance on the hydrogen permeation behavior of the composite membrane. They observed that the permeation flux was affected by the permeation direction and the permeation flux obtained from the support to film (SF) mode was higher than that from the reverse mode (FS mode).

Ryi et al. [34] prepared defect-free Pd–Cu–Ni ternary alloy membranes of 12 μm thickness by sputtering Pd and Cu on the polished porous nickel support (250 nm) followed by the Cu-reflow method. The hydrogen permeance through the membrane was 3.8×10^{-7} mol m^{-2} s^{-1} Pa^{-1} with infinite H_2/N_2 selectivity. The permeance value obtained in this study was three times higher than that obtained in their previous study [31] of the similar membrane with a lower support pore size.

Zhang et al. [35] deposited Pd–Ag alloy on V–15Ni circular membranes of 12 mm diameter by co-sputtering of separate pure Pd and Ag targets using a multi-target sputtering system. They found that the hydrogen permeation of the composite membranes was mainly bulk diffusion limited at a temperature higher than 473 K and at the temperatures lower than 473 K, the hydrogen permeability of the composite membranes increased with increasing the Ag content until 30 at%.

Checchetto et al. [36] deposited thin Pd films of 5 μm thick by r.f. magnetron sputtering on porous stainless steel discs steel support after the deposition of a polycarbonate (PC) layer by spin coating technique for hydrogen purification. The as-prepared Pd–PC composite membrane had a hydrogen permeance of 5×10^{-7} mol $m^{-2}s^{-1}Pa^{-1}$ and high H_2 to N_2 selectivity.

O'Brien et al. [37] deposited thin Pd/Ag coating layer of 1 µm thickness by unbalanced magnetron sputtering on porous α-alumina (pore size: 50–500 nm) and γ-alumina (pore size: 5–20 nm) tubular membranes. They observed that the hydrogen permeance depended strongly on the type of substrate (2×10^{-5} mol m^{-2} s^{-1} Pa^{-1} for α-alumina and $2–8\times10^{-7}$ mol m^{-2} s^{-1} Pa^{-1} for γ-alumina) and the H_2/N_2 selectivity ranged from 4 to 80.

Zhao et al. [38] prepared Pd and Pd–Ag (24 wt.%) alloy composite membrane (thickness 1 µm) by electroless plating and magnetron sputtering, respectively on commercial microfiltration ceramic membrane coated with γ-Al_2O_3 based layer. The membranes exhibited a high permeation rate of H_2 and a H_2/N_2 selectivity of higher than 60 in the optimized operation conditions.

Gielens et al. [39] co-sputtered a 750 nm dense layer of $Pd_{77}Ag_{23}$ on non-porous silicon nitride. After sputtering 0.5µm openings were created on the silicon nitride layer by etching. With 0.2 bar hydrogen partial pressure in the feed the hydrogen flux was 0.16–7.7×10^{-3} m^3/m^2h at 350 and 450°C. The H_2/He selectivity was above 1500.

Athayde et al. [40] sputtered $Pd_{76}Ag_{24}$ on micro-porous polymer supports that were coated with a suitable polymer (dimethylsiloxane). The pore free and smooth substrate did not offer any resistance to gas permeation. Membranes with 2.5–10 µm thick alloy layer were obtained by controlling the sputtering time.

1.3.3 Electrodeposition

Chen et al. [41] prepared palladium membrane by electroplating on AISI 316L porous stainless steel tubular supports (200 nm pore size) for producing high-purity hydrogen in methanol steam reformer. They observed that the electroplated Pd membrane had an excellent H_2/He permselectivity (>100,000) and resisted hydrogen embrittlement under the phase-transition temperature of 280°C, when operated in the temperature range of 250–350°C. They also observed that high membrane rotation speed (200 rpm) resulted in a very homogenous grain size.

Nam et al. [42] fabricated pinhole-free palladium/nickel (78% Pd and 22% Ni) alloy membranes (1 μm thick) deposited on a disk shaped porous stainless steel (SUS) support (pore size 500 nm) by vacuum electrodeposition technique. The prepared Pd/Ni membranes by the application of vacuum on the opposite side yielded excellent separation performance for hydrogen: hydrogen permeance of 5.79×10^{-2} cm^3/cm^2 cmHg s and H_2/N_2 selectivity of 4700 at 823 K.

Nam and Lee [43] prepared thin (<2 μm) and dense composite Pd/Ni alloy membrane on mesoporous stainless steel (SUS) support modified with submicron nickel powder and CuCN solution by the vacuum electrodeposition technique employing Pd/Ni complex reagent. They observed that the current density had an important effect on thickness, composition, and microstructure of the deposited film and the films prepared with lower current density (6.5 mA/cm^2) resulted in smaller grain size and higher Pd content and showed higher hydrogen permeance (2.0×10^{-2} cm^3/cm^2 cmHg s) and greater hydrogen/nitrogen selectivities (3000) at 723 K.

Choi et al. [44] deposited thin platinum layer (150 nm) on the surface of the electrode for proton exchange membrane fuel cells by pulse electrodeposition. They observed that higher current density (50 mA/cm^2) resulted in poor performance because of the growth of dendritic crystals and the loss of the deposition layer due to rapid generation of hydrogen.

Nam et al. [45] prepared Pd–Cu/SS composite membranes for hydrogen separation on a porous stainless steel (SS) support (pore size 500 nm) by the vacuum electrodeposition. They observed that the Pd–Cu (60/40 wt%) alloy membranes prepared by vacuum electrodeposition showed long term stability (>3 months) with infinite selectivity.

Lertviriyapaisan and Tantavichet [46] deposited platinum (Pt) catalyst layer on commercial carbon cloth for proton exchange membrane fuel cell (PEMFC) by electrodeposition. They applied two sublayers on the substrate and found that the hydrophilic (top) sublayer played a substantial role in Pt electrodeposition. They found that a PTFE to carbon black weight ratio of 30:70 in the hydrophobic sublayer yielded the best Pt catalyst layer for PEMFC.

Kim et al. [47] deposited Pt on carbon electrodes for PEM fuel cell using pulse electrodeposition technique. They observed that the peak current density and the pulse duty cycle controlled the nucleation rate and decreased the catalyst dendric growth while the amount of platinum loading was controlled by the total charge density. They obtained a high catalyst performance of 380 mA/cm^2 at 0.8 V using a peak current density of 400 mA/cm^2, a duty cycle of 2.9% and a total charge density of 8 C/cm^2.

Wei et al. [48] deposited metallic manganese in an electrolytic membrane reactor by electrodeposition. They obtained a maximum current efficiency of 85.86% at an electrolyte composition of 35 g/L Mn and 130 g/L $(NH_4)_2SO_4$ at a temperature of 40°C and a pH of 7.5 in the presence of additives and with a cathode current density of 400 A/m^2.

Hrapovic et al. [49] deposited Ni on gas diffusion cathodes by electrodeposition for hydrogen production in a continuous flow microbial electrolysis cell (MEC). These gas diffusion cathodes with electrodeposited Ni exhibited excellent stability for hydrogen production compared to expensive Pt cathodes.

Lee et al. [50] prepared nickel membranes with tunable pore size by electrodeposition on colloidal monolayer template. They controlled the pore size by varying the deposition time.

1.3.4 Electroless plating

Ayturk and Ma [51] studied the electroless Pd and Ag deposition kinetics of the composite Pd and Pd/Ag membranes synthesized from agitated plating baths. They utilized atomic absorption spectroscopy (AAS) for the measurement of the Pd and Ag ion concentrations in the plating baths and to elucidate the effects of temperature, initial metal ion and reducing agent concentrations and agitation on the electroless plating kinetics of Pd and Ag metals. They found that the electroless plating of both Pd and Ag were strongly affected by the external mass transfer limitation in the absence of bath agitation. The external mass transfer limitations for both Pd and Ag deposition were minimized at or above an agitation rate of 400 rpm, resulting in a maximum conversion of the plating reaction with the added advantage of uniform deposition morphology. Bath agitation indicated a 60% improvement of the plating bath efficiency in comparison to that of the Pd and Ag runs conducted under the static conditions. They conducted non-linear regression analysis based on the method of initial rates for the derivation of the differential rate laws and the estimation of the reaction orders and the activation energies for the electroless Pd and Ag kinetics and solved the integrated rate law for a constant-volume batch reactor to calculate the conversion and the reactant concentrations as a function of plating time. The model was in good agreement with the experimental data. They synthesized 16–20 μm thick composite Pd/Ag membranes (10–12 wt% Ag) and a pure-Pd membrane with a hydrogen selective dense Pd layer as thin as 4.7 μm. The H_2 permeance for the 4.7 μm thick pure-Pd membrane at 400°C was as high as 63 $m^3/m^2\text{-h-atm}^{0.5}$. The long-term permeance testing of all the membranes synthesized from agitated plating baths resulted in a relatively slow leak growth due primarily to the improved morphology obtained via the bath agitation and modified plating conditions.

Zeng et al. [52] sealed the defects in Pd and Pd–Ag membranes by directed electroless plating, which was achieved by feeding the metal source and the reducing agent from opposite directions to the defect zone. They showed that the surface texture of the metal layers was well preserved in the vicinity of cracks and pinholes, indicating that Pd deposition was effectively restricted to defect sites. The ideal H_2/N_2 selectivity was improved by more than an order of magnitude during these point plating experiments while the very high H_2 permeability of the membrane was completely retained, indicating that the overall metal layer thickness had not increased.

Seshimo et al. [53] investigated a method of electroless plating to fabricate a novel functionally graded Pd/γ-alumina/anodic alumina composite membrane. They carried out electroless plating reactions on catalyzed anodic alumina surfaces and on catalyzed nanoporous γ-alumina in an electroless plating solution and observed that the reactions readily formed a smooth Pd membrane on the catalyzed nanoporous γ-alumina, but failed to form a Pd membrane on the catalyzed anodic alumina. They noticed that the Pd membrane grew into the nanoporous γ-alumina in the direction of depth from 2 h up to 5 h during the electroless plating reaction, and then grew upward in the direction of thickness after 5 h. They found that the agitation speed of the electroless plating bath influenced the Pd deposition, and also influenced the crystalline growth of the Pd. At a high agitation speed, the Pd grew in the direction of depth, promoting the growth of the Pd/γ-alumina graded layer and at a low agitation speed, the Pd grew upward in the direction of thickness and a pure Pd membrane grew on the surface of the nanoporous γ-alumina. When grown under an increased agitation speed, the Pd membrane had a smoother surface. The Pd/γ-alumina graded layer between the Pd and γ-alumina layers provided a buffer against the stress generated by the difference between the thermal expansion coefficients of the Pd and γ-alumina and improved its durability.

Gade et al. [54] fabricated unsupported palladium alloy foil membranes by electroless plating upon mirror-finished (polished) stainless steel supports followed by mechanical removal. They produced high quality pure palladium films as thin as 7.2 μm that showed hydrogen permeabilities comparable to cold-rolled unsupported foils, and high H_2/N_2 selectivity as high as 40,000. They prepared palladium-copper membranes by sequential electroless plating of copper onto palladium foils followed by in situ annealing to produce films of desired composition. They showed that the annealing process did not produce defects in the film and their membranes performed 15 days without increased leak rates.

Zhang et al. [55] prepared thin dense Pd/Al_2O_3 composite membranes by a vacuum electroless plating (VELP) technique. They noticed that thin dense Pd composite membranes with finer and more uniform microstructure were rapidly deposited by the influence of vacuum effect on both sides of the tubular substrate. These features significantly improved hydrogen permeation performance and enhanced stability as compared with the conventional electroless plating method. Their membranes were thermally stable over a period of 470 h and over 10 temperature cycles and gas-exchanging cycles over the temperature range of 350–480°C under H_2 or Ar atmosphere without any significant changes for hydrogen permeation performance and exhibited good chemical stability over a period of 2000 h. They obtained hydrogen permeance up to 22.4 m^3/m^2.h.bar and the ideal permselectivity over 3000 at 500°C.

Ke et al. [56] prepared thin palladium composite membranes by a modified electroless plating method on α-alumina supports and obtained a dense Pd/α-$A1_2O_3$ composite membrane with high hydrogen flux and good selectivity for hydrogen. They added sodium dodecyl sulfate to enhance the stability of the plating solution. The hydrogen permeance of the corresponding membrane was as high as 2.45×10^{-6} $mol.m^{-2}.s^{-1}.Pa^{-1}$ and H_2/N_2 selectivity over 700 at 623 K and a pressure difference of 0.1 MPa and the membrane exhibited good thermal stability at 623K for over 200h. They found that the main resistance of the composite membrane to H_2 permeation lied in the alumina ceramic support rather than the thin Pd layer.

Nair et al. [57] carried out electroless plating (ELP) synthesis and permeation characterization of a series of Pd and Pd/Ag membranes supported on α-Al_2O_3 hollow fibers. They noticed that the electroless plating carried out at ambient temperature (25°C), resulted in smaller grains and Pd deposition rate exhibited a maximum while the Ag growth rate demonstrated autocatalytic behavior and was enhanced by Pd and they also found that the grain size and morphology were sensitive functions of the plating temperature. They obtained initial binary separation factors of 1000–10000 with the low temperature ELP. The transport of hydrogen was limited by the diffusion of hydrogen in the metallic membrane while non-selective transport was by a combination of Knudsen diffusion and convective transport. The Pd/Ag alloy membrane exhibited high permselectivity for extended operation with the separation factor (α) decreasing from an initial value of 970 to 650 after 300 h with the H_2 flux sustained at 0.5 mol/m^2s at 550°C for a transmembrane pressure gradient (ΔP_{H_2}) of ~4×10^5 Pa. They showed that the use of an intermediate layer (γ-Al_2O_3) of reduced pore size enabled the synthesis of thinner membranes of higher flux without loss of permselectivity.

Huang and Dittmeyer [58] prepared composite palladium membranes on sinter-metal supports (stainless steel) with a ceramic barrier against intermetallic diffusion. They used Zirconia (ZrO_2), yttria-stabilized zirconia (YSZ), and titania (TiO_2) as porous barriers between the palladium membrane and the sinter-metal support. They coated the ceramic layers by magnetron sputtering (MS-ZrO_2, thickness ~2μm), atmospheric plasma spraying (APS-YSZ, thickness 10–70μm), and wet powder spraying (WPS-TiO_2, thickness 40–60μm), respectively which differ considerably in terms of thickness, pore size, surface roughness, and open porosity. They demonstrated the barrier function against intermetallic diffusion between the palladium and the metals from the support by annealing of membrane samples in pure hydrogen at 600°C for up to 23 days. Palladium membranes on APS-YSZ layer had to be significantly thicker (15–20μm) due to its extremely rough surface while the smooth and uniform surface of WPS-TiO_2 allowed plating of very thinner (8–10μm) and selective palladium membranes. Pd/MS-ZrO_2 membranes (thickness ~14μm) showed intermetallic diffusion at locations where direct contact between the palladium and the sinter-metal support persisted. They identified APS-YSZ to be the most promising barrier against intermetallic diffusion amongst the three membrane types. They demonstrated that Pd/WPS-TiO_2 had the best hydrogen permeance, i.e. 0.154

$m^3m^{-2}h^{-1}Pa^{-0.5}$, as well as the best H_2/N_2-permselectivity (~800), at 500°C. They obtained the highest hydrogen permeability from Pd/APS-YSZ (1.6 $m^3\mu mm^{-2}h^{-1}Pa^{-0.5}$ at 500°C).

Huang et al. [59] investigated the co-deposition behavior of palladium and silver on porous alumina by means of electroless plating technique. They also investigated fabrication parameters of the membranes in electroless plating process for the preparation of Pd–Ag composite membrane. For the Pd_{90}–Ag_{10}/α-alumina composite membrane prepared at 333 K, the thickness of the Pd–Ag layer on the α-Al_2O_3 support for plating 8 h was 20 μm. They used the Pd_{90}–Ag_{10}/α-alumina composite membrane (20 μm) for hydrogen and nitrogen permeation experiments under 473–616 K and 80–250 kPa and found that the ideal separation factor of H_2/N_2 through the membrane was in the range 30–178. They used a resistance model to account for the simultaneous transport of hydrogen through the α-alumina support and skin layer of the Pd_{90}–Ag_{10}/α-alumina composite membrane which revealed that the transport behavior of hydrogen through the skin layer of the membrane was a combination of solution-diffusion and Knudsen diffusion with minimal contribution of viscous flow.

Roa et al. [60] made Pd–Cu composite membranes by successive electroless deposition of Pd and then Cu onto various tubular porous ceramic supports viz. symmetric α-alumina (nominal 200 nm in pore size), asymmetric zirconia on α-alumina (nominal 50 nm pore size), and asymmetric γ-alumina on α-alumina (nominal 5 nm pore size). They heat-treated the resulting metal/ceramic composite membranes between 350 and 700°C for times ranging from 6 to 25 days to induce intermetallic diffusion and obtain homogeneous metal films. They obtained an ideal hydrogen/nitrogen separation factor as 1150 at the same conditions and found that the support pore size controlled the required metal film thickness to insure a leak-free membrane and the internal structure of the support (symmetric or asymmetric) affected the mass transfer resistance. The support with the 200 nm pores required more Pd to plug the pores than the asymmetric membranes with smaller pore sizes. However, they failed to deposit leak-free films on the support with the smallest pore size (5 nm γ-alumina), due to lack of adhesion between the metal film and the membrane surface.

Cheng and Yeung [61] studied the effects of plating chemistry on palladium deposition, plating efficiency and membrane microstructure for hydrazine-based and hypophosphite-based plating baths. They determined the electroless plating kinetics of palladium onto seeded supports for hypophosphite-based plating bath, and developed a simple kinetic model. They observed that the deposition rate, plating efficiency and Pd film microstructure were different for the hydrazine and hypophosphite-based plating baths. They demonstrated that the plating chemistry played a vital role on both plating performance and film microstructure. The hypophosphite-based plating bath had a slower plating rate, but provided better plating efficiency than a hydrazine-based plating bath. The presence of hydrogen that was produced during the oxidation of hypophosphite resulted in the de-lamination of palladium membrane upon its removal from the hydrogen saturated plating bath. In contrast, they obtained dense palladium membranes with excellent support adhesion using hydrazine as the reducing agent. They suggested that chemical reducers that generate hydrogen were not suitable for electroless plating of palladium membrane.

Zheng and Wu [62] prepared palladium–ceramic composite membranes on porous α-Al_2O_3 supports by electroless plating using a novel hydrothermal method to control the systemic pressure for the fabrication of palladium membrane. They found that the pore size shrinkage of the hydrothermally deposited palladium membrane was significantly higher than that produced under conventional conditions due to better mechanical contact between the plating bath and the pore walls. They proposed that control of the systemic pressure of the plating process could be a novel route for the preparation of dense palladium composite membranes.

Zhao et al. [63] prepared Pd and Pd–Ag (24 wt %) alloy composite membranes by electroless plating and magnetron sputtering. They used commercial microfiltration ceramic membrane coated with γ-Al_2O_3-based layer by sol–gel method as the substrate for Pd and Pd–Ag alloy film. They showed that both the as-prepared membranes were He gas-tight at room temperature with a thickness of less than 1 μm and the H_2 flux through the Pd-based composite membranes is proportional to the trans-membrane pressure difference of H_2. Their membranes exhibited a high permeation rate of H_2 and a H_2/N_2 permselectivity of higher than 60 in the optimized operating conditions.

Keuler et al. [64] prepared palladium alloy membranes by successive electroless plating steps on an alumina–zirconia support membrane. They deposited palladium–silver and palladium–nickel in layers and then heat treated the metal films for 5 h in a hydrogen atmosphere at 650°C. They characterized the topography of the metal coatings and cross-sections of the films (before and after heating) using scanning electron microscopy (SEM) and the crystal phase of the alloy coatings using XRD. In addition to the surface information, they also extracted depth information of the alloy coating using micro-PIXE (proton induced X-ray emission). They constructed concentration profiles across the thickness of the films to determine penetration of the coating into the support membrane pores during electroless plating and to investigate diffusion of coated layers during the heating step. Their observations were as follows:

- The palladium to nickel ratio remained constant across the thickness of the film. Smaller nickel particles penetrated deeper into the support membrane pores and resulted in a higher nickel concentration inside the support.
- When palladium was deposited first (for both Pd–Ag and Pd–Ni films), the Pd penetrated at least 3 μm into the support. Coatings, where silver was deposited first, showed very little pore penetration (in the order of 1 μm) and hence poor metal to ceramic adhesion.
- Variable concentration profiles were obtained (after heating) when silver was deposited on palladium. The silver concentration declined from a high percentage at the outer edge of the film to a low value at the edge of the support. A constant palladium to silver ratio, across the thickness of the film, was obtained when palladium was deposited on silver and the coating heat treated.

Li et al. [65] fabricated a thin-film (10.3 μm), defect-free Pd/α-Al_2O_3 composite membrane by the electroless plating technique combined with osmosis. They found that the apparent activation energy for the membrane was 12.3 kJ/mol in the temperature range of 320–577°C. They also found that both sweep gas and a higher total feed flow rate improved the hydrogen permeation through the membrane.

Yeung et al. [66] prepared thin supported palladium membranes using electroless plating technique and determined the intrinsic plating kinetics for hydrazine-based palladium plating baths. They developed mathematical models to predict film thickness and plating rate as a function of plating parameters (i.e., reactant concentrations, temperature and time). They found that the surface grain structure was dependent on both plating chemistry and plating rate. They also demonstrated that film structure had a significant influence on the permeation performance of the palladium membrane. They proposed that the structural transformation during annealing was responsible for the increase in permeation rate of palladium supported membranes.

Keuler et al. [67] prepared palladium and silver coated membranes using electroless plating and palladium–silver alloy membranes by successive palladium and silver depositions on the same membrane support and heat treated the metal coated membranes for 5 h in a hydrogen atmosphere at 650°C. They found that by depositing first silver and then palladium, the palladium to silver ratio across the thickness of the film remained constant after heat treatment and it resulted in only a small amount of the alloy penetrating into the support membrane pores. However, when palladium was deposited first, the alloy penetrated at least 3 µm into the support and the palladium and silver concentration profiles across the thickness of the film were asymmetric. They noticed that the palladium deposit was about 99.75% pure with the main impurities being tin (deposited during the pretreatment step), 700 ppm silver, 100 ppm mercury and 100 ppm lead and the silver film was about 99.5% pure with tin (0.49%) and 250 ppm iron as the main impurities. They found that the palladium deposit was column-like, but formed a continuous dense layer covering the entire substrate surface. The silver deposit was non-homogeneous and clusters were deposited randomly over the palladium film or the activated substrate. No layer of even thickness was formed.

Zhao et al. [68] produced a thin palladium composite membrane by modified electroless plating procedure that consisted of the activation of a ceramic substrate by the sol-gel process of a Pd (II)-modified boehmite sol and with a higher concentration of hydrazine in the plating bath. They employed infiltration of the electroless plating solution to the porous substrate during the deposition of palladium with a filter device to improve adherence of a palladium layer to the substrate. They obtained a membrane with a thickness of about 1 μm and was gas-tight for helium, had a high compactness that showed a hydrogen selectivity of 20−130 for H_2/N_2, and a hydrogen flux of 1.8–87 $m^3/m^2.h$, depending on operation conditions.

Kathirgamanathan [69] studied ultrasound-assisted electroless deposition of copper onto and into microporous membranes for electromagnetic shielding. The author noticed that ultrasonication reduced the plating time for electroless deposition of copper onto microporous membranes, improved adhesion of the metal to the surface of the membrane and also helped to eliminate the need for pretreatment or chemical etching of the membranes. These membranes had high bulk conductivities (up to 0.82 S cm^{-1}) to give electromagnetic shielding efficiencies of 55±5 dB in the frequency range 10 kHz to 1 GHz.

Kikuchi and Uemiya [70] studied the characterization of composite membranes, consisting of a palladium–silver alloy film on the outer surface of an inorganic porous support (alumina), for hydrogen separation. They prepared the membranes by consecutive electroless-plating of palladium and silver, and then heat treatment in a stream of inert gas (argon) at 1173 K for 12 h. The prepared membranes had a complete selectivity for hydrogen separation and they exhibited an extremely high rate of hydrogen permeation compared with commercial palladium-based membranes. They found that the hydrogen permeation was about 30 times faster when 23 wt% silver was melted to give a film thickness of 5.7 μm. The high rate of hydrogen permeation was a result of enhanced hydrogen solubility into the metal film as well as its reduced thickness.

Tang et al. [71] studied a new palladium free activation process for Ni electroless plating on acrylonitrile butadiene styrene (ABS) plastic. The activation was carried out by immobilizing Ni nanoparticles as catalyst site on the ABS plastic surface. This method consisted of etching and activation of the substrate surface. Etching was performed on the surface of degreased ABS foils by dipping in a mix solution of 40 ml hydrogen peroxide (30%) and 160 ml sulfuric acid (98%) at room temperature for 5 min. After etching, the foils were dipped into 1% acetic acid solution containing 15 g/l chitosan (CTS) for 5 min at room temperature, and then dried at 60 °C for 15 min. After that, the foils (ABS–CTS) were immersed in a nickel sulfate solution ($NiSO_4.6H_2O$: 2.0 g/l) at 40 °C for 10 min, rinsed and then reduced in a solution of KBH_4 (3.0 g/l) at 40 °C for 5 min. ABS–CTS–Ni was obtained. The electroless nickel deposition was catalytically achieved by dipping the pre-nucleated substrates (ABS–CTS–Ni) into a solution containing sodium citrate as complexing agent and sodium hypophosphite as reducing agent at 40°C for 20 min. It is a cost effective activation method since Ni nanoparticles were successfully used as catalyst and a glossy and smooth Ni–P plating layer was obtained.

Ma et al. [72] obtained a nano-composite coating of Ni–P/Ag by adding silver nanoparticles (1×10^{-7} mol/l) to the Ni–P electroless plating solution operated at 85°C. Silver nanoparticles were obtained by adding $AgNO_3$ (1×10^{-3} M) solution to $NaBH_4$ (4×10^{-3} M) solution containing sodium oleate (2.5×10^{-4} M) with vigorous stirring at an ice-cold temperature. They noticed that the silver nanoparticles changed the properties of the composite coating. They found that the Ni–P/Ag composite coating had better hardness and less P content than that of Ni–P alloy coating. Further, the hardness was increased by 70% upon heat treatment at 400°C.

Zhang et al. [73] undertook the direct electroless Ni–P plating on Mg–10Li–1Zn alloy using nickel sulfate as the main salt. They investigated that the pre-treatment processes were indispensable steps to obtain a compact and uniform Ni–P coating on Mg–10Li–1Zn alloy. They developed a pre-treatment process that consisted of three steps namely ultrasonic cleaning with acetone for 10 min to remove soils and greases, acid pickling with H_3PO_4 and HNO_3 for 20 s to remove oxide/hydroxide and other chemical layer and fluoride activation with HF for 10 min. They observed that the scratches almost vanished after acid pickling and the substrate surface became smoother and flatter after fluoride activation. After pre-treatment, they carried out electroless nickel plating using sodium hypophosphite as the reducing agent. The obtained Ni–P coating layer was amorphous and had a phosphorus content of 7.5 wt%. Their results indicated that electroless Ni–P plating could obviously improve the corrosion resistance of Mg–10Li–1Zn alloy.

Mahmoud [74] investigated electroless deposition of nickel and copper over the pre-anodized titanium substrates. The obtained specimens were heat treated at 400°C for 2 h and used as anodes in the process of the electrochemical degradation of Methylene Blue (MB) dye in simulated wastewater. It was shown that complete degradation of the dye is dependent primarily on the type and concentration of conductive electrolyte. The highest electrocatalytic activity was achieved in the presence of NaCl (2 g/l) and could be attributed to indirect oxidation of the investigated dye by the electrogenerated hypochlorite ions formed from the chloride ions oxidation.

Sahoo [75] reported an experimental study of wear characteristics of electroless Ni–P coatings sliding against steel. Coating process parameters are optimized for minimum wear with four process parameters, viz., bath temperature, concentration of nickel source solution, concentration of reducing agent and annealing temperature. It is observed that annealing temperature and bath temperature have the most significant influence on wear characteristics of electroless Ni–P coating. The interaction of bath temperature and concentration of nickel source solution has some significant influence on wear. The wear mechanism in electroless nickel coatings is found to be abrasive wear.

Novakovic and Vassiliou [76] prepared composite NiP–TiO_2 layers by simultaneous electroless deposition of Ni–P and TiO_2 on steel substrate, from a solution in which TiO_2 particles were kept in suspension by stirring. They found that the chemical composition of Ni–P matrix was influenced by the incorporation of TiO_2 particles. An improvement (up to 20%) in microhardness was observed in both as-plated and vacuum heat-treated composite coatings compared to Ni–P coatings. Electroless deposited composite coatings exhibit an amorphous structure of the nickel matrix in which crystalline titanium oxide is incorporated. Vacuum heat treatment leads to the formation of a crystalline layer in which the Ni and Ni_3P crystallites appear apart from those of the TiO_2 (anatase). As-plated and heat-treated composite coatings have less corrosion resistance.

Aal and Aly [77] applied Ni–Cu–P coatings onto open cell stainless steel foams from Ni–P bath containing $CuSO_4.5H_2O$ as a source of Cu ions. They studied the influence of $CuSO_4.5H_2O$ addition on the deposition rate, chemical composition and surface morphology of coatings and examined the corrosion performance of coated foam in 1 M HCl using weight loss technique. Their results revealed that wt% of Cu in deposit increased with $CuSO_4.5H_2O$ concentration, while wt% of Ni and P was reduced. Better corrosion resistance, finer-grained deposit and lower deposition rate were observed by increasing Cu content into Ni–P matrix.

Wu et al. [78] prepared nickel nanoparticles supported on metal oxides by a modified electroless nickel-plating method. They showed that the dispersion of nickel nanoparticles was dependent on the interface reaction between the metal oxide and the plating solution or the active metal and the plating solution. The Ag loading and acidity of the metal oxide mainly affected the interface reaction to change the dispersion of nickel nanoparticles. They observed that the use of ultrasonic waves and microwaves and the change of solvents from water to ethylene glycol in the electroless plating could affect the dispersion and size of nickel nanoparticles.

Song et al. [79] proposed a novel and facile surface activation for electroless nickel plating, avoiding complex surface functionalization or pretreatment. The results indicated that the coatings of Ni/polystyrene (Ni/PS) microspheres were smooth, compact and uniform, and the Ni coatings thickness was about 0.15 µm. They concluded that the novel surface activation was effective for the uniform nickel deposition on the surfaces of PS microspheres, due to more palladium catalytic active sites generated on the surfaces of PS microspheres.

Liu et al. [80] deposited electroless Ni–Co–P films on Fe film in plating baths using sodium hypophosphite as reducing agent and nickel and cobalt sulphates as ion source at pH value of 9 and plating temperature from 60 to 85°C. They studied the effect of the mole ratio of $CoSO_4/CoSO_4 + NiSO_4$ in plating bath on the growth behavior of electroless Ni–Co–P films. They observed that the electroless Ni–Co–P films can be deposited on Fe films without the step of sensitization and activization and the surface of electroless Ni–Co–P film on Fe was quite even. It was found that the more the Co^{2+} ion in plating bath, the larger is the activation energy and the smaller is the plating rate of electroless Ni–Co–P films; and the mole ratio of Co/Co + Ni in film is larger than that in plating bath.

Kong et al. [81] used electroless plating technique to coat Sn–Ni alloy on copper substrate with high Sn content by adding the amounts of thiourea as special complexing agent and sodium hypophosphite as reducing agent to an acidic electroless plating bath of $SnCl_2$ and $NiCl_2$, which avoided activation pretreatment in plating process. They observed that the Sn content of the Sn–Ni layer increased with lowing temperature which reached

60 wt% under optimum plating conditions. The Sn–Ni alloy layer showed good corrosion-resistance and had crystalline structure and exhibited a compact and low porosity surface. Meanwhile, the Sn–Ni alloy exhibited a good anticorrosion ability in 3.5% sodium chloride solution than those of electroless plated nickel and tin.

Shibata et al. [82] fabricated a Pd–Ni–P film by electroless alloy plating and found that the fabricated Pd–Ni–P film was a metallic glass on the basis of two features, namely, an amorphous structure and a glass transition followed by crystallization during heating. The composition of the fabricated Pd–Ni–P film was controlled by adjusting the mixture ratio of the plating solutions or the plating temperature. The fabricated Pd–Ni–P film had a non-uniform microstructure that resulted from the inhomogeneous distribution of the free volume accompanying the electroless alloy plating reaction.

Kar and Sathiyamoorthy [83] studied the nickel–phosphorous (Ni–P) coating on carbon fibers, using sodium hypophosphite as a reducing agent in alkaline medium and investigated the effect of process parameters such as time, stabilizer concentration, pH of the plating bath and bath temperature on the electroless Ni–P coating efficiency. They observed that the coating thickness and nickel content increased with an increase of coating time and temperature. They found that the bath temperature of 80°C, pH of 9, and stabilizer concentration of 25 g/L were optimum to get a good and uniform coating of Ni on carbon fiber and the nickel coating increased thermal stability of the nickel-coated carbon fiber and the Ni-coated fiber was more conducting in nature. The Ni–P coating with low phosphorous content on the carbon fiber surface led to an increase in two phases, viz. microcrystalline and amorphous due to the increase of NiP_2, Ni_3P and Ni metal.

Yan et al. [84] deposited Ni–P alloy coatings with the addition of Yb^{3+} in the electroless plating solution. They investigated the effect of Yb^{3+} concentration on the corrosion resistance and deposition rate of electroless Ni–P coatings. They showed that the addition of Yb^{3+} could significantly improve the corrosion resistance of the coatings without any significant co-deposition. With an increase of Yb^{3+} concentration up to 0.20 g L^{-1}, the corrosion potential (E_{corr}) of the electroless Ni–P coating in 3.5% NaCl solution increased from –0.381 to –0.08 V, and the corrosion current density (I_{corr}) decreased from 7.36 to 0.62 mA cm^{-2}. At 0.20 g L^{-1} Yb^{3+}, the coating could be as long as 960 h (288 h for the case without Yb^{3+}) free of corrosion in the neutral salt spray. In addition, the deposition rate can also be accelerated by Yb^{3+} addition.

Elansezhian et al. [85] presented the effect of surfactants on the surface roughness, microhardness and microstructure of electroless Nickel–Phosphorus (EN) surface protective coating obtained from an alkaline bath. They investigated the influence of surfactants sodium dodecylsulfate (SDS) and cetyl trimethyl ammonium bromide (CTAB) on the surface roughness, microhardness and microstructure of coated samples. EN deposits with addition of surfactant SDS and CTAB at a concentration of 0.6 g/l produced a smooth surface with an average roughness value (Ra) of 1.715 µm for SDS and 1.607 µm for CTAB which were less than the Ra value of EN deposit without surfactant addition (1.885 µm). The mean average roughness value (Ra) with addition of surfactant was 1.796 µm. They found that without surfactant the micro hardness value of as-coated condition was 450 Hv. The micro hardness value increased to 685 Hv with addition of SDS and 675 Hv with addition of CTAB. The surface finish of the coated layer significantly improved when the concentration of the surfactant exceeds 0.6 g/l. By adding the surfactants during deposition of Ni–P, the phosphorus content had increased and contributed to the improved quality of the deposits in terms of corrosion resistance.

Hazan et al. [86] studied the dispersion stability of aluminum oxide colloidal particles stabilized with comb-polyelectrolytes in an electroless nickel (EN) solution under plating conditions (80–90°C). The nanodispersions which were stable at room temperature for several weeks flocculate rapidly as the temperature approached ~65°C. They found that hydrotropes such as propylene glycol and urea induce stability under plating conditions. The co-deposition of stabilized and non-stabilized nanoparticle dispersions resulted in very different particle density and distribution in the composite coatings. Stabilized baths resulted in highly homogeneous Ni–P/alumina nanocomposite coatings with improved co-deposition efficiency.

Cheng et al. [87] studied the effect of the microstructure on the anti-fouling property of the electroless Ni–P coating with different contents of nanocrystalline phase (phosphorus). They found that the electroless Ni–P coatings have better antifouling property than that of uncoated sample and fouling increased with increasing the nanocrystalline phase.

Grande et al. [88] studied the suitability of nickel electroless plating for anode deposition on electrolyte-supported solid oxide fuel cells (SOFCs) based on yttrium-stabilized zirconia (YSZ). Their study was carried out on YSZ disk-shaped pellets sintered at different temperatures ranging from 1000°C to 1400°C with analysis of the influence of sintering temperature on the Ni–YSZ interface microstructure and fuel cell performance. Lower pre-sintering temperature resulted in higher Ni penetration into the YSZ matrix, forming a graded anode and improving the anode-electrolyte interfacial strength. The optimized electrode showed good mechanical stability under redox cycling which resulted in an enhancement of electrode porosity. The higher Ni penetration on YSZ substrates pre-sintered at low temperature resulted in an improvement of one order of magnitude of power output compared to a cell in which a metal Ni anode was coated over a fully dense (i.e. high pre-sintering temperature) electrolyte surface.

Liu et al. [89] investigated the effects of two organic additives, 3-S isothiuronium propyl sulfonate (UPS) and thiourea (TU) on the properties of electroless nickel (EN) deposit and showed that TU and UPS had different influences on the morphology of EN deposits. The two additives decreased phosphorus content and increased sulfur content and enhanced the crystallization of the EN deposits but the EN coating with TU or UPS had a lower corrosion resistance because of the lower phosphorous content and S co-deposition of EN coating with TU or UPS. In addition, the Ni–P–S–O–C–N organic film formed on the EN deposit with UPS during nitric acid corrosion test could act as a protection layer between the inner deposit and the corrosion medium, thus contributing to an increase in nitric acid corrosion resistance.

Huang and Cui [90] studied the effect of complexing agent on the morphology and microstructure of electroless deposited Ni–P alloy using aminoacetic as the main complexing agent. They found that the nucleation processes strongly depend on the complex content. With the content of the complex increasing in the bath solution, the morphologies of the initial priority depositing points changed from coniform shapes to planers. Coniform growth centers grew up to hemispherical microstructure depositions, and planar growth centers caused smooth plane microstructure depositions.

Changrong et al. [91] prepared microfiltration nickel membranes on porous alumina supports by electroless plating using sol–gel process to activate the alumina supports. They observed that the membrane thickness and amount of nickel increased with plating time and the pore size decreased greatly as electroless coating is processed for 15 min after which the pore size decreased slightly. They obtained a thickness of 4.5 µm in 90 min with the mean pore radius of 0.13 µm with a narrow distribution without any cracks or pinholes in the membrane.

Xue and Deng [92] prepared a new amorphous Ni–B alloy/ceramic composite membrane by an improved electroless plating technique by pumping away the gases trapped in the porous ceramic substrate and the resultant film with the application of vacuum on the opposite side of the membrane along with rigorous stirring in the plating bath. The new membrane exhibited not only high permeability, but also high separation efficiency while the membrane prepared by the conventional plating method suffered from defects and low separation efficiency.

Haag et al. [93] deposited pure nickel coating on an asymmetric alumina support having a mesoporous top layer composed of γ-alumina using hydrazine as reducing agent for use in high temperature hydrogen separation. They found that the metallic nickel was dispersed both in and on the γ-alumina. After heat treatment at high temperature (900°C), they obtained a compact (thin) and uniform pure nickel layer of about 1–1.5 µm thickness. Their results indicated that the hydrogen transport phenomenon was mainly governed by the Knudsen diffusion, suggesting the presence of small pinholes on the surface of the nickel film.

1.4 Prominent issues in literatures

1.4.1 Membrane support parameters

Membrane performance characteristics are combinatorially influenced by the support characteristics, support pore size and fabrication method variables. The composition, porosity and pore size distribution of the substrate are some factors that affect the thickness of the membrane, thus the hydrogen flux, as well as the stability of the membrane at elevated temperatures. Typically asymmetric supports with a skin layer pore size of 5–10 nm are used. State of the art is largely biased towards electroless plating based metal membrane fabrication and therefore, it is in accordance with the summary presented in 1.2.7. The final thickness of the metal layer is strongly dependent on the pore size distribution of the support. Thinner membranes can be prepared with supports that have a smaller and narrower pore size distribution. Mardilovich et al. [94] deposited Pd on PSS supports of three different grades, 0.1, 0.2, 0.5 μm by electroless plating. The mercury porosimetry of the original supports showed that they had a different pore size distribution and that maximum pore size increased with higher grades. They reported that the final palladium thickness was approximately three times the diameter of the largest pore on the surface. Independent of the deposition technique, much thinner membranes can be prepared using porous glass and alumina [37, 95] support which have very small and narrow pore size distribution compared to the PSS. Surface roughness also contributes to the resulting coating structure. O`Brien et al. [37] sputter coated α-alumina (50–500 nm pore size) and γ-alumina (5–20 nm pore size) with Pd. γ-alumina substrates facilitated much denser coatings than α-alumina on which enhanced growth encircled around pinholes were formed. The roughness and the porosity of the support also affect the quality of the Pd seeds during the activation step and the adhesion of the metal to the substrate.

Considering the contribution of substrate properties to the performance of the membranes, ceramic supports are used in lab scale studies, basically on alloy formation and/or permeation characteristic of membranes as a function of microstructure. On the other hand, they suffer from peeling problems. Porous stainless steel supports are advantageous due to their thermal expansion coefficient close to that of Pd based films, ease of fabrication, high mechanical strength and high resistance to corrosion. However, in addition to their high cost, PSS composite membranes have other disadvantages such as relatively large pore size distribution (yielding thicker membranes) and intermetallic diffusion at high temperatures (that causes deterioration of the hydrogen flux).

1.4.2 Fabrication process variables

Controlling parameters in electrodeposition are peak current density, pulse duty cycle, total charge density, temperature, pH, deposition time and electrolyte concentration [44, 47, 48]. The optimal values of these parameters reported in literatures are: a charge density of 8 C/cm^2 [47], a cathode current density of 400 A/m^2 [47, 48], a temperature of 40°C and a pH of 7.5 [48]. Higher H_2/N_2 separation factors (>3000) were achieved with the application of vacuum during the electrodeposition of palladium [42, 43, 45].

Since a systematic investigation towards performance characteristics of Pd/Ni electroless plating is not available, it is not possible to deduce upon the proper choice of plating process parameters from much investigated research towards palladium membrane fabrication is not systematic. As far as loading ratio is concerned, various researchers used various values of loading ratio without indicating their efficacy. Collins and Way [98] used a high A/V ratio of 527 cm^2/L where as Yeung et al. [66] used a moderate A/V ratio of 350 cm^2/L during the electroless deposition of Pd on tubular membrane supports. In agreement with these values, Bhandari and Ma [6] used an A/V ratio of 460 cm^2/L while Ayturk and Ma [51] used a lower A/V ratio of 250 cm^2/L for electroless Pd and Ag deposition on tubular stainless steel porous supports. On the other hand, experimental studies involving disc type membranes did not adopt A/V ratios as high as those used for tubular membranes. Altinisik et al. [96] used a bath loading value of 30 cm^2/L while Dogan and Kilicarslan [99] used a loading ratio of 80 cm^2/L for Pd electroless plating on porous (2.6 μm) glass disks of 2.5 cm diameter. In a similar way, Huang et al. [59] used a bath loading ratio of 60 cm^2/L in the electroless co-deposition of Pd–Ag alloy membrane on a γ-Al_2O_3 substrate. Some of the above researchers also used diverse metal solution concentrations. For instance, Huang et al. [59] used a metal solution concentration of 0.0033 mol/L (at a loading ratio of 60 cm^2/L) whereas Collins and Way [98] used a metal solution concentration of 0.0307 mol/L (at a loading ratio of 527 cm^2/L).

However, when higher Pd metal precursor concentrations (about 0.0307 mol/L) were used [100], the loading ratio was increased to 785 cm^2/L. In other words, it appears that loading ratio is proportionally adjusted to the metal concentration without much technical justification. In summary, the combinatorial effects of loading ratio and metal solution concentration on process efficiency, membrane thickness and pore densification have not been reported.

Haag et al. [93] inferred that a nickel solution concentration of 0.12 mol/L is optimal to obtain membranes that have separation factors achievable with Knudsen diffusion transport mechanism. They did not emphasize upon the relationships between process parameters and membrane characteristics.

Several experimental investigations on nickel hypophosphite plating baths emphasized with respect to the surface engineering studies [80, 101, 102], without giving much insight into the choice of various process parameters such as concentrations of nickel, hypophosphite and stabilizer, coating time, pH, temperature and loading ratio. Process engineering studies towards nickel electroless plating need to address simultaneously two objectives namely identification of optimal process parameters that maximize plating conversion and efficiency and quality of plating with respect to the substrate. Very few literatures are available that emphasize upon the combinatorial optimization of both process and coating characteristics. Kar and Sathiyamoorthy [83] inferred that a stabilizer concentration of 25 g/L, bath temperature of 80°C and a pH of 9 provided the most uniform coating for Ni–P deposition on carbon fibers. Bi et al. [103]

indicated that a plating time of 20 min at a pH of 9.0 and plating bath temperature of 70°C is optimal to yield low phosphorous nickel coated microcoils. All in all, these literatures also did not relate upon the plating efficiency and were directed to surface engineering studies. Jappes et al. [104] used 0.23 mol/L of Ni^{+2} solution concentration, 0.38 mol/L sodium hypophosphite solution concentration and obtained a bath conversion of 22% and a plating efficiency of 68% at an optimal bath temperature of 87°C. In their work as well, the authors did not study upon the influence of loading ratio on the performance characteristics of the plating baths.

As presented in the earlier section (1.3), Cheng and Yeung [61] used two different reducing agents namely sodium hypophosphite and hydrazine to study the influence of plating chemistry on deposition rate in electroless plating, plating efficiency and Pd film microstructure. They observed that hypophosphite-based plating bath had a slower plating rate than a hydrazine-based plating bath. Also, the presence of hydrogen that was produced during the oxidation of hypophosphite resulted in the de-lamination of palladium layer from the support. In contrast, they obtained dense palladium membranes with excellent support adhesion using hydrazine as reducing agent. They suggested that chemical reducers that generate hydrogen such as sodium hypophosphite were not suitable for electroless plating of palladium membrane.

1.4.3 Mass transfer enhancements

Metal deposition using electroless plating technique is a severely mass transfer limited process. Therefore, enhancement in metal deposition rate is very much desired. Various suggested mass transfer enhancement techniques for nickel hypophosphite baths include bath agitation [51], gas sparging [96] and sonication [69, 105]. Jiang et al. [105] indicated that sonication assisted electroless plating can provide efficient deposition of nickel even at 40°C, a temperature which is considered to be very inefficient for the conventional nickel electroless plating baths due to extremely low reaction rates. Amongst these, bath agitation and gas sparging would be attractive options due to lower additional costs to the conventional electroless plating setup when compared to sonication. For all these cases as well, we did not find literatures that present the combinatorial performance characteristics of the nickel plating baths.

Zheng and Wu [62] reported upon the effectiveness for palladium electroless plating under hydrothermal conditions. The authors observed that using a support of nominal pore size 800 nm, the average membrane pore size was reduced to about 360 nm in a single electroless plating deposition step. This corresponds to a pore densification of about 79.75% in only two hours of Pd electroless plating. However, process inefficiency and selective conversion have not been reported in this work.

Mass transfer enhancements are considered with the fact that electroless plating technique suffers with the basic problem of gas generation on the membrane surface due to which metal attrition and poor conversions are at place. Few researchers have conveyed that due to the gas generation at the membrane surface, electroless deposition is not favored in the pores but on the surface thus contributing to larger metal film thickness and poor membrane pore densification per unit metal film. Therefore, electroless plating being severely mass transfer controlled process, it needs to accommodate the mass transfer coupling effects to improve both nickel plating rate and uniformity of plating. In summary, both process parameters and mass transfer coupling effects can contribute significantly towards the permeation characteristics of the metal–ceramic composite membranes. So far, various suggested mass transfer enhancement techniques for nickel plating baths include bath agitation [51], gas sparging [96] and sonication [69]. However, a parametric study that emphasizes towards surface property optimization is not targeted so far. Therefore, electroless plating in comparison to other deposition techniques encourages both fundamental and applied research to identify the optimal conditions for metal composite membrane fabrication.

Chen et al. [41] prepared palladium membranes by stirring assisted Pd electrodeposition on porous stainless steel tubular supports and observed that high membrane rotation speed (200 rpm) resulted in a very homogenous grain size.

Ayturk and Ma [51] studied the electroless Pd and Ag deposition kinetics of the composite Pd and Pd/Ag membranes synthesized from agitated plating baths. They observed that bath agitation indicated a 60% improvement of the plating bath efficiency in comparison to that of the Pd and Ag runs conducted under the static conditions.

Kathirgamanathan [69] studied ultrasound-assisted electroless deposition of copper onto and into microporous membranes for electromagnetic shielding. The author noticed that ultrasonication reduced the plating time for electroless deposition of copper onto microporous membranes, improved adhesion of the metal to the surface of the membrane and also helped to eliminate the need for pretreatment or chemical etching of the membranes.

Altinisik et al. [96] prepared palladium membranes (15 µm) by electroless plating technique on porous glass supports whose average pore size was 1.3 µm with a bulk porosity of 0.46. They applied gas sparging (helium bubbling) together with solution stirring and observed that these mass transfer enhancements created uniform concentration in the solution and removed the produced hydrogen gas from the surface of the membrane. The prepared membranes had a selectivity of 7 for H_2/N_2 at 200°C.

1.4.4 New generation supports

Among the supports, non-metals such as ceramic and glass have week adhesion to metallic thin films and difficulty to seal into commercial component. The week adhesion, different thermal expansion coefficients and the volume change of the membrane in contact with hydrogen may cause stability problems. On the other hand, porous stainless steel support has been used to improve mechanical strength of the support. From the viewpoint of a practical application, porous stainless steel has the merit of getting more readily sealed into a commercial unit. However, atomic interdiffusion of metals between the thin dense Pd/Pd alloy layer and the porous stainless steel components occur during high temperature processing.

Ryi et al. [97] prepared symmetric nickel membranes with a nominal pore size of 33 nm from nickel powder using compression (333 MPa) and sintering (650°C) technique. They found that the porous nickel support had very small pores with uniformity and smooth enough surface to be applied as the support for metallic dense membrane without surface modification. Later, the same authors [31, 33] prepared Pd–Cu–Ni alloy membrane of 4 μm thick on porous nickel support (33 nm) by multi-target sputtering and Cu-reflow technique. They observed that the nickel support was very stable and a very high H_2/N_2 separation factor (∞) was obtained. However, flexibility to vary the surface pore size and average porosity has not been addressed by the authors. In addition, fabrication using electroless plating has not been yet studied. In a similar study, Vichaphund and Atong [106] prepared nickel–alumina membranes using both powder and bulk impregnation methods for hydrogen separation. In this study as well, various important issues such as controlling film pore size, thickness and average effective porosity have not been addressed which influence to a significant extent the permeation and separation characteristics of the membrane.

Xiong et al. [32] prepared porous nickel supports by uniaxial compression of nickel powders for the fabrication of $Nb_{40}Ti_{30}Ni_{30}$ membranes by magnetron sputtering for hydrogen separation and purification. They found that the $Pd/Nb_{40}Ti_{30}Ni_{30}/Pd$/porous nickel support composite membrane exhibited excellent permeation capability and satisfactory mechanical properties.

Ryi et al. [34] prepared defect-free Pd–Cu–Ni ternary alloy membranes of 12 μm thickness by sputtering Pd and Cu on the polished porous nickel support (250 nm) followed by the Cu-reflow method. The hydrogen permeance through the membrane was 3.8×10^{-7} mol m^{-2} s^{-1} Pa^{-1} with infinite H_2/N_2 selectivity. The permeance value obtained in this study was three times higher than that obtained in their previous study [31] of the similar membrane with a lower support pore size.

In summary, nickel membranes appear to be promising as new generation supports for thin and dense Pd film integrated composite membranes. There is a need to address the ability of electroless plating to prepare these new generation supports that possess nickel layer as the intermediate diffusion barrier.

1.5 Possible scope for further research

It is evident from the literature survey that electroless plating process received maximum research attention to achieve membranes with desired performance characteristics [51–96]. Based on extensive literature survey, it is apparent that the following areas in the field of metal composite membrane fabrication need to be thoroughly investigated.

a) **Membrane support parameters:** The development of low cost ceramic membrane supports with a nominal pore size of about 200–300 nm is an important issue.

b) **Combinatorial performance characteristics:** The effect of metal solution concentration and loading ratio parameters of the metal plating baths on conversion, plating efficiency, metal film thickness, pore size and pore densification should be considered.

c) **Mass transfer enhancements:** The existing literature is scarce and the impact of various mass transfer enhancements such as agitation, sonication and hydrothermal processes on the combinatorial performance characteristics of electroless plating baths needs to be addressed.

d) **New generation supports:** Electroless plating can be explored to identify new generation nickel composite membranes with diverse nickel film characteristics (film thickness and nominal pore size) can be obtained by the selection of appropriate combination of metal solution concentration and bath loading ratio. It is important to note that the existing nickel powder impregnation method may not offer such flexibility and hence further engineering of dense Pd membranes may be restricted.

In summary, mass transfer enhanced electroless plating process characteristics for nickel deposition on porous supports is anticipated to provide a sound technical overview with which further engineering of thin dense Pd composite membranes is easily accomplished.

1.6 Objectives of present study

The fundamental challenge that we wish to consider in this work is to achieve 100% pore densification using 8 hours of sequential plating using nickel precursors and a low cost ceramic support that has wider pore size distribution. The consideration of a support with wider pore size distribution is to identify the potential of mass transfer enhancements in driving pore densification. The selection of nickel as the plating precursor is due to the hypothesis that nickel membrane depositional characteristics are inferior to palladium membrane depositional characteristics and therefore, the greater role of mass transfer enhancements can be thoroughly examined. Alternatively, the supplementary objective of this work is to prepare nickel ceramic composite membranes with variant average pore size values (5–100 nm), metal film thickness (5–50 microns) in order to serve as diverse membrane supports for the deposition of ultra-thin palladium films on these supports. Other objectives of this work are presented as follows:

a) Investigate the combinatorial performance characteristics (conversion, efficiency and pore densification) of sodium hypophosphite and hydrazine electroless plating bath variables (nickel solution concentration and loading ratio).

b) To critically examine and identify potential mass transfer enhancement techniques that can enable higher pore densification values at lower metal precursor concentrations. These include stirring, sonication, hydrothermal and sonication coupled hydrothermal plating processes.

c) To identify electroless plating variables (especially metal solution concentration and loading ratio) for which mass transfer enhancements do not play a greater role in enhancing the pore densification.

d) To define conceptual benchmarks for various mass transfer enhanced electroless plating processes based on tradeoffs associated to selective conversion and pore densification.

1.7 Organization of the thesis

Chapter 2 presents the preparation and characterization of ceramic membrane support along with the experimental procedure for electroless plating process adopted in this study.

Chapter 3 addresses the performance characteristics of conventional electroless plating baths for nickel–ceramic composite microfiltration membranes.

Chapter 4 summarizes the performance characteristics of agitated plating baths for nickel composite membrane fabrication.

Chapter 5 summarizes the performance characteristics of ultrasound assisted electroless plating baths for nickel composite membrane fabrication.

Chapter 6 summarizes the effect of hydrothermal condition (with and without sonication) on the performance characteristics of nickel plating baths for membrane fabrication. All in all, the sole objective of this work is to achieve a near 100% pore densification by targeting rigorous experimentation with various mass transfer enhancement techniques.

Chapter 7 briefly presents the concluding remarks and recommended future work as an extension of the work carried out in this thesis.

EXPERIMENTAL

This chapter is divided into three sections. The first section presents the preparation and characterization of ceramic membrane supports. The second section presents the methodology adopted for electroless plating experiments for the fabrication of nickel–ceramic composite membranes and the third section summarizes the evaluation of various parameters for characterizing the electroless plating process as well as the membrane performance. The disk type ceramic membranes were prepared manually by paste method. Their average pore size was evaluated to be 275 nm by both air and water permeation experiments.

2.1 Support preparation and characterization

2.1.1 Raw materials

Seven inorganic raw materials viz. kaolin, feldspar, quartz, sodium carbonate, pyrophyllite, boric acid and sodium metasilicate were used in the fabrication of ceramic membrane supports. Kaolin was obtained from CDH Ltd., India, feldspar and pyrophyllite from National Chemicals, India, quartz from Research-lab Fine Chem Industries, India, sodium metasilicate from SD Fine-chem Ltd., India and the other inorganic precursors (sodium carbonate and boric acid) were obtained from Merck Ltd., India. Composition of various raw materials used for the fabrication of ceramic membrane supports is presented in the following table (Table 2.1). This composition is chosen as it yielded the lowest average pore size and better corrosion resistance among the other compositions tested by trial and error method.

Table 2.1: Composition of raw materials for the fabrication of membrane supports

Material	**Composition on dry basis** (wt %)	**Composition on wet basis** (wt %)
Kaolin	40	32
Feldspar	15	12
Quartz	15	12
Sodium carbonate	10	8
Pyrophyllite	10	8
Boric Acid	5	4
Sodium metasilicate	5	4
Water	–	20

2.1.2 Support fabrication

The ceramic membrane supports were fabricated manually by paste method. As shown in the figure (Figure 2.1), the fabrication methodology consists of the following hierarchical steps: mixing of raw materials to make a paste; casting of the paste into circular moulds; drying of the raw discs; sintering; polishing of the membranes and cleaning. All the raw materials except water were taken based on the above composition with a total dry weight of 20 g per each membrane. These raw materials were manually mixed and ground to make a uniform powder and then mixed thoroughly using a laboratory blender. This dry mixture was taken into a petri dish and water was added to it (approx. 5 ml for each membrane) and was mixed to form a uniform paste. The paste was then placed into a circular mould (stainless steel) to make disk shaped membranes. Weights (2 kg each) were placed on the wet membranes to recover structural deformations and for about 12 hours and then the membranes were dried for 24 hours at ambient conditions (298 K).

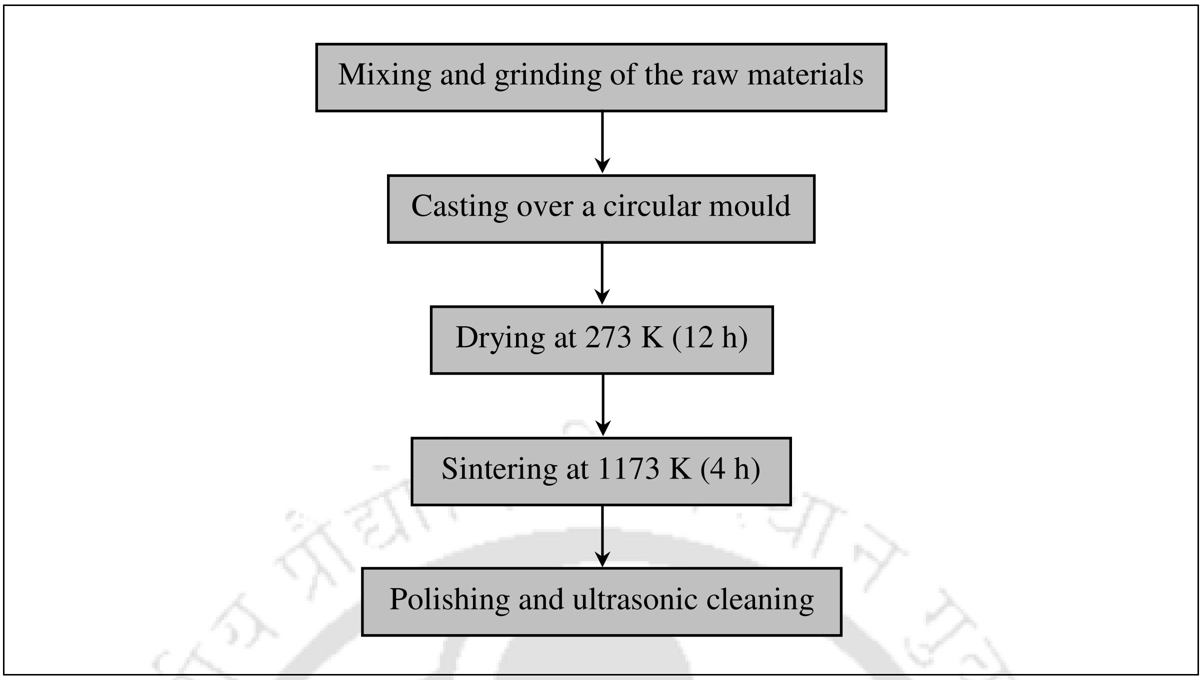

Figure 2.1: An outline of ceramic membrane preparation procedure.

Then, the membranes were dried in a muffle furnace at 373 K for 12 hours to remove the moisture content of the membranes. Finally, the membranes were sintered at 1173 K for four hours. The temperature of the furnace was raised in two steps. Initially, heating was carried out at a slower rate (1 K/min) up to 523 K to avoid bending/cracking of membranes followed by a slightly higher heating rate (2 K/min) up to the sintering temperature (1173 K). This sintering temperature was chosen because no considerable weight loss was observed beyond this temperature in the thermogravimetric analysis (TGA) of the raw material paste formulation (Figure 2.2). Sintering was carried out for four hours and the membranes were allowed to cool down slowly to the room temperature. The sintered membranes were polished on silicon carbide abrasive paper (No. C–220) to obtain a smooth surface finishing with required dimensions (52.5 mm diameter and 4.5 mm thickness) and were subjected to ultrasonic cleaning for 15 minutes to remove any loose particles created during surface polishing. After cleaning the membranes with de-ionized water, they were dried in a hot air oven to make them moisture free.

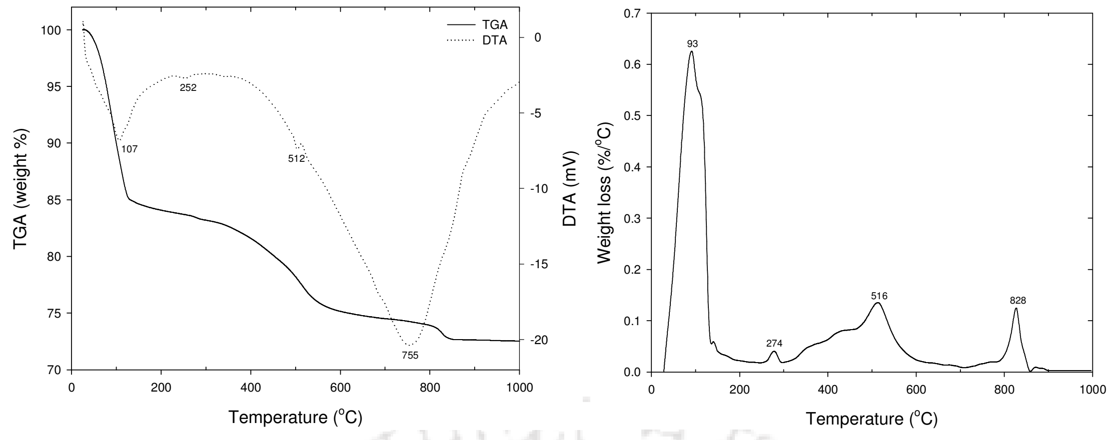

(a) **(b)**

Figure 2.2: (a) TGA and DTA curves of the raw material paste; (b) weight loss of the mixture.

2.1.3 Support characterization

Membrane characterization was studied using various preliminary methods. The surface characterization was performed by scanning electron microscopy (SEM). The mean pore size of the bulk membrane was estimated from air and water permeation experiments. Membrane porosity was obtained by pycnometric method. Finally, the prepared membranes were tested for their corrosion resistance by measuring their weight loss after keeping them in standard (0.1 N) solutions of HCl and NaOH respectively for a period of 7 days.

2.1.3.1 Surface characterization

Figure 2.3 presents the SEM surface micrograph and pore size distribution of the membrane support, respectively. The average pore size obtained from the surface SEM image analysis using ImageJ software was 258 nm (Figure 2.3b). For this analysis, more than 100 points were considered from 6 different SEM images taken at various locations of the support membrane. However, it is risky to estimate the average pore size from SEM

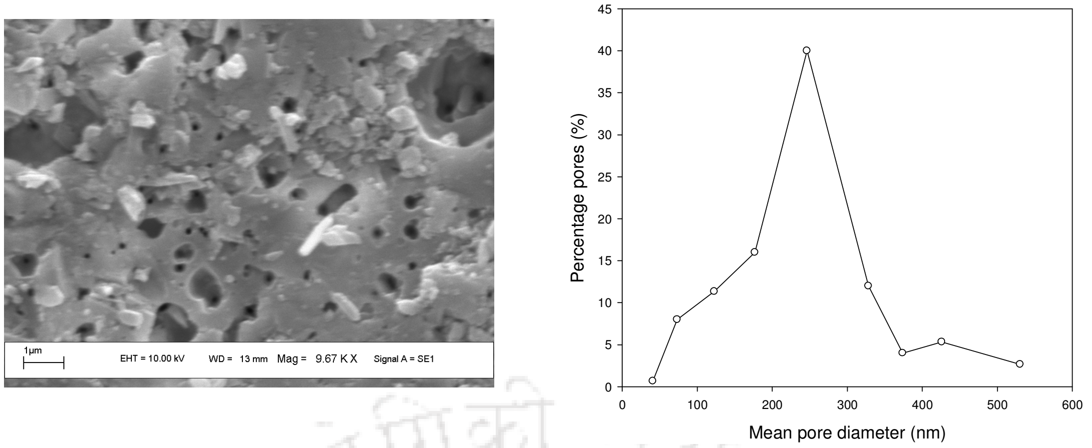

(a) **(b)**

Figure 2.3: (a) Surface SEM image of the ceramic support; (b) pore size distribution.

image analysis as the surface area scanned by SEM is too small to represent the overall surface morphology of the membrane.

2.1.3.2 Permeation experiments

Both gas (air) and liquid (water) permeation experiments were carried out to evaluate the membrane performance and identify the presence of defects in the interior of the membranes using a laboratory made permeation setup (shown in Figure 2.4) of capacity 200 ml. The setup consisted of a Teflon tubular cell with a flat rectangular Teflon base plate. The membrane was placed in the membrane housing provided on the base plate

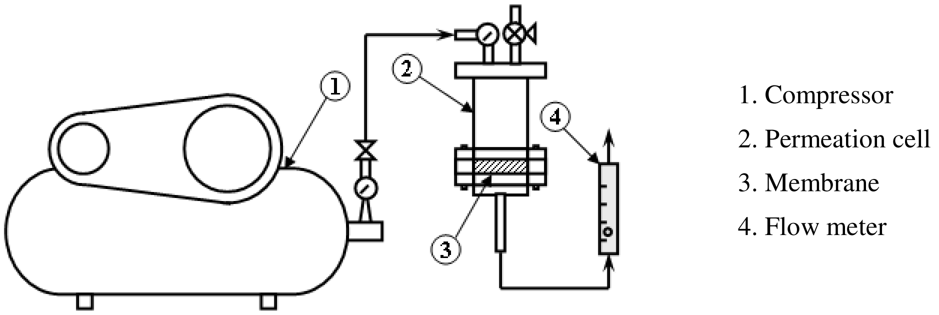

Figure 2.4: Experimental setup for the permeation tests.

and was sealed with epoxy resin. The cell was pressurized with compressed air and the outlet was connected to a gas flow meter for measuring the gas flow rate at various trans-membrane pressures. The hydraulic permeability and corresponding pore diameter and porosity of the membranes were also determined. All permeation experiments were conducted at room temperature (298 K). The flux data of the ceramic membrane support is presented in Figure 2.5.

2.1.3.2.1 Gas permeation

Based on the gas permeation data, average pore radius (r_g) and effective porosity (ε/q^2) can be estimated according to the following expression [107, 108].

$$K = 2.133\frac{r_g v}{l}\frac{\varepsilon}{q^2} + 1.6\frac{r_g^2}{l\eta}\frac{\varepsilon}{q^2}\bar{P} \tag{2.1}$$

Here, $\bar{P}$ is the average pressure on the membrane, v (m/s) is the molecular mean velocity of the gas, l (m) is the pore length, q is the tortuosity, η (Pa.s) is the viscosity of gas, and K (m/s) is the effective permeability factor evaluated as:

$$K = \frac{QP_2}{S\Delta P} \tag{2.2}$$

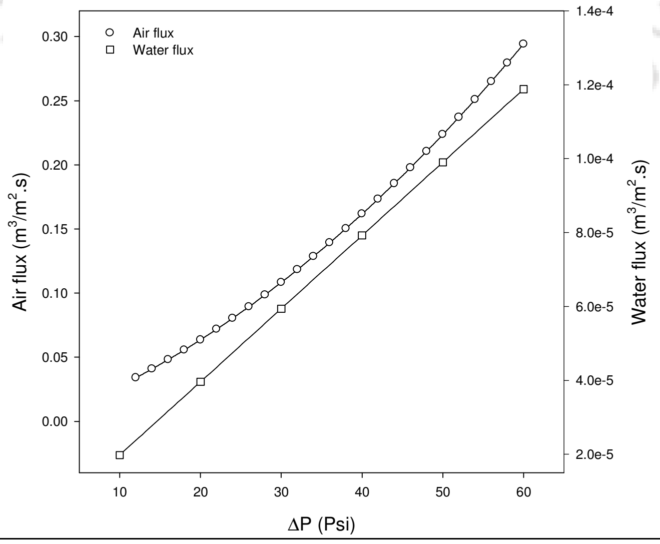

Figure 2.5: Air and water flux data for the ceramic membrane support.

where S (m^2) is the permeable area of the membrane, Q (m^3/s) is the volumetric flow rate, P_2 (Pa) is the membrane pressure at permeate side and ΔP (Pa) is the trans-membrane pressure drop.

Equation (2.1) is in the form of a straight line:

$$K = A\bar{P} + B \tag{2.3}$$

for which 'A' and 'B' are the slope and the intercept respectively. Here 'K' can be evaluated for different values of '$\bar{P}$' using Equation (2.2) and a straight line fit to these data (Figure 2.6) can yield the values of 'A' and 'B' from which the average pore radius can be obtained as follows.

$$r_g = 1.333\frac{A}{B}v\eta \tag{2.4}$$

Using the value of r_g, the effective porosity can be calculated as:

$$\frac{\varepsilon}{q^2} = \frac{B}{2.133}\frac{l}{r_g v} \tag{2.5}$$

As shown in the figure (Figure 2.6), the slope and intercept values for the ceramic support

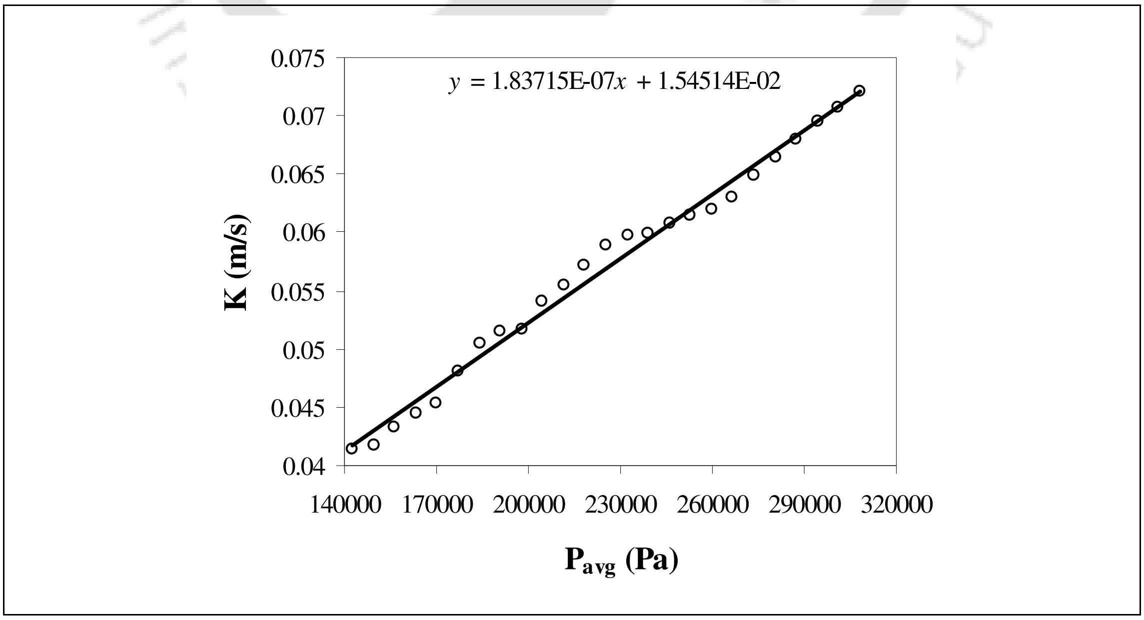

Figure 2.6: Plot of effective permeability factor versus average pressure.

were obtained to be 1.84×10^{-7} and 1.54×10^{-2} respectively. Substitution of these values into Equation (2.4) gives the average pore radius from which the average pore diameter can be evaluated. The average pore diameter and the effective porosity of the ceramic support as obtained from the above analysis were 275.46 nm and 0.4497 respectively.

2.1.3.2.2 Liquid permeation

Based on the liquid permeation data, hydraulic permeability (L_h) and the average pore radius (r) can be estimated according to the following expression [107, 108].

$$J = \frac{n\pi r^4 \Delta P}{8\mu l} = L_h \Delta P \tag{2.6}$$

where J (m/s) is the flow density (flux) of permeated water, n is the pore density (number of pores per m^2), μ is the water viscosity, l is the pore length (m), ΔP (Pa) is the trans-membrane pressure difference. Here L_h is the slope of the straight line fitted for 'J' versus 'ΔP' (Figure 2.7). By using the porosity, $\varepsilon = n\pi r^2$ in Equation (2.6), the corresponding pore radius can be obtained as follows.

$$r = \left[\frac{8\mu l}{\varepsilon} L_h\right]^{1/2} \tag{2.7}$$

As shown in the figure (Figure 2.7), the slope of the straight line was 2.97×10^{-10} which is the value of hydraulic permeability (L_h). By substituting this value and the values of other variables in Equation (2.7) gives the average pore radius from which the pore diameter can be evaluated. The average pore diameter as obtained from the above calculation was 274.18 nm which is very close to that obtained from the gas permeation experiment (275.46 nm). The higher value of pore size in permeation studies is due to those smaller pores that were not continuous but were observed in the surface SEM analysis. The porosity determination is described in the next sub-section (2.1.3.3).

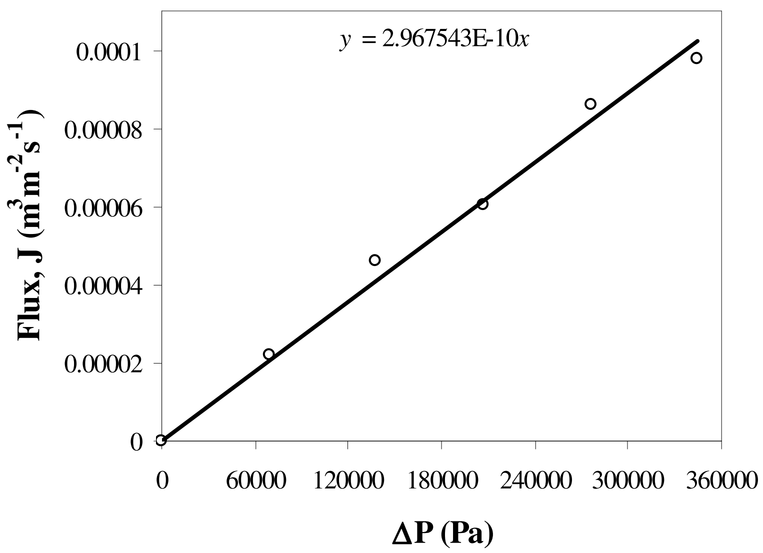

Figure 2.7: Plot of liquid permeate flux versus trans-membrane pressure difference.

2.1.3.3 Porosity estimation

Bulk porosity of the ceramic membrane was estimated by pycnometric method [109] using water as the wetting medium. In this method, the dry membrane was wetted by water for about 15 minutes in a sonication bath and the weight gain was measured. Thereby, the volume of water absorbed into the pores was evaluated to get the pore volume. The ratio of pore volume to the total volume of the membrane gives the bulk porosity of the prepared membrane.

$$\text{Porosity, } \phi = \frac{\text{Volume of pores}}{\text{Total volume of the membrane}} \qquad (2.8)$$

Using the above equation, porosity was found to be 0.4021. And also the structural density of the membrane is found to be 1653 kg/m^3. The porosity value obtained by this method is in good agreement to that obtained from the gas permeation experiment (0.44).

2.1.3.4 Corrosion resistance

The prepared membranes were tested for their corrosion resistance by keeping them in standard (0.1 N) solutions of hydrochloric acid (HCl) and sodium hydroxide (NaOH) for a period of one week. These membranes were then washed with water and were dried at a temperature of 393 K for four hours to take their dry weight. The weight loss of the membranes was measured in order to evaluate their corrosion resistance. No weight loss was observed for the membrane placed in NaOH solution but a considerable amount (5%) of weight loss was observed for the membrane placed in HCl solution. Results showed that the prepared membranes have better resistance to alkaline (base) atmosphere and are very much suitable for electroless plating in alkaline baths.

2.1.4 Summary

From the air permeation experiments, the average pore diameter and the effective porosity of the ceramic membrane support were obtained as 275 nm and 0.44 respectively. From the water permeation experiments, the average pore diameter was evaluated to be 274 nm which is very close to that obtained from the air permeation experiments (275 nm). From the pycnometric analysis of the ceramic membrane, porosity was found to be 0.402 while its structural density was 1653 kg/m^3. Corrosion resistance studies indicate that no weight loss (0%) was observed for the membrane placed in NaOH solution (0.1 N) but a considerable amount (5%) of weight loss was observed for the membrane placed in HCl solution (0.1 N). Therefore, these results indicate that the prepared membranes have very good corrosion resistance in alkaline (base) atmosphere and poor resistance in acidic atmosphere. Henceforth, it is very likely that the support morphology does not get affected by the alkaline nature of the plating baths and the suggested inorganic precursor formulation is suitable for extended studies upon the plating and metal–ceramic composite membrane characteristics.

2.2 Electroless plating

Substrate pre-treatment to remove the presence of contaminants on membrane surface involved two sequential steps. These were cleaning with trichloroethylene in a sonication bath for 30 minutes to remove any greasy materials present on its surface and rinsing in de-ionized water for 5 minutes. Later, sensitization and activation were carried out to seed palladium metal on the support surface selectively by covering the other surfaces with adhesive tape (Teflon) prior to nickel plating. Conventional procedure involving sequential steps of sensitization, activation and rinsing using baths of various compositions (Table 2.2) was deployed to carry out the Pd seeding process. The ceramic membrane was dipped in the sensitization bath containing tin chloride solution for 2 minutes, rinsed with water and then dipped in the activation bath containing palladium chloride solution followed by acid (0.1 N HCl) bath for 2 minutes each and finally rinsed with de-ionized water. The operation was repeated 4 to 5 times to get sufficient seeding of Pd over the ceramic substrate. After seeding, the membrane was dried overnight in an oven at 373 K to measure its dry weight (w_1).

Plating experiments were carried out using typical compositions summarized in Tables 2.3 and 2.4 for hypophosphite and hydrazine based electroless plating baths respectively. The plating experiments were designed to evaluate plating characteristics for wide range of initial nickel solution concentration (0.04–0.16 mol/L) and loading ratio

Table 2.2: Compositions of sensitization and activation baths

Constituent	**Amount used in each bath**	
	Sensitization	**Activation**
$SnCl_2.2H_2O$ (g/L)	1.0	–
$PdCl_2$ (g/L)	–	0.1
35% HCl (ml/L)	1.0	0.5

Table 2.3: Compositions and parameters for hypophosphite electroless plating baths

S. No	**Component**	**Amount (mol/L)**	**Unit cost ($/kg)**
1	Nickel sulfate ($NiSO_4.7H_2O$)	0.04–0.16	70
2	Sodium hypophosphite ($NaH_2PO_2.H_2O$)	0.08–0.32	29
3	Trisodium citrate ($Na_3C_6H_5O_7.2H_2O$)	0.2	12
4	Ammonium sulfate ($(NH_4)_2SO_4$)	0.5	7
Plating temperature (K)		353	
Loading ratio (cm^2/L)		196–393	

(196–393 cm^2/L). A 100% excess reducing agent was used in all the cases and the pH of the plating bath was maintained around 10–11 using NaOH for hydrazine baths. Trisodium citrate was used as the stabilizer agent to control the rate of release of free metal ions for the reduction reaction.

Eight sequential steps (with equal initial nickel solution concentration) involving intermediate rinsing of membrane with de-ionized water were carried out to yield the nickel–ceramic composite membrane. For each plating step, all the components excluding the reducing agent were taken in a beaker and were mixed thoroughly to obtain homogeneous solution and the beaker was placed in a silicone oil bath (Figure 2.8a) to maintain the plating temperature (353 K). After reaching the required temperature inside the beaker, the reducing agent was added and the solution was mixed thoroughly. Then the substrate was kept in the plating bath for 60 minutes to get sufficient plating. After eight

Table 2.4: Compositions and parameters for hydrazine electroless plating baths

S. No	**Component**	**Amount (mol/L)**	**Unit cost ($/kg)**
1	Nickel sulfate ($NiSO_4.7H_2O$)	0.04–0.16	70
2	Hydrazine hydrate ($N_2H_4.H_2O$)	0.08–0.32	46
3	Trisodium citrate ($Na_3C_6H_5O_7.2H_2O$)	0.05–0.20	12
4	Sodium hydroxide (NaOH)	pH: 10–11	32
Plating temperature (K)		353	
Loading ratio (cm^2/L)		196–393	

such depositions, the membrane was rinsed with de-ionized water for 30 minutes so as to clean the surface from free particles followed with drying for 3 hours at 373 K. The dry weight of the membrane after plating was measured (w_2) to evaluate the amount of nickel plated on the ceramic support. A total of twenty four (24) nickel–ceramic composite membranes were fabricated using solutions of four different concentrations (0.04, 0.08, 0.12 and 0.16 mol/L), three different loading ratios (196, 262 and 393 cm^2/L) and two different reducing agents to study the combinatorial performance characteristics of electroless plating baths (bath conversion, plating efficiency, selective conversion, deposition rate, average mass transfer coefficient, mean pore size of the composite membrane, porosity of the deposited nickel layer, percent pore densification (PPD) and metal layer thickness).

For agitated electroless plating case, the activated ceramic membrane substrate was rotated with the help of a mechanical stirrer as shown in Figure 2.8b. The substrate was fixed to a membrane holder connected to the stirrer shaft. The plating solution was heated to the desired temperature (353 K) in a silicon oil bath equipped with a digital control to maintain the plating temperature. After reaching the desired temperature inside the plating bath, the activated ceramic membrane substrate along with the stirrer shaft was immersed into the plating solution such that the activated surface of the substrate was kept at one half of the liquid level. Membrane rotation speed was varied between 0–200 rpm at the intervals of 50 rpm to study the effect of stirring speed on the combinatorial performance characteristics of electroless plating baths. A total of forty eight (48) nickel–ceramic composite membranes were fabricated using solutions of three different concentrations (0.04, 0.08 and 0.16 mol/L), two different loading ratios (196 and 393 cm^2/L), four different stirrer speeds (0, 50, 100 and 200 rpm) and two different reducing agents to study the combinatorial performance characteristics of electroless plating baths.

For sonication assisted electroless plating case (Figure 2.8c), the plating bath along with the activated substrate was placed in an ultrasonic bath (Elmasonic, S30H) provided with an internal heater to maintain the plating temperature at 353 K. The sonication bath was operated at a constant frequency of 37 kHz. The total power consumption of the sonicator was 280 W. After heating the plating solution to the desired temperature (353 K), the activated ceramic membrane substrate was placed in the bath and the sonicator was run continuously during the plating process. A total of sixteen (16) nickel–ceramic composite membranes were fabricated in the sonication bath using solutions of four different concentrations (0.04, 0.08, 0.12 and 0.16 mol/L), two different loading ratios (196 and 393 cm^2/L) and two different reducing agents to study the effect of ultrasound on the performance characteristics of electroless plating baths.

For plating under hydrothermal conditions, all the components were mixed thoroughly to obtain a homogeneous solution and placed in the hydrothermal setup (shown in Figure 2.9) preloaded with the activated ceramic support. Flexible PTFE rings were used as gaskets to make the container leak-proof. The total volume of the setup was 100 ml of which 50% was filled with the plating solution for all the hydrothermal plating experiments to maintain a constant loading ratio of 393 cm^2/L (which was found to be optimal and more economical from the previous experiments). For pure hydrothermal experiments, the setup was placed in a water bath to maintain the plating temperature (353 K) while for the hydrothermal experiments combined with sonication (hydrothermal + sonication), the setup was placed in a sonication bath (Elmasonic, S30H) provided with a heater to maintain the bath temperature. A total of sixteen (16) nickel–ceramic composite membranes were fabricated to study the plating characteristics under hydrothermal conditions with and without sonication using four different initial nickel solution

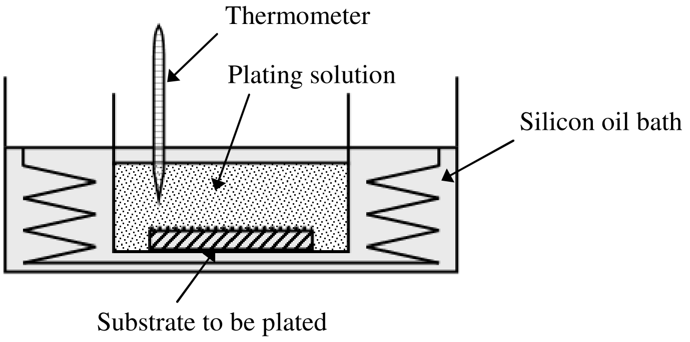

(a) Conventional electroless plating

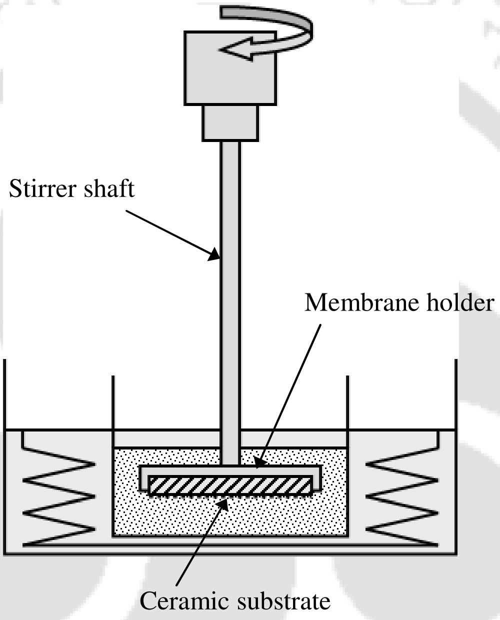

(b) Agitated electroless plating

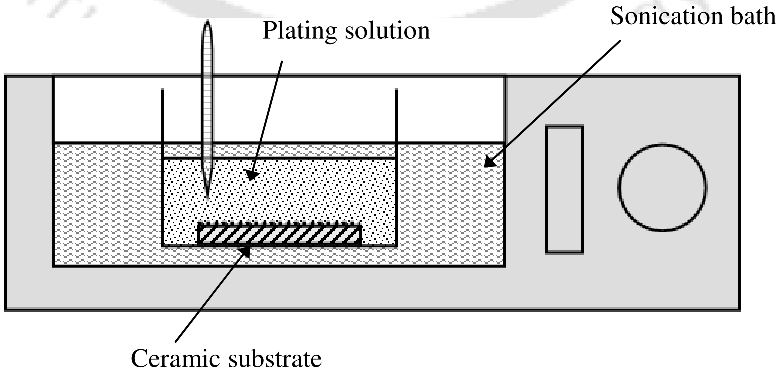

(c) Ultrasonic electroless plating

Figure 2.8: Typical electroless plating setup for various cases.

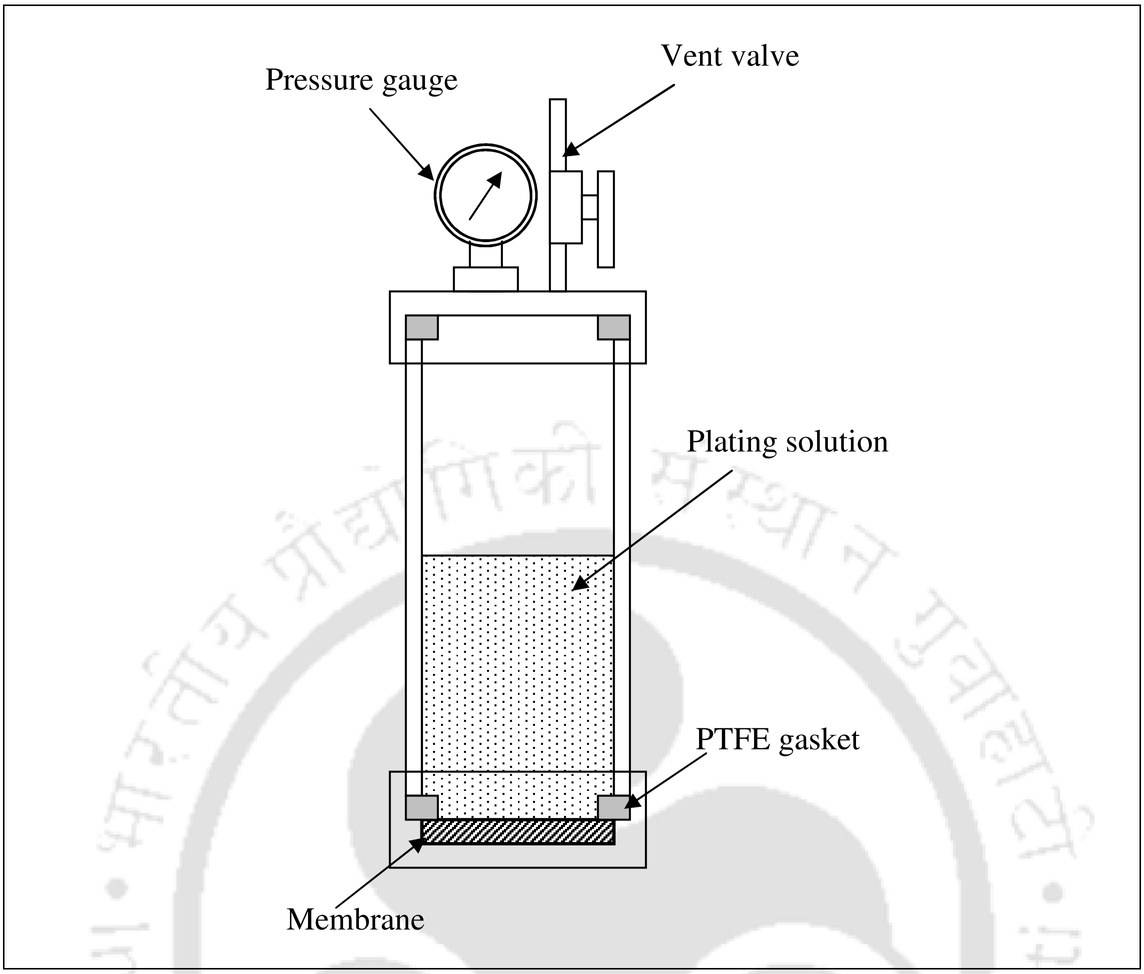

Figure 2.9: Hydrothermal electroless plating setup.

concentrations (0.04, 0.08, 0.12 and 0.16 mol/L) and two different reducing agents (sodium hypophosphite and hydrazine).

For all plating experiments, a 100% excess reducing agent was used. Water loss during the plating experiments was compensated by adding hot water into the bath so that the liquid level of the plating solution (and hence the loading ratio) remains constant. Concentration of nickel ions in the plating baths before and after electroless deposition were estimated from complexometric titration with EDTA using xylenol orange indicator under specified conditions (stirring and heating). Average pore size and porosity of the composite membranes were estimated from gas permeation experiments. Average thickness of the nickel layer deposited on the ceramic substrate was estimated from weight gain method. The results are presented in the subsequent chapters (Chapters 3–6). For all the cases studied, few experiments were randomly repeated to ensure consistency of the obtained results.

2.3 Evaluation of plating characteristics

2.3.1 Plating parameters

Parameters evaluated for conventional electroless plating are conversion, plating efficiency selective conversion, plating thickness and pore densification. Further, the effect of bath loading, metal ion concentration and mass transfer enhancements on these parameters is also studied. Analysis of the bath solution was carried out by complexometric titration (refer section 2.3.2) with standard ethylene diamine tetra-acetic acid (Na_2–EDTA) using xylenol orange as the indicator to estimate the average solution concentration of nickel before and after eight electroless plating.

Eventually, the conversion (x) in the plating bath is evaluated using the following expression (Eq. (2.9)).

$$x = \frac{C_i - C_f}{C_i} \qquad (2.9)$$

where, C_i (mol/L) is the initial concentration of Ni^{+2} in the plating solution and C_f (mol/L) is the average Ni^{+2} solution concentration after plating (obtained from titration analysis). Plating efficiency (η) is the ratio of amount of nickel metal plated on the ceramic membrane support to that converted in the plating reaction.

$$\eta = \frac{w_2 - w_1}{w_0 x} \qquad (2.10)$$

where, w_1 (g) is the dry weight of the membrane before plating, w_2 (g) is the dry weight of the membrane after plating and w_0 is the total amount of nickel (g) originally available in the plating bath (for 8 sequential plating steps) expressed as follows.

$$w_0 = (nV_0C_i)\,M_{Ni} \tag{2.11}$$

where, n is the number of plating cycles (= 8), V_0 is the volume of plating solution in each plating cycle (L) and M_{Ni} is the molecular weight (g/mol) of nickel metal.

The nickel film thickness (δ) is evaluated using the weight gain method and was expressed as follows.

$$\delta = \frac{w_2 - w_1}{\rho_{Ni} A_m} \times \frac{1}{1-(\varepsilon/q^2)_{film}} \tag{2.12}$$

where, ρ_{Ni} is the density of nickel metal (g/cm^3), A_m is the membrane surface area (m^2) and $(\varepsilon/q^2)_{film}$ is the effective porosity of the deposited metal layer evaluated from air permeation experiments. Pore densification during the plating process is defined as the fractional volume of the pores covered by the deposited metal and it is generally expressed as percent pore densification (PPD). It is given by the following expression (2.13).

$$PPD = \left(\frac{d_i^{\,2} - d_o^{\,2}}{d_i^{\,2}}\right) \times 100 \tag{2.13}$$

where, d_i and d_o are average pore diameters of the substrate (before plating) and nickel–ceramic composite membrane (after plating) respectively. Both the average pore diameters were determined from air permeation experiments.

2.3.2 Titration analysis

Concentration of Ni^{+2} in the plating bath before and after plating is analyzed by complexometric titration (Figure 2.10) with ethylenediaminetetraacetic acid (EDTA) using xylenol orange (1% in KNO_3) as indicator at a temperature of 353 K with added buffering agents (NaOH + CH_3COOH (glacial), 5:8 mole ratio) under continuous agitation.

The sequence of steps involved in the titration process was as follows.

(i) 5 ml of bath sample was taken into a 250 ml beaker.

(ii) The sample was then diluted (10 times) with de-ionized water.

(iii) Buffer solution was added until the solution becomes colorless (≈10 ml).

(iv) The solution was heated (≈353 K) on a hot plate under continuous stirring.

(v) Xylenol orange indicator was added (solution becomes red).

(vi) Standardized (0.1 N) EDTA solution was added drop by drop (using burette) until the equivalence point was reached (color changes to yellow).

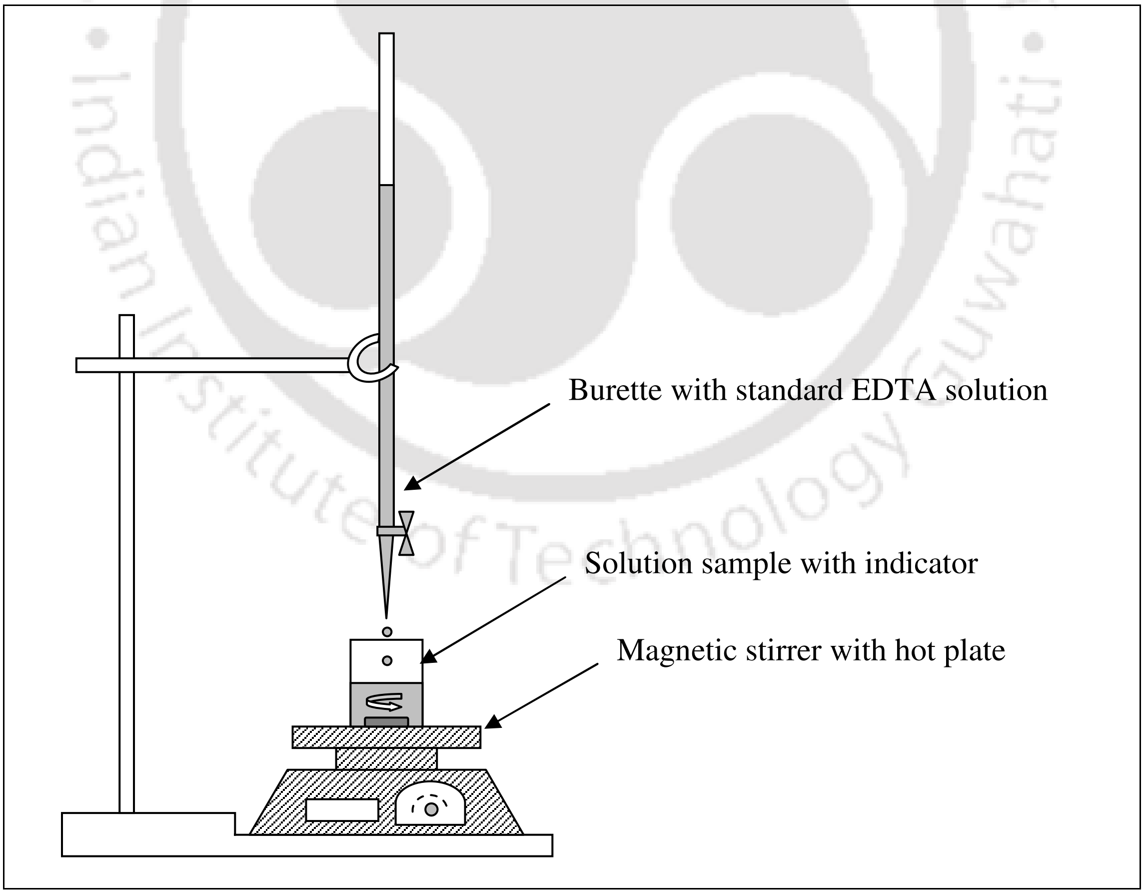

Figure 2.10: Typical setup for titration experiments.

The above procedure (steps i–vi) was repeated 3–4 times for accuracy. From the volume (V_2) of standard (N_2) EDTA solution run down during the titrations, the concentration (N_1) of Ni^{+2} in the plating bath can be evaluated using the following expression (Eq. (2.14)).

$$N_1 \times V_1 = N_2 \times V_2 \tag{2.14}$$

where, (V_1) is the volume of bath sample taken for analysis (5 ml).

2.3.3 Permeation analysis of composite membrane

The average pore diameter of the composite membrane (d_o) and the effective porosity of the deposited metal layer ($(\varepsilon/q^2)_{film}$) were evaluated from the air permeation experiments using the following procedure.

a) For the metal–ceramic composite membrane, the air permeation data is represented as follows.

$$K = A\overline{P} + B \tag{2.15}$$

Here, A and B are related as follows

$$A = 0.4\left(\frac{d_o^{\,2}}{\eta_g \delta}\right)\left(\frac{\varepsilon}{q^2}\right)_{film} \tag{2.16}$$

$$B = 1.066\left(\frac{d_o v}{\delta}\right)\left(\frac{\varepsilon}{q^2}\right)_{film} \tag{2.17}$$

The effective permeability factor (K) can be evaluated experimentally as

$$K = \frac{QP_2}{S\Delta P} \tag{2.18}$$

b) The average pore diameter of the metal–ceramic composite membrane is evaluated using the expression:

$$d_o = 2.666\frac{A}{B}v\eta_g \tag{2.19}$$

c) The effective porosity of the metal–ceramic composite membrane is evaluated using the expression

$$\left(\frac{\varepsilon}{q^2}\right)_{film} = \frac{B\delta}{1.066 d_o v} \tag{2.20}$$

Metal layer thickness (δ) itself is a function of the effective film porosity ($(\varepsilon/q^2)_{film}$). Substituting for δ (Eq. (2.12)) in the above expression (Eq. (2.20)), we get the following expression for effective porosity.

$$\left(\frac{\varepsilon}{q^2}\right)_{film} = \frac{1}{2}\left(1 - \sqrt{1 - \frac{4B(w_2 - w_1)}{1.066 d_o v \rho_{Ni} A_m}}\right) \tag{2.21}$$

2.3.4 Kinetic studies

A model was developed assuming that the nickel deposition during electroless plating is strongly governed by mass transfer limitations. The plating rate is therefore represented as a function of the average mass transfer coefficient ($\bar{k}$) and the available average driving force $(\bar{C}_B - \bar{C}_S)$:

$$\bar{r}_{\text{model}} = \bar{k}(\bar{C}_B - \bar{C}_S) \tag{2.22}$$

where $\bar{r}_{\text{model}}$ is the average reaction rate, $\bar{C}_B$ is the average bulk concentration of nickel ions in the plating bath and $\bar{C}_S$ is the average nickel ions concentration at the liquid–substrate interface. Subsequently, $\bar{C}_S$ is defined as:

$$\bar{C}_s = \frac{\bar{C}_M}{\bar{\gamma}} \tag{2.23}$$

where $\bar{\gamma}$ is the partition coefficient and $\bar{C}_M$ is the average metallic nickel concentration on the substrate and is evaluated using the following expression.

$$\bar{C}_M = \frac{w_2 - w_1}{M_{Ni} \times A_m \delta} \tag{2.24}$$

The parameters $\bar{k}$ and $\bar{\gamma}$ in the above equations are determined by solving the following non-linear regression model as an optimization problem using generalized reduced gradient (GRG) method:

$$\text{Minimize: } \sum\left(\frac{\bar{r}_{\text{e}}-\bar{r}_{\text{model}}}{\bar{r}_{\text{e}}}\right)^2 \qquad (2.25)$$

such that $\bar{k}, \bar{\gamma} \geq 0$

Here, $\bar{r}_{\text{e}}$ is the average deposition rate during the plating time t obtained experimentally using the following expression (Eq. (2.26)).

$$\bar{r}_{\text{e}} = \frac{C_i - C_f}{t} \times \eta \qquad (2.26)$$

2.4 Summary

An important objective of this work is to obtain a comparative technical overview of electroless plating baths assisted with various mass transfer enhancements. Since literature is dovetailed towards the performance characteristics of Pd membranes, the achievement of a dense membrane using laboratory fabricated membrane supports that have wider pore size distribution is regarded as a formidable challenge. A laboratory support with a nominal pore size of 200–300 nm is first targeted be adopting trial and error fabrication method procedures. This is also due to the fact that Collins and Way [98] reported upon the requirement of 8 sequential one-hour electroless plating steps using a stainless steel membrane support of 500 nm to achieve a dense Pd membrane. Therefore, the selection of (a) laboratory supports with an average pore size of 275 nm and (b) conceptualizing towards 8 one-hour sequential depositions in this work has relevance with the findings in the literature.

PERFORMANCE CHARACTERISTICS OF CONVENTIONAL ELECTROLESS PLATING BATHS

This chapter is divided into three sections. The first section presents the performance characteristics of conventional hypophosphite electroless plating baths and the second section presents the performance characteristics of hydrazine based electroless plating baths. The third section presents a brief summary and conclusions based on the results obtained for both hypophosphite and hydrazine baths.

3.1 Performance characteristics of hypophosphite baths

Sodium hypophosphite is the most commonly used reducing agent in electroless nickel deposition. It is generally used in the pH range of 7–10. The plating reactions are presented as follows (Eq. (3.1a–c)).

$$Ni^{+2} + H_2PO_2^- + H_2O \longrightarrow Ni + H_2PO_3^- + 2H^+ \qquad (3.1a)$$

$$H_2PO_2^- + H_2O \xrightarrow{\text{catalyst}} H_2PO_3^- + H_2 \qquad (3.1b)$$

Overall reaction can be obtained by adding the above two reactions as follows.

$$Ni^{+2} + 2H_2PO_2^- + 2H_2O \xrightarrow{\text{catalyst}} Ni + 2H_2PO_3^- + 2H^+ + H_2 \uparrow \qquad (3.1c)$$

The plating experiments were carried out using the typical setup shown in Figure 2.8a (Chapter 2) to evaluate the performance characteristics of conventional electroless plating baths. The results with respect to the hypophosphite baths are presented in four sub-sections. The first sub-section summarizes the characteristics of the electroless plating process in terms of conversion and plating efficiency. The second sub-section presents the characteristics of composite nickel–ceramic membrane in terms of average membrane pore size and percent pore densification. The third sub-section summarizes the cost tradeoffs with respect to PPD and average membrane thickness. Finally, the fourth sub-section presents the tradeoffs associated with plating efficiency and PPD.

3.1.1 Efficacy of electroless plating

Figures 3.1a and 3.1b summarize the variation of conversion and plating efficiency with nickel solution concentration and loading ratio (θ) respectively. As shown, nickel conversion in hypophosphite baths varied from 10–36%, 11–37% and 12–39% for a variation in nickel sulfate solution concentration of 0.04–0.16 mol/L and θ values of 196, 262 and 393 cm^2/L respectively. Corresponding plating efficiencies varied from 97–61.6%, 98–61.9% and 99.2–62.1% for a variation in nickel sulfate solution concentration of 0.04–0.16 mol/L and θ values of 196, 262 and 393 cm^2/L respectively. The plating efficiency trends indicate that the loading ratio did not influence the efficiency

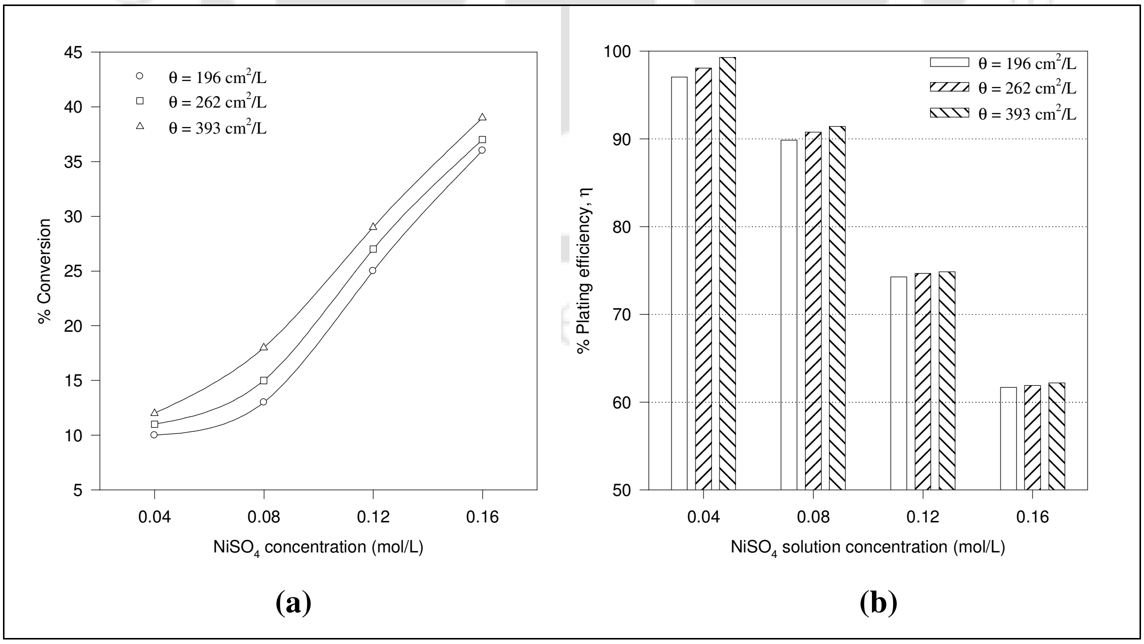

Figure 3.1: (a) Conversion and (b) efficiency profiles for conventional hypophosphite electroless plating baths.

significantly for a chosen nickel plating solution concentration. In summary, the plating characteristics are indicative of low conversions (10–40%) and variant efficiency profiles (97–60%) with respect to the solution concentration and loading ratio parameters.

Table 3.1 presents the variation of selective conversion values (defined as the product of fractional conversion and efficiency) with concentration and loading ratio. It was observed that the selective conversion values increased with increasing initial nickel solution concentration as well as loading ratio. However, the effect of loading ratio on the selective conversion is not as significant as the solution concentration.

Figure 3.2 presents the variation of nickel deposition rate (mol/L.s) with the electroless plating process parameters. It can be observed that the average efficient nickel plating rate varied from 1.08–9.86, 1.19–10.18 and 1.32–10.78 $\times 10^{-6}$ mol Ni/L.s with a variation in initial nickel solution concentration of 0.04–0.16 mol/L and loading ratio values of 196, 262 and 393 cm^2/L respectively. The deposition rate is found to increase nonlinearly with the solution concentration and loading ratio. However, the effect of loading ratio is insignificant in comparison with the solution concentration.

Model parameters evaluated using the equations described in section 2.3.4 (Chapter 2) are summarized in Table 3.2. The average mass-transfer coefficient ($\bar{k}$) varied from 37.0–98.8, 41.4–105.2 and 46.2–136.8 s^{-1} with a variation in initial nickel solution

Table 3.1: Selective conversion data for conventional hypophosphite baths.

Initial $NiSO_4$ concentration (mol/L)	**Selective conversion** (%) **for various θ** (cm^2/L)		
	196	262	393
0.04	9.70	10.79	11.91
0.08	11.68	13.61	16.46
0.12	18.57	20.16	21.71
0.16	22.20	22.91	24.25

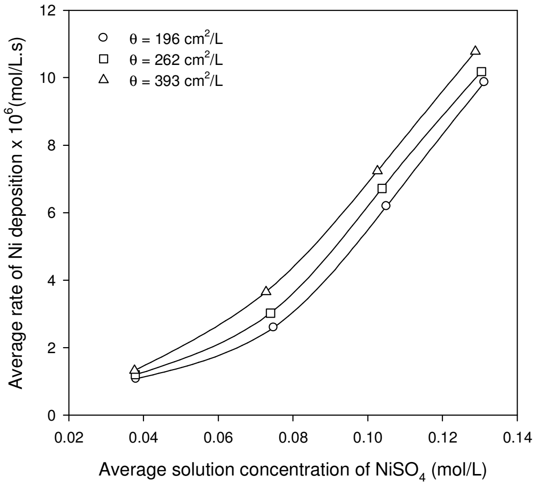

Figure 3.2: Average nickel deposition rate for conventional hypophosphite baths.

concentration from 0.04–0.16 mol/L for the loading ratios of 196, 262 and 393 cm^2/L respectively. It is observed that the average mass-transfer coefficient ($\bar{k}$) increases significantly with increasing the metal-ion concentration in the plating solution which indicates that the transfer of reacting species to the substrate surface is favored at higher concentrations. However, corresponding increase in the average mass-transfer coefficient

Table 3.2: Model parameters for conventional hypophosphite baths.

θ (cm^2/L)	$\bar{C}_B$ (mol/L)	$\bar{k}$ (s^{-1})	$\bar{\gamma}$	**% Error** ×10^5
196	0.038	37.0	999.3	5.34
196	0.075	41.3	999.6	5.31
196	0.105	86.9	1000.4	3.10
196	0.131	98.8	1000.6	2.91
262	0.038	41.4	999.6	5.33
262	0.074	54.0	999.8	6.06
262	0.104	92.3	1000.5	3.34
262	0.130	105.2	1000.8	1.20
393	0.038	46.2	999.6	5.04
393	0.073	68.9	999.8	6.14
393	0.103	96.4	1001.3	3.77
393	0.129	136.8	1005.5	3.35

($\bar{k}$) with the loading ratio is not much significant. For all the cases, the partition coefficient ($\bar{\gamma}$) value is around 1000 and it varied a minimum (<1%), indicating that it is relatively independent of both parameters namely concentration and loading ratio. In other words, it can be concluded that the average mass transfer coefficient is strongly influenced by nickel concentration as well as loading ratio. Nonetheless, the obtained kinetic model parameters could be used for the scale-up and design studies associated with the large scale manufacture of metal–ceramic membranes in the near future.

3.1.2 Surface characterization

Figure 3.3 presents the surface SEM micrographs for all 12 membranes fabricated using various combinations of nickel solution concentration (0.04–0.16 mol/L) and loading ratio (196–393 cm^2/L). The micrographs are reported at different magnifications so as to aid analyzing the micrographs, as membranes with insignificant nickel film thickness are produced at low nickel solution concentration and high loading ratio value and membranes with substantial nickel film thickness yield at high nickel solution concentration and low loading values. It is observed that the presence of nickel metal grains is more prevalent in those cases where the deposited nickel layer thickness is more than 10 microns. A critical observation of the SEM images indicates that the membranes could be defect free. A further confirmation of the defect-freeness of the membranes is ensured using air permeation experiments.

To further confirm the presence of nickel on the membrane surface, the surfaces of the composite membranes were subjected to X-ray diffraction (XRD) study. Figure 3.4 presents the XRD pattern of the metal film deposited for good plating conditions (nickel concentration of 0.08 mol/L and loading ratio of 393 cm^2/L) which matches very closely with relevant peaks associated to quartz and nickel. Similar XRD patterns are observed

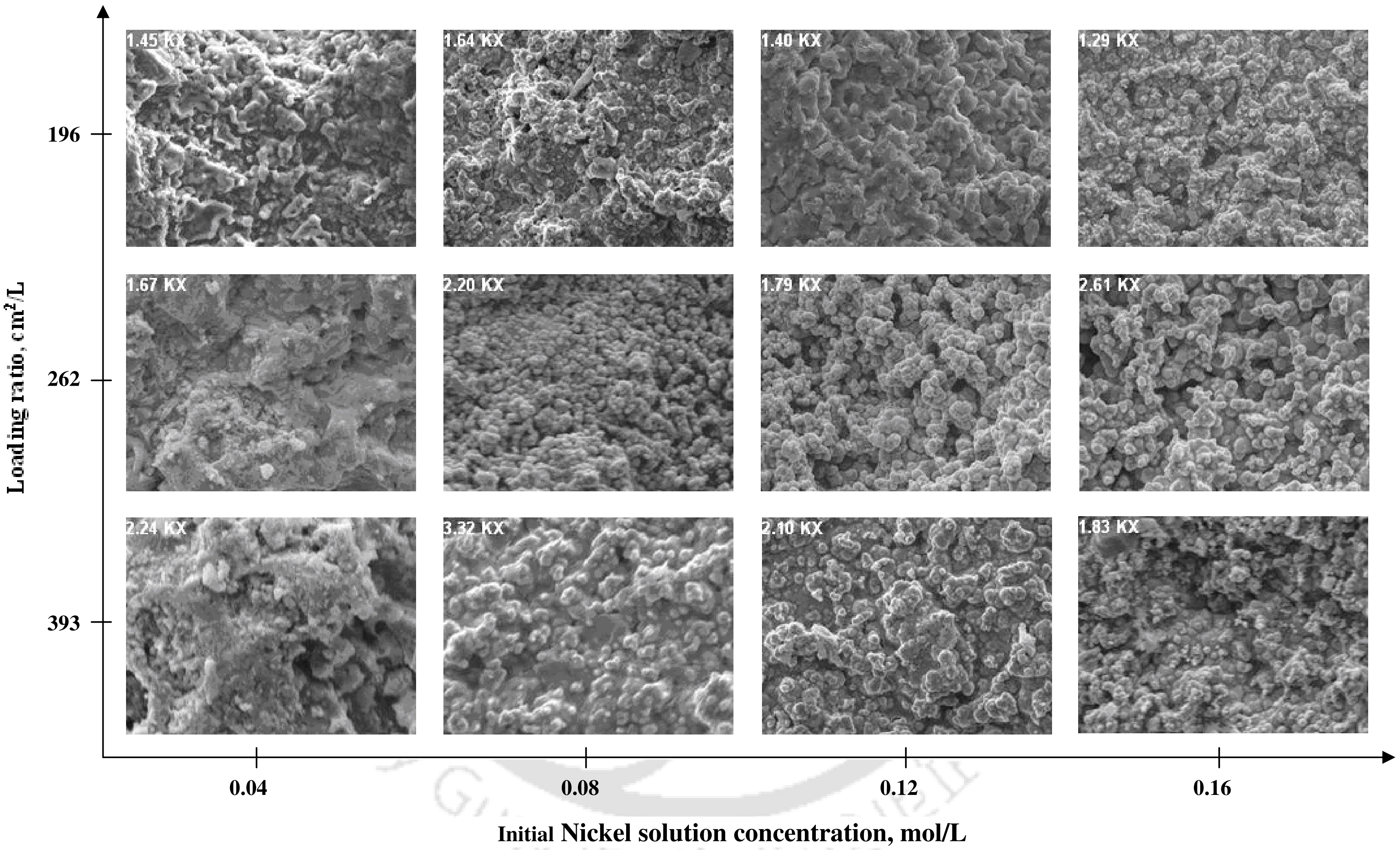

Figure 3.3: Surface SEM micrographs of the composite membranes fabricated in conventional hypophosphite baths.

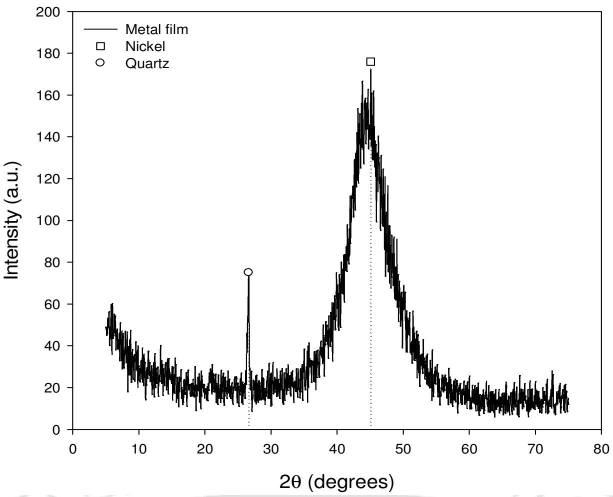

Figure 3.4: XRD pattern of metal film deposited in conventional hypophosphite baths.

for the other membranes as well. The nature of the spectra indicates that the nickel films deposited using hypophosphite electroless plating baths is amorphous. The presence of quartz (a constituent of the ceramic support) could be an indication of the porous nature of the composite membranes which is further confirmed by the air permeation experiments presented in the next section.

3.1.3 Permeation characteristics of composite membrane

The average pore size of the composite membranes is evaluated using gas permeation experiments. Figure 3.5 presents the variation of average pore diameter and porosity of the nickel–ceramic composite membranes with plating process parameters. It is observed that the average pore diameter (Figure 3.5a) of the membranes did not vary significantly with plating parameters and only varied between 128–89 nm, which corresponds to a variation in PPD values from 78.3–89.5% (Table 3.3). In other words, varying electroless process parameters does not contribute to substantial densification of the membrane. These results are in good agreement with the results presented by Changrong et al. [91] who reported the fabrication of nickel–ceramic composite

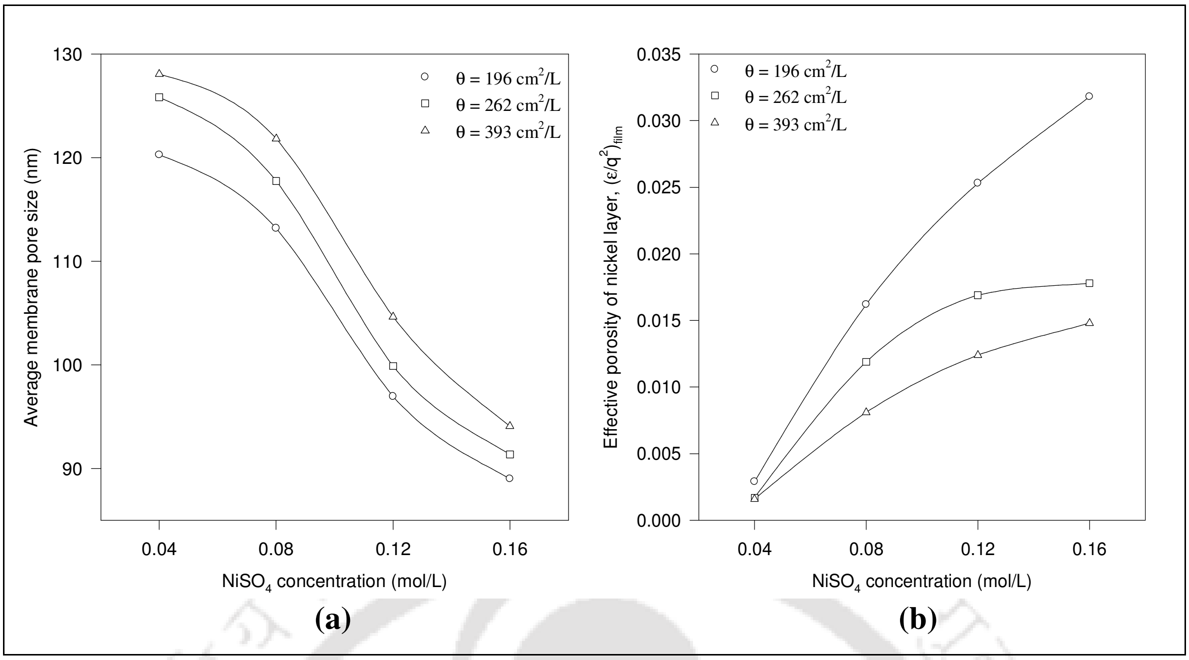

Figure 3.5: (a) Average pore size and (b) porosity profiles for conventional hypophosphite electroless plating baths.

membranes using sodium hypophosphite based plating baths. The authors found that for a support with 900 nm and a plating time variation of 15–100 min, the film thickness varied between 2.2–4.5 µm with an average pore size variation from 170–140 nm. Effective porosity (Figure 3.5b) of the deposited nickel layer increased with increasing the solution concentration but a reduction in porosity values with increasing the loading ratio is observed. Table 3.3 presents the variation of percent pore densification (PPD) with solution concentration and loading ratio. From this table it can be observed that the PPD increased with increasing the metal concentration in the solution indicating that a higher concentration favors the PPD as a result of faster deposition of the metal on the membrane surface at higher concentrations. On the other hand, PPD reduced to a small extent by increasing the bath loading ratio but this variation is insignificant when compared to the effect of metal ion concentration in the solution.

Table 3.3: Pore densification data for conventional hypophosphite baths.

Initial $NiSO_4$ concentration (mol/L)	**PPD** (%) **for various θ** (cm^2/L)		
	196	262	393
0.04	80.87	79.06	78.31
0.08	83.06	81.66	80.37
0.12	87.57	86.81	85.52
0.16	89.53	88.96	88.30

The average metal film thickness was evaluated with the weight gain method (Eq. (2.12)). Figure 3.6 presents the variation of average metal film thickness with electroless plating process parameters. It can be observed that the average nickel metal film varied from 2.58–23.67, 2.15–18.32 and 1.59–12.93 µm for a variation in initial nickel metal solution concentration of 0.04–0.16 mol/L and loading ratio values of 196, 262 and 393 cm^2/L respectively. It is generally observed that higher metal film thickness is obtained for higher values of nickel solution concentration and low loading values.

Figure 3.7 presents the cross-sectional SEM images of the nickel–ceramic composite membranes for a loading ratio of 196 cm^2/L. These micrographs (Figures 3.7a–d) correspond to the evaluated average film thicknesses of 2.6, 6.2, 14.8 and 23.7 µm

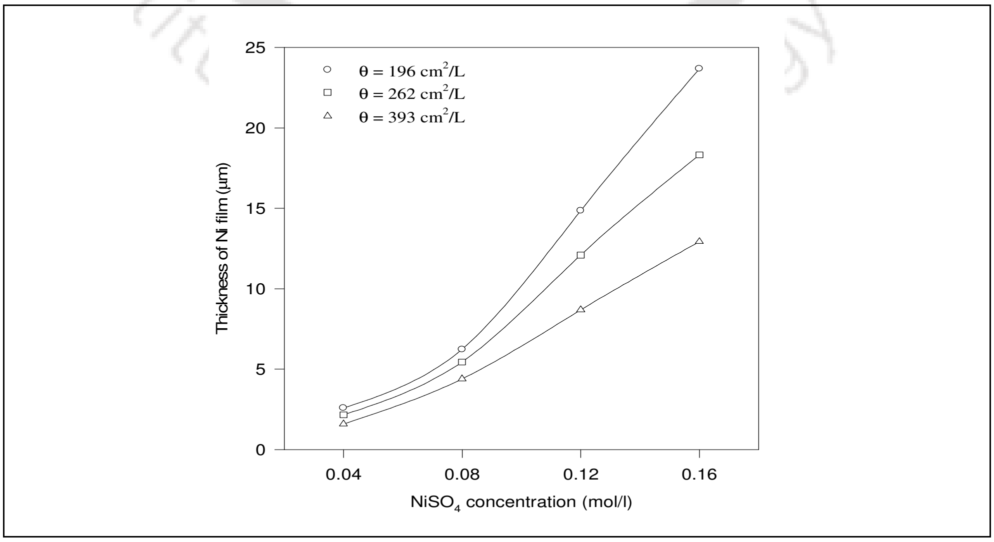

Figure 3.6: Film thickness profiles for conventional hypophosphite baths.

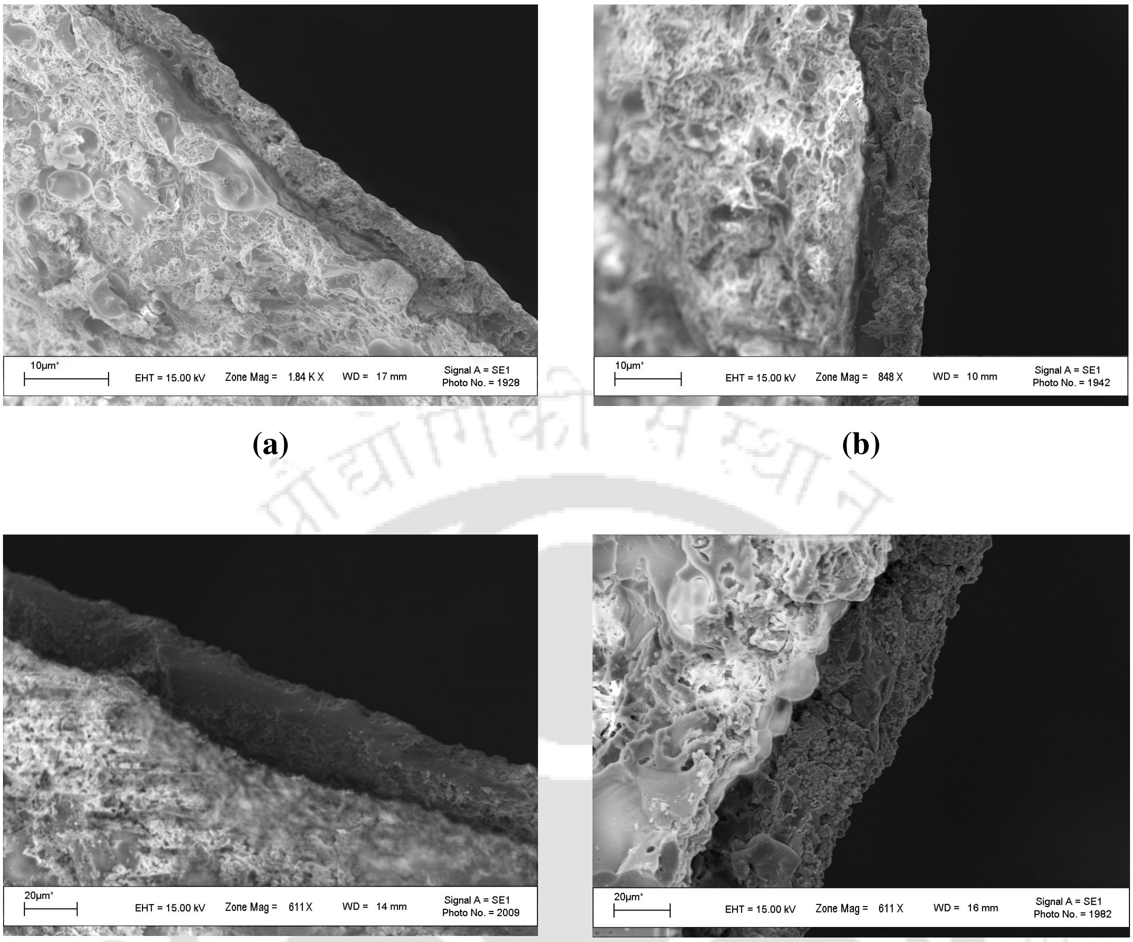

(a) **(b)** **(c)** **(d)**

Figure 3.7: Cross-sectional SEM images of composite membranes fabricated in conventional hypophosphite baths ($\theta = 196\ \text{cm}^2/\text{L}$).
(a) 0.04 mol/L; (b) 0.08 mol/L; (c) 0.12 mol/L; (d) 0.16 mol/L.

respectively. Similar micrographs are obtained for the other membranes also. Estimation of nickel layer thickness from cross-sectional SEM micrographs is erroneous especially at higher magnification when the layer thickness is too low (figure 3.7a). A deviation of about ±2 µm from the evaluated average nickel layer thickness was observed at some locations in the cross-sectional SEM image. This may be due to the fact that the surface of the porous substrate is uneven. In addition, SEM image couldn't represent the overall membrane characteristics since a very small area can be scanned by this method.

3.1.4 Cost tradeoffs

Since the objective of electroless plating in this work is to evaluate the plating as well as membrane characteristics, the cost tradeoffs associated to electroless plating need to account for the satisfaction of both thickness (δ) and densification (PPD) constraints. This is due to the fact that a mere densification of the support surface does not accomplish the desired attributes for its functional application as a critical minimum thickness is always desired for several reasons such as mechanical strength, resistance to temperature cycling etc. Therefore, the cost tradeoffs shall aim to explore the existence of combinatorial dependence of cost on both PPD and metal thickness on the membrane. It is further interesting to note that the associated tradeoffs assume paramount significance for noble metals due to their high cost. Figure 3.8 summarizes the variation in the chemicals cost (evaluated using retail costs of the bath constituents summarized in Table 2.3) and metal film thickness with PPD. It is observed that a non-linear dependence of cost and thickness on PPD is existent indicating complex associated trade-offs. The figure indicates

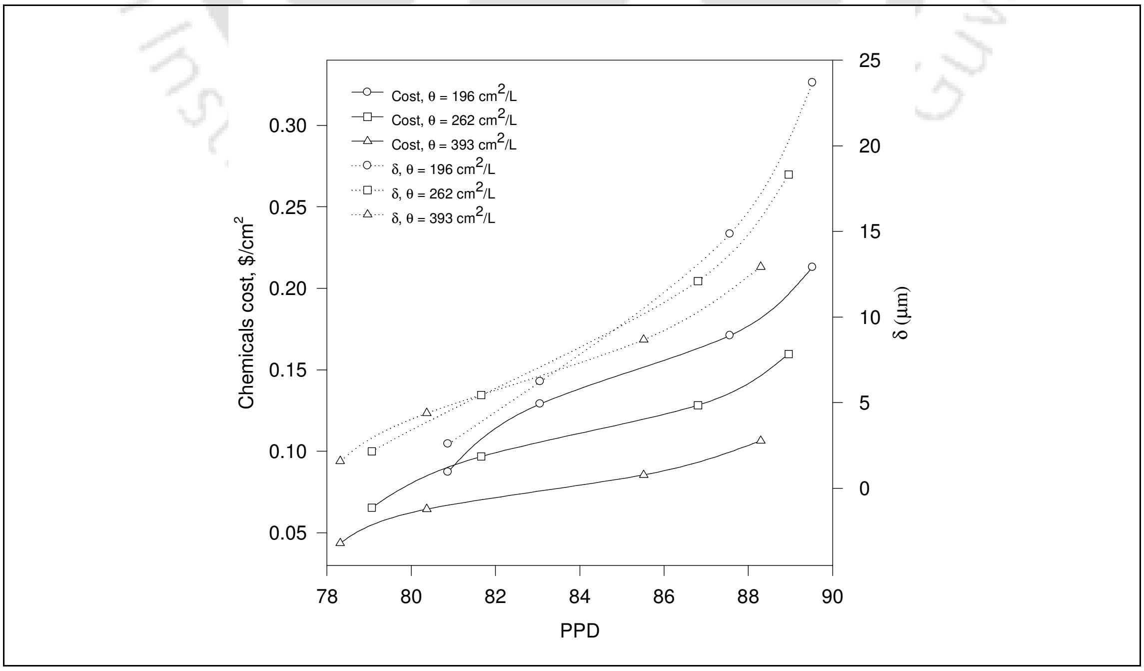

Figure 3.8: Cost tradeoffs for conventional hypophosphite baths.

that the chemicals cost varied between 0.04–0.21 \$/cm^2 for a variation in PPD from 78–89% and film thickness from 1.5–24 microns. Thereby, the cost-tradeoffs are anticipated to be useful for the rigorous design and scale-up purposes. Similar cost trade-off profiles are expected for noble metal electroless deposition targeting dense composite membrane fabrication.

3.1.5 PPD and efficiency tradeoffs

To determine the optimal concentration of nickel that provides the best combination of plating efficiency (η) and the percent pore densification (PPD), an objective function (f) is defined as follows.

$$f = f_1(\eta) + f_2(\mathrm{PPD}) \tag{3.2}$$

$$f_1 + f_2 = 1 \ \text{ and } \ 0 \le f_1, f_2 \le 1 \tag{3.3}$$

where f_1 and f_2 are the weight factors corresponding to the plating efficiency (η) and PPD respectively which depend on their relative preference. Figure 3.9 summarizes the variation of the objective function for the best value of loading ratio (θ = 393 cm^2/L).

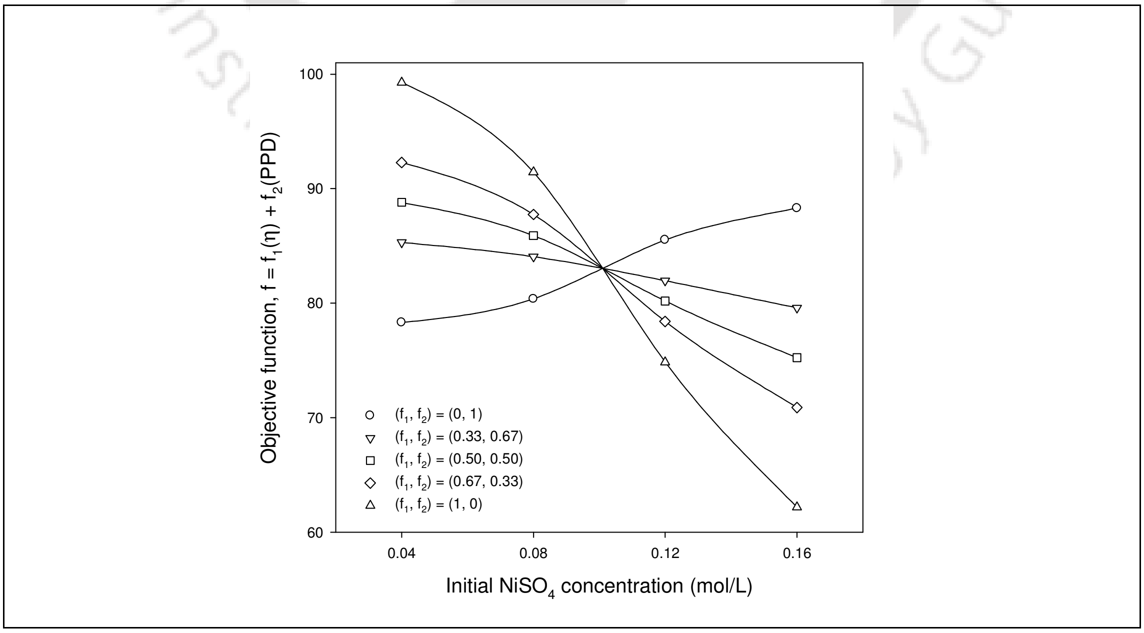

Figure 3.9: PPD and efficiency tradeoffs for conventional hypophosphite baths.

From Figure 3.9, it is evident that the plating efficiency (η) which minimizes the metal loss during the electroless plating is favored by a lower initial concentration of nickel while the pore densification (PPD) which improves the separation performance of the plated membrane is favored by a higher concentration. An initial nickel concentration of 0.04 mol/L is found to be optimal for all the cases excepting $f_1 = 0$.

3.1.6 Summary

This work addresses the preparation of nickel–ceramic composite membranes using electroless plating technique from the process perspective. An inexpensive laboratory fabricated ceramic membrane support with a nominal pore size of 275 nm was used in the experimental study. It is observed that though dense membrane is not accomplished various inherent relationships between process parameters and plating/membrane characteristics are unveiled. Firstly, sodium hypophosphite based nickel baths are not efficient as they resulted in lower conversions (10–40%). Secondly, it is observed that the loading ratio does not contribute to a significant variation in process efficiency. Thirdly, higher solution concentrations provide lower process efficiencies that amount to significant metal deposition in the solution and on the surfaces other than the substrate. Fourthly, the optimal concentration of $NiSO_4$ in hypophosphite baths for electroless plating is evaluated to be 0.08 mol/L, as this concentration resulted in a good combination of plating efficiency and PPD. Finally, complex non-linear tradeoffs with respect to cost, percent pore densification and metal thickness are evaluated. In the near future, the evaluated inherent relationships between various parameters need to be also judged for the case of dense membrane fabrication so as to provide a general guideline upon the process parameters for noble/regular metal–ceramic composite membranes. In addition, simple process modifications that target higher combinations of conversion, plating efficiency and percent pore densification (PPD) as well need to be investigated. A

PPD value of about 78 to 89% along with the experimental inference of porous membranes presumably indicates that the utilization of supports with lower surface pore sizes (as those obtained using γ-alumina) could yield a dense nickel–ceramic composite membrane in about 4–5 sequential electroless plating steps.

3.2 Performance characteristics of hydrazine baths

Hydrazine is a powerful reducing agent in aqueous alkaline solutions. Nickel deposition by hydrazine can be represented by the following equations (Eq. 3.4 a–c).

$$Ni^{+2} + 2OH^{-} \longrightarrow Ni(OH)_2 \qquad (3.4a)$$

$$2Ni(OH)_2 + N_2H_4 \xrightarrow{\text{catalyst}} 2Ni + 4H_2O + N_2 \uparrow \qquad (3.4b)$$

Now the overall reaction is given by,

$$2Ni^{+2} + N_2H_4 + 4OH^{-} \xrightarrow{\text{catalyst}} 2Ni + 4H_2O + N_2 \uparrow \qquad (3.4c)$$

The plating experiments were carried out using the typical setup shown in Figure 2.8a (Chapter 2) to evaluated the performance characteristics of conventional electroless plating baths using hydrazine as the reducing agent. In this section the results are presented in three sub-sections. The first sub-section summarizes the characteristics of the electroless plating process in terms of conversion and plating efficiency. The second sub-section presents the characteristics of nickel–ceramic composite membrane in terms of average membrane pore size and percent pore densification. Finally, the third sub-section presents associated cost tradeoffs with respect to PPD and average membrane thickness.

3.2.1 Efficacy of electroless plating

Figure 3.10 summarizes the variation of conversion and plating efficiency with nickel solution concentration and loading ratio (θ). As shown, nickel conversion varied from 14.5–46.8%, 16–49.8% and 17.5–54% for a variation in nickel solution concentration of 0.04–0.16 mol/L and θ values of 196, 262 and 393 cm^2/L respectively. Corresponding plating efficiencies varied from 97.2–82.0%, 98.3–82.3% and 99.9–82.6% for a variation in nickel solution concentration of 0.04–0.16 mol/L and θ values of 196, 262 and 393 cm^2/L respectively.

The plating efficiency trends indicate that the loading ratio does not influence the efficiency significantly for a chosen nickel plating solution concentration. In summary, the plating characteristics are indicative of a low to moderate conversion (14.5–54%) and good efficiency profiles (99.9–82.0%) with variation in solution concentration and loading ratio parameters. The selective conversion values (defined as the product of fractional conversion and efficiency) presented in Table 3.4 increased with increasing the solution concentration as well as loading ratio.

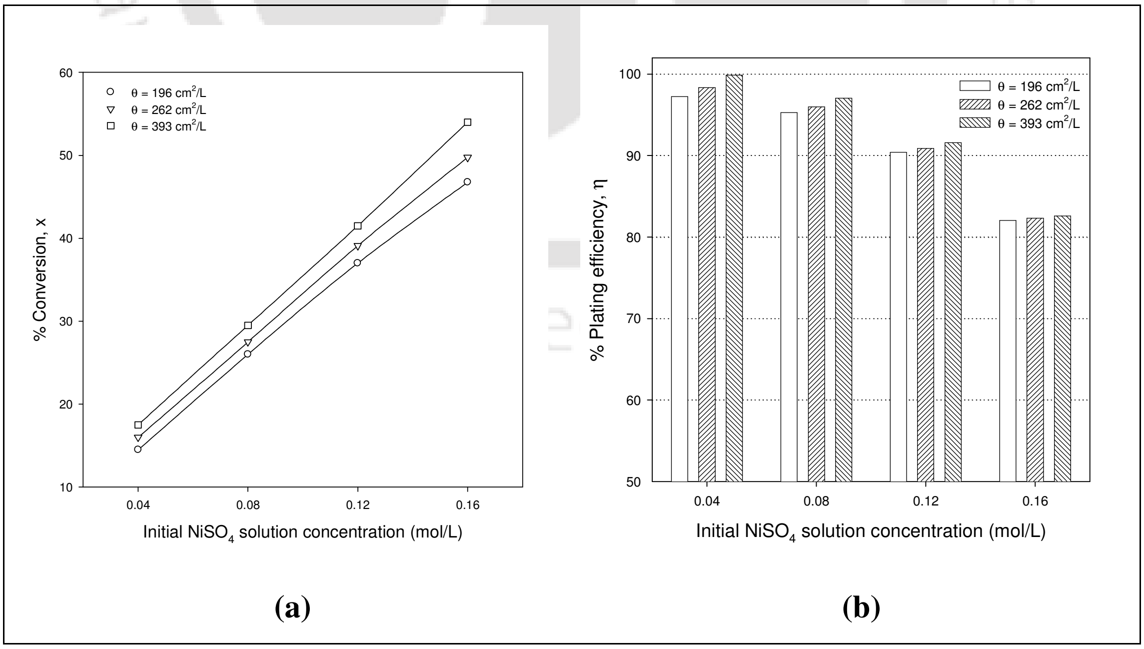

(a) **(b)**

Figure 3.10: (a) Conversion and (b) efficiency profiles for conventional hydrazine electroless plating baths.

Table 3.4: Selective conversion data for conventional hydrazine baths.

Initial $NiSO_4$ concentration (mol/L)	**Selective conversion** (%) **for various θ** (cm^2/L)		
	196	262	393
0.04	14.10	15.73	17.48
0.08	24.77	26.39	28.63
0.12	33.45	35.54	38.01
0.16	38.35	40.94	44.60

Figure 3.11 presents the variation of average efficient nickel plating rate (mol/L.s) with the electroless plating process parameters. It can be observed that the average deposition rate of nickel varied from 1.57–17.05, 1.75–18.20 and 1.94–19.82 $\times 10^{-6}$ mol/L.s with a variation in initial nickel solution concentration from 0.04–0.16 mol/L for the loading ratio (θ) values of 196, 262 and 393 cm^2/L respectively. The average nickel deposition rate increases with increasing the solution concentration. The effect of loading ratio on the deposition rate is found to be insignificant compared to solution concentration especially at lower concentrations.

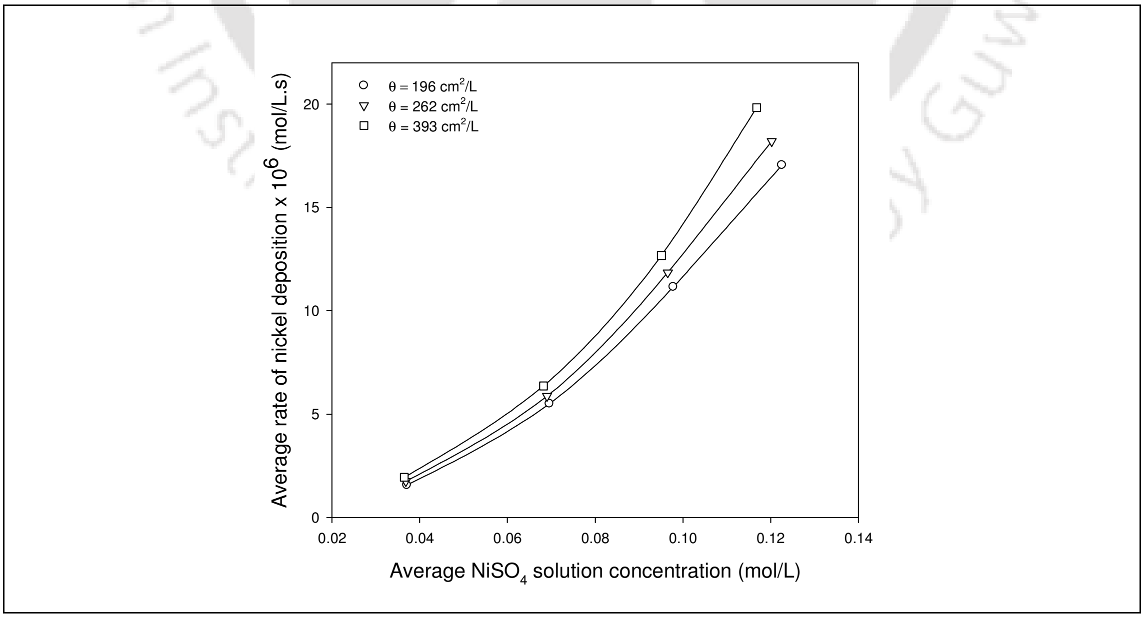

Figure 3.11: Average nickel deposition rate for conventional hydrazine electroless plating baths.

Model parameters evaluated using the equations described in section 2.3.4 (Chapter 2) are summarized in Table 3.5. The average mass-transfer coefficient ($\bar{k}$) varied from 67.2–343.4, 67.7–369.9 and 83.6–487.0 s^{-1} with a variation in initial nickel solution concentration from 0.04–0.16 mol/L for the loading ratios of 196, 262 and 393 cm^2/L respectively. These values are much higher than those of the hypophosphite baths presented in Table 3.2 especially at higher concentrations. It is observed that the average mass-transfer coefficient ($\bar{k}$) increased significantly with increasing initial solution concentration of $NiSO_4$. However, corresponding increase in the average mass-transfer coefficient ($\bar{k}$) with the loading ratio is not much significant. For all the cases, the partition coefficient ($\bar{\gamma}$) value is around 1000 and it varied a minimum (<6%), indicating that it is relatively independent of both the parameters namely concentration and loading ratio. In other words, it can be concluded that the average mass transfer coefficient is strongly influenced by nickel concentration as well as loading ratio.

Table 3.5: Model parameters for conventional hydrazine baths.

θ (cm^2/L)	$\bar{C}_B$ (mol/L)	$\bar{k}$ (s^{-1})	$\bar{\gamma}$	% Error ×10^5
196	0.037	67.2	984.4	5.17
196	0.070	117.5	990.2	4.68
196	0.098	293.8	1024.2	6.17
196	0.123	343.4	1042.3	5.64
262	0.037	67.7	994.2	1.99
262	0.069	160.3	994.2	1.68
262	0.097	294.0	1028.4	4.47
262	0.120	369.9	1061.5	5.20
393	0.037	83.6	998.0	5.01
393	0.068	178.3	994.4	6.51
393	0.095	295.0	1035.0	4.91
393	0.117	487.0	1066.8	6.11

3.2.2 Surface characterization

Figure 3.12 presents surface SEM micrographs (magnification: 1KX) of all the membranes fabricated using various combinations of nickel solution concentration (0.04–0.16 mol/L) and loading ratio (196–393 cm^2/L). Membranes with insignificant nickel film thickness are produced at lower nickel solution concentration and higher loading ratio and membranes with substantial nickel film thickness are yielded at higher nickel solution concentrations and low loading values. It is further observed that the presence of nickel metal grains is more prevalent in those cases where the nickel metal film thickness is more than 10 microns. A critical observation of the SEM images indicates that the membranes could be defect free. A further confirmation of the defect freeness of the membranes is ensured using air permeation experiments.

To confirm that the membrane fabrication is crystalline, the surfaces of the composite membranes were subjected to X-ray diffraction (XRD) study. Figure 3.13 presents the XRD pattern of the metal film deposited for good plating conditions (nickel concentration of 0.12 mol/L and loading ratio of 393 cm^2/L) which matches very closely with the relevant peaks associated to nickel (JCPDS: 00–001–1260 (D)). Sharp peaks further confirm that the metal film was crystalline. Similar XRD patterns were observed for the other membranes.

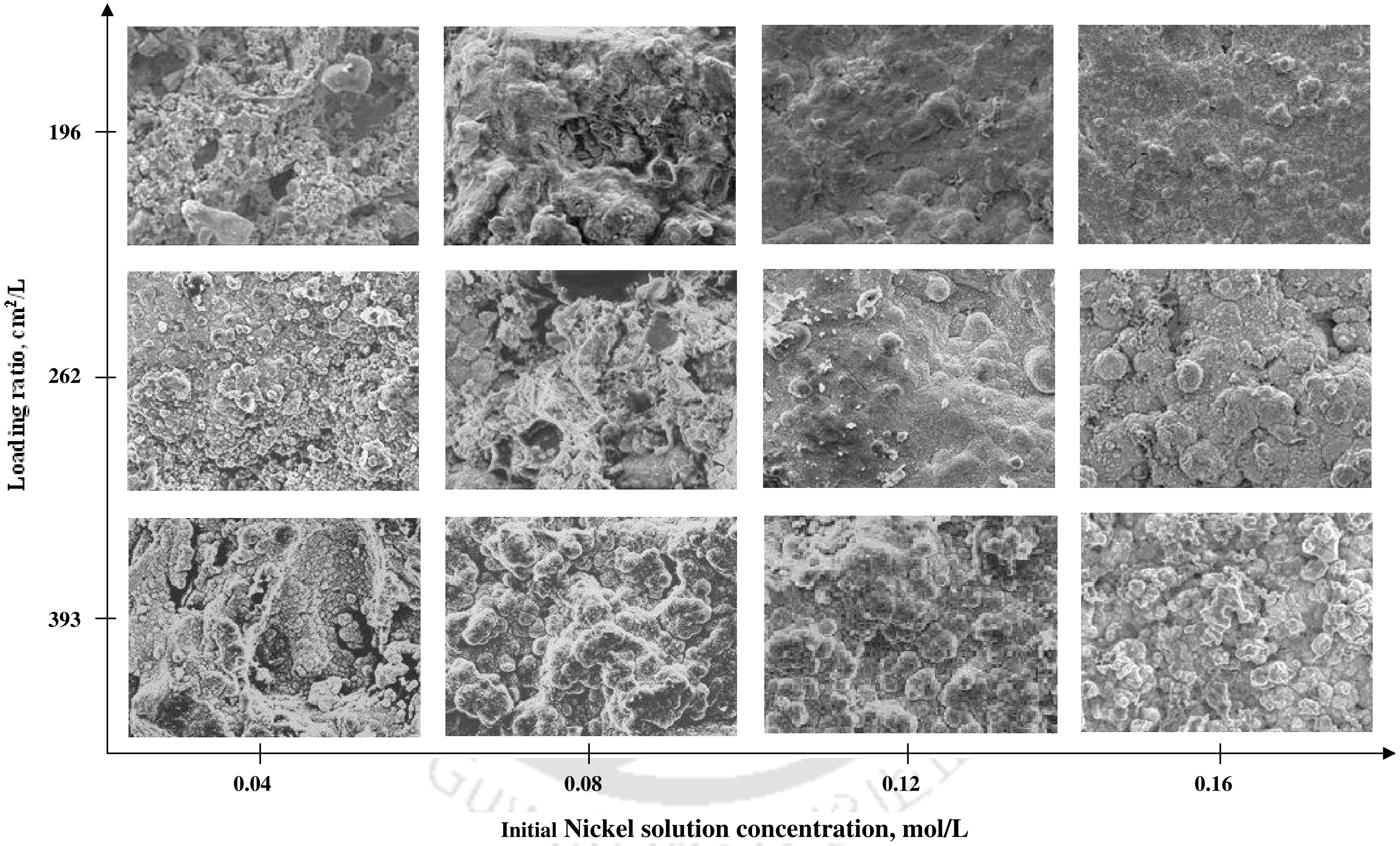

Figure 3.12: Surface SEM micrographs of the composite membranes fabricated in conventional hydrazine baths.

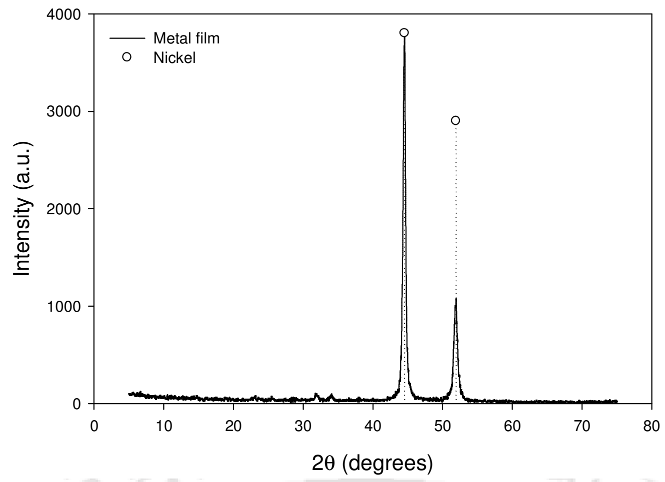

Figure 3.13: XRD pattern of metal film deposited in conventional hydrazine baths.

3.2.3 Permeation characteristics of composite membrane

To further assess the quality of nickel plating on the membrane surface, the average pore size and porosity of the membrane were evaluated using gas permeation experiments. Figure 3.14a presents the variation of composite membrane average pore diameter and Figure 3.14b presents the variation of effective porosity of the deposited nickel layer with plating process parameters. It is observed that the average pore diameter

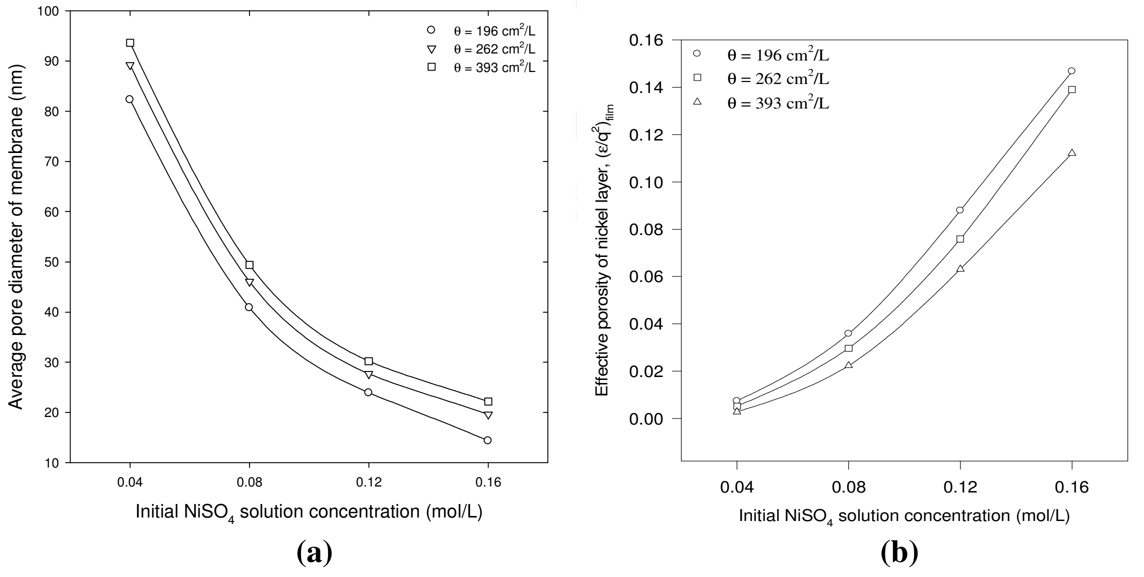

(a) **(b)**

Figure 3.14: (a) Pore size and (b) porosity profiles for conventional hydrazine baths.

of the membrane (Figure 3.14a) varied significantly from plating process parameters between 94–14 nm, which corresponds to a variation in PPD values from 88.4 to 99.7% (Table 3.6). Obtaining near 100% values for PPD is encouraging for the used precursor concentration, plating temperature, pH and membrane morphology. In summary, varying electroless process parameters significantly contributes to substantial densification of the membrane. Obtaining a PPD value of 99.7% thereby indicates that choosing a proper support whose top layer pore size is lower than 10 nm does in turn enable the fabrication of dense metal–ceramic composite membrane.

Based on experimental observations, it can be inferred that the performance characteristics of the electroless plating baths are significantly affected by the solution concentration than the loading ratio. For instance, when the loading ratio value is doubled for a nickel solution concentration of 0.08 mol/L, a marginal variation in the values of PPD, conversion and efficiency is observed. However, when the initial nickel solution concentration is doubled from 0.08 to 0.16 mol/L for a fixed loading ratio value of 393 cm^2/L, the bath conversion enhanced significantly from 29.5 to 54.5%, plating efficiency reduced from 97.6 to 82.7% and PPD increased from 96.8 to 99.3%.

The average metal film thickness was evaluated by the weight gain method (Eq. (2.12)). Figure 3.15 presents the variation of average metal film thickness with electroless plating process parameters. It can be observed that the average nickel metal film varied

Table 3.6: Pore densification data for conventional hydrazine baths.

Initial $NiSO_4$ concentration (mol/L)	**PPD** (%) **for various θ** (cm^2/L)		
	196	262	393
0.04	91.05	89.48	88.42
0.08	97.79	97.20	96.78
0.12	99.24	98.99	98.79
0.16	99.73	99.49	99.35

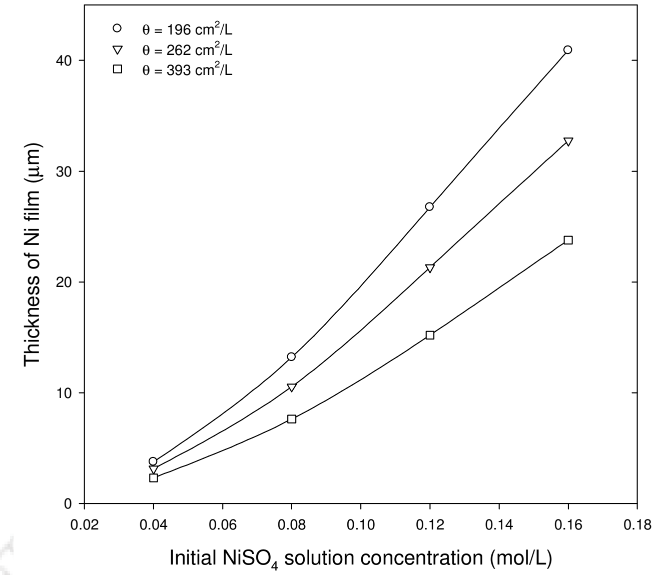

Figure 3.15: Film thickness profiles for conventional hydrazine baths.

from 3.76–40.9, 3.14–32.8 and 2.33–23.7 µm for a variation in initial nickel metal solution concentration of 0.04–0.16 mol/L for the loading ratio values of 196, 262 and 393 cm^2/L respectively. It is generally observed that higher solution concentrations and lower loading values result in thicker metal films.

These results are in good agreement with the results presented by Haag et al. [93] who deposited nickel on a γ-alumina layer using hydrazine based plating bath. They found that for a support with an average pore size of 4.7 nm and a plating time of 3 h, the film thickness varied between 1–1.5 µm for a solution concentration of 0.004–0.2 mol/L.

Figure 3.16 presents the cross-sectional SEM images of the nickel–ceramic composite membranes for a loading ratio of 393 cm^2/L. These micrographs (Figures 3.16a–d) correspond to the evaluated average film thicknesses of 2.3, 7.6, 15.2 and 23.8 µm respectively. Similar micrographs are obtained for the other membranes also. Estimation of nickel layer thickness from cross-sectional SEM micrographs is erroneous

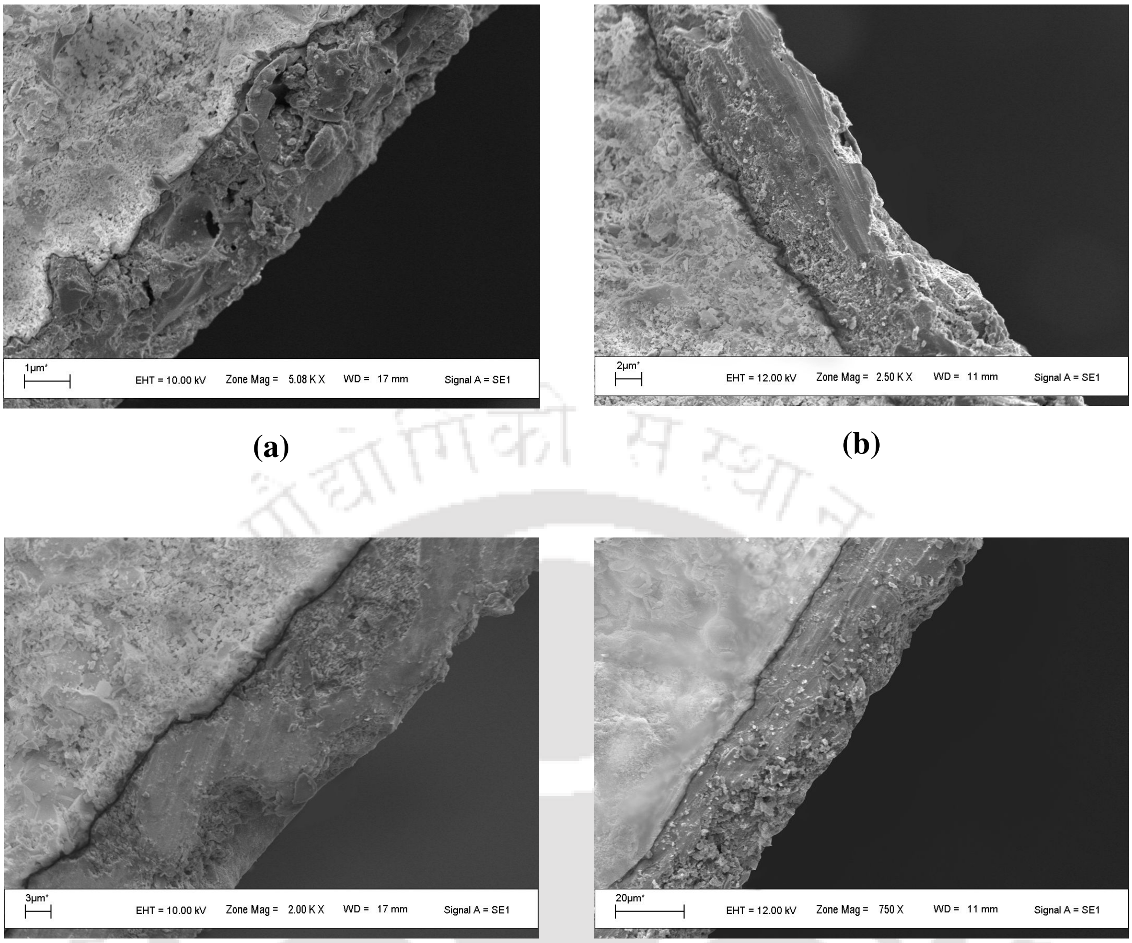

(a) **(b)**

(c) **(d)**

Figure 3.16: Cross-sectional SEM images of composite membranes fabricated in conventional hydrazine baths ($\theta = 393\ cm^2/L$). (a) 0.04 mol/L; (b) 0.08 mol/L; (c) 0.12 mol/L; (d) 0.16 mol/L.

especially at higher magnification when the layer thickness is too low (figure 3.16a). This may be due to the fact that the surface of the porous substrate is uneven.

3.2.4 Cost tradeoffs

Figure 3.17 summarizes the variation in the chemicals cost (evaluated using retail cost of the bath constitutes summarized in Table 2.4) and metal film thickness with PPD. It was observed that for both cases, non-linear dependence on PPD is existent indicating complexity in the associated tradeoffs. The figure indicates that the chemicals cost varied

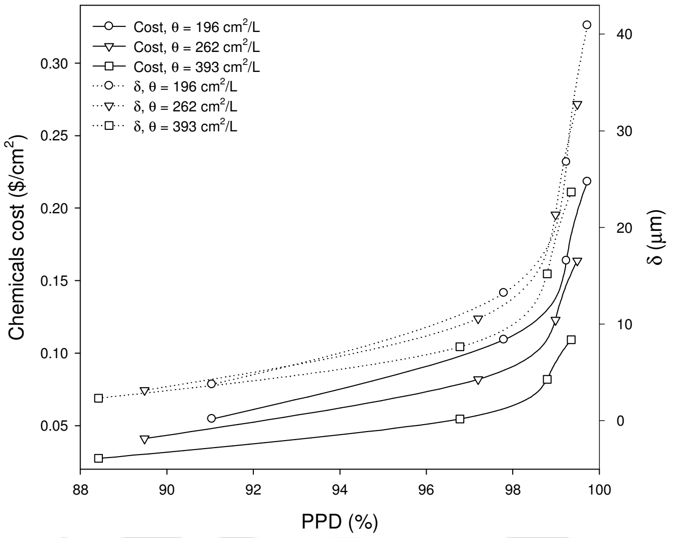

Figure 3.17: Cost tradeoffs for conventional hydrazine baths.

between 0.03–0.22 $/cm^2 for a variation in PPD from 88.4–99.7% and film thickness from 2.3–40.9 microns. Thereby, the cost tradeoffs are anticipated to be useful for the rigorous design and scale up purposes. Similar cost tradeoff profiles are expected for noble metal electroless deposition targeting dense metal–ceramic membrane fabrication.

3.2.5 PPD and efficiency tradeoffs

Figure 3.18 summarizes the variation of the objective function defined in equation (3.2) for the best value of loading ratio (θ = 393 cm^2/L). The optimal values of the initial $NiSO_4$ solution concentration ($C_{i,\ opt}$) obtained by maximization of the objective function (f_{max}) by a non-linear regression analysis for various combinations of f_1 and f_2 for a loading ratio of 393 cm^2/L are presented in Table 3.7. From Figure 3.18, it is evident that the plating efficiency (η) which minimizes the metal loss during the electroless plating is favored by a lower initial concentration of nickel while the pore densification (PPD) which improves the separation performance of the plated membrane is favored by a higher concentration. From Table 3.7, it can be noticed that lower metal concentrations result in

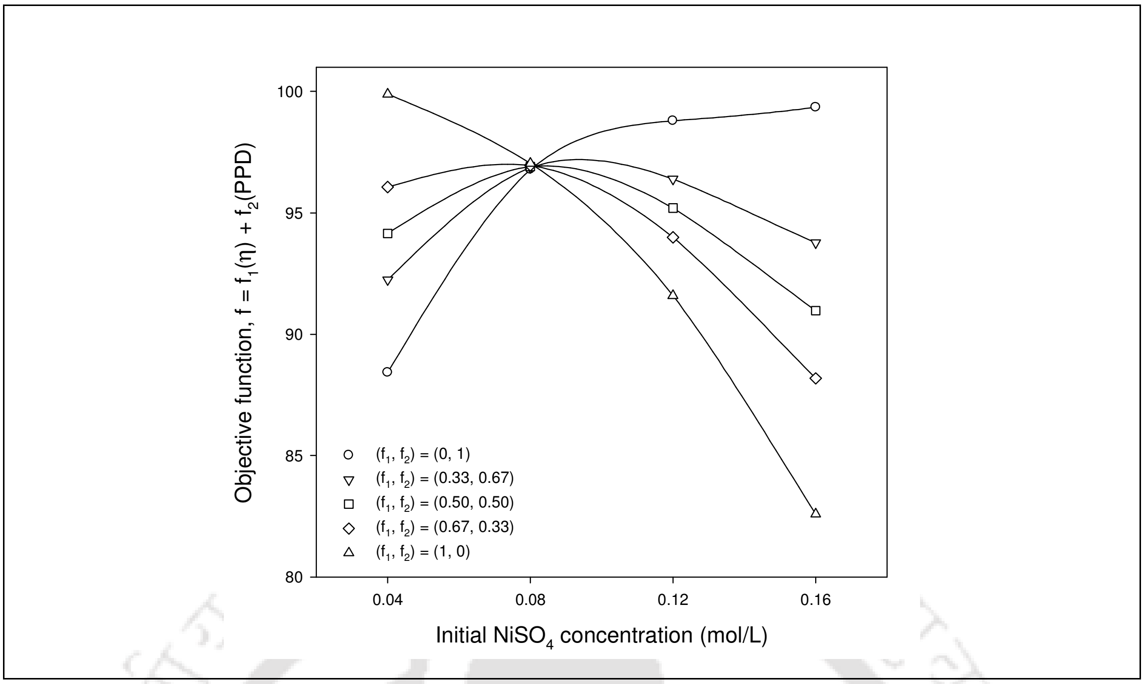

Figure 3.18: PPD and efficiency tradeoffs for conventional hydrazine baths.

efficient plating while higher concentrations result in dense membrane. An initial nickel concentration of 0.08 mol/L is found to be optimal for the combination of equal weights assigned to both efficiency and PPD.

3.2.6 Summary

In this work, an attempt is made to quantify the performance characteristics of hydrazine based electroless plating baths for metal–ceramic composite membrane fabrication. Firstly, it is observed that for a nominal membrane pore size of 275 nm, the optimal conditions of plating using hydrazine based electroless plating baths are identified

Table 3.7: Optimal nickel concentration data for various combinations of weight factors.

S. No.	**f_1**	**f_2**	**f_{max} (%)**	**$C_{i,\,opt}$ (mol/L)**
1	0	1	99.3501	0.1600
2	0.33	0.67	97.1287	0.0938
3	0.50	0.50	96.9116	0.0817
4	0.67	0.33	97.1326	0.0680
5	1	0	99.8856	0.0400

as 0.12 mol/L initial concentration of nickel and 393 cm^2/L of loading ratio, which provide 41.5% conversion, 91.6% plating efficiency and 98.8% PPD. The prepared nickel–ceramic composite membranes are porous in nature and this is possibly due to the larger pore size of the membrane support. Secondly, it is observed that the variation in loading ratio does not provide significant variation in conversion, efficiency and PPD. Thirdly, process inefficiencies in metal deposition are observed to be arising due to metal removal from membrane surface because of the shear effects induced by the released N_2 gas. Fourthly, based on the combinatorial tradeoffs associated to plating efficiency and PPD, an initial $NiSO_4$ solution concentration of 0.08 mol/L is found to be optimal. Finally, complex non-linear tradeoffs with respect to cost, percent pore densification and metal film thickness are evaluated.

The evaluated performance characteristics for the hydrazine based nickel electroless plating baths are encouraging to further develop and design sequential plating process steps for the simultaneous maximization of both plating efficiency and PPD. The deployment of suitable mass-transfer coupling to the process is expected to enhance conversions by 20–30% at higher concentrations. In addition, the evaluated inherent relationships between various parameters need to be also judged for the case of dense membrane fabrication so as to provide a general guideline upon the process parameters for noble metal–ceramic composite membranes. The obtained optimal parameters are expected to provide a dense metal–ceramic composite membrane for supports with lower surface pore sizes (5–50 nm) within 4–5 sequential plating process steps, which needs to be experimentally verified. These observations are anticipated to be useful for the scale-up and design of electroless plating processes for the large scale fabrication of metal–ceramic composite membranes.

3.3 Conclusions

The effect of metal concentration in the plating solution and loading ratio on electroless plating process parameters is presented in this chapter. Table 3.8 summarizes a comparative assessment of various process and membrane morphological parameters obtained for the cases with two different reducing agents namely sodium hypophosphite and hydrazine. It can be observed that all process as well as morphological parameters including conversion, efficiency, PPD, average pore size, average effective porosity and average mass-transfer coefficient for the hydrazine based baths are significantly higher than those obtained using the hypophosphite based baths. The selective conversion values for hydrazine based baths varied between 14.1–44.6% and are far better than those obtained for hypophosphite baths (9.7–24.2%) even at higher concentrations. To have a minimum plating efficiency of 90% without compromising upon the conversion and PPD, the optimal initial $NiSO_4$ concentrations for hypophosphite and hydrazine baths are evaluated to be 0.08 mol/L and 0.12 mol/L respectively. In comparison with the hypophosphite baths, hydrazine baths resulted in higher values of conversion, efficiency, film thickness and pore densification. Hence, it can be concluded that the hydrazine as a reducing agent serves better than sodium hypophosphite for the electroless deposition of

Table 3.8: Comparison between conventional hypophosphite and hydrazine baths.

Parameter	Hypophosphite baths	Hydrazine baths
Conversion (%)	10–39	14.5–54.0
Efficiency (%)	99.3–61.7	99.9–82.0
Pore diameter (nm)	128–89	94–14
PPD (%)	78.3–89.5	88.4–99.7
Porosity of metal layer	0.0016–0.032	0.0028–0.147
Thickness (µm)	1.59–24.4	2.34–47.9
Average mass transfer coefficient, $\bar{k}$ (s^{-1})	37–137	67–487
Optimal concentration (mol/L)	0.08	0.12
Optimal loading ratio (cm^2/L)	393	393

nickel. However, it is observed that hydrazine based baths tend to decompose soon at high temperatures and require more careful selection of process parameters such as temperature and pH and mode of operation.

The mean pore diameter of the nickel–ceramic composite membrane as obtained from the gas permeation experiments can also be visualized from the surface FESEM micrographs (Figure 3.19). Figure 3.19a corresponds to an evaluated mean pore size of 89 nm for the membrane fabricated in hypophosphite bath (C_i = 0.16 mol/L and θ = 196 cm^2/L) while Figure 3.19b corresponds to a mean pore size of 14 nm for the membrane fabricated in hydrazine bath (C_i = 0.16 mol/L and θ = 196 cm^2/L). These micrographs show the presence of micro-pores on the surfaces of the nickel–ceramic composite membranes fabricated in hypophosphite as well as hydrazine electroless plating baths.

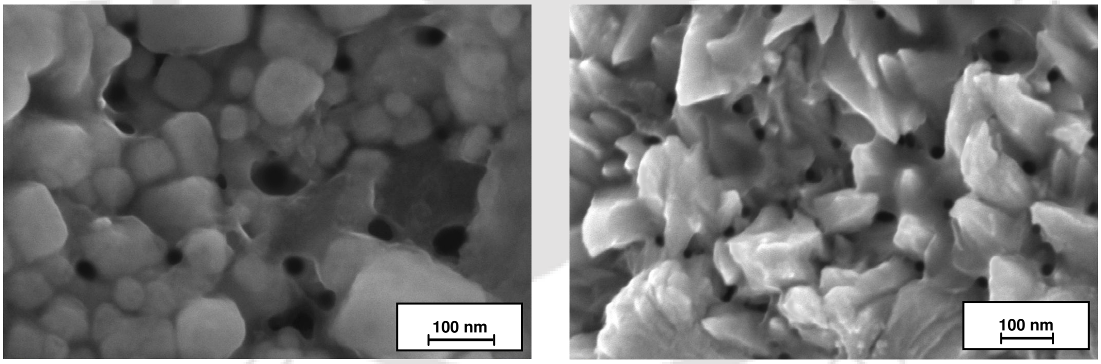

(a) **(b)**

Figure 3.19: Surface FESEM micrographs of the nickel–ceramic composite membranes prepared by conventional electroless plating:
(a) hypophosphite bath (361 KX); (b) hydrazine bath (286 KX).

PERFORMANCE CHARACTERISTICS OF AGITATED ELECTROLESS PLATING BATHS

In this chapter, the results are presented in two sections. The first section summarizes the performance characteristics agitated hypophosphite based electroless plating baths for nickel–ceramic composite membrane fabrication and the second section elaborates upon the effect of agitation on the performance characteristics of hydrazine based electroless plating baths for nickel–ceramic composite membrane fabrication. Finally, a summary of the obtained results is presented.

4.1 Agitated hypophosphite electroless plating baths

4.1.1 Efficacy of electroless plating

The plating experiments were carried out using the typical setup shown in Figure 2.8b (Chapter 2) to evaluate the performance characteristics of agitated electroless plating baths using hypophosphite as the reducing agent. From a theoretical perspective, mass transfer enhancement brought forward using membrane stirring principle shall enhance conversion. Figure 4.1 presents the variation in bath conversion with stirrer speed at various initial $NiSO_4$ solution concentrations for the loading ratios of 196 and 393 cm^2/L. As shown in the figure, the conversion increases with increasing stirrer speed and increasing nickel solution concentration for both the loading ratio values. For instance, at a loading ratio of 196 cm^2/L and for an enhancement in stirrer speed (ω) from 50 to 200 rpm, the conversion increased from 12.5 to 17.5%, 17.5 to 22.5% and 37.5 to 43.75% for the initial solution concentrations of 0.04, 0.08 and 0.16 mol/L respectively. Similarly, for the other loading ratio (393 cm^2/L) also, an enhancement in stirrer speed from 50 to 200

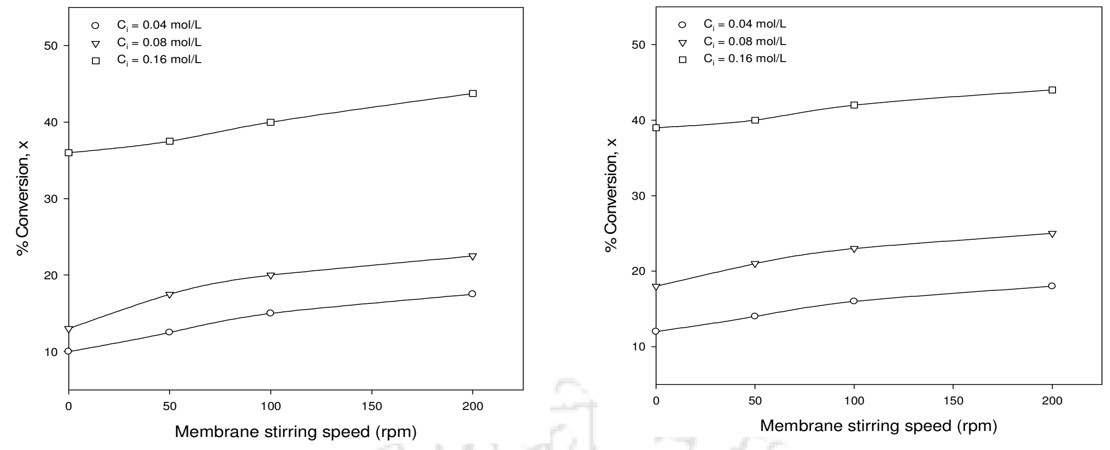

(a) **(b)**

Figure 4.1: Conversion profiles for agitated hypophosphite baths.
(a) $\theta = 196$ cm^2/L; (b) $\theta = 393$ cm^2/L.

rpm resulted in an increased conversion from 14 to 18%, 21 to 25% and 40 to 44% for the initial nickel solution concentrations of 0.04, 0.08 and 0.16 mol/L respectively. In other words, lower loading ratios do not favor significant enhancements in bath conversion and therefore loading ratio as such need not be considered as an important parameter in the due course of the plating process. However, from waste minimization perspective, higher loading ratio values are recommended for large scale membrane fabrication. In comparison with the available values in literature [104], it can be observed that the evaluated nickel conversions in our case (36–43.7% and 39–44%) are about 63–100% excess to the value reported (conversion = 22%). This is probably due to the consideration of 100% excess reducing agent in our case (which was added after 30 minutes during each of the one-hour plating steps) and enhanced transportation of metal ions to the substrate surface by the stirring principle.

Theoretically, mass transfer enhancements such as stirring reduce plating efficiency. This is because of the turbulence generated by enhanced mass transfer, which gives rise to a higher level of nucleation in the solution and thereby promotes metal deposition at these sites causing plating inefficiency. Therefore, it is important to quantitatively evaluate the parametric effect of mass transfer enhancement on plating efficiency. Figure 4.2 presents the variation in percent metal plating efficiency with stirrer speed at various initial nickel solution concentrations for the loading ratios of 196 and 393 cm^2/L. It is observed that stirring as a mass transfer enhancement technique contributes to a substantial reduction in metal plating efficiency especially at higher solution concentrations. For instance, for an initial nickel solution concentration of 0.04 mol/L, with an enhancement in stirrer speed from 0 to 200 rpm, the metal plating efficiency reduced from 97% to 86.3% for the loading ratio of 196 cm^2/L and from 99.2 to 93.7% for the loading ratio of 393 cm^2/L. However, for a higher initial nickel solution concentration of 0.16 mol/L, with an enhancement in stirrer speed from 0 to 200 rpm, the metal plating efficiency significantly reduced from 61.6 to 41.9% for the loading ratio of 196 cm^2/L and from 62.1 to 52.2% for the loading ratio of 393 cm^2/L.

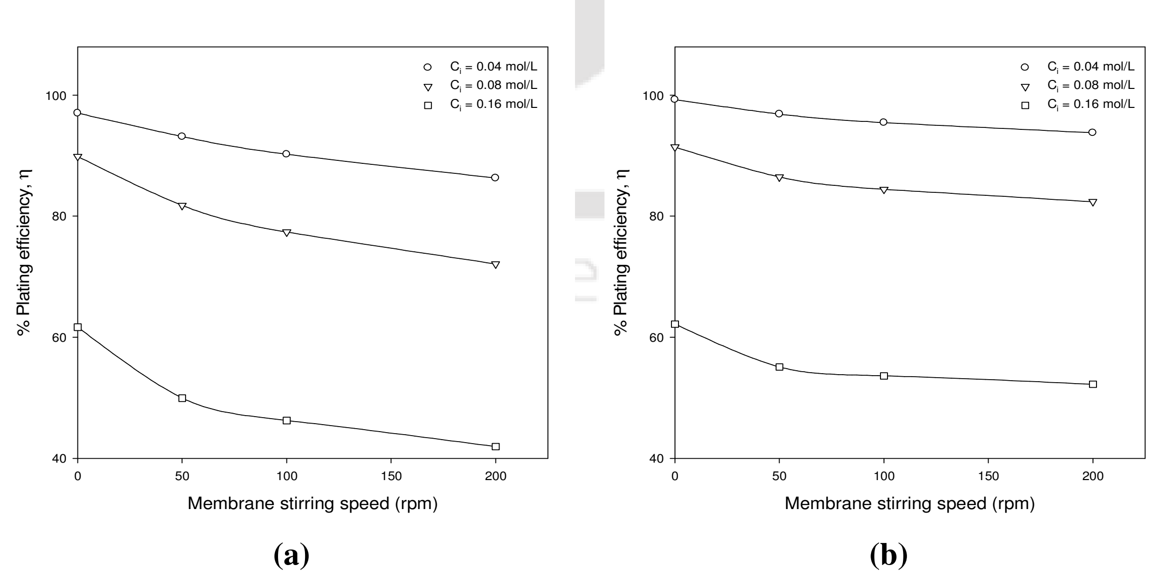

Figure 4.2: Efficiency profiles for agitated hypophosphite baths.

(a) $\theta = 196\ cm^2/L$; (b) $\theta = 393\ cm^2/L$.

In comparison, the literature [104] plating efficiency value was about 68% for a bath initial nickel concentration of 0.23 mol/L, which is comparable with the evaluated plating efficiency values of this work. The data trends indicate that plating efficiency is significantly affected by the initial nickel solution concentration and stirrer speed than the loading ratio. The possible reason for significant reduction in metal plating efficiency is accounted for significant metal deposition on the beaker surface, membrane holder (base plate) and in the plating solution at higher stirrer speeds and higher initial nickel solution concentrations. A higher loading ratio (393 cm^2/L), lower solution concentrations (0.04 and 0.08 mol/L) and lower stirrer speeds (0 to 100 rpm) are recommended as these resulted in higher plating efficiencies. Considering upon the fact that higher values of loading ratio, concentrations and stirrer speeds enable better conversion profiles, the optimal choice of operation would refer to an initial solution concentration of 0.08 mol/L, a stirrer speed of 100 rpm and the higher loading ratio (393 cm^2/L). This corresponds to about 23% metal conversion, which is significantly lower for acceptance towards industrial scale fabrication process. In other words, it is necessary to identify potential parameters of mass transfer enhanced electroless plating process that indicate good combinations of plating conversion (>60%) and plating efficiency (>80%) for hypophosphite based electroless plating baths in the near future.

Table 4.1 presents the variation of selective conversion (fractional conversion multiplied by plating efficiency) with stirrer speed for both cases of loading ratios. It can be seen from the table that the selective conversion varied between 9.7% and 23%, which is far lower than that acceptable for good industrial practice. It can be further observed that enhancing stirrer speed does enhance the selective conversion significantly at lower initial nickel concentrations (0.04 and 0.08 mol/L) but not at higher solution concentration (0.16 mol/L) where the selective conversion is reducing with increasing the stirrer speed.

Table 4.1: Selective conversion data for agitated hypophosphite baths.

Stirring speed (rpm)	**Selective conversion** (%) **for various values of** C_i (mol/L)					
	θ = 196 cm^2/L			θ = 393 cm^2/L		
	0.04	0.08	0.16	0.04	0.08	0.16
0	9.7	11.7	22.2	11.9	16.5	24.3
50	11.6	14.3	18.7	13.6	18.2	22.0
100	13.5	15.5	18.5	15.3	19.4	22.5
200	15.1	16.2	18.3	16.9	20.6	23.0

Therefore, higher solution concentration (0.16 mol/L) is not recommended for the fabrication of nickel–ceramic composite membranes in agitated electroless plating baths. Further, it can be observed that the loading ratio also affects the selective conversion values and higher loading ratio (393 cm^2/L) resulting in an increased selective conversion (by 2–5%).

Figure 4.3 presents the variation of average efficient nickel plating rate (mol/L.s) with average solution concentration for various stirrer speeds and two different loading ratios (196 and 393 cm^2/L). It can be observed that the average efficient nickel plating rate varied from 1.08–9.87, 1.29–8.32, 1.50–8.22 and 1.68–8.15 $\times 10^{-6}$ mol/L.s with a variation in initial nickel solution concentration of 0.04–0.16 mol/L for stirrer speeds of 0, 50, 100 and 200 rpm respectively at the loading ratio value of 196 cm^2/L. Similarly, the average efficient nickel plating rate varied from 1.32–10.78, 1.51–9.79, 1.70–10.01 and 1.88–10.21 $\times 10^{-6}$ mol/L.s with a variation in initial nickel solution concentration of 0.04–0.16 mol/L and stirrer speed of 0, 50, 100 and 200 rpm respectively for the loading ratio value of 393 cm^2/L. From this figure (Fig. 4.3), it can be observed that the average nickel deposition rates increase with increasing the stirrer speed for the initial solution concentrations of 0.04 and 0.08 mol/L and are higher than those of the base case (0 rpm) for both the loading ratios. However, this is not the case with the higher initial solution concentration (0.16 mol/L) where the values of the average nickel deposition with stirring

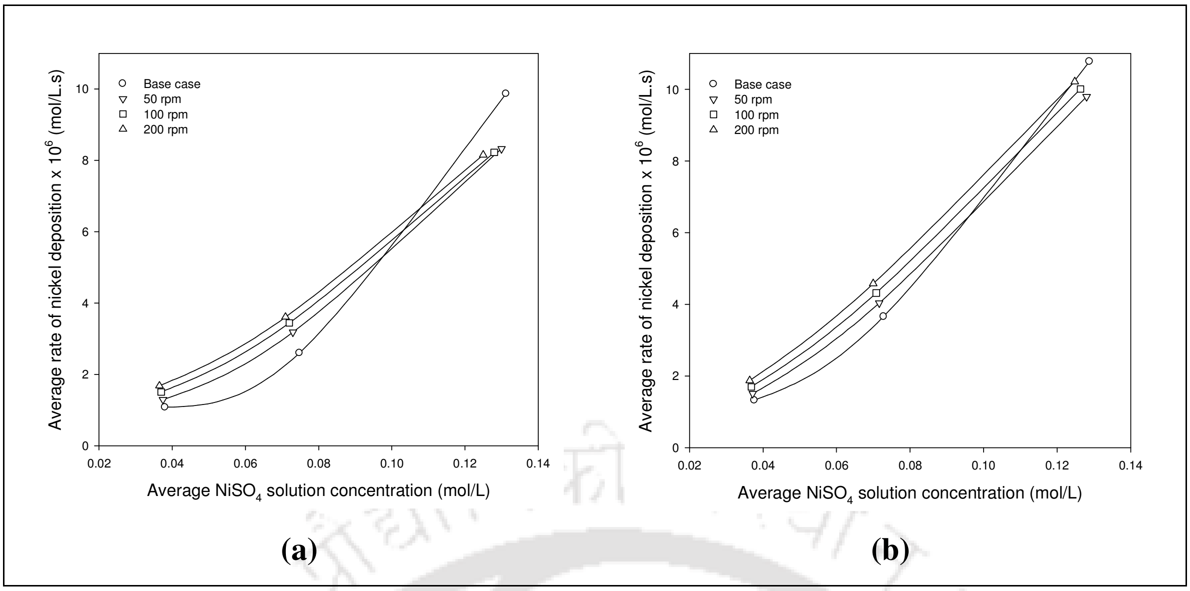

(a) **(b)**

Figure 4.3: Average nickel deposition rate for agitated hypophosphite baths. (a) $\theta = 196$ cm^2/L; (b) $\theta = 393$ cm^2/L.

are lower than those of the base case (without stirring). Though the values of average deposition rate at the lower loading ratio (196 cm^2/L) are slightly lower than that of the other (393 cm^2/L), they are significantly affected by stirring. For instance, for a loading ratio of 196 cm^2/L, the efficient average reaction rate increases by 56% and 39% for an enhancement in stirrer speed from 0 to 200 rpm for the initial nickel concentrations of 0.04 and 0.08 mol/L respectively. Corresponding values for the other loading ratio (393 cm^2/L) are 42% and 25%. On the other hand, the average reaction rate at higher initial nickel solution concentration (0.16 mol/L) reduces by 17% and 5% for the loading ratios of 196 and 393 cm^2/L respectively.

Table 4.2 presents the model parameters obtained from the non-linear regression analysis described in section 2.3.4 (Chapter 2). It can be observed that for a loading ratio of 196 cm^2/L (Table 4.2a), the average nickel mass transfer coefficient ($\overline{k}$) varied between 37.0–98.8, 50.3–100.6, 82.0–106.4 and 100.3–116.6 s^{-1} for the stirrer speeds of 0, 50, 100 and 200 rpm respectively. The average mass transfer coefficient values strongly

Table 4.2: Model parameters for agitated hypophosphite baths. (a) θ = 196 cm^2/L; (b) θ = 393 cm^2/L.

Stirrer speed (rpm)	$\bar{C}_B$ (mol/L)	$\bar{k}$ (s^{-1})	$\bar{\gamma}$	**% Error** ×10^5
0	0.038	37.0	999.3	5.34
0	0.075	41.3	999.8	5.31
0	0.131	98.8	1000.6	2.91
50	0.038	50.3	992.2	1.36
50	0.073	56.8	996.5	3.32
50	0.130	100.6	1015.9	4.99
100	0.037	82.0	990.3	5.00
100	0.072	83.9	991.5	5.00
100	0.128	106.4	1020.9	4.99
200	0.036	100.3	984.9	5.02
200	0.071	100.4	982.2	5.00
200	0.125	116.6	975.0	4.88

(a)

Stirrer speed (rpm)	$\bar{C}_B$ (mol/L)	$\bar{k}$ (s^{-1})	$\bar{\gamma}$	**% Error** ×10^5
0	0.038	46.2	999.6	5.04
0	0.073	68.9	999.8	6.14
0	0.129	136.8	1005.5	3.35
50	0.037	60.5	992.4	0.66
50	0.072	86.3	996.9	4.02
50	0.128	141.1	1015.4	1.15
100	0.037	107.8	989.6	2.48
100	0.071	122.0	991.5	5.00
100	0.126	149.7	1020.8	5.87
200	0.036	139.3	983.8	3.05
200	0.070	141.3	981.9	3.46
200	0.125	153.6	975.1	5.07

(b)

depend on stirrer speed especially at lower initial nickel solution concentration (0.04 mol/L) with almost 100% enhancement. However, this is not the case at higher initial nickel solution concentration (0.16 mol/L), where the change in mass transfer coefficient with stirrer speed is insignificant. Further, it can be observed that the effect of solution concentration on the mass transfer coefficient is nullified at the highest stirrer speed (200 rpm). This observation once again confirms that bath agitation can be applied at lower solution concentrations to enhance mass transfer rate of the reactants but not at higher nickel solution concentration where there is a possibility of larger nucleation in the solution. When the loading ratio is increased to 393 cm^2/L (Table 4.2b), the average nickel mass transfer coefficient varied between 46.2–136.8, 60.5–141.1, 107.8–149.7 and 139.3–153.6 s^{-1} for stirrer speeds of 0, 50, 100 and 200 rpm respectively. Bath loading ratio also affects the mass transfer coefficient values but to a small extent. For all these cases, the partition coefficient ($\bar{\gamma}$) value is around 1000 and varied a minimum (2%), indicating that it is relatively independent of stirrer speed, concentration and loading ratio. In other words, it can be concluded that the average mass transfer coefficient is strongly influenced by all the three parameters namely nickel concentration, loading ratio and stirrer speed.

4.1.2 Metal–ceramic membrane characteristics

A composite membrane is said to be dense if it satisfies the following three conditions. Firstly, its surface must be fully covered by the deposited material, which can be evidenced from the surface characterization. Secondly, the value of PPD shall be 100 and thirdly, the effective porosity of the deposited film is zero.

4.1.2.1 Surface characterization

The surface characterization was carried out using scanning electron microscopy (SEM) (LEO, 1430VP) and X-ray diffraction (XRD) (Bruker AXS, D8 ADVANCE) methods. Figure 4.4 presents the surface SEM micrographs of all membranes fabricated at a stirrer speed of 100 rpm with different initial nickel concentrations (0.04–0.16 mol/L) and loading ratios (196 and 393 cm^2/L). These micrographs indicate the presence of metallic nickel grains on the ceramic surface. It can be observed that the surface texture is strongly affected by the solution concentration than the loading ratio. Metal layer is not fully developed at lower solution concentration (0.04 mol/L) and hence the surfaces are

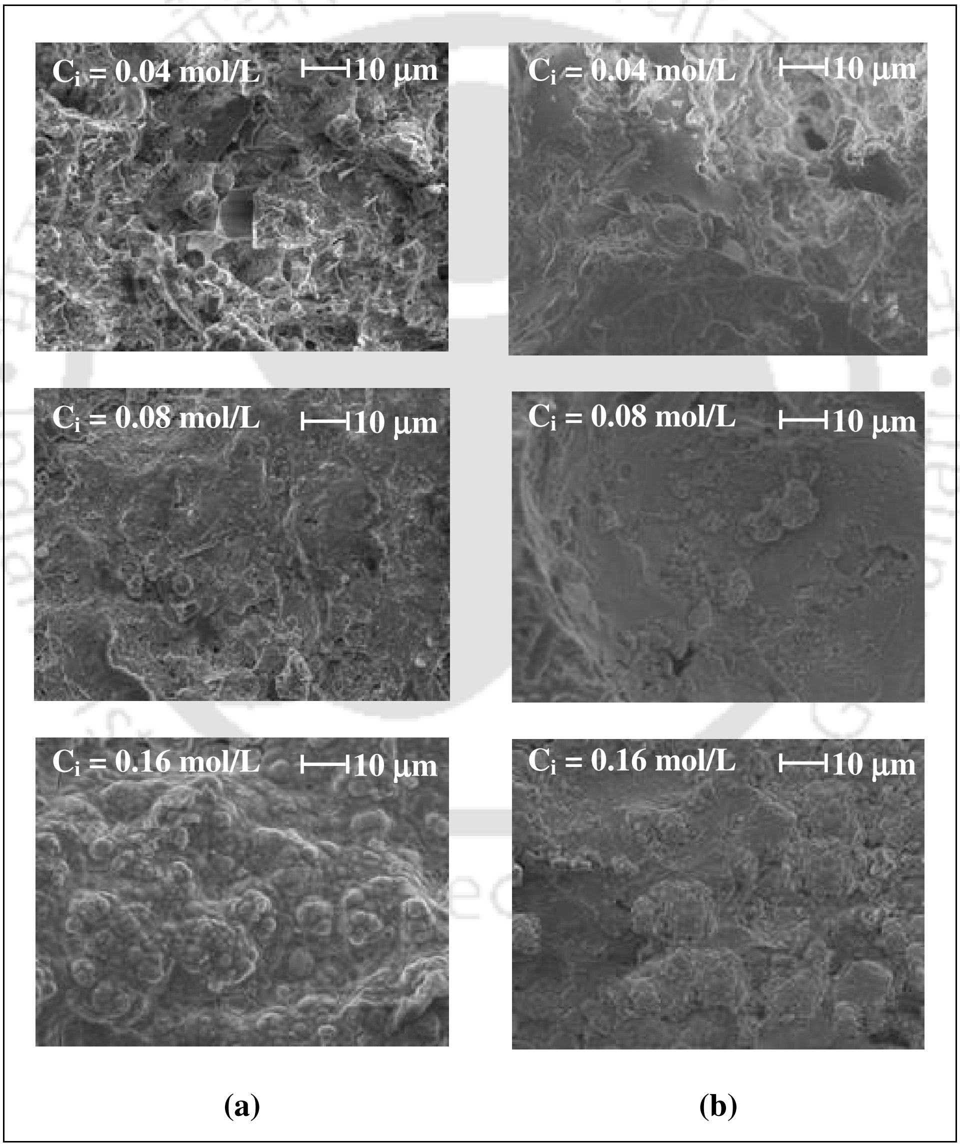

Figure 4.4: Surface SEM micrographs (magnification: 1 KX) of nickel–ceramic composite membranes prepared in agitated hypophosphite baths at a stirrer speed of 100 rpm. (a) $\theta = 196\ cm^2/L$; (b) $\theta = 393\ cm^2/L$.

non-uniform. A more uniformity in the metal coating is observed at a concentration of 0.08 mol/L and coarser nickel grains are resulted at higher solution concentration (0.16 mol/L) for all stirrer speeds. Further, it is observed that stirring has a minimal effect on the coating morphology and higher stirrer speeds result in more uniform and smoother coatings. The pore characterization of the composite membranes is anticipated from air permeation data and is presented in the next section (4.1.2.2).

Figure 4.5 presents the XRD pattern of the metal film deposited under good plating conditions (initial nickel concentration of 0.08 mol/L, stirring speed of 100 rpm and a loading ratio of 393 cm^2/L). Similar XRD spectra were observed for the other cases also. The observed peaks matches very closely with the relevant peaks associated to quartz (JCPDS: 01–075–0443 (A)) and nickel (JCPDS: 00–001–1266 (D)). Presence of quartz, an ingredient of the ceramic substrate is perhaps identified either from the open pores of the deposited metal layer or due to higher penetration depth of the X-rays than the metal layer thickness. The nature of the spectra indicates that the metal films are amorphos.

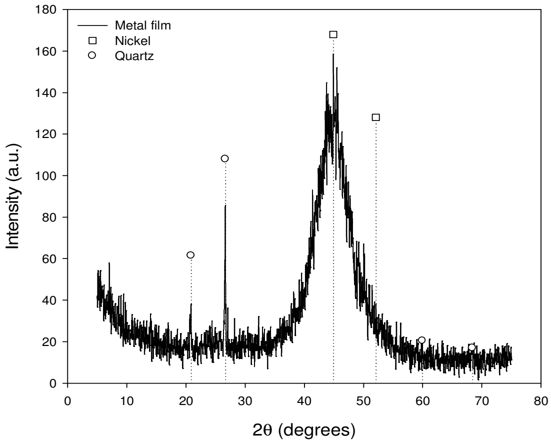

Figure 4.5: XRD pattern of the metal film deposited in agitated hypophosphite baths. (C_i = 0.08 mol/L, θ = 393 cm^2/L and ω = 100 rpm).

4.1.2.2 Permeation characteristics

Air permeation experiments were carried out to evaluate the membrane performance and identify the presence of any defects (such as cracks) in the membrane structure. Variant permeability profiles are observed at different concentrations and loading ratios indicating that the permeation characteristics of the composite membranes are largely influenced by mass transfer enhancement techniques. In addition, the average pore size of the composite membranes and the effective porosity of the deposited metal layers are evaluated using the procedure described in section 2.3 (Chapter 2).

4.1.2.2.1 Pore diameter

The data corresponding to the average pore diameter of composite membranes is presented in Table 4.3. It is found that agitated electroless plating baths are effective to significantly reduce the average pore size of the surface from 275 nm to 128–59 nm. Solution concentration plays a significant role in pore size reduction and increasing the bath concentration resulted in a decrease in the pore size. Further, it is observed that the effect of stirrer speed in reducing the pore size is predominant at all the solution concentrations.

Table 4.3: Average pore size data for agitated hypophosphite baths.

Stirring speed (rpm)	**Average pore size** (nm) **of composite membrane for various values of C_i** (mol/L)					
	$\theta = 196$ cm^2/L			$\theta = 393$ cm^2/L		
	0.04	0.08	0.16	0.04	0.08	0.16
0	120	113	89	128	122	94
50	85	78	69	100	93	85
100	78	70	62	90	83	76
200	75	68	59	86	80	73

4.1.2.2.2 Effective porosity

Porous nature of the nickel films deposited in hypophosphite based electroless plating baths can be attributed to the hydrogen gas which evolves during the reaction. The rate of hydrogen generation is directly proportional to the rate of electroless plating reaction, which increases with increasing solution concentration. This hydrogen gas forms bubbles at the membrane surface and when not removed causes voids in the metal film and hence contribute to the pore volume of the nickel film.

Figure 4.6 presents the variation in effective porosity of the metal film with stirrer speed for various initial metal solution concentrations and loading ratios. For a loading ratio of 196 cm^2/L, the effective porosity varied with the stirrer speed from 0 to 200 rpm as 0.003–0.001, 0.016–0.011 and 0.032–0.020 for the initial nickel concentrations of 0.04, 0.08 and 0.16 mol/L respectively. Corresponding values for the other loading ratio (393 cm^2/L) are 0.002–0.001, 0.008–0.006 and 0.015–0.009 respectively. It is observed that the effective porosity of the metal layer is strongly affected by all the three parameters

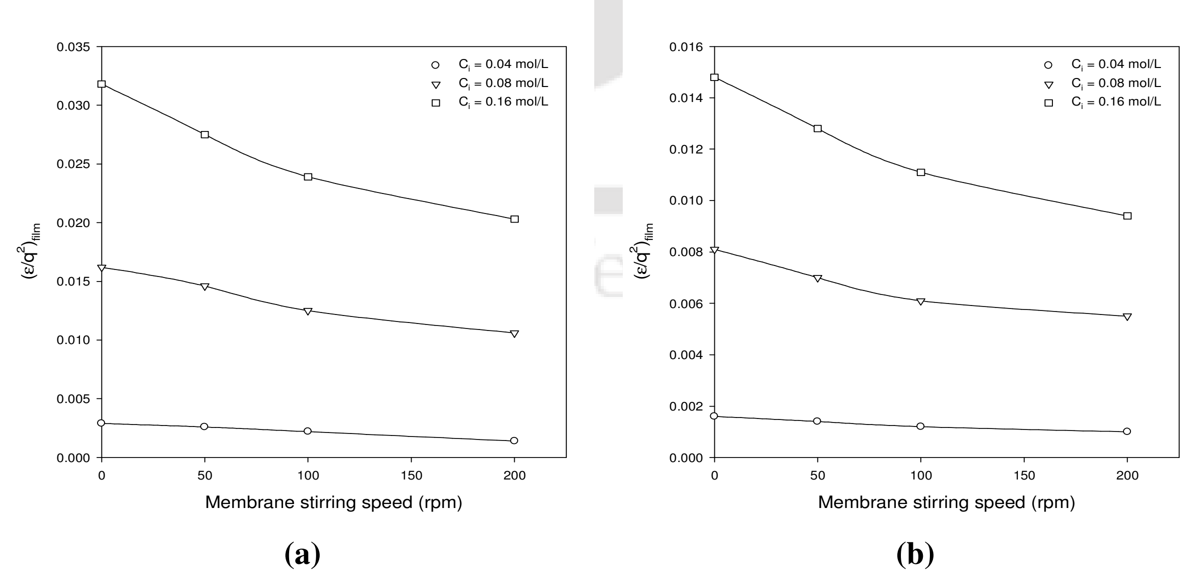

Figure 4.6: Effective porosity ($(\varepsilon/q^2)_{film}$) profiles for agitated hypophosphite baths. (a) θ = 196 cm^2/L; (b) θ = 393 cm^2/L.

(solution concentration, loading ratio and stirrer speed). Higher values of effective porosity are observed at higher solution concentration (0.16 mol/L) due to rapid generation of hydrogen at the surface. Membrane stirring as a mass transfer enhancement provides subsequent removal of gas bubbles at higher stirrer speeds resulting in lower values of effective porosity of the metal film. Initially there is a significant reduction in effective porosity values up to 100 rpm and thereafter, no significant reduction is observed by increasing the stirrer speed from 100 to 200 rpm. Hence, a stirrer speed of 100 rpm is found to be the optimal speed. Further, higher loading ratio (393 cm^2/L) is recommended as it produced less porous metal films with more uniformity which can be observed from the surface SEM images (Figure 4.4).

4.1.2.2.3 Percent pore densification

Percent pore densification (PPD), a measure of pore size reduction is an important parameter to quantify the quality of deposition. Figure 4.7 presents the variation of PPD with stirrer speed and initial metal solution concentration for the loading ratios of 196 and 393 cm^2/L. For the lower loading ratio (196 cm^2/L) case, PPD values varied with the stirrer speed (0–200 rpm) as 80.9–92.7, 83.1–93.9 and 89.5–95.5 for the initial nickel concentrations of 0.04, 0.08 and 0.16 mol/L respectively. Corresponding values for the higher loading ratio (393 cm^2/L) are 78.3–90.1, 80.4–91.6 and 88.3–93.0 respectively. Amongst all data, the case of $C_i = 0.16$ mol/L, $\theta = 196$ cm^2/L and stirrer speed of 200 rpm provided the best value of the PPD (95.5%). The PPD values are more affected by the solution concentration than the loading ratio. However, it is important to note that the PPD varied non-linearly with stirrer speed and the enhancement in these values is predominantly higher at lower agitation speeds (0–100 rpm). No significant improvement in PPD is observed beyond 100 rpm indicating this as the optimal speed (100 rpm). In

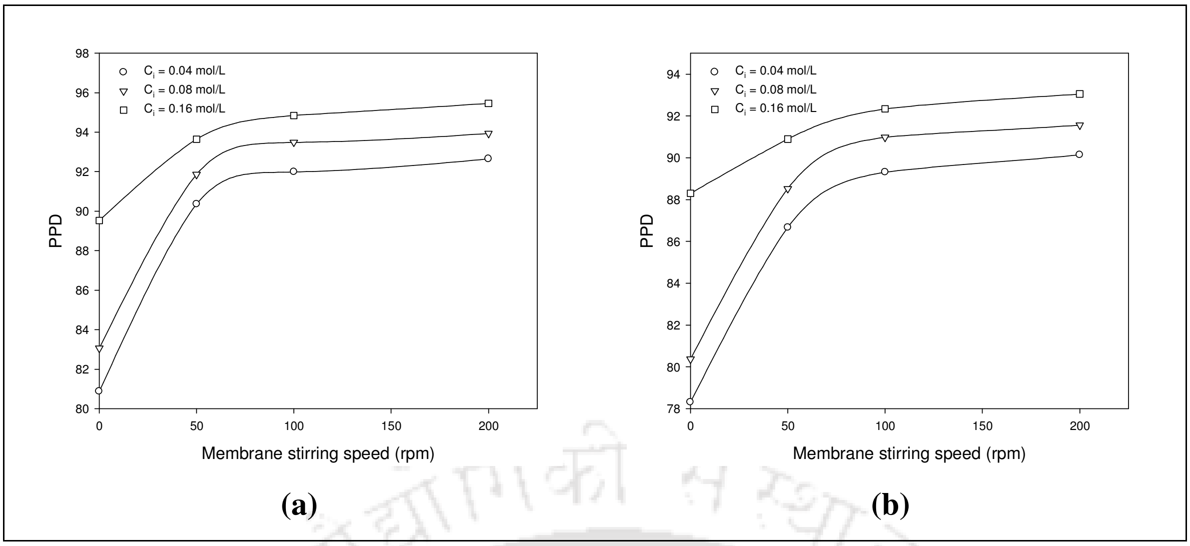

Figure 4.7: PPD profiles for agitated hypophosphite baths.
(a) $\theta = 196\ cm^2/L$ and (b) $\theta = 393\ cm^2/L$.

summary, it is observed that lower values of PPD (78.3–95.5%) are obtained despite conducting 8 hours of sequential plating in sodium hypophosphite baths.

4.1.2.2.4 Film thickness

Thickness of the deposited metal layer depends primarily on the quantity of metal deposited over the surface of the substrate and its effective porosity (Eq. (2.12)). Table 4.4 presents the variation in bulk average thickness of the nickel layer with stirrer speed for various values of initial metal solution concentration and loading ratios. It is observed that at lower metal solution concentrations (0.04–0.08 mol/L), stirring contributes to substantial enhancement in film thickness, which is not the case with higher metal solution concentration (0.16 mol/L) wherein the metal film thickness reduces with increasing stirrer speed due to lower efficiency. Further, it can be observed that the average thickness of the porous nickel layer is inversely proportional to the bath loading ratio. Doubling the loading ratio (from 196 to 393 cm^2/L) contributes to a reduction in film thickness by about 50% (from 2.59–24.45 μm to 1.59–13.12 μm). Since lower film thickness is always preferred, a higher loading ratio (393 cm^2/L) would be the optimal choice. The maximum

Table 4.4: Average film thickness data for agitated hypophosphite baths.

Stirring speed (rpm)	**Average nickel layer thickness** (μm) **for various values of** C_i (mol/L)					
	θ = 196 cm^2/L			θ = 393 cm^2/L		
	0.04	0.08	0.16	0.04	0.08	0.16
0	2.59	6.33	24.45	1.59	4.42	13.12
50	3.11	7.74	20.54	1.81	4.88	11.90
100	3.62	8.36	20.21	2.04	5.21	12.15
200	4.03	8.74	19.97	2.25	5.52	12.37

film thickness (24.45 μm) is observed for the case of C_i = 0.16 mol/L, θ = 196 cm^2/L and 0 rpm (without mass transfer enhancement). In summary, it is observed that all the three parameters namely stirrer speed, solution concentration and loading ratio largely influence the metal film thickness during the fabrication of composite membranes by electroless plating.

4.1.3 PPD and Efficiency tradeoffs

An efficient design of electroless plating processes needs to maximize both PPD and efficiency. Conventionally, there exists a tradeoff between PPD and efficiency with the fact that higher plating efficiency does not contribute to good quality of plating and vice-versa. Figure 4.8 presents the PPD versus efficiency tradeoffs for both loading ratio values considered in this work. The four points of each plot from bottom to top (or from right to left) correspond to the stirrer speeds of 0, 50, 100 and 200 rpm respectively. Several possible combinations of PPD and efficiency can be chosen depending upon the requirement. If at least 75% plating efficiency and 90% PPD are desired, then there exist five feasible options for the lower loading ratio (196 cm^2/L) and only two for the higher loading ratio (393 cm^2/L). The five feasible points (represented as pairs of (C_i, ω)) for the first case (θ = 196 cm^2/L) are (0.08, 100), (0.08, 50), (0.04, 200), (0.04, 100) and (0.04,

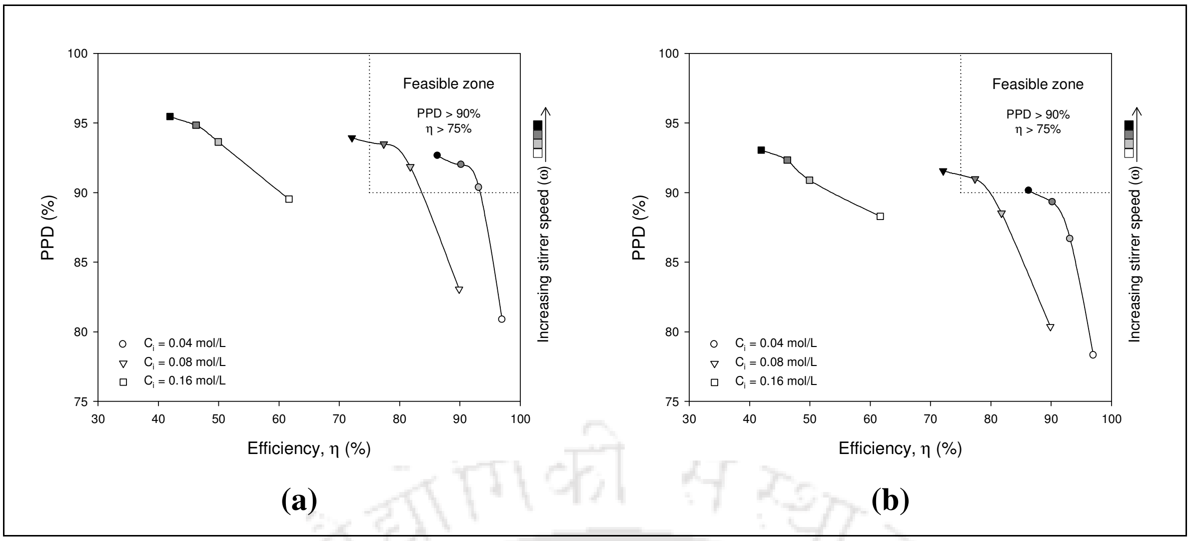

(a) **(b)**

Fig. 4.8: PPD and efficiency tradeoffs (a) θ = 196 cm^2/L and (b) θ = 393 cm^2/L.

50) where as for the second case (θ = 393 cm^2/L), they are (0.08, 100), (0.04, 200). A careful selection of an optimal combination should be made from amongst these feasible options based on the other important parameters. If we consider the second case (θ = 393 cm^2/L) which has comparatively higher values of selective conversion and lower thickness, two feasible options does exist. Either of the two optimal combinations namely 0.08 mol/L initial nickel concentration with 100 rpm stirrer speed or 0.04 mol/L with 200 rpm can be used.

4.2 Agitated hydrazine electroless plating baths

4.2.1 Efficacy of electroless plating

Figure 4.9 presents the variation in bath conversion with stirrer speed at various initial nickel solution concentrations and loading ratios. Conversion increases with loading ratio, nickel concentration and stirrer speed. For a loading ratio of 196 cm^2/L, the conversion varied with stirring speed from 14.5–20.5%, 26–32% and 46.8–50.2% for 0.04, 0.08 and 0.16 mol/L initial nickel concentrations respectively. For the other loading ratio (393 cm^2/L), the conversions varied with stirrer speed from 17.5–24, 29.5–35% and 56–

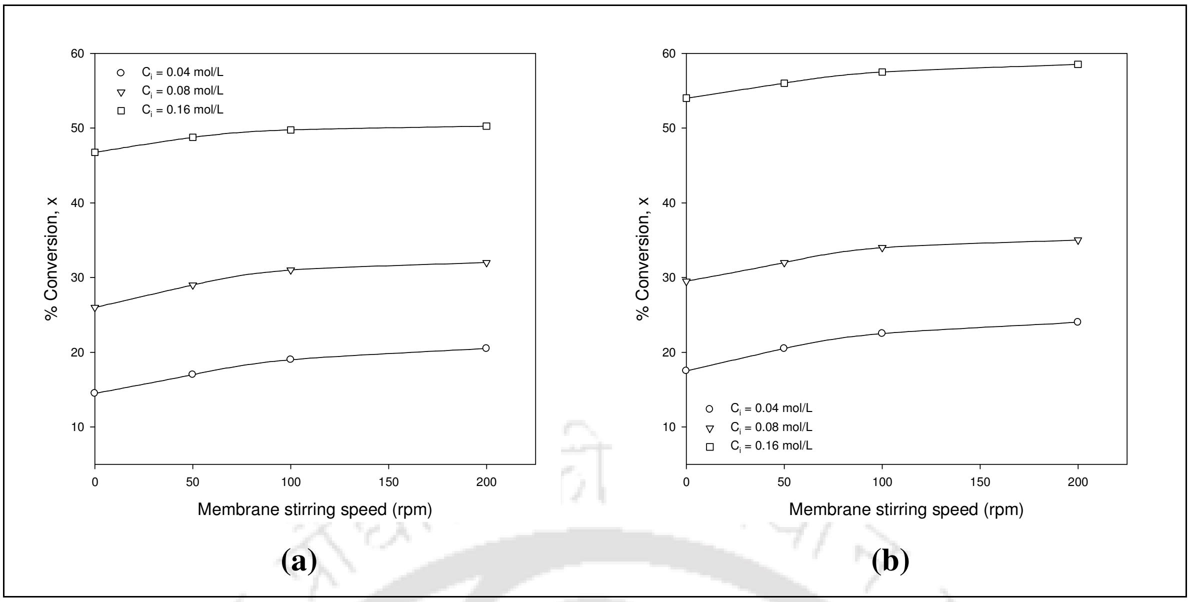

(a) **(b)**

Figure 4.9: Conversion profiles for agitated hydrazine baths.
(a) $\theta = 196\ cm^2/L$ and (b) $\theta = 393\ cm^2/L$.

58.5% for 0.04, 0.08 and 0.16 mol/L initial nickel concentrations respectively. Obtaining higher conversions at higher metal solution concentrations is encouraging even from the waste minimization perspective.

Due to enhancement in nucleation at higher stirrer speeds, it is expected that enhancement in stirrer speeds would reduce plating efficiency. Figure 4.10 presents the variation in percent metal plating efficiency with stirrer speed at various initial nickel solution concentrations and loading ratios. The decline in plating efficiency with increasing stirrer speeds is prominent for higher metal solution concentrations (0.16 mol/L). On the other hand, it is interesting to note that the plating efficiency is not significantly affected with the loading ratio. For example, the metal plating efficiency in the case of 0.04 initial nickel solution concentration reduced from 97–91% and 99.9–96.3% with increasing stirrer speeds (up to 200 rpm) and loading ratios of 196 and 393 cm^2/L respectively. Similarly, for the case of 0.16 initial nickel solution concentration, the plating efficiencies reduced from 82–74% and 82.6–77.9% for loading ratios of 196 and

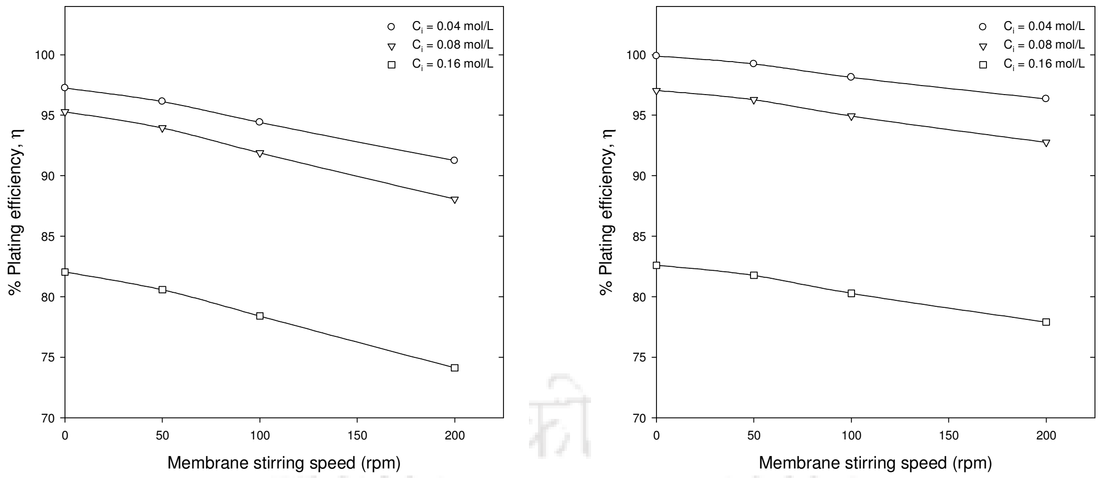

(a) **(b)**

Figure 4.10: Efficiency profiles for agitated hydrazine baths. (a) θ = 196 cm^2/L; (b) θ = 393 cm^2/L.

393 cm^2/L respectively. In other words, the reduction in loading ratio is not favored for higher metal plating efficiency. This is also due to the fact that lower loading ratios indicate larger risk of greater nucleation in the solution due to stirring and hence enhanced reaction rates lead to inefficient plating. Therefore, based on both conversion and plating efficiency profiles, the optimal loading ratio is 393 cm^2/L. In addition, if a minimal plating efficiency of 90% is set, the optimal conditions would indicate to 0.08 mol/L initial nickel solution concentration at a stirrer speed of 100 rpm. This work also recognizes the immediate need to identify suitable mass transfer enhanced electroless plating processes that provide good combinations of plating conversion (≥60%) and plating efficiency (≥90%).

Table 4.5 presents the variation of selective conversion (fractional conversion multiplied by plating efficiency) with stirrer speed for both cases of loading ratios. The selective conversion increased from 14.1–45.6% with increasing metal concentration. Due to pertinent lower selective conversion values (14.1–23.1%), lower solution concentrations

Table 4.5: Selective conversion data for agitated hydrazine baths.

Stirring speed (rpm)	**Selective conversion** (%) **for various values of C_i** (mol/L)					
	$\theta = 196$ cm^2/L			$\theta = 393$ cm^2/L		
	0.04	0.08	0.16	0.04	0.08	0.16
0	14.1	24.8	38.4	17.5	28.6	44.6
50	16.3	27.2	39.3	20.3	30.8	45.8
100	17.9	28.5	39.0	22.1	32.3	46.2
200	18.7	28.2	37.3	23.1	32.5	45.6

of 0.04 and 0.08 mol/L may not be recommendable for large scale fabrication. It is also apparent that loading ratio affects selective conversion. Further, dividends in selective conversions exist with stirrer speeds for lower solution concentrations (0.04–0.08 mol/L) but not higher solution concentrations (0.16 mol/L). This indicates that higher solution concentrations do not require mass transfer enhancement techniques to supplement the conventional electroless plating process.

Figure 4.11 presents the variation of average efficient nickel plating rate (mol/L.s) with average solution concentration for various stirrer speeds and two different loading

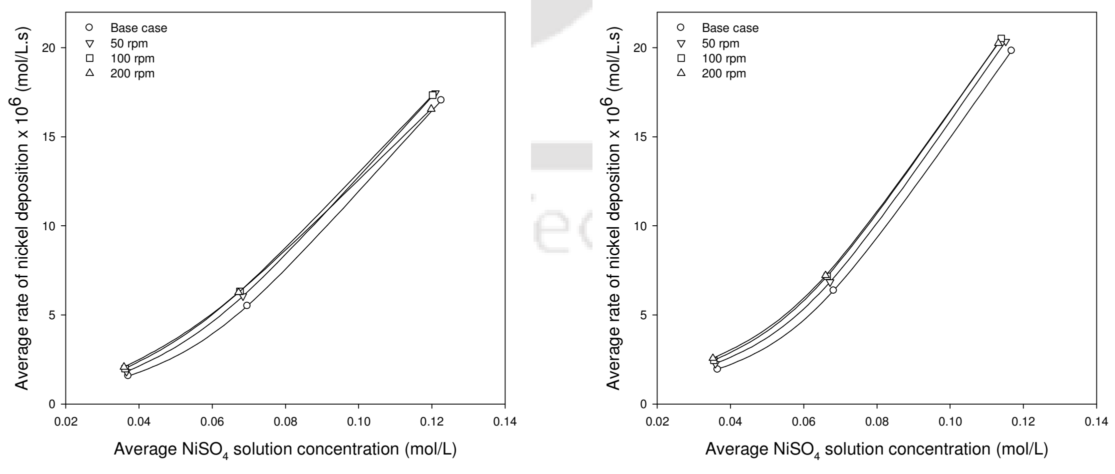

(a) **(b)**

Figure 4.11: Average deposition rate profiles for agitated hydrazine baths. (a) $\theta = 196$ cm^2/L; (b) $\theta = 393$ cm^2/L.

ratios (196 and 393 cm^2/L). From this figure, it is clear that the deposition rate strongly depends on the average solution concentration but not the loading ratio and stirrer speed, which only provided incremental enhancements.

Model parameters evaluated using the equations described in section 2.3.4 (Chapter 2) are summarized in Table 4.6. For a loading ratio of 196 cm^2/L (Table 4.6a), the average nickel mass transfer coefficient ($\bar{k}$) varied between 67.2–343.4, 80.4–390.6, 167.8–419.1 and 178.7–498.4 s^{-1} for the stirrer speeds of 0, 50, 100 and 200 rpm respectively and for the other loading ratio (393 cm^2/L), it varied between 83.6–487.0, 104.5–426.7, 208.4–532.4 and 216.4–573.1 s^{-1} for the stirrer speeds of 0, 50, 100 and 200 rpm respectively. For all the cases, the average mass-transfer coefficient ($\bar{k}$) increases significantly with increasing the solution concentration, loading ratio as well as stirrer speed. Hence it can be concluded that agitation as a mass transfer enhancement is recommended for hydrazine based electroless plating baths for all solution concentrations and loading ratios. For all these cases as well, the partition coefficient ($\bar{\gamma}$) value is around 1000 and it varied a minimum (≤4%), indicating that it is relatively independent of all the three parameters namely solution concentration, loading ratio and stirrer speed.

Table 4.6: Model parameters for agitated hydrazine baths.

(a) θ = 196 cm^2/L; (b) θ = 393 cm^2/L.

Stirrer speed (rpm)	$\bar{C}_B$ (mol/L)	$\bar{k}$ (s^{-1})	$\bar{\gamma}$	**% Error** ×10^5
0	0.038	67.2	984.4	5.17
0	0.075	117.5	990.2	4.68
0	0.131	343.4	1042.3	5.64
50	0.037	80.4	992.2	4.94
50	0.072	176.3	996.5	4.09
50	0.128	390.6	1015.9	4.25
100	0.037	167.8	990.3	4.83
100	0.071	282.0	991.5	3.48
100	0.126	419.1	1020.9	4.62
200	0.036	178.7	984.9	1.88
200	0.070	321.1	982.2	2.40
200	0.125	498.4	975.0	2.20

(a)

Stirrer speed (rpm)	$\bar{C}_B$ (mol/L)	$\bar{k}$ (s^{-1})	$\bar{\gamma}$	**% Error** ×10^5
0	0.038	83.6	998.0	5.01
0	0.073	178.3	994.4	6.51
0	0.129	487.0	1066.8	6.11
50	0.036	104.5	987.3	–1.97
50	0.067	225.0	972.1	0.60
50	0.115	426.7	1010.0	3.47
100	0.036	208.4	984.6	6.65
100	0.066	317.2	992.3	5.59
100	0.114	532.4	1026.0	2.45
200	0.035	216.4	994.7	2.38
200	0.066	420.9	990.3	5.09
200	0.113	573.1	1044.9	2.06

(b)

4.2.2 Metal–ceramic membrane characteristics

4.2.2.1 Surface characterization

The surface characterization was carried out using scanning electron microscopy (SEM) (LEO, 1430VP) and X-ray diffraction (XRD) (Bruker AXS, D8 ADVANCE) methods. Figure 4.12 presents the surface SEM micrographs of all membranes fabricated at a stirrer speed of 100 rpm with different initial nickel concentrations (0.04–0.16 mol/L)

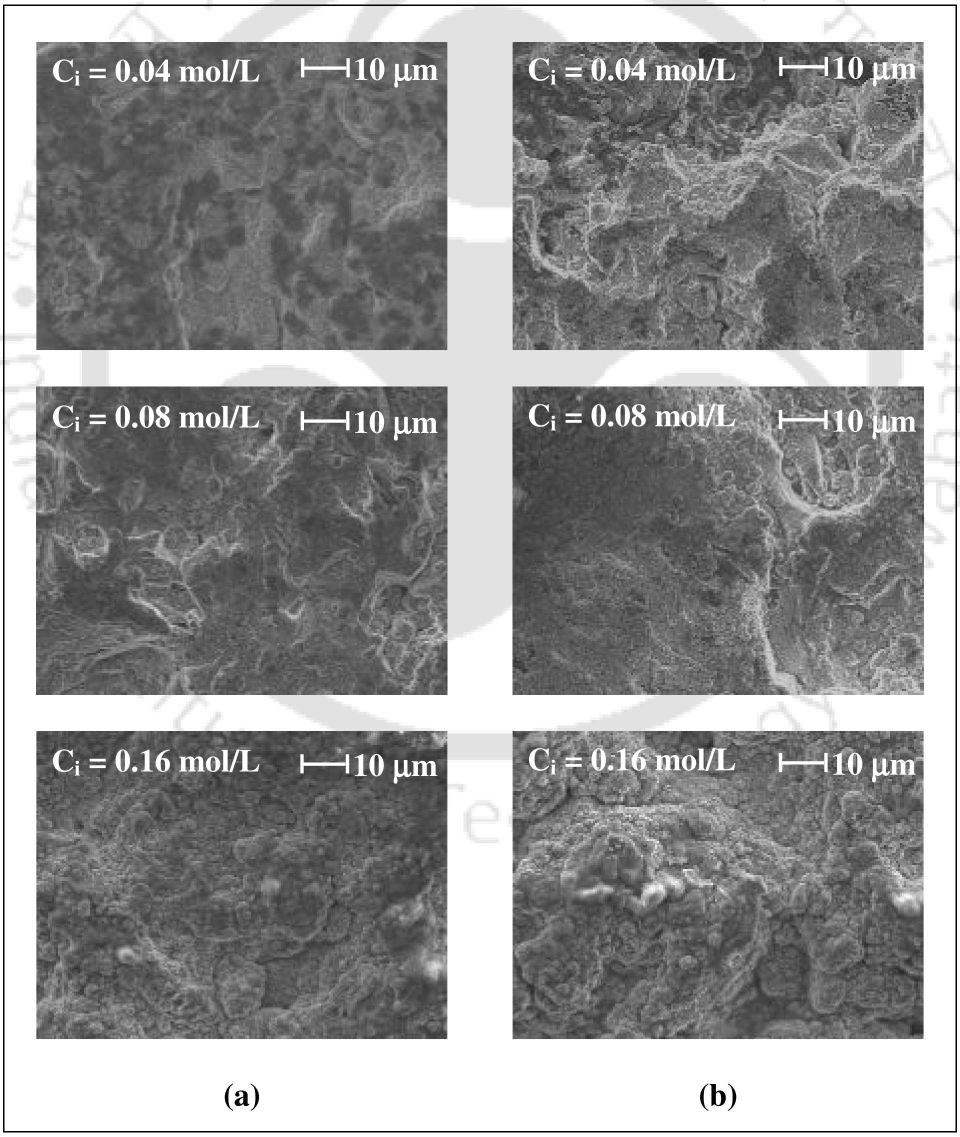

Fig. 4.12: Surface SEM micrographs (magnification: 1 KX) of composite membranes prepared in agitated hydrazine baths. (a) $\theta = 196$ cm^2/L; (b) $\theta = 393$ cm^2/L.

and loading ratios (196 and 393 cm^2/L). These micrographs indicate the presence of metallic nickel grains on the ceramic surface. It can be observed that the surface texture is strongly affected by the solution concentration than the loading ratio. Metal layer is not fully developed at lower solution concentration (0.04 mol/L) and hence the surfaces are non-uniform. A more uniformity in the metal coating is observed at a concentration of 0.08 mol/L and coarser nickel grains are resulted at the higher solution concentration (0.16 mol/L) for all stirrer speeds. Further, it is observed that stirring has a minimal effect on the coating morphology and higher stirrer speeds resulted in more uniform and smoother coatings.

The composite membranes prepared at various conditions and stirrer speeds were subjected to XRD analysis. Figure 4.13 presents the XRD pattern of the metal film deposited under good plating conditions (initial nickel concentration of 0.08 mol/L, stirring speed of 100 rpm and loading ratio of 393 cm^2/L). Similar XRD spectra were observed for the other cases also. Observed XRD peaks matches very closely with the relevant peaks associated to quartz (JCPDS: 01–075–0443 (A)) and nickel (JCPDS: 00–

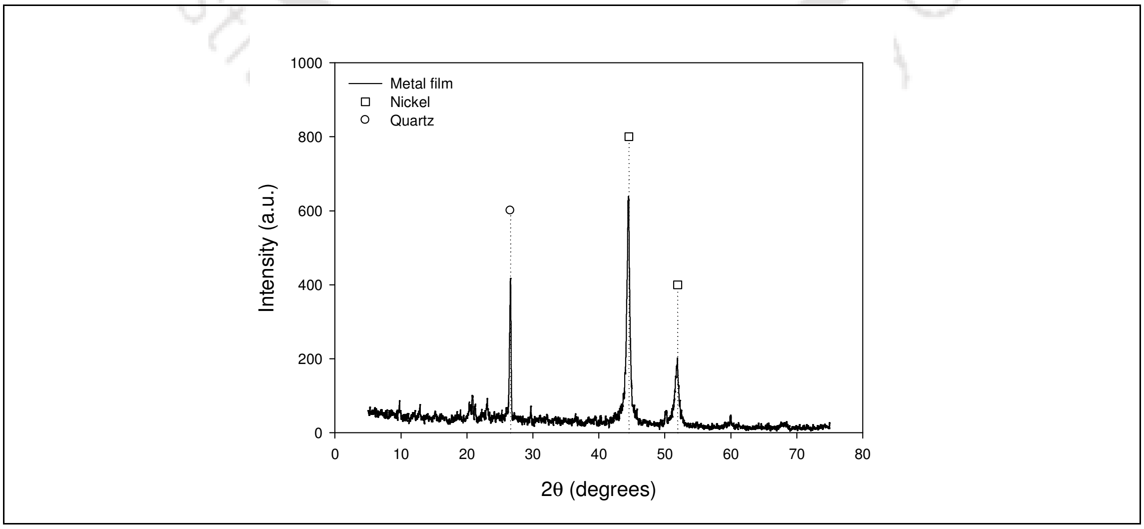

Fig. 4.13: XRD pattern of metal film deposited in agitated hydrazine baths. (C_i = 0.08 mol/L, θ = 393 cm^2/L and ω = 100 rpm).

001–1266 (D)). Presence of quartz, an ingredient of the ceramic substrate indicates that the metal film may be porous. This is further confirmed by the gas permeations experiments. The nature of the spectra indicates that the metal film resulting from the agitated hydrazine electroless plating baths is microcrystalline.

4.2.2.2 Permeation characteristics

4.2.2.2.1 Pore diameter

The data corresponding to the average pore diameter of composite membranes is presented in Table 4.7. As is presented, hydrazine based plating baths are effective to drastically reduce the average pore size of the surface from 275 nm to 82–15 nm. Some salient features to observe from these results are (a) the film pore size is not significantly dependent on the loading ratio (b) metal solution concentration plays a significant role in pore densification and (c) the effect of stirrer speed in enhancing pore densification is predominant at lower metal solution concentrations and is negligible at higher solution concentrations.

4.2.2.2.2 Effective porosity

Figure 4.14 presents the variation in effective porosity of the metal film with stirrer speed for various initial metal solution concentrations and loading ratios. For a loading

Table 4.7: Average pore size data for agitated hydrazine baths.

Stirring speed (rpm)	**Average pore size** (nm) **of composite membrane for various values of** C_i (mol/L)					
	$\theta = 196\ cm^2/L$			$\theta = 393\ cm^2/L$		
	0.04	0.08	0.16	0.04	0.08	0.16
0	82	41	14	94	49	22
50	66	32	16	81	41	20
100	59	26	14	72	36	18
200	53	28	15	67	34	20

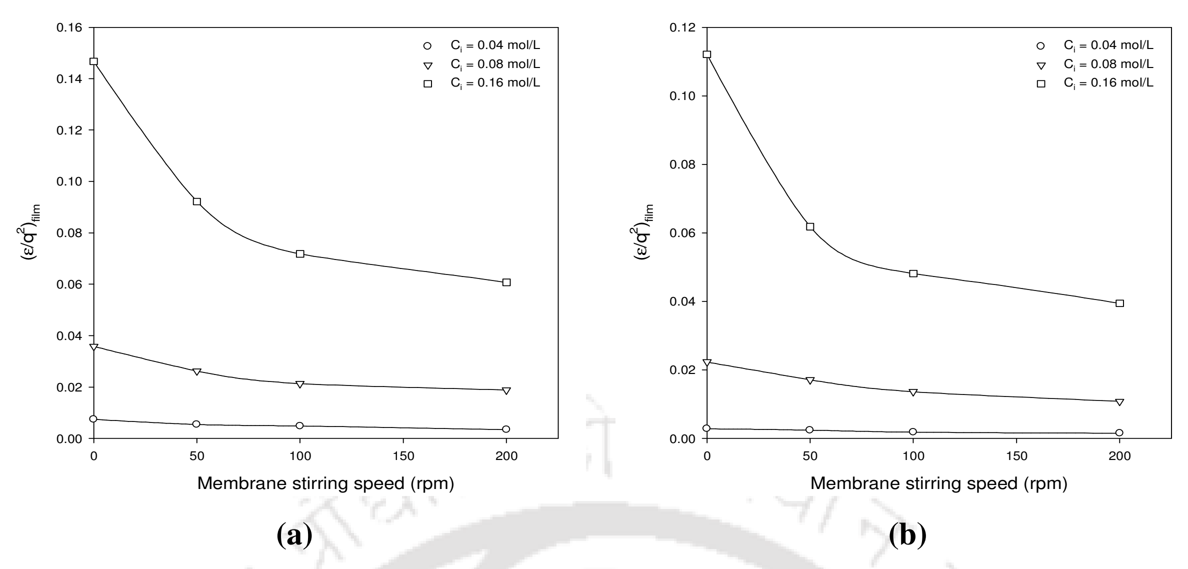

Figure 4.14: Effective porosity ($(\varepsilon/q^2)_{film}$) profiles for agitated hydrazine baths. (a) θ = 196 cm^2/L and (b) θ = 393 cm^2/L.

ratio of 196 cm^2/L, the effective porosity varied with the stirrer speed from 0 to 200 rpm as 0.007–0.003, 0.036–0.019 and 0.147–0.061 for the initial nickel concentrations of 0.04, 0.08 and 0.16 mol/L respectively. Corresponding values for the other loading ratio (393 cm^2/L) are 0.003–0.002, 0.022–0.011 and 0.112–0.039 respectively. It is observed that the effective porosity of the metal layer was strongly affected by all the three parameters (solution concentration, loading ratio and stirrer speed). Higher values of effective porosity are observed at higher solution concentration (0.16 mol/L) due to rapid generation of nitrogen at the surface. Membrane stirring as a mass transfer enhancement provides subsequent removal of gas bubbles at higher stirrer speeds resulting in lower values of effective porosity of the metal film. Initially there is a significant reduction in effective porosity values up to 100 rpm and thereafter, no significant reduction is observed by increasing the stirrer speed from 100 to 200 rpm. Hence, a stirrer speed of 100 rpm is found to be the optimal speed. Further, higher loading ratio (393 cm^2/L) is recommended as it produces less porous metal films with more uniformity which can be observed from the surface SEM images (Figure 4.12).

4.2.2.2.3 Percent pore densification

Figure 4.15 presents the variation of PPD with stirrer speed and initial metal solution concentration for the loading ratios of 196 and 393 cm^2/L. The PPD values varied between 88.4–99.7% for variation in metal solution concentration and loading ratio. The effect of loading ratio on PPD is insignificant when compared to the metal solution concentration. The observed PPD trends are similar to those obtained for conversion i.e., enhancement in PPD with stirrer speed is evident for both 0.04 and 0.08 mol/L initial nickel metal solution concentrations but not 0.16 mol/L initial nickel solution concentration. The PPD enhancement with stirrer speed is evaluated to be about 6% and 1.7% for initial metal solution concentrations of 0.04 and 0.08 mol/L respectively. All in all, it is apparent that mass transfer enhancement is required at lower nickel solution concentrations (0.04 and 0.08 mol/L) but not at the higher concentration (0.16 mol/L).

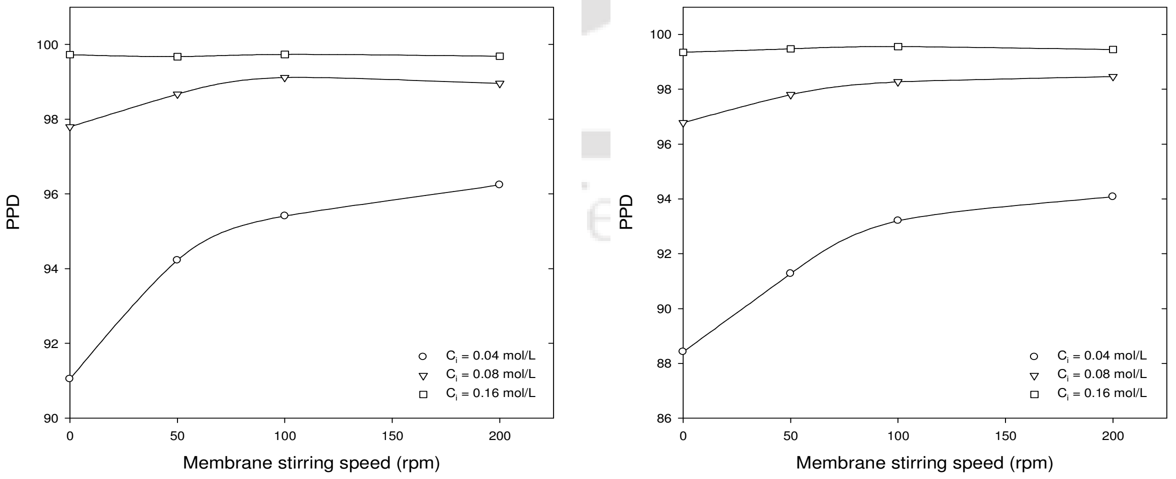

(a) **(b)**

Figure 4.15: PPD profiles for agitated hydrazine baths.
(a) $\theta = 196$ cm^2/L and (b) $\theta = 393$ cm^2/L.

4.2.2.2.4 Film thickness

Table 4.8 presents the variation in average thickness of the nickel layer with stirrer speed for various values of initial metal solution concentration and loading ratios evaluated using Eq. (2.12). The porous nickel film thickness varied from 2.34–55.17 μm. The porous nickel film thickness is observed to be more strongly dependent on the solution concentration as well as loading ratio. A near inversely proportional dependence of thickness is observed with the loading ratio at higher metal solution concentration thereby indicating that higher amount of metal in the solution provides nickel films with higher thickness. Stirring contributes to about 20–30% additional enhancement in the metal film thickness, thereby indicating greater metal transport to the membrane surface. The observed data trends in thickness indicate that electroless plating is capable to provide thicker nickel films as intermediate diffusion barriers that are required for better mechanical strength and permeation characteristics.

4.3 Summary and conclusions

In this work, a systematic study is presented that targets the measurement of combinatorial performance characteristics of agitated electroless plating baths for the fabrication of microfiltration range nickel–ceramic composite membranes. The

Table 4.8: Average film thickness data for agitated hydrazine baths.

Stirring speed (rpm)	**Average nickel layer thickness** (μm) **for various values of C_i** (mol/L)					
	$\theta = 196$ cm^2/L			$\theta = 393$ cm^2/L		
	0.04	0.08	0.16	0.04	0.08	0.16
0	3.79	13.70	47.93	2.34	7.79	26.78
50	4.38	15.26	51.42	2.72	8.38	28.44
100	4.81	16.06	53.78	2.95	8.81	29.60
200	5.03	16.44	55.17	3.09	9.02	33.00

combinatorial performance characteristics are evaluated in terms of conversion, plating efficiency, metal film thickness, average pore diameter and PPD.

A comparative assessment of the performance of the two reducing agents in agitated electroless plating baths is presented in Table 4.9. From this table (Table 4.9), it can be noticed that the hydrazine based electroless plating baths result in higher values of conversion, efficiency, PPD, metal film thickness and average mass transfer coefficient indicating that these are superior to hypophosphite baths. Lack of competence of hypophosphite based electroless plating baths with hydrazine based baths even under agitation is due to the basic problem of hydrogen generation in the prior case. However, the optimal values of the process parameters namely concentration, loading ratio and stirrer speed are found to be the same (0.08 mol/L, 393 cm^2/L and 100 rpm respectively) for both the cases.

The mean pore diameter of the nickel–ceramic composite membrane as obtained from the gas permeation experiments is also confirmed by the surface FESEM micrographs (Figure 4.16). Further, it can be observed from the Figure 4.16 that agitation

Table 4.9: Comparison between agitated hypophosphite and hydrazine baths.

Parameter	**Agitated hypophosphite baths**	**Agitated hydrazine baths**
Conversion (%)	12.5–44.0	17–58.5
Efficiency (%)	96.9–41.9	99.2–74.1
Pore diameter (nm)	100–59	81–14
PPD (%)	86.7–95.5	91.3–99.7
Porosity of metal layer	0.001–0.028	0.002–0.092
Thickness (μm)	1.8–20.5	2.7–41.9
Average mass transfer coefficient, $\overline{k}$ (s^{-1})	60–154	104–573
Optimal concentration (mol/L)	0.08	0.08
Optimal loading ratio (cm^2/L)	393	393
Optimal stirrer speed (rpm)	100	100

results in smoother surface of the metal film than the base case (Figure 3.17) and the surface smoothness increases with increasing the stirrer speed from 50 to 200 rpm. A

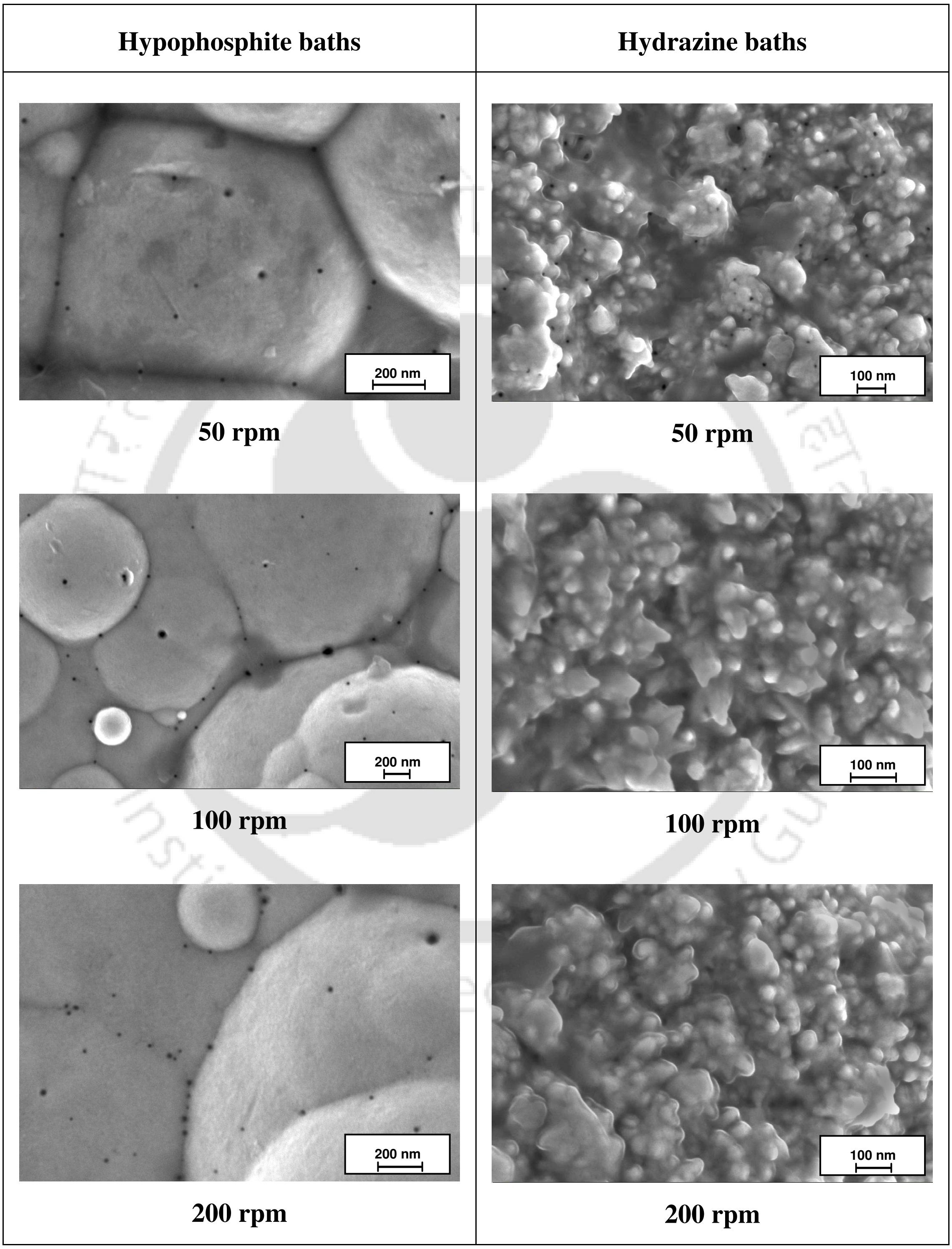

Figure 4.16: Surface FESEM micrographs of composite membranes prepared in agitated electroless plating baths. ($C_i = 0.16$ mol/L and $\theta = 196$ cm^2/L).

number of pin holes are observed on the surfaces of the nickel films deposited in hypophosphite baths, which is not the case with hydrazine baths.

Based on thorough experimental investigations, it is found that the bath agitation by means of membrane stirring improves the performance of electroless plating baths but results in lower plating efficiencies compared to the base case. The following observations have been concluded from the experimental investigations.

a) Based on conversion, plating efficiency, PPD, metal thickness, average reaction rates, the optimal conditions of electroless plating for both the reducing agents are initial nickel solution concentration of 0.08 mol/L, stirrer speed of 100 rpm and a loading ratio of 393 cm^2/L.

b) The influence of loading ratio is significant on the parameters such as metal film thickness and effective porosity but not with respect to the other parameters such as average metal film pore size, conversion, plating efficiency and PPD.

c) Mass transfer enhancement in the form of membrane stirring brings about 20–56% enhancement in the average nickel deposition rate (efficient plating). Stirred electroless hypophosphite baths do not function efficiently at higher stirrer speeds and higher solution concentrations. This is attributed to the enhanced nucleation under these conditions in the solution, which contributes significantly to inefficient metal plating.

d) Even with the well known versatility of nickel–hypophosphite plating baths in metal finishing industries, these baths are characterized with low conversions (10–44%), moderately good plating efficiencies (42–99%) and PPD values (78–96%). Therefore, further improvement to the plating process that target doubling conversions while maintaining similar trends in plating efficiencies and PPD values is desired.

e) Data analysis based on air permeation experiments is a novel approach that can effectively capture the quality of metal plating on membrane surfaces. The approach can eventually replace the usually followed convention of physical examination using scanning electron and atomic force microscopy methods.

f) The approach presented in this work can be used as a new methodology for the assessment of nickel electroless plating baths with variant process parameters and conditions of operations.

The effect of process parameters such as concentration and loading ratio on the performance characteristics of the nickel–ceramic composite membranes is presented in the previous chapter (Chapter 3) while studies on the effect of mass transfer enhancement through membrane rotation is presented in this chapter. The next chapter (Chapter 5) presents the effect of sonication on the performance of electroless plating baths. Finally, the performance of electroless plating baths under hydrothermal conditions is presented in Chapter 6.

PERFORMANCE CHARACTERISTICS OF ULTRASONIC ELECTROLESS PLATING BATHS

In this chapter, the results are presented in two sections. The first section summarizes the performance characteristics of sonication assisted hypophosphite based electroless plating baths and the second section elaborates upon the effect of sonication on the performance characteristics of hydrazine based electroless plating baths. A few cases of stirring are also shown along with the sonication results for comparison purpose.

5.1 Ultrasonic hypophosphite electroless plating baths

5.1.1 Efficacy of sonication assisted electroless plating

The plating experiments were carried out using the typical setup shown in Figure 2.8c (Chapter 2) to evaluate the performance characteristics of ultrasonic electroless plating baths. Figure 5.1 presents the effect of initial nickel solution concentration on conversion for various cases namely the base case (conventional electroless plating), strirring at 100 and 200 rpm and sonication. For all cases, conversion increases with the solution concentration and the sonication assisted baths provided better conversion profiles than the base case as well as stirring. The conversions obtained for sonication assisted electroless plating baths (28–76%) are almost twice compared to the base case (10–39%) and are far better than the cases with stirring (15–44%). Bath loading has no significant effect (4–5.5%) on conversion since the obtained profiles are similar for both the loading ratios 196 and 393 cm^2/L. Similar trends in conversion profiles were indicated by Jiang et al. [105]. This is because of the fact that ultrasonic waves could enhance the rate of electroless plating due to the cavitation effect.

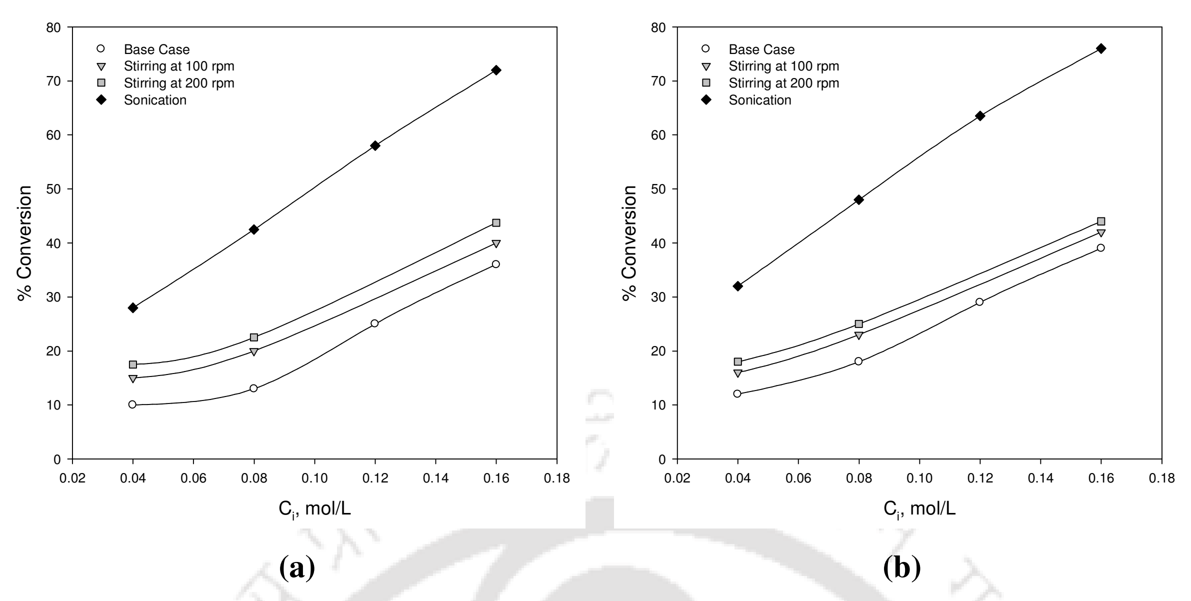

(a) **(b)**

Figure 5.1: Conversion profiles for ultrasonic hypophosphite baths. (a) $\theta = 196$ cm^2/L; (b) $\theta = 393$ cm^2/L.

Figure 5.2 presents the variation of plating efficiency with initial nickel solution concentration (0.04–0.16 mol/L) for various cases and loading ratios of 196 and 393 cm^2/L. From this figure, it can be observed that the plating efficiency reduced with stirring speed (95.5–41.9%) while it is slightly improved for the sonication assisted baths (99.5–66.2%) when compared to the base case (99.3–61.7%). For all the cases, plating efficiency decreased significantly with increasing the solution concentration from 0.04 to 0.16 mol/L. Bath loading slightly affects the plating efficiency and a higher loading ratio (393 cm^2/L) is recommended for efficient plating. These observations are in good agreement with those indicated conceptually by Wu et al. [78], Lu [110] and Touyeras et al. [111]. They inferred that ultrasonic degassing promotes the adhesion of metal deposition to the substrate surface by removing gas bubbles (hydrogen) immediately after generation during electroless plating process. Touyeras et al. [111] also inferred that ultrasonic irradiation improves deposit adhesion strength by decreasing internal stress. Therefore, sonication is

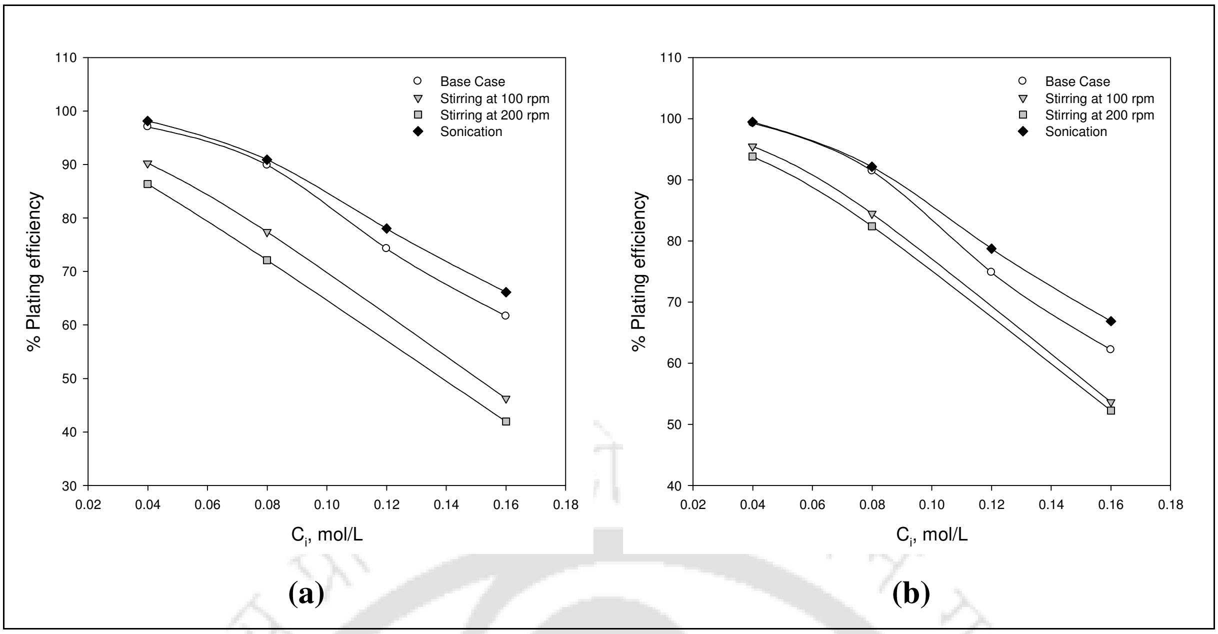

(a)

(b)

Figure 5.2: Efficiency profiles for ultrasonic hypophosphite plating baths. (a) $\theta = 196$ cm^2/L; (b) $\theta = 393$ cm^2/L.

expected to improve the plating efficiency as it provides better adhesion of depositing metal to the surface of the substrate.

The possible reason for significant reduction in metal plating efficiency is accounted for the peeling of deposited metal from the substrate at high stirrer speeds (100–200 rpm) as well as significant depositions on the beaker surface and in the plating solution at higher initial nickel solution concentrations. If a minimum plating efficiency of 90% is desired, then the optimal conditions of operation would refer to 0.08 mol/L initial nickel solution concentration and a loading ratio of 393 cm^2/L. This corresponds to about 48% metal conversion and 92.1% plating efficiency. In other words, it appears that sonication can be regarded as a potential mass transfer coupling process for hypophosphite based electroless plating baths.

Table 5.1 presents the selective conversion (defined as the product of fractional conversion and percent plating efficiency) data for various cases and loading ratios (196 and 393 cm^2/L). It can be seen from the table that the selective conversion is about 9.7–

Table 5.1: Selective conversion data for ultrasonic hypophosphite baths.

Case study	**Selective conversion** (%) **for various values of** C_i (mol/L)							
	θ = 196 cm^2/L				θ = 393 cm^2/L			
	0.04	0.08	0.12	0.16	0.04	0.08	0.12	0.16
Base case	9.7	11.7	18.6	22.2	11.9	16.5	21.7	24.3
Stirring at 100 rpm	13.5	15.5	–	18.5	15.3	19.4	–	22.5
Stirring at 200 rpm	15.1	16.2	–	18.3	16.9	20.6	–	23.0
Sonication	27.5	38.6	45.3	47.6	31.8	44.2	50.0	50.8

24.3% for the base case, which is far lower than that acceptable for good industrial performance. Stirring brought about some considerable improvement in selective conversion at lower concentrations (0.04–0.08 mol/L) but not at higher concentration (0.16 mol/L). Sonication results in a tremendous increase in selective conversion even at higher concentrations due to simultaneous improvement in bath conversion without compromising upon plating efficiency, which is well desired for efficient metal utilization. For instance, sonication provided 230% excess selective conversion compared to the base case at an initial nickel solution concentration of 0.08 mol/L and a loading ratio of 196 cm^2/L. Selective conversions as high as 50% are achieved at higher concentrations (0.12–0.16 mol/L) with higher loading ratio (393 cm^2/L).

Figure 5.3 presents the effect of average solution concentration on average nickel deposition rate (mol/L.s) at two different loading ratios (196 and 393 cm^2/L). From this figure, it is evident that the deposition rate in sonication assisted electroless plating baths is twice faster than all other cases including stirring. These observations are in good agreement with the trends indicated by Kathirgamanathan [69] who inferred that sonication enhances metal deposition rate and improves adhesion of the metal to the membrane surface. However, insights with respect to the metal film properties such as porosity and pore size were not addressed by the author.

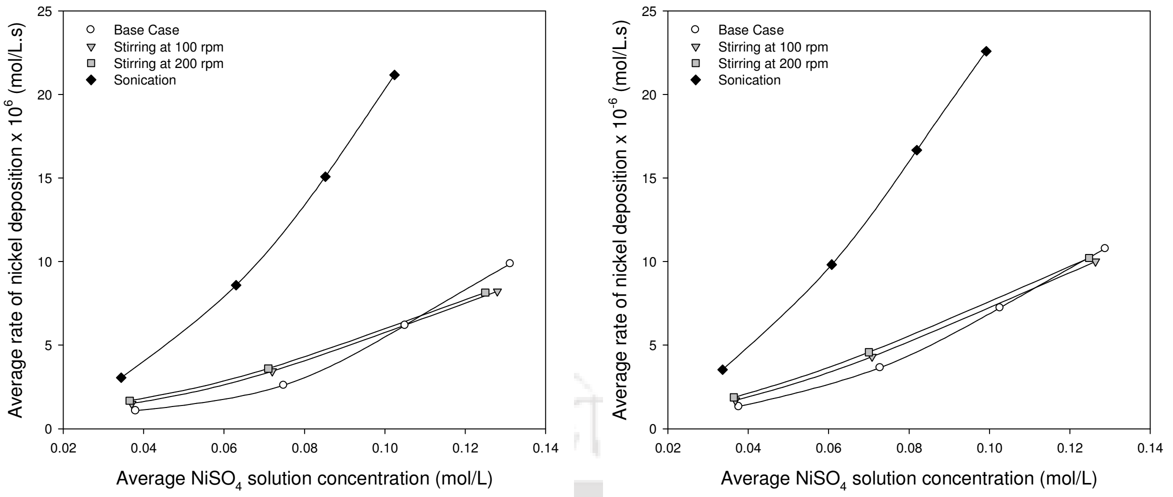

(a) **(b)**

Figure 5.3: Average deposition rate profiles for ultrasonic hypophosphite baths. (a) θ = 196 cm^2/L; (b) θ = 393 cm^2/L.

Table 5.2 presents the model parameters obtained from the non-linear regression analysis for sonication assisted hypophosphite based electroless plating baths. It can be observed that the average nickel mass transfer coefficient ($\bar{k}$) is between 195–370 s^{-1} and 214–423 s^{-1} for the loading ratios of 196 and 393 cm^2/L respectively. These values are significantly higher than the base case (37–137 s^{-1}) and stirring (50–154 s^{-1}). Stirring improved $\bar{k}$ values significantly at lower concentrations but not at high concentrations (Table 4.6). However, sonication results in a tremendous increase in the mass transfer coefficient ($\bar{k}$) values for all the concentrations. On the other hand, no significant change in the partition coefficient ($\bar{\gamma}$) values is observed. Bath loading ratio (θ) has no significant effect on the model parameters.

Table 5.2: Model parameters for ultrasonic hypophosphite baths.

θ (cm^2/L)	$\bar{C}_B$ (mol/L)	$\bar{k}$ (s^{-1})	$\bar{\gamma}$	**% Error** ×10^5
196	0.034	194.6	989.1	3.69
196	0.063	282.5	991.5	4.61
196	0.085	346.3	1013.1	4.58
196	0.102	370.5	1033.5	5.03
393	0.034	214.4	994.0	2.56
393	0.061	296.1	998.6	4.26
393	0.082	375.5	1027.5	4.91
393	0.099	422.8	1051.3	4.38

5.1.2 Metal–ceramic membrane characteristics

5.1.2.1 Surface characterization

The surface characterization was carried out using scanning electron microscopy (SEM) (LEO 1430VP). Figure 5.4 presents the surface SEM micrographs for all membranes fabricated in sonication bath at various nickel solution concentrations (0.04–0.16 mol/L) and loading ratios (196 and 393 cm^2/L). These micrographs indicate the presence of metallic nickel grains on the ceramic surface. Well-developed nickel layers are obtained at higher nickel solution concentrations. The pore characterization of the membranes is anticipated from air permeation data presented in Section 5.1.2.3.

The composite membranes were also subjected to X-ray diffraction (XRD) (Bruker AXS, D8 ADVANCE) study. Figure 5.5 presents the XRD pattern of the metal film deposited in sonication assisted plating bath at an initial nickel concentration of 0.08 mol/L and a loading ratio of 393 cm^2/L which matches very closely with the relevant peaks associated to quartz (JCPDS: 01–075–0443 (A)) and nickel (JCPDS: 00–001–1266 (D)). The nature of the spectra indicates that the deposited metal layer is amorphous. The presence of quartz peaks further confirms that the metal film might be porous.

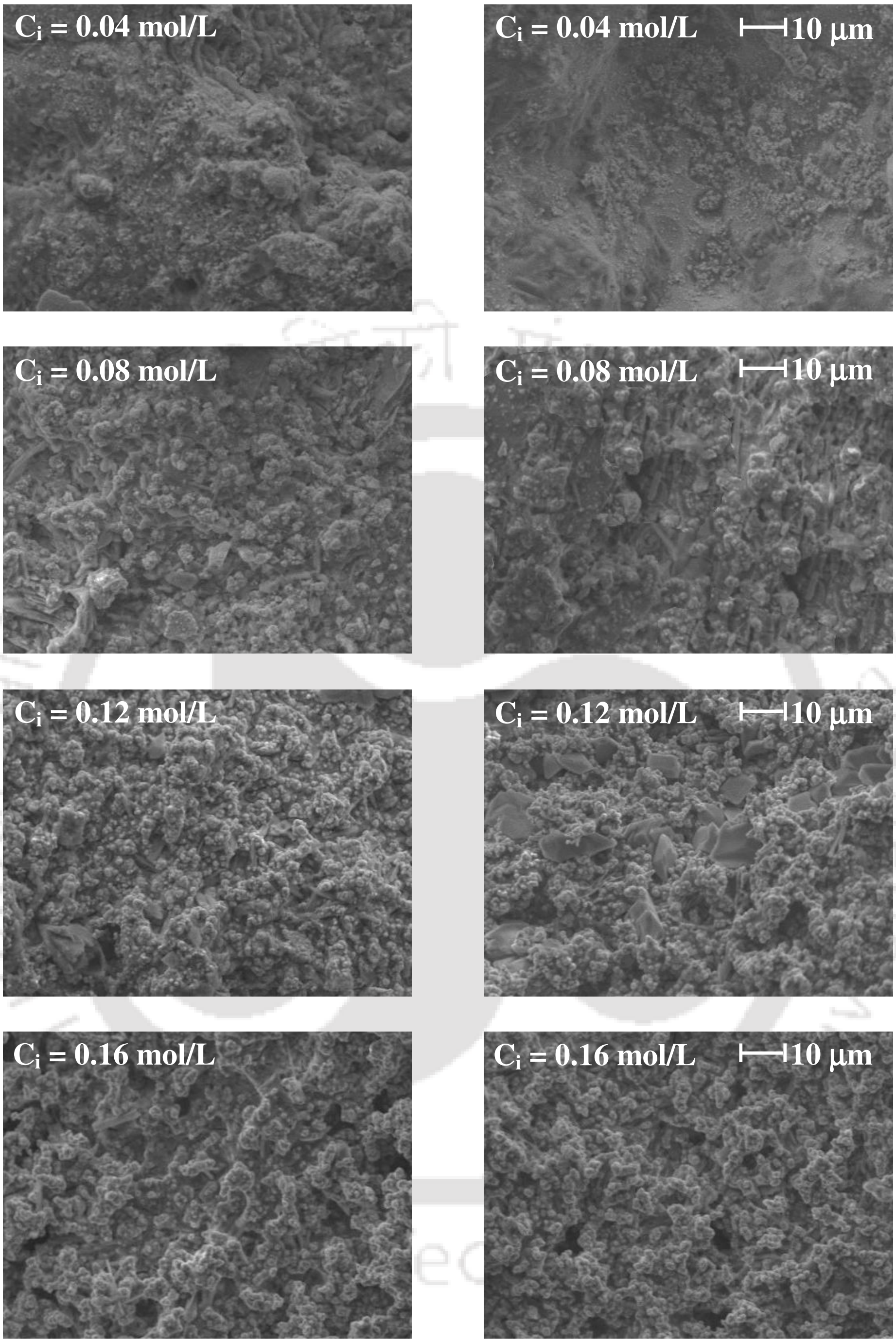

(a) **(b)**

Figure 5.4: Surface SEM micrographs (magnification: 1 KX) of composite membranes prepared in ultrasonic hypophosphite baths. (a) $\theta = 196$ cm^2/L; (b) $\theta = 393$ cm^2/L.

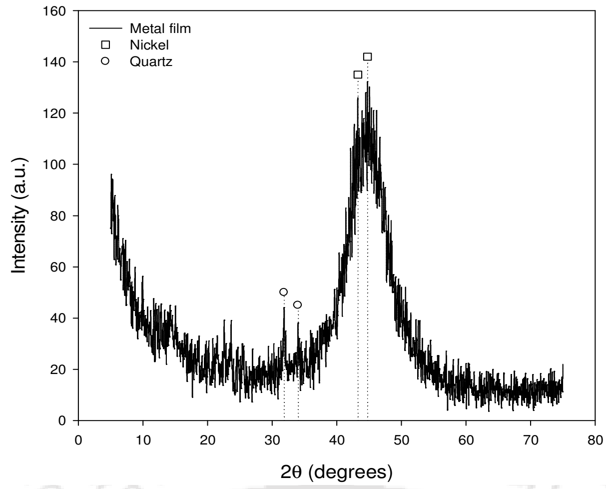

Figure 5.5: XRD pattern of metal film deposited in ultrasonic hypophosphite baths. ($C_i = 0.08$ mol/L and $\theta = 393$ cm^2/L).

This observation is also evident from the permeation experiments for estimating average pore size and porosity of the composite membranes. Similar XRD patterns were observed for the other membranes prepared at different conditions of plating.

5.1.2.2 Film thickness

Tables 5.3 presents the variation of nickel layer thickness (evaluated using Eq. (2.12)) with initial metal solution concentration for various cases with loading ratios of 196 and 393 cm^2/L. Metal layer thickness is strongly affected by the initial $NiSO_4$ concentration. Thickness increases nonlinearly with solution concentration indicating that it is related to several other factors including bath conversion and plating efficiency. It can be observed that at lower metal solution concentrations (0.04–0.08 mol/L), stirring contributed to significant enhancement in film thickness, which is not the case for higher metal solution concentration (0.16 mol/L) where in the metal film thickness reduced due to inefficient plating. Sonication improves the metal film thickness tremendously irrespective of the solution concentration due to enhanced plating rate and efficient

Table 5.3: Film thickness data for ultrasonic hypophosphite baths.

Case study	**Thickness** (µm) **for various values of** C_i (mol/L)							
	θ = 196 cm^2/L				θ = 393 cm^2/L			
	0.04	0.08	0.12	0.16	0.04	0.08	0.12	0.16
Base case	2.6	6.3	15.2	24.5	1.6	4.4	8.8	13.1
Stirring at 100 rpm	3.6	8.4	–	20.2	2.0	5.2	–	12.1
Stirring at 200 rpm	4.0	8.7	–	20.0	2.3	5.5	–	12.4
Sonication	7.3	20.8	36.6	51.5	4.2	11.8	20.1	27.3

deposition. Also, it can be observed that the film thickness is strongly influenced by the loading ratio values i.e., doubling the loading ratio (from 196 to 393 cm^2/L) contributes to a reduction in the metal film thickness by about 50% for all the cases (from 2.6–51.5 to 1.6–27.3 µm). Maximum film thickness (51.5 µm) is observed for the sonication assisted electroless plating bath with C_i = 0.16 mol/L and θ = 196 cm^2/L. In summary, it is observed that sonication greatly influences the metal film thickness than membrane stirring at similar process parameters (solution concentration and loading ratio) during the fabrication of metal–ceramic composite membranes by electroless deposition technique. As lower metal film thickness is always preferred for composite membranes to enable better separation characteristics, a higher loading ratio (θ = 393 cm^2/L) can be recommended for this purpose.

5.1.2.3 Permeation characteristics

Figure 5.6 illustrates the effective permeability factor (K) versus P_{avg} data at a loading ratio of 393 cm^2/L and initial nickel solution concentrations of 0.04, 0.08 and 0.16 mol/L respectively. Similar data trends are obtained for the case of lower loading ratio (196 cm^2/L) also. For all the cases, it can be observed that the permeability coefficient values are the lowest for sonication case compared to membrane stirring and base case.

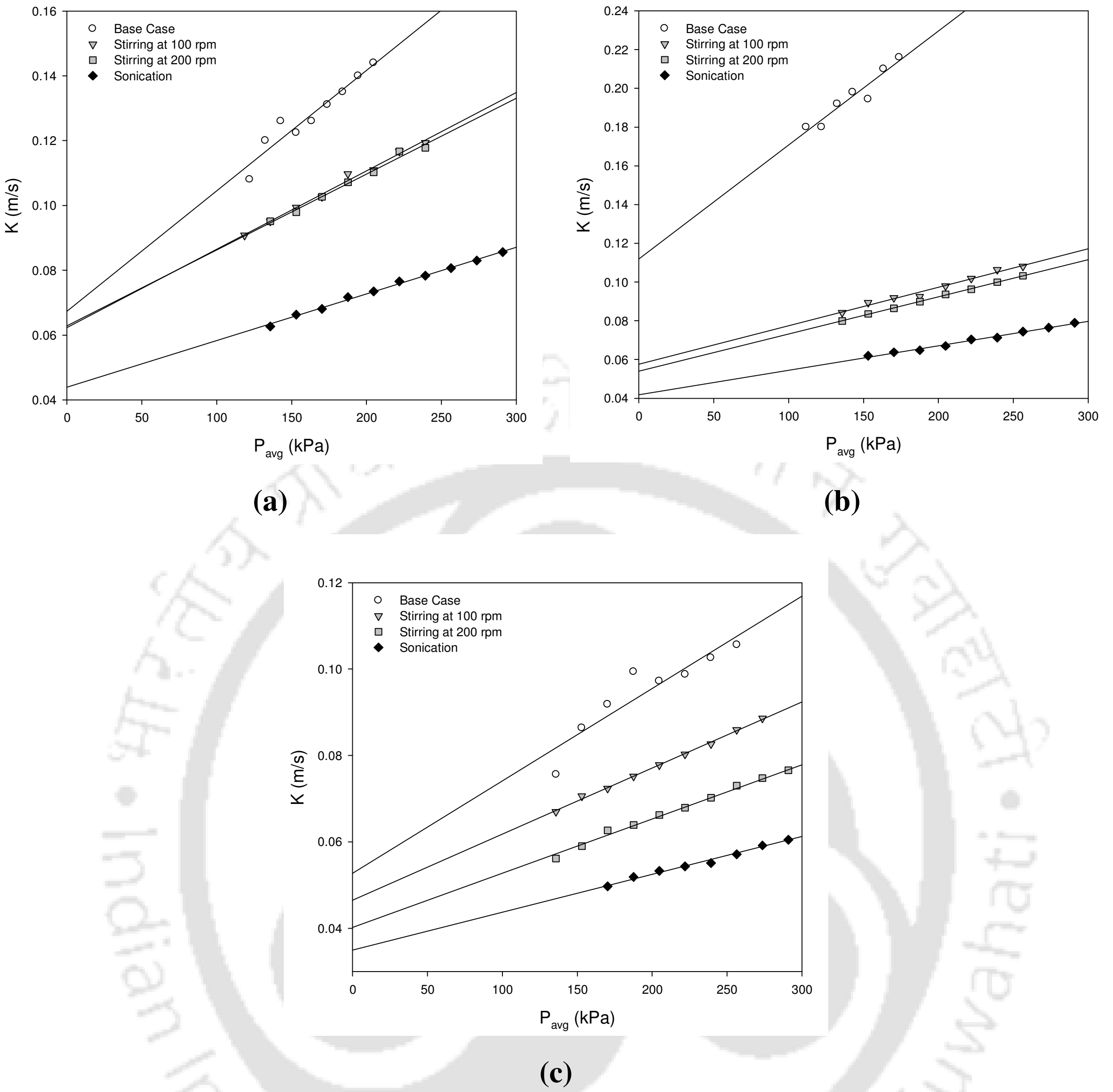

(a) **(b)**

(c)

Figure 5.6: Plots of effective permeability factor (K) versus average pressure (P_{avg}) for membranes synthesized at various conditions in hypophosphite baths ($\theta = 393\ cm^2/L$). (a) 0.04 mol/L; (b) 0.08 mol/L; (c) 0.16 mol/L.

This observation indicates that sonication assisted electroless plating baths result in membranes with lowest values of average pore size. Further, it can be observed that identical permeability coefficient profiles exist for both membrane-stirring cases of 100 rpm and 200 rpm at a lower solution concentration of 0.04 mol/L (Figure 5.6a). This observation indicates that higher stirrer speeds are not necessary for lower solution concentrations (0.04–0.08 mol/L). Therefore, it is apparent that the permeation characteristics of the metal film are largely influenced by the type of mass transfer enhancement as well as solution concentration.

5.1.2.3.1 Pore diameter

The data corresponding to the average pore diameter of composite membranes evaluated from gas permeation experiments (using equation 6) are presented in Figure 5.7. As presented in this figure, hypophosphite based plating baths are effective to significantly reduce the average pore size of the surface from 275 nm to 128–54 nm. Sonication enables better reduction in pore size than membrane stirring especially at higher loading ratio (393 cm^2/L). Solution concentration plays a significant role in pore size reduction. However, it is important to note that the film pore size does not significantly dependent upon the loading ratio (as the film thickness did). Hence a higher loading ratio (θ = 393 cm^2/L) is recommended for efficient and cost effective fabrication.

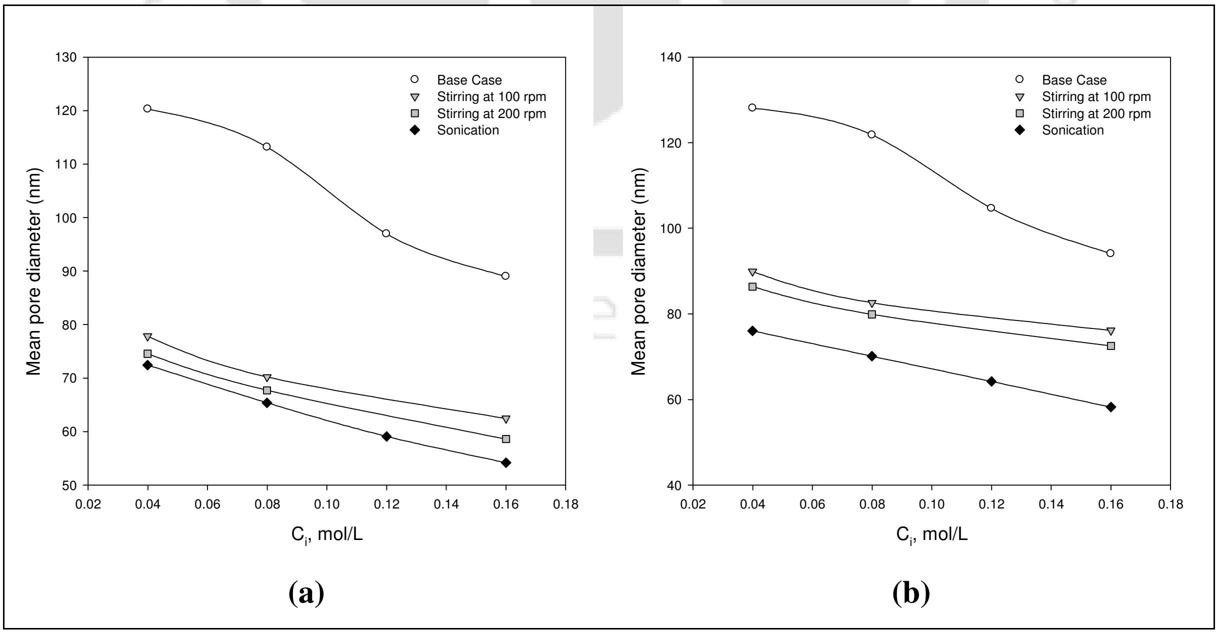

(a) **(b)**

Figure 5.7: Pore size profiles for ultrasonic hypophosphite plating baths. (a) $\theta = 196$ cm^2/L; (b) $\theta = 393$ cm^2/L.

5.1.2.3.2 Effective porosity

Figures 5.8a and 5.8b present the change in metal film effective porosity with initial metal solution concentration for the loading ratios of 196 and 393 cm^2/L respectively. It can be observed that the bath concentration as well as loading ratio significantly affects the effective porosity values. For all cases, the effective porosity values obtained for lower loading ratio (196 cm^2/L) are nearly twice to those obtained for the higher loading ratio (393 cm^2/L) and increase with the solution concentration. A non-linear dependence of porosity values on initial nickel solution concentration is noticed. For both loading ratios, sonication resulted in significantly lower values of effective porosity than the other cases. Theoretically, uniformity of metal deposition that results in a dense membrane shall have a value of zero effective porosity. Higher values of effective porosity at higher concentrations even with sonication are indicative of the existence of fundamental problem of surface shear induced by hydrogen generation during the reaction. Therefore, possible alterations to minimize the hydrogen production rate at the surface need to be

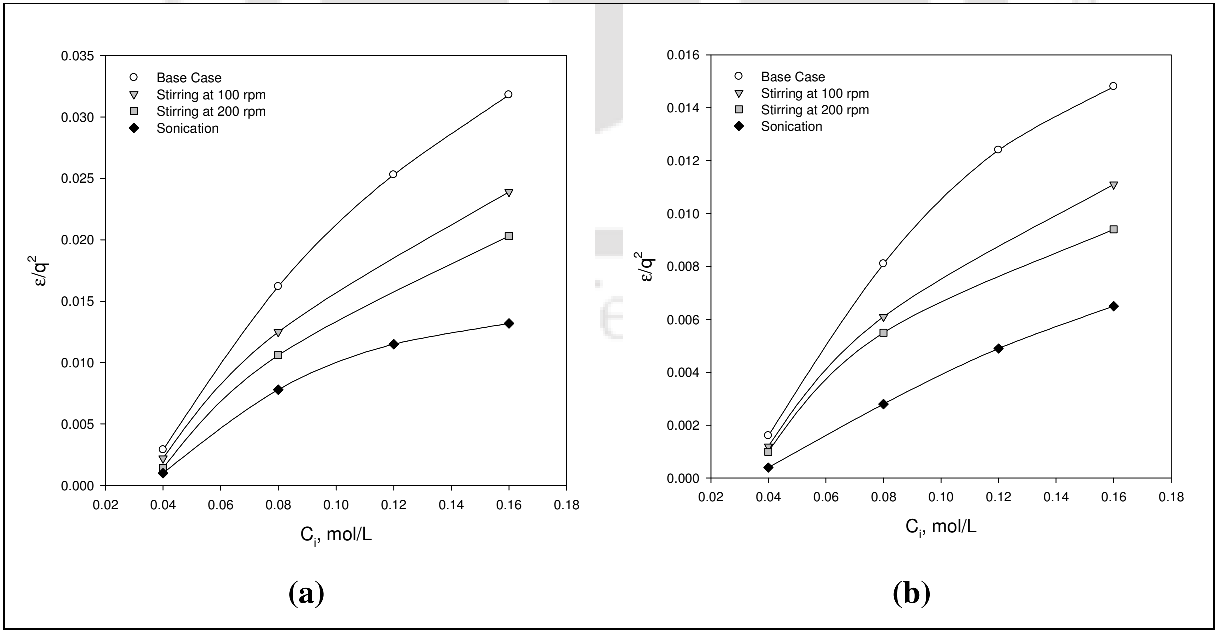

(a) (b)

Figure 5.8: Porosity profiles for ultrasonic hypophosphite plating baths.
(a) θ = 196 cm^2/L; (b) θ = 393 cm^2/L.

investigated. All in all, it is observed that the uniformity in metal deposition is strongly influenced by initial metal solution concentration, loading ratio and mass transfer enhancement techniques.

5.1.2.3.3 Percent pore densification

Percent pore densification (PPD), a measure of pore size reduction is an important parameter for composite membranes. Figures 5.9a and 5.9b present the change in PPD values for various cases with initial nickel solution concentration for the loading ratios of 196 and 393 cm^2/L respectively. It is observed that mass transfer enhancements (stirring and sonication) favor PPD predominantly at lower metal solution concentrations and sonication provides significant enhancement in PPD. In summary, it is observed that comparatively lower values of PPD (78–96 %) are obtained despite conducting 8 hours of sequential plating in sodium hypophosphite baths. This is again an indication of the basic problem of hydrogen generation at the membrane surface and its contribution of induced shear stress to PPD.

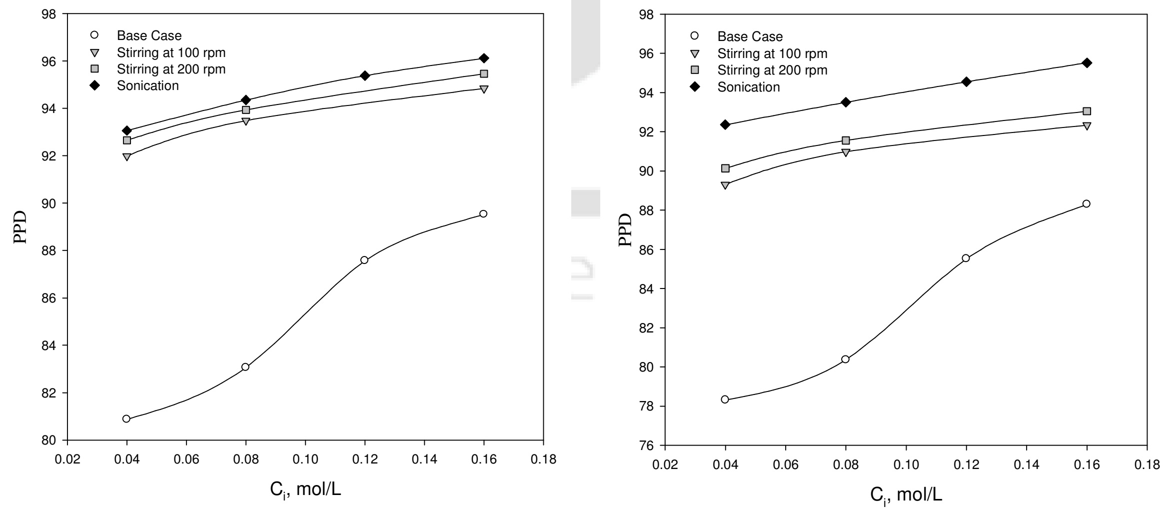

(a) **(b)**

Figure 5.9: PPD profiles for ultrasonic hypophosphite plating baths.
(a) θ = 196 cm^2/L; (b) θ = 393 cm^2/L.

5.1.2.3.4 PPD and efficiency tradeoffs

The efficient design of electroless plating process needs to maximize both PPD and efficiency. However, a tradeoff between PPD and efficiency exists because higher plating efficiency does not contribute to good quality of plating and vice-versa. Figure 5.10 presents the PPD versus efficiency trade offs for both loading ratio values considered in this work. It can be observed that sonication assisted plating baths provide better PPD profiles than all the other cases. Though stirring improved the PPD values to a significant extent, it suffered from a significant reduction in plating efficiencies. On the other hand, sonication results in a simultaneous improvement in both PPD as well as plating efficiency. Lower loading ratio (196 cm^2/L) enables better pore densification while higher loading value (393 cm^2/L) provides more efficient plating. This is possibly due to the fact that larger amount of plating solution (at lower loading ratio) enables greater nucleation of nickel metal in the solution at higher solution concentrations and therefore maximizes the probability of nickel deposition in the solution than the substrate. It is further interesting to

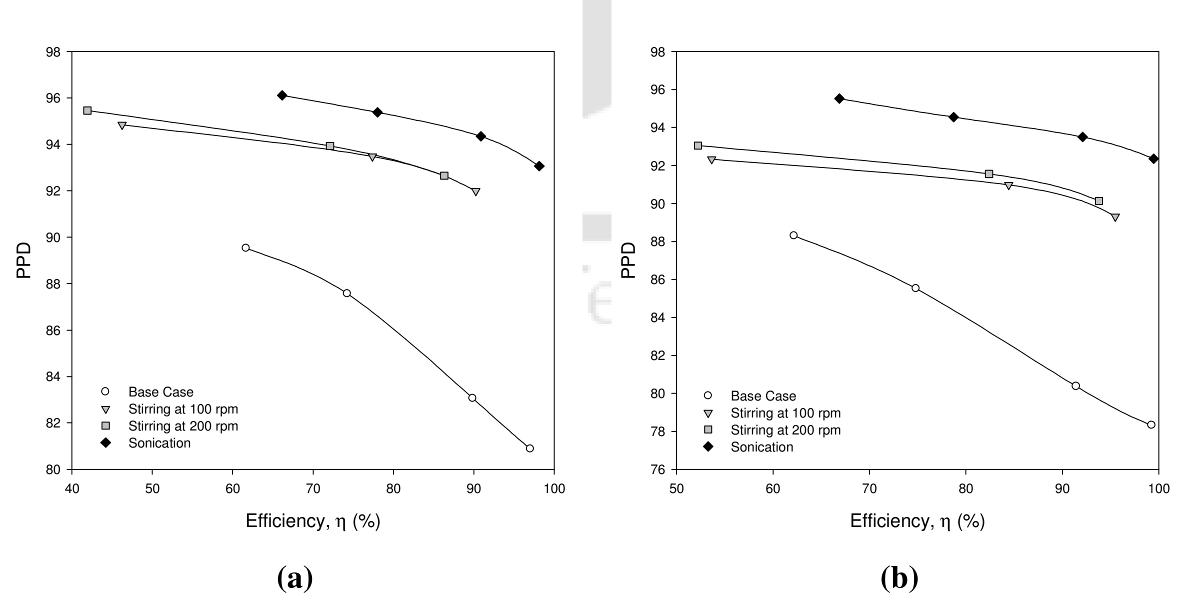

Figure 5.10: Plots of PPD versus efficiency for ultrasonic hypophosphite baths. (a) θ = 196 cm^2/L; (b) θ = 393 cm^2/L.

note that sonication provides plating efficiency values similar to those obtained for the base case, which is not the case with membrane stirring.

5.1.3 Summary

This work addresses the effect of process parameters and mass transfer enhancement techniques on the properties of the porous nickel metallic films fabricated by ultrasonic electroless plating using sodium hypophosphite baths. The following conclusions are obtained from the experimental as well as theoretical investigations. Firstly, the selective conversion of nickel–hypophosphite plating baths for all the cases without sonication is too low (<25%) even at higher nickel concentrations (0.16 mol/L). Secondly, sonication contributes significantly towards maintaining higher plating efficiency, selective conversion, faster plating rate, higher metal thickness and lower values of effective porosity. Thirdly, it is observed that the mass transfer limitations are very effectively handled by sonication than membrane stirring. Finally, despite carrying out eight 1-hour sequential depositions using sonication assisted hypophosphite baths, the average pore size of the skin layer only reaches the value of 54 nm. Corresponding values of effective porosity and thickness of the nickel film are 0.013 and 51.5 μm respectively. All these observations indicate that the inherent limitation of shear stress induced due to hydrogen generation which needs to be addressed in both fundamental and applied research in the field of nickel–hypophosphite electroless plating baths.

5.2 Ultrasonic hydrazine electroless plating baths

5.2.1 Efficacy of sonication assisted electroless plating

Figure 5.11 presents the variation in conversion with initial nickel solution concentration for various cases for the loading ratios of 196 and 393 cm^2/L. For all the cases, conversion increases with solution concentration and the sonication assisted baths provides better conversion profiles than the other cases. The conversions obtained for sonication assisted electroless plating baths (30–80%) are far better than those of the base case (14.5–54%) and stirring (19–58.5%). Bath loading has no significant effect (3.5–5%) on conversion as the obtained profiles are similar for both the loading ratios (196 and 393 cm^2/L).

Lu [110] found that ultrasonic coupling during electroless copper plating generates a specific agitation resulting from the cavitation phenomenon that results in high quality metal coating. Touyeras et al. [111] also showed that ultrasound irradiation improves deposit adhesion strength by decreasing internal stress. Therefore, sonication would

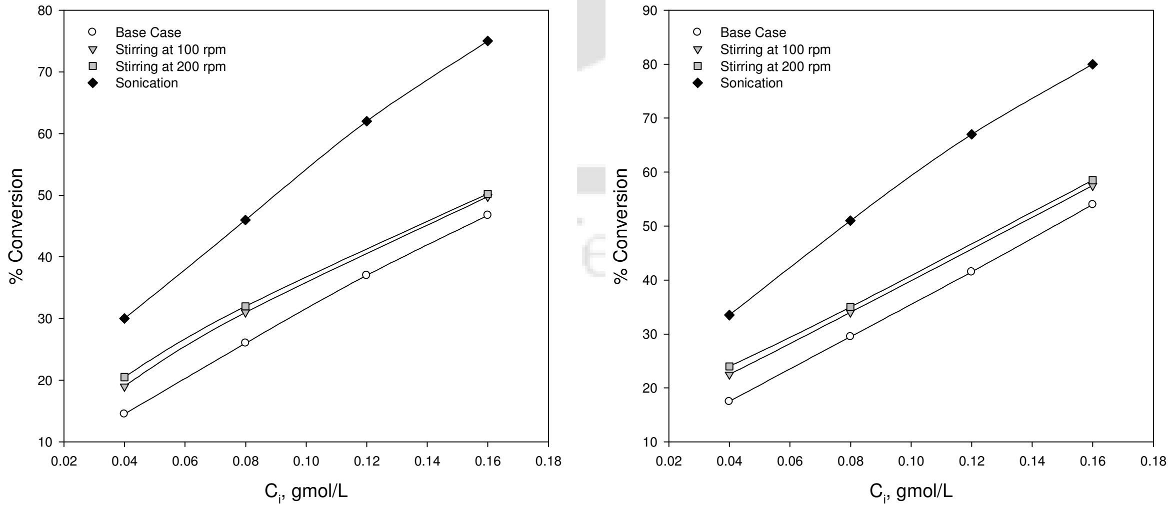

(a) **(b)**

Figure 5.11: Conversion profiles for ultrasonic hydrazine plating baths.
(a) $\theta = 196$ cm^2/L; (b) $\theta = 393$ cm^2/L.

improve the plating efficiency as it provides better adhesion of depositing metal to the surface of the substrate. Figure 5.12 presents the variation in metal plating efficiency with initial nickel concentration for various cases. Sonication slightly improves the plating efficiency (about 1–2%) compared to the base case due to better adhesion of deposited metal to the substrate surface by removing N_2 immediately after forming. On the other hand, stirring resulted in a significant reduction (4–6%) in the plating efficiency due to peeling effect. For all the cases, plating efficiency decreases significantly with increasing the solution concentration from 0.04 to 0.16 mol/L. Bath loading slightly affects the plating efficiency and a higher loading ratio (393 cm^2/L) is recommended for efficient plating.

The overall yield of the plating process can better be defined in terms of selective conversion (the product of fractional conversion and percent plating efficiency). The selective conversion values shown in Table 5.4 varied between 14.1–44.6% for the base case, which are far lower than those acceptable for good industrial performance.

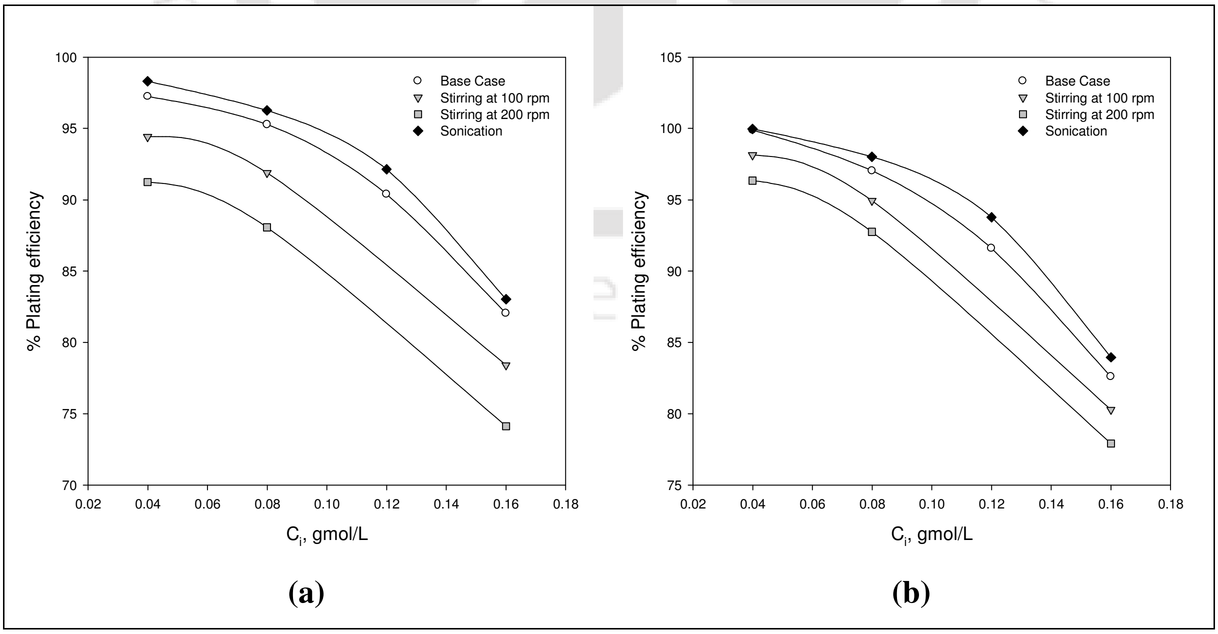

Figure 5.12: Efficiency profiles for ultrasonic hydrazine plating baths. (a) θ = 196 cm^2/L; (b) θ = 393 cm^2/L.

Table 5.4: Selective conversion data for ultrasonic hydrazine baths.

Case study	**Selective conversion (%) for various values of C_i (mol/L)**							
	θ = 196 cm^2/L				θ = 393 cm^2/L			
	0.04	0.08	0.12	0.16	0.04	0.08	0.12	0.16
Base case	14.1	24.8	33.4	38.4	17.5	28.6	38.0	44.6
Stirring at 100 rpm	17.9	28.5	–	39.0	22.1	32.3	–	46.2
Stirring at 200 rpm	18.7	28.2	–	37.3	23.1	32.5	–	45.6
Sonication	29.5	44.3	57.1	62.3	33.5	50.0	62.8	67.2

Sonication results in a tremendous increase in selective conversion at all concentrations due to simultaneous improvement in deposition rate and plating efficiency. For instance, sonication provides 100% excess selective conversion (29.5%) compared to the base case (14.1%) at an initial nickel solution concentration of 0.04 mol/L and a loading ratio of 196 cm^2/L. However, stirring brought about some considerable improvement in selective conversion only at lower concentrations. Selective conversions as high as 60% are achieved in sonication assisted plating baths at higher concentrations (0.12–0.16 mol/L) and higher loading ratio (393 cm^2/L).

Figure 5.13 presents the variation of average nickel deposition rate (mol/L.s) with average solution concentration for various cases with the loading ratios of 196 and 393 cm^2/L. Similar trends in reaction rates with slightly higher values are observed for the higher loading ratio (393 cm^2/L) than the lower one (196 cm^2/L). The deposition rate in sonication assisted electroless plating baths is found to be twice faster than all other cases including stirring. This observation indicates that ultrasound enhances the speed of electroless plating by accelerating the transport of materials in the plating solution due to cavitation effect. Wu et al. [78] inferred that the plating rate could be increased by introducing ultrasound waves during electroless nickel deposition. Jiang et al. [105] also found that the electroless plating process could be completed in a shorter time when ultrasonic waves are applied than mechanical agitation is applied.

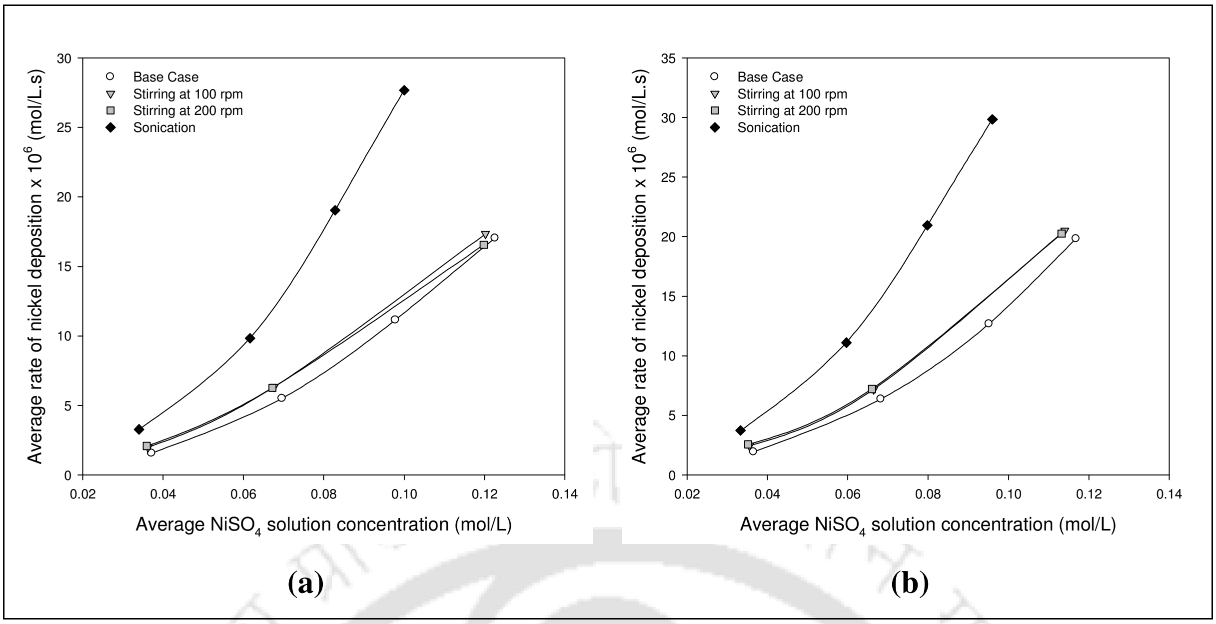

Figure 5.13: Average deposition rate profiles for ultrasonic hydrazine baths. (a) $\theta = 196$ cm^2/L; (b) $\theta = 393$ cm^2/L.

Table 5.5 presents the model parameters obtained from the non-linear regression analysis for sonication assisted hydrazine based electroless plating baths. It can be observed that the average nickel mass transfer coefficient ($\bar{k}$) varied between 224–789 s^{-1} and 300–809 s^{-1} for the loading ratios of 196 and 393 cm^2/L respectively. These values are significantly higher than the base case (67.2–487 s^{-1}) and stirring (104.5–573.1 s^{-1}). Stirring improved $\bar{k}$ values significantly at lower concentrations than high concentrations (Table 4.6). However, sonication results in a tremendous increase in the mass transfer coefficient ($\bar{k}$) values for all the concentrations. On the other hand, no significant change in the partition coefficient ($\bar{\gamma}$) values is observed. Bath loading ratio (θ) has no significant effect on the model parameters for ultrasonic electroless plating.

Table 5.5: Model parameters for ultrasonic hydrazine baths.

θ (cm^2/L)	$\bar{C}_B$ (mol/L)	$\bar{k}$ (s^{-1})	$\bar{\gamma}$	**% Error** ×10^5
196	0.034	223.5	1003.5	6.47
196	0.062	485.4	1020.2	7.41
196	0.083	683.6	1046.5	7.75
196	0.100	788.6	1058.5	6.48
393	0.033	299.6	1011.8	5.84
393	0.060	514.9	1035.5	5.91
393	0.080	738.4	1056.7	6.74
393	0.096	809.0	1082.8	1.79

5.2.2 Metal–ceramic membrane characteristics

5.2.2.1 Surface characterization

The surface characterization was carried out using scanning electron microscopy (SEM) (LEO 1430VP). Figure 5.14 presents surface SEM micrographs of all membranes fabricated under sonication using different nickel solution concentrations (0.04–0.16 mol/L) and loading ratios (196 and 393 cm^2/L). These micrographs indicate the presence of metallic nickel grains on the ceramic surface. It is observed that the metal films deposited under sonication are found to be smoother in texture than those of the base case, but are not as smooth as those processed at higher stirrer speeds presented earlier. As shown in the figure, surface morphology of the deposited metal layer depended on the solution concentration as well as the loading ratio. Higher concentrations (0.12–0.16 mol/L) provide more uniform deposition. A lower loading ratio (196 cm^2/L) results in coarser and more compact metal grains on the surface. This is probably due to higher film thickness of the deposited metal at this loading ratio (196 cm^2/L) than at 393 cm^2/L as discussed earlier.

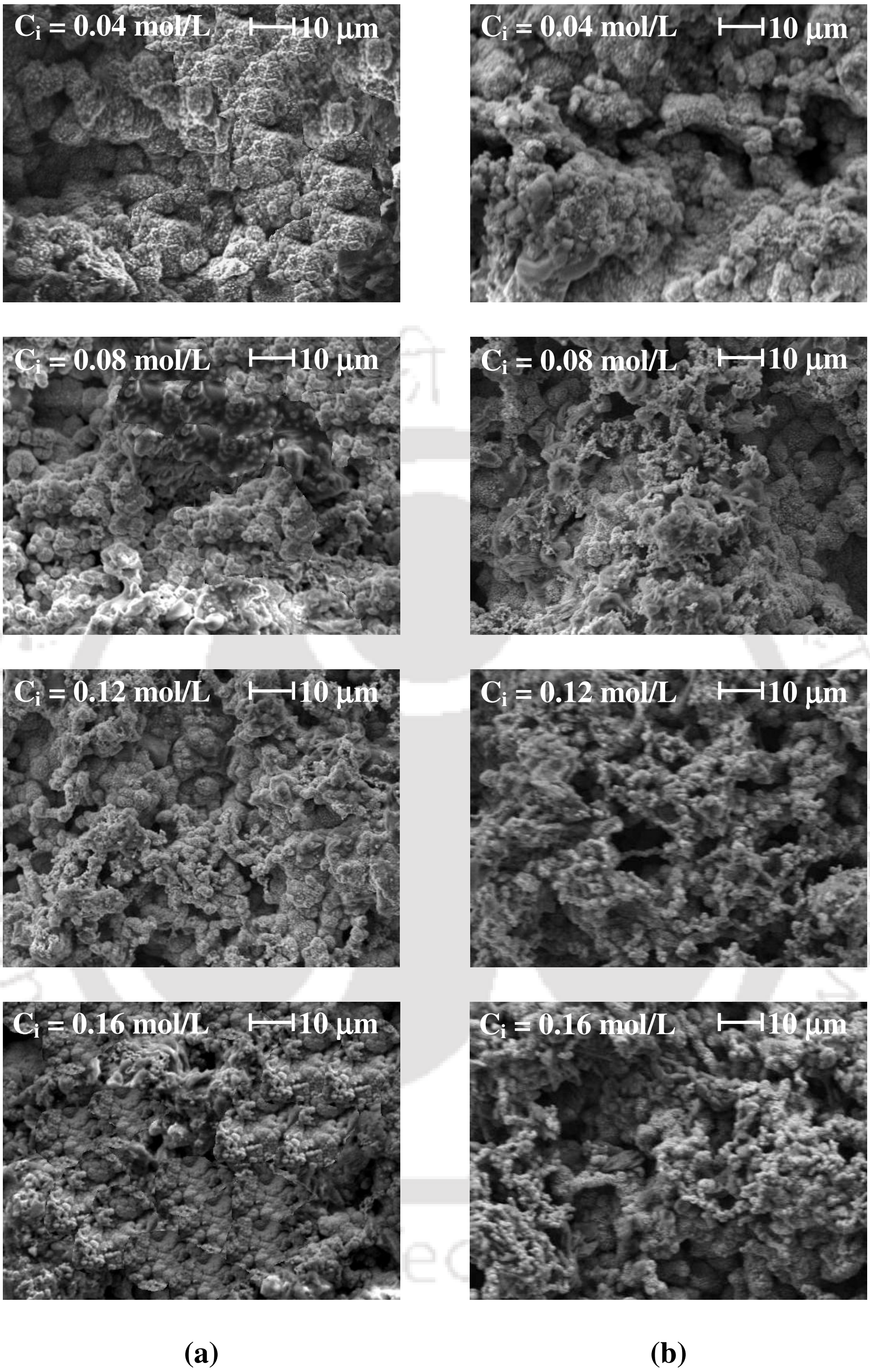

Figure 5.14: Surface SEM micrographs (magnification: 1 KX) of composite membranes prepared in ultrasonic hydrazine baths. (a) $\theta = 196$ cm^2/L; (b) $\theta = 393$ cm^2/L.

Surfaces of the composite membranes were also subjected to X-ray diffraction (XRD) (Bruker AXS, D8 ADVANCE) analysis. Figure 5.15 presents the XRD pattern of the metal film deposited in ultrasonic baths (initial nickel concentration of 0.08 mol/L and loading ratio of 393 cm^2/L) which matches very closely with the relevant peaks associated to nickel (JCPDS: 00–001–1260 (D)). Similar XRD patterns were observed for the other membranes processed in sonication bath and were influenced neither by solution concentration nor by loading ratio. The nature of the spectra indicates that the deposited metal layer is crystalline. Absence of quartz peaks (which were present in the earlier case with membrane stirring) further implies that the surface of the membranes processed in ultrasound assisted plating baths are fully covered by the deposited metal (i.e. nickel).

5.2.2.2 Film thickness

The average film thickness of the deposited metal layer was measured by weight gain method using the expression given by Eq. (2.12). Table 5.6 presents the variation in metal layer thickness with initial metal solution concentration for various cases. It can be observed that stirring contributed for significant enhancement in film thickness at lower

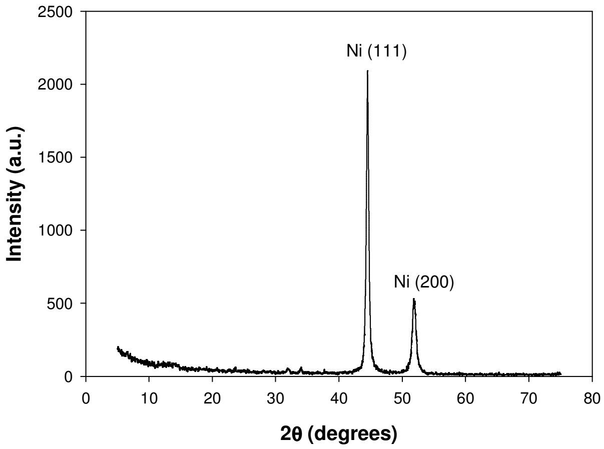

Figure 5.15: XRD pattern of metal film deposited in ultrasonic hydrazine baths. ($C_i = 0.08$ mol/L and $\theta = 393$ cm^2/L).

Table 5.6: Film thickness data for ultrasonic hydrazine baths.

Case study	Thickness (μm) for various values of C_i (mol/L)							
	θ = 196 cm^2/L				θ = 393 cm^2/L			
	0.04	0.08	0.12	0.16	0.04	0.08	0.12	0.16
Base case	3.8	13.2	26.8	40.9	2.3	7.6	15.2	23.8
Stirring at 100 rpm	4.8	15.2	–	41.6	2.9	8.6	–	24.6
Stirring at 200 rpm	5.0	15.0	–	39.7	3.1	8.7	–	24.3
Sonication	7.9	23.6	45.7	66.4	4.5	13.3	25.1	35.8

solution concentrations (0.04–0.08 mol/L), but not at higher solution concentration (0.16 mol/L) wherein the metal film thickness reduced due to inefficient plating. Sonication improves the metal film thickness tremendously irrespective of the solution concentration due to enhanced plating rate and efficient deposition. In addition, it is observed that the film thickness is strongly influenced by loading ratio i.e., doubling the loading ratio (from 196 to 393 cm^2/L) contributes to a reduction in the metal film thickness by about 50% for all the cases (from 7.9–66.4 to 4.5–35.8 μm). Maximum film thickness (66.4 μm) is observed for the sonication assisted electroless plating bath with $C_i = 0.16$ mol/L and θ = 196 cm^2/L. In summary, it is observed that sonication greatly influences the metal film thickness than membrane stirring besides the other parameters namely solution concentration and loading ratio during the fabrication of metal–ceramic composite membranes by electroless deposition technique. As lower metal film thickness is always preferred for composite membranes to enable better separation characteristics, a higher loading ratio (θ = 393 cm^2/L) can be recommended for this purpose.

5.2.2.3 Permeation characteristics

Figure 5.16 illustrates the effective permeability factor (K) versus P_{avg} data at a loading ratio of 393 cm^2/L, for the initial nickel solution concentrations of 0.04, 0.08 and

0.16 mol/L. Similar data trends are obtained for the case of lower loading ratio (196 cm^2/L) also. For all the cases, it can be observed that the permeability coefficient values are the lowest for sonication case compared to membrane stirring and base case. This observation indicates that sonication assisted electroless plating baths result in membranes with lowest values of average pore size. Further, it can be observed that variant permeability coefficient profiles exist for different cases (base case, membrane-stirring

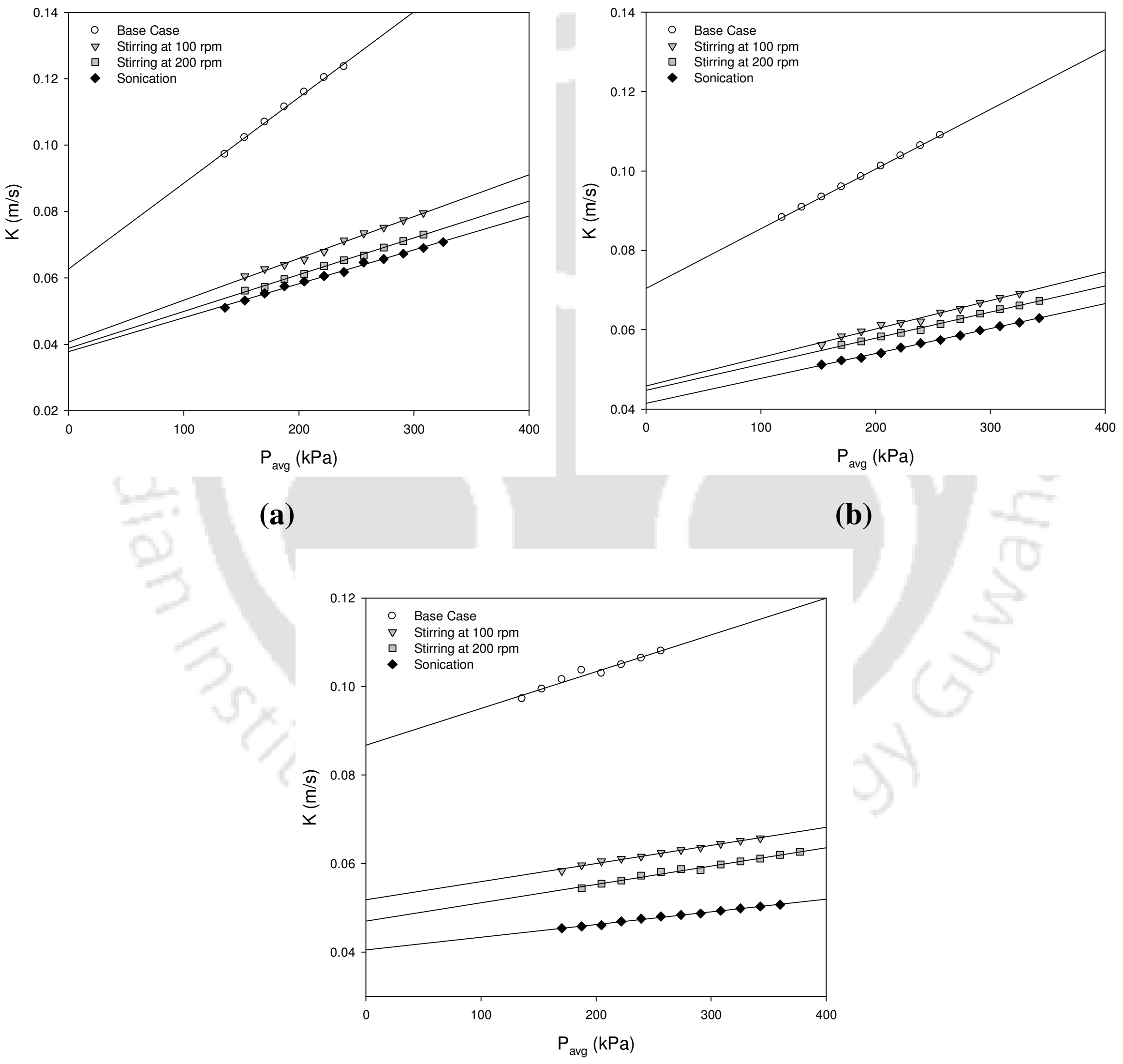

(a) **(b)**

(c)

Figure 5.16: Plots of effective permeability factor (K) versus average pressure (P_{avg}) for membranes synthesized at various conditions in hydrazine baths (θ = 393 cm^2/L). (a) 0.04 mol/L (b) 0.08 mol/L; (c) 0.16 mol/L.

and sonication) indicating that there is a flexibility in obtaining desired permeation properties for specific purposes with the mass-transfer enhancement techniques. It is also apparent that the permeation characteristics of the metal film are largely influenced by the type of mass transfer enhancement as well as solution concentrations.

5.2.2.3.1 Pore Diameter

The data corresponding to the average pore diameter of composite membranes (θ = 393 cm^2/L) evaluated from gas permeation experiments is presented in Table 5.7. Hydrazine based plating baths are effective to reduce the average pore size of the surface significantly from 275 nm to 51–11 for θ = 196 cm^2/L and 58–16 nm for θ = 393 cm^2/L. Sonication enables better reduction in pore size than membrane stirring at all concentrations and loading ratios. Though sonication improves the plating rate and film thickness, it does not provide significant pore size reduction compared to membrane stirring. The minimum pore size of 11 nm obtained from the sonication assisted plating baths (C_i = 0.16 mol/L and θ = 196 cm^2/L) is only 3 nm lower than that obtained with membrane stirring at 100 rpm (14 nm). Solution concentration plays a significant role in pore size reduction and higher concentrations (0.12–0.16 mol/L) result in smaller pores. However, it is important to note that the film pore size does not significantly depend upon the loading ratio (as the film thickness did). Hence a higher loading ratio (θ = 393 cm^2/L)

Table 5.7: Average pore size data for ultrasonic hydrazine baths.

Case study	**Average pore size** (nm) **for various values of** C_i (mol/L)							
	θ = 196 cm^2/L				θ = 393 cm^2/L			
	0.04	0.08	0.12	0.16	0.04	0.08	0.12	0.16
Base case	82	41	24	14	94	49	30	22
Stirring at 100 rpm	59	26	–	14	72	36	–	18
Stirring at 200 rpm	53	28	–	15	67	34	–	20
Sonication	51	27	17	11	58	31	21	16

is recommended for efficient and cost effective fabrication.

5.2.2.3.2 Effective porosity

Figures 5.17a and 5.17b present the change in metal film effective porosity with initial metal solution concentration for the loading ratios of 196 and 393 cm^2/L respectively. It can be observed that the bath concentration as well as loading ratio significantly affects the effective porosity values. For all the cases, the effective porosity values obtained for lower loading ratio (196 cm^2/L) are about 50% excess to that of those obtained for the higher loading ratio (393 cm^2/L) and increase with the solution concentration. A non-linear dependence of porosity values on initial nickel solution concentration is noticed. For both loading ratios, sonication results in significantly lower values of effective porosity than the other cases. This observation indicates that sonication as a mass-transfer enhancement, is effective to eliminate the problem of gas (nitrogen) bubbles at the membrane surface by detaching them instantaneously after generation. All in all, it is observed that the uniformity in metal deposition is strongly influenced by initial metal

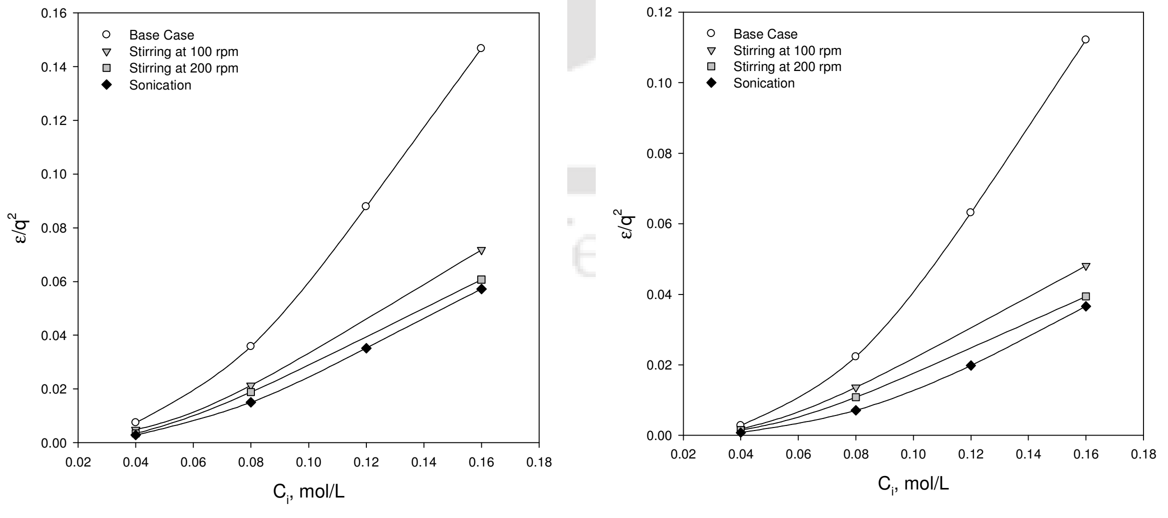

(a) **(b)**

Figure 5.17: Porosity profiles for ultrasonic hydrazine plating baths.
(a) $\theta = 196$ cm^2/L; (b) $\theta = 393$ cm^2/L.

solution concentration, loading ratio and mass transfer enhancement techniques.

5.2.2.3.3 Percent pore densification

Percent pore densification (PPD), a measure of surface coverage by the deposited material is an important parameter for asymmetric membranes. Figure 5.18 presents the variation of PPD with initial metal solution concentration for the loading ratios of 196 and 393 cm^2/L. It is observed that mass transfer enhancements favor PPD predominantly at lower metal solution concentrations. Slightly higher values of PPD (95.5–99.8 %) are achievable with sonication assisted electroless plating compared to membrane stirring case (94–99.7 %) using hydrazine baths. There is no significant improvement in PPD at higher concentrations in both cases (stirring and sonication) as the PPD values are very close to that of the base case and these mass transfer enhancements does not provide dense membranes despite conducting sequential deposition for eight hours. This is again an indication of the basic problem of nitrogen generation at the membrane surface and the greater contribution of induced shear stress to PPD.

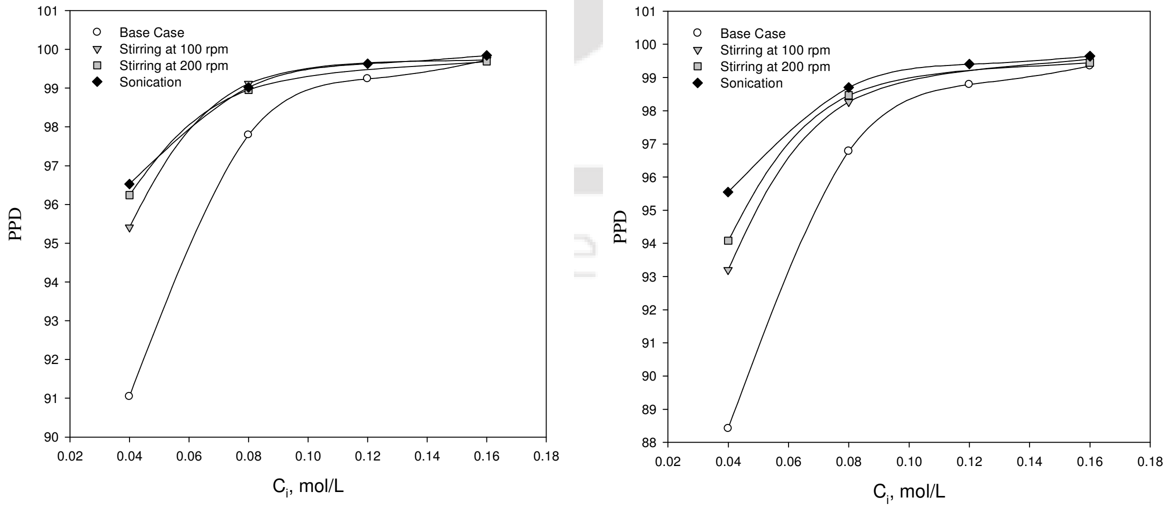

(a) **(b)**

Figure 5.18: PPD profiles for ultrasonic hydrazine plating baths.
(a) θ = 196 cm^2/L; (b) θ = 393 cm^2/L.

5.2.3 Summary

Based on several experimental investigations, this work addresses the effect of process parameters and mass transfer enhancement techniques on the morphological and transport properties of the porous nickel metallic films fabricated using ultrasonic hydrazine electroless plating baths. The selective conversions of nickel–hydrazine plating baths are in the acceptable range for industrial applications (>60% at higher nickel solution concentrations (0.12–0.16 mol/L) with sonication at a loading ratio of 393 cm^2/L). Sonication contributes significantly towards maintaining higher plating efficiency, selective conversion, faster plating rate, higher metal thickness and higher values of effective porosity. These observations are indicating that the mass transfer limitations are very effectively handled by sonication than membrane stirring. However, sonication does not suffice much towards morphological characteristics in terms of drastic pore size reduction and PPD enhancement. Despite conducting 8 hours sequential deposition with sonication using hydrazine baths, the average pore size of composite membrane reached a value of 11 nm, which is close to that of membrane stirring (14 nm). Corresponding thickness of the nickel film (66 μm) is significantly higher than membrane stirring case (40 μm). All these conclusions imply that sonication can be the best choice from process perspective while stirring is recommended from morphological perspective.

5.3 Conclusions

The effect of ultrasound on electroless plating process parameters is presented in this chapter. Table 5.8 summarizes a comparative assessment of various process and membrane morphological parameters obtained for the cases with two different reducing agents namely sodium hypophosphite and hydrazine in sonication coupled electroless

Table 5.8: Comparison between ultrasonic hypophosphite and hydrazine baths.

Parameter	**Hypophosphite baths**	**Hydrazine baths**
Conversion (%)	28–76	30–80
Efficiency (%)	99.5–66.2	99.9–83.0
Pore diameter (nm)	76–54	58–11
PPD (%)	92.4–96.1	95.5–99.8
Porosity of metal layer	0.0004–0.0132	0.0008–0.0572
Thickness (μm)	4.2–50.8	4.5–66.4
Average mass transfer coefficient, $\overline{k}$ (s^{-1})	194–423	224–809
Optimal concentration (mol/L)	0.08	0.12
Optimal loading ratio (cm^2/L)	393	393

plating baths. It can be observed that all process as well as morphological parameters including conversion, efficiency, PPD, average pore size, average effective porosity and average mass-transfer coefficient for the hydrazine based baths are significantly higher than those obtained using the hypophosphite based baths. The selective conversion values for hydrazine based baths varied between 29.5–67.2% and are higher than those obtained for hypophosphite baths (27.5–50.8%) especially at higher concentrations. To have a minimal plating efficiency of 90% without compromising upon the conversion and PPD, the optimal initial $NiSO_4$ concentrations for hypophosphite and hydrazine baths are evaluated to be 0.08 mol/L and 0.12 mol/L respectively. In comparison with hypophosphite baths, hydrazine baths results in higher values of conversion, efficiency, film thickness and pore densification. Hence, it can be concluded that hydrazine as a reducing agent serves better than sodium hypophosphite for the electroless deposition of nickel under ultrasonic conditions.

The presence of micro-pores on the surfaces of the nickel–ceramic composite membranes is also confirmed by the surface FESEM micrographs (Figure 5.19). Figure

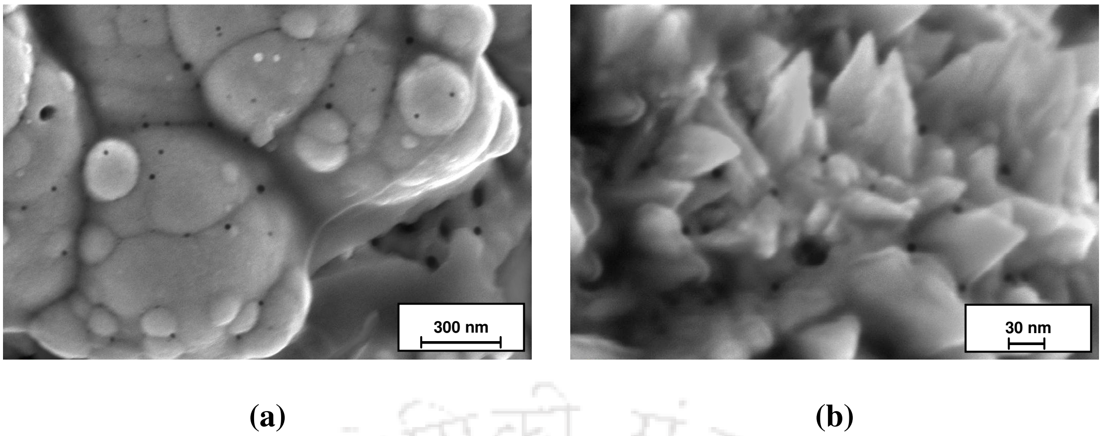

(a) **(b)**

Figure 5.19: Surface FESEM micrographs of the nickel–ceramic composite membranes prepared by ultrasonic electroless plating.
(a) hypophosphite bath (139 KX); (b) hydrazine bath (604 KX).

5.19a corresponds to a mean pore size of 54 nm for the membrane fabricated in hypophosphite bath (C_i = 0.16 mol/L and θ = 196 cm^2/L) while Figure 5.19b corresponds to a mean pore size of 11 nm for the membrane fabricated in hydrazine bath (C_i = 0.16 mol/L and θ = 196 cm^2/L).

Chapter 6

PERFORMANCE CHARACTERISTICS OF ELECTROLESS PLATING BATHS UNDER HYDROTHERMAL CONDITIONS

In this chapter, the results are presented in three sections. The first section summarizes the performance characteristics of hydrothermal assisted electroless plating baths in terms of conversion, efficiency, selective conversion, deposition rate and model parameters and the second section elaborates upon the characteristics of the composite membranes in terms of film thickness, pore size, porosity and PPD along with the physical characteristics of the composite membrane surface. The third section summarizes the efficacy of hydrothermal conditions in comparison with the other mass-transfer enhancement techniques for electroless plating process. Two cases namely hydrothermal condition (HT) and hydrothermal condition in combination with sonication (HTSO) are considered for both the reducing agents (sodium hypophosphite and hydrazine).

6.1 Electroless plating process characteristics

The plating experiments were carried out using the typical setup shown in Figure 2.9 (Chapter 2) to evaluate the performance characteristics of electroless plating baths under hydrothermal conditions. The systemic pressure (autogenous pressure) under hydrothermal conditions gradually increases with electroless plating time because the generated gas (H_2/N_2) cannot escape from the closed container. A similar observation had been reported by Zheng and Wu [62] for palladium deposition on alumina membrane. In the subsequent sections, conventional electroless plating without any mass transfer enhancement is referred to as ‘Base case’ while simple hydrothermal condition is denoted as ‘HT’ and hydrothermal condition coupled with sonication is denoted as ‘HTSO’ for convenience.

Figure 6.1 presents the variation of nickel conversion in the hypophosphite as well as hydrazine based plating baths. Similar to the base case results presented in chapter 3, conversion increases with increasing the solution concentration. For the case of hypophosphite based electroless plating baths (Figure 6.1a), an increase in initial $NiSO_4$ concentration from 0.04 to 0.16 mol/L resulted in a corresponding increase in the bath conversion from 37.5 to 65% for the hydrothermal case and from 42.5 to 77.5% for HTSO. These values are significantly higher than the conversion values of the base case. Similarly for the hydrazine based electroless plating baths (Figure 6.1b), conversion values varied from 40 to 78.1% for simple hydrothermal case (HT) and from 45 to 81.9% for HTSO which are again significantly higher than those of the base case.

Figure 6.2 presents the variation of plating efficiency with initial $NiSO_4$ solution concentration. Plating efficiency decreases with increasing nickel solution concentration. Lower plating efficiencies are observed at higher solution concentrations due to significant

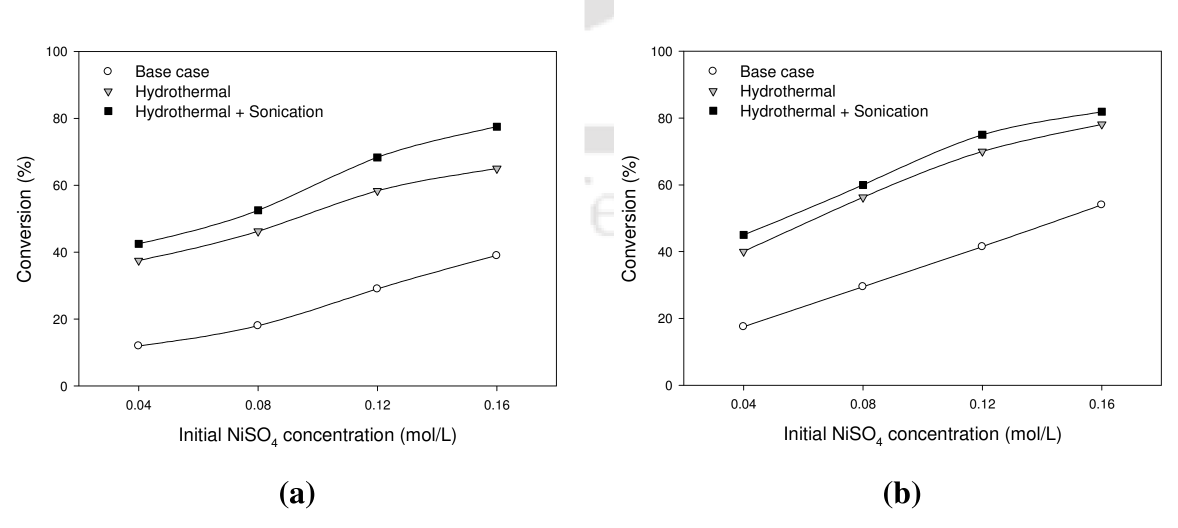

Figure 6.1: Conversion profiles for hydrothermal electroless plating. (a) hypophosphite baths; (b) hydrazine baths.

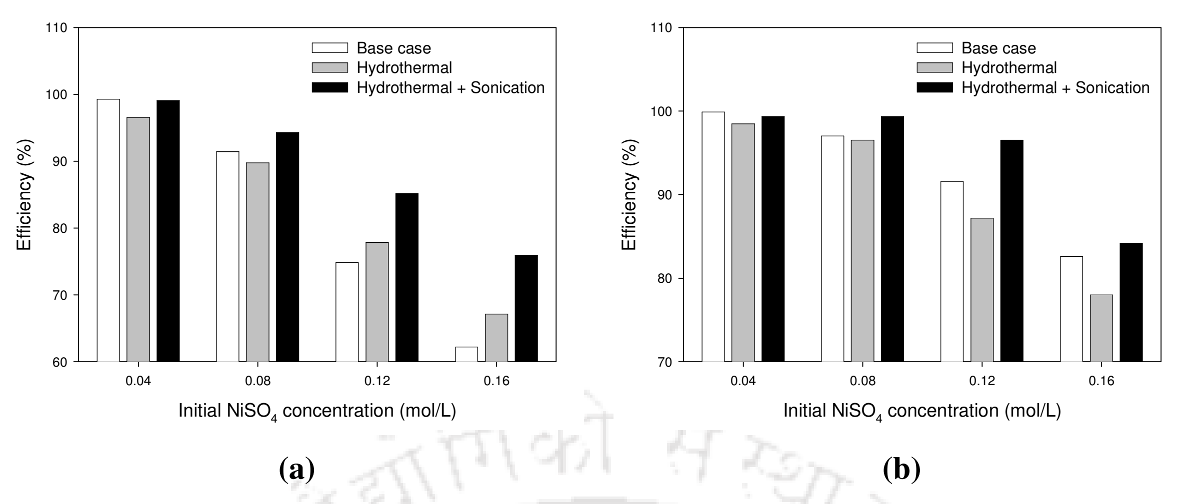

Figure 6.2: Efficiency profiles for hydrothermal electroless plating. (a) hypophosphite baths; (b) hydrazine baths.

enhancement in the amount of H_2/N_2 generation at the solid–liquid interface which contributes to additional attrition of deposited nickel on the surface. As shown in the figure, hydrazine baths (Figure 6.2b) are more efficient than the hypophosphite baths (Figure 6.2a) and sonication coupling improves the plating efficiency. The plating efficiency values of hypophosphite baths varied from 96.5 to 67.2% for hydrothermal assisted case and 99.1 to 75.9% for HTSO which are slightly lower than the corresponding values obtained for the base case. Corresponding values for hydrazine baths are 98.5 to 78.0% for hydrothermal case and 99.4 to 84.2% for HTSO case.

Table 6.1 presents the selective conversion (defined as the product of fractional conversion and plating efficiency) values for various cases. Selective conversion increases with increasing solution concentration up to the initial concentration of 0.12 mol/L and hydrazine baths results in higher values of selective conversion than hypophosphite baths. Sonication coupling significantly improves the selective conversion by promoting simultaneous enhancement in both conversion and efficiency values discussed earlier.

Table 6.1: Selective conversion data for hydrothermal plating baths.

Initial $NiSO_4$ concentration (mol/L)	**Selective conversion** (%)			
	Hypophosphite baths		Hydrazine baths	
	HT	HTSO	HT	HTSO
0.04	36.2	42.1	39.4	44.7
0.08	41.5	49.5	54.3	59.6
0.12	45.4	58.2	61.0	72.4
0.16	43.6	58.8	60.9	68.9

HT: Hydrothermal
HTSO: Hydrothermal + Sonication

Obtained selective conversion values are almost twice of the base case values. Therefore, the mass transfer enhancement techniques can be observed to be very effective.

Figure 6.3 presents the variation of average reaction rate with solution concentration. For the hypophosphite baths, it can be observed that the average reaction rate varied from 1.32×10^{-6} to 10.8×10^{-6} mol/L.s for base case, 4.17×10^{-6} to 28.9×10^{-6} mol/L.s for hydrothermal (HT) case and 4.72×10^{-6} mol/L.s to 34.4×10^{-6} mol/L.s for HTSO. This corresponds to about 268–314% and 319–356% enhancement in average reaction rate for hydrothermal and HTSO cases respectively with respect to the base case. Also, it can be observed that for both hydrothermal and HTSO cases, the average solution concentration reduced and this is due to the enhancement in bath conversion. On the other hand, for hydrazine baths, the average reaction rate varied from 1.94×10^{-6} to 19.8×10^{-6} mol/L.s for base case, 4.44×10^{-6} to 34.7×10^{-6} mol/L.s for hydrothermal case and 5×10^{-6} to 36.4×10^{-6} mol/L.s for HTSO. This corresponds to an enhancement of 228 to 175.1% for hydrothermal case and 257–183% for HTSO. In conclusion, it can be observed that mass transfer enhancements enable similar average reaction rate values for both hypophosphite and hydrazine baths and this observation once again conveys the efficacy of mass transfer enhancement in enhancing the metal deposition rates.

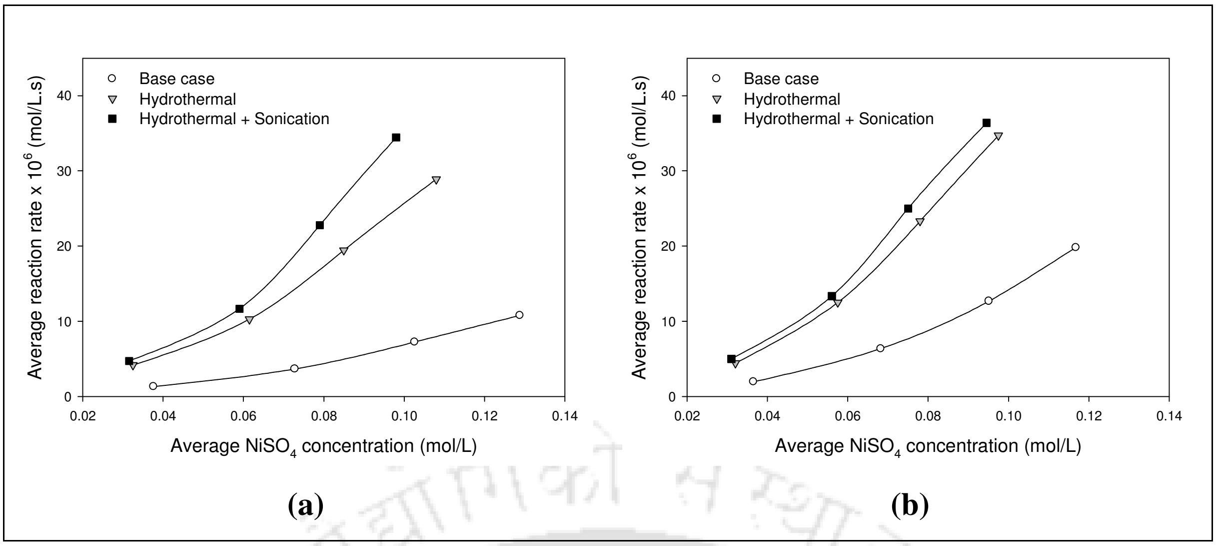

Figure 6.3: Average reaction rate profiles for hydrothermal electroless plating. (a) hypophosphite baths; (b) hydrazine baths.

Table 6.2 presents the model parameters obtained from the non-linear regression analysis for electroless plating baths under hydrothermal conditions. It can be observed that the average nickel mass transfer coefficient ($\bar{k}$) is between 251–372 s^{-1} and 304–566 s^{-1} for HT and HTSO cases with hypophosphite based baths (Table 6.2a) and 349–810 s^{-1} and 429–984 s^{-1} for HT and HTSO cases with hydrazine based baths (Table 6.2b). These values are significantly higher than the base case (Chapter 3), stirring (Chapter 4) as well as sonication (Chapter 5). However, no significant change in the partition coefficient ($\bar{\gamma}$) values is observed.

Table 6.2: Model parameters for hydrothermal electroless plating baths.
(a) hypophosphite baths; (b) hydrazine baths.

Case	$\bar{C}_B$ (mol/L)	$\bar{k}$ (s^{-1})	$\bar{\gamma}$	**% Error ×10^5**
HT	0.033	251.4	999.9	0.29
HT	0.062	306.5	999.8	2.02
HT	0.085	366.7	999.7	0.47
HT	0.108	372.2	999.6	0.38
HTSO	0.032	304.1	993.8	0.82
HTSO	0.059	384.0	997.9	0.86
HTSO	0.079	512.9	1001.8	0.22
HTSO	0.098	566.1	1001.7	0.53

(a)

Case	$\bar{C}_B$ (mol/L)	$\bar{k}$ (s^{-1})	$\bar{\gamma}$	**% Error ×10^5**
HT	0.032	348.6	999.8	0.13
HT	0.058	629.9	1003.7	–2.18
HT	0.078	732.2	1005.3	–0.09
HT	0.098	809.8	1004.6	2.16
HTSO	0.031	429.2	1005.5	1.15
HTSO	0.056	629.8	1004.8	4.33
HTSO	0.075	895.0	1003.4	–1.26
HTSO	0.095	984.0	1004.0	–0.42

(b)

HT: Hydrothermal
HTSO: Hydrothermal + Sonication

6.2 Composite membrane characteristics

6.2.1 Physical characteristics

The top surface of the composite membranes was subjected to Field Emission Scanning Electron Microscopy (FESEM). Figure 6.4 presents the surface FESEM micrographs of the nickel layer deposited using hypophosphite bath and hydrazine bath with an initial nickel sulfate concentration (C_i) of 0.16 mol/L prepared under hydrothermal

Hypophosphite baths	**Hydrazine baths**
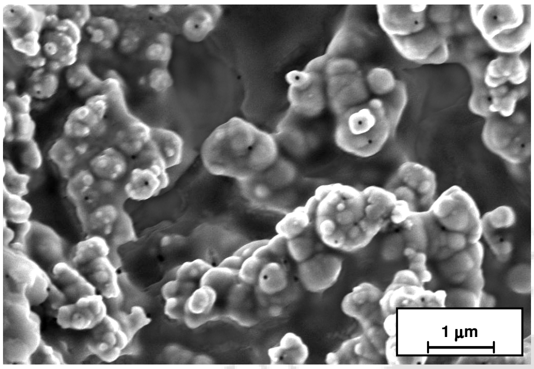 **Hydrothermal**	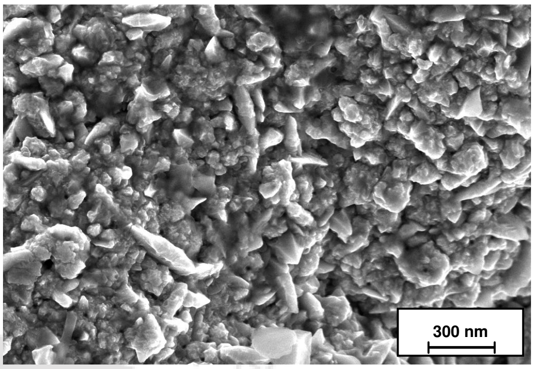 **Hydrothermal**
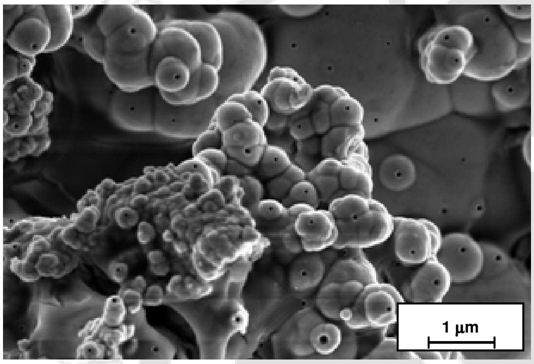 **Hydrothermal + Sonication**	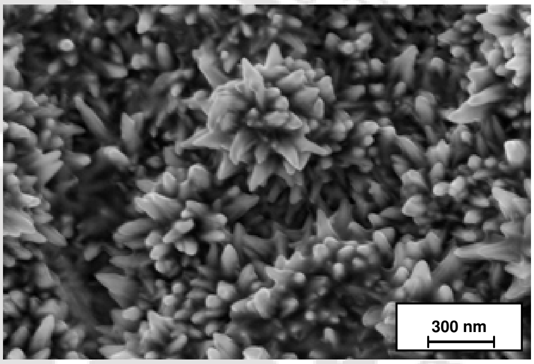 **Hydrothermal + Sonication**

Figure 6.4: Surface FESEM micrographs of the nickel–ceramic composite membranes prepared by hydrothermal electroless plating (C_i = 0.16 mol/L and θ = 196 cm^2/L).

conditions which correspond to the average pore size of 45, 21, 33 and 8 nm respectively. It can be observed that hydrogen gas generated from hypophosphite baths is responsible for the presence of pin holes on the surface. On the other hand, no such pin holes are observed in case of hydrazine baths despite having an average pore size of 8 nm. Thus, hydrazine can be regarded as better reducing agent than sodium hypophosphite.

Figure 6.5 presents the X-ray diffraction (XRD) spectra of the membranes fabricated in hypophosphite as well as hydrazine baths at an initial nickel concentration

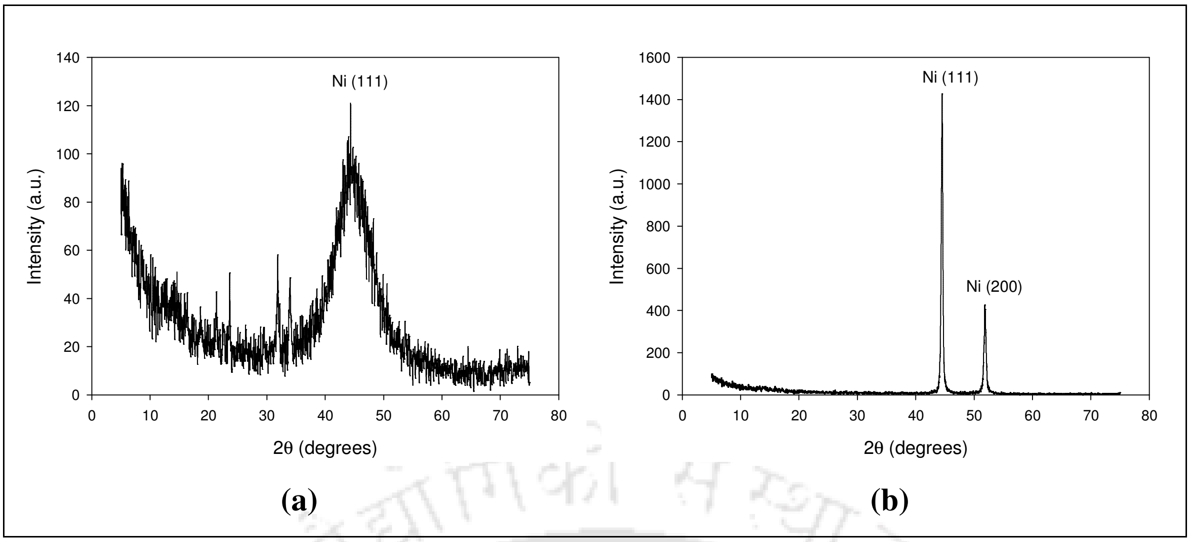

(a) **(b)**

Figure 6.5: XRD spectra of membranes fabricated under sonication coupled hydrothermal conditions (C_i = 0.16 mol/L). (a) hypophosphite baths; (b) hydrazine baths.

(C_i) of 0.16 mol/L prepared under hydrothermal condition combined with sonication (HTSO). Similar patterns were observed for the other membranes as well. From the figure, it can be observed that hypophosphite baths (Figure 6.5a) results in wider spectral distribution whereas hydrazine baths (Figure 6.5b) results in sharp peaks indicating that the nickel layer deposited from hydrazine baths is crystalline.

6.2.2 Film thickness

Figure 6.6 presents the average nickel layer thickness values evaluated from weight gain method (Eq. (2.12)). The average metal layer thickness increases with increasing the solution concentration due to an increase in the amount of metal deposited on the substrate at higher concentrations. Sonication coupling also enhances the metal layer thickness. Hydrazine baths (Figure 6.6b) results in slightly higher values (5.2–36.8 μm) of average metal film thickness compared to the thickness values (4.8–31.4 μm) of hypophosphite baths (Figure 6.6a). These values are significantly higher than the thickness values of the base case with respect to hypophosphite (1.6–12.9 μm) and hydrazine (2.3–23.8 μm) electroless plating baths. Once again mass transfer enhancements can be

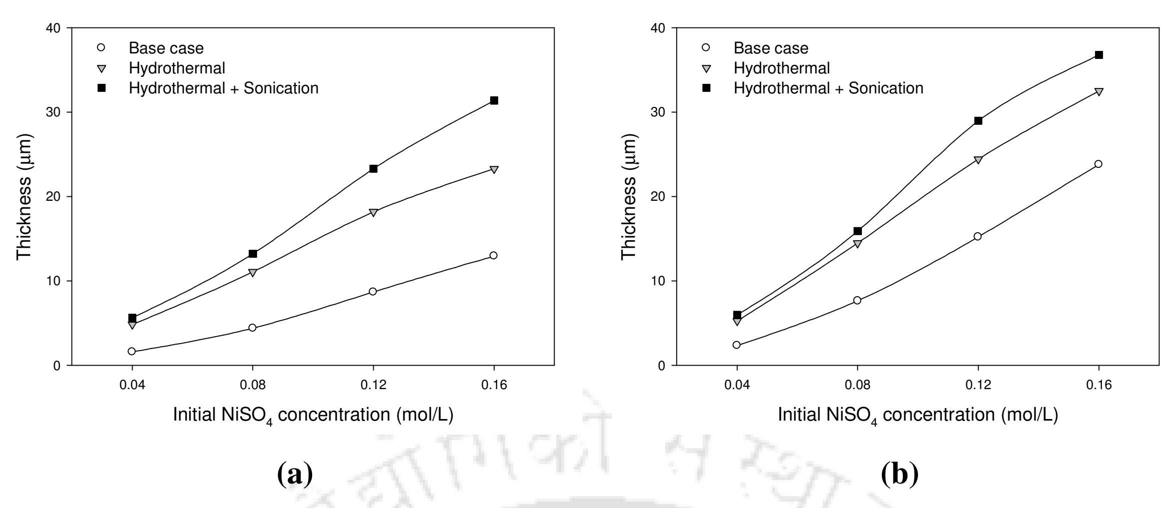

Figure 6.6: Film thickness profiles for hydrothermal electroless plating baths. (a) hypophosphite baths; (b) hydrazine baths.

observed to yield membranes with similar thickness for both hypophosphite and hydrazine baths.

6.2.3 Permeation characteristics

6.2.3.1 Pore size

Table 6.3 presents the average pore diameter values of the nickel–ceramic composite membranes evaluated from the gas permeation experiments described earlier. Average pore diameter of the ceramic membrane support was initially 275 nm which upon plating with nickel reduces to as low as 8 nm as presented in the table (Table 6.3). The average pore size of the composite membranes is found to reduce with increasing the solution concentration and hydrazine based electroless plating baths result in better reduction in pore size compared to the hypophosphite baths. The pore sizes of the composite membranes fabricated under hydrothermal conditions (86–45 nm for hypophosphite baths and 66–21 nm for hydrazine baths) are comparable to the values obtained for membranes fabricated with base case conditions (128–94 nm for hypophosphite baths and 94–22 nm for hydrazine baths). On the other hand, the HTSO

Table 6.3: Average pore size data for hydrothermal plating baths.

Initial $NiSO_4$ concentration (mol/L)	**Average pore size** (nm)			
	Hypophosphite baths		Hydrazine baths	
	HT	HTSO	HT	HTSO
0.04	86	63	66	41
0.08	72	54	38	20
0.12	58	45	27	11
0.16	45	33	21	8

HT: Hydrothermal
HTSO: Hydrothermal + Sonication

coupled electroless plating baths yielded membranes with average pore size values ranging from 63–33 nm for hypophosphite case and 41–8 nm for hydrazine baths. It can be observed here that both hydrothermal and HTSO are highly successful to enhance the pore densification at all metal solution concentrations and this is a good indication of the chosen mass transfer coupling techniques.

6.2.3.2 Effective porosity

Figures 6.7a and 6.7b present the change in metal film effective porosity with initial metal solution concentration under hydrothermal conditions for hypophosphite and hydrazine baths respectively. It can be observed that the bath concentration, reducing agent as well as hydrothermal conditions (HT and HTSO) significantly affect the effective porosity values. For all the cases, the effective porosity values obtained for hydrazine baths are nearly six times that of those obtained for the hypophosphite baths and increase with increasing the solution concentration. A non-linear dependence of porosity values on initial nickel solution concentration is noticed. For both loading ratios, hydrothermal condition (HT) results in significantly higher values of effective porosity than the base case while sonication coupled hydrothermal condition (HTSO) results in significantly

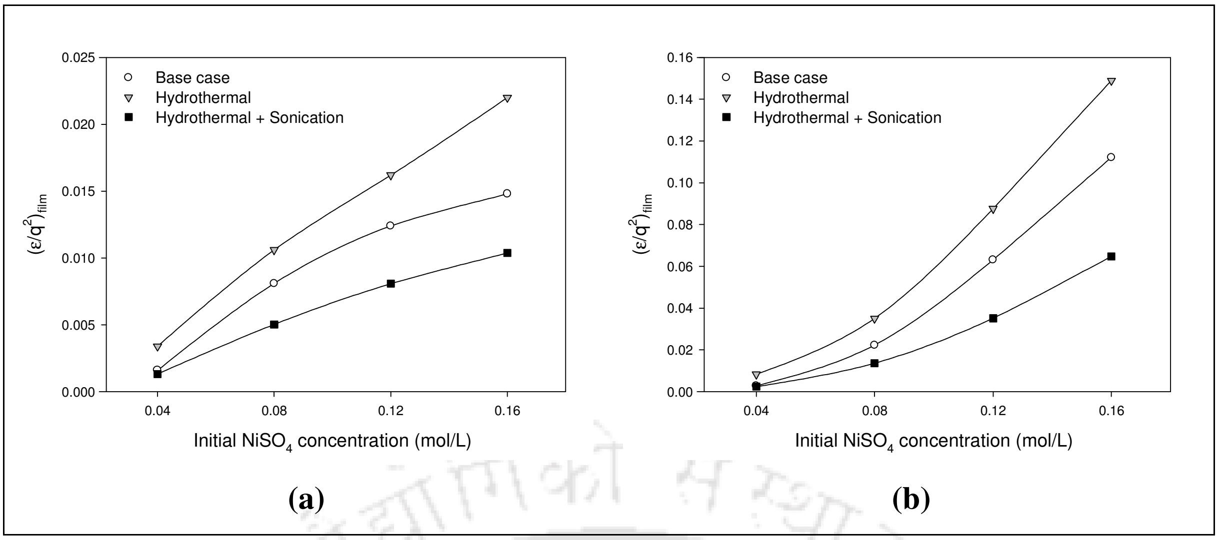

Figure 6.7: Porosity profiles for hydrothermal electroless plating baths. (a) hypophosphite baths; (b) hydrazine baths.

lower values of effective porosity than the base case. This observation indicates that hydrothermal condition (HT) causes the bubbles (H_2/N_2) to retain on the membrane surface because of its autogenous pressure. On the other hand, sonication coupling phenomena as a mass-transfer enhancement is effective to eliminate the problem of gas (H_2/N_2) bubbles at the membrane surface by detaching them instantaneously after generation. However, uniformity of metal deposition that results in a dense membrane shall have a value of zero effective porosity. All in all, it is observed that the uniformity in metal deposition is strongly influenced by initial metal solution concentration, reducing agent and mass transfer enhancement techniques.

6.2.3.3 Percent pore densification

Figure 6.8 presents the variation in percent pore densification (PPD) values with initial $NiSO_4$ concentration for various cases. Distinct PPD profiles have been observed for both hypophosphite baths and hydrazine baths. A significant enhancement in PPD is observable for hypophosphite baths due to mass transfer enhancements in the form of hydrothermal or HTSO conditions (Figure 6.8a). However, for the case of hydrazine baths,

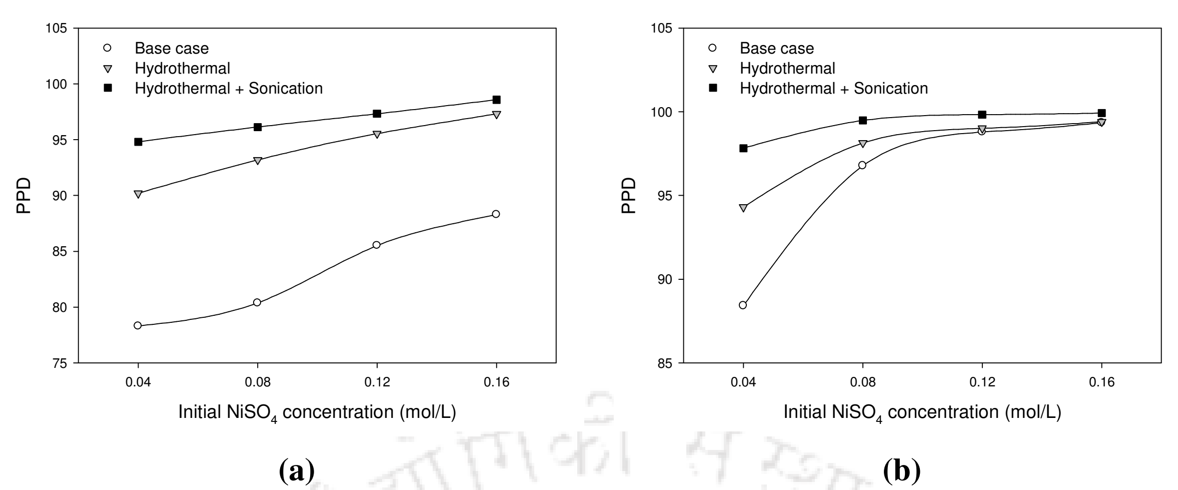

Figure 6.8: PPD profiles for hydrothermal electroless plating baths. (a) hypophosphite baths; (b) hydrazine baths.

it can be observed that mass transfer enhancements are relatively ineffective at higher metal solution concentrations (Figure 6.8b). Therefore, the PPD increases linearly with solution concentration for hypophosphite baths (Figure 6.8a) while the variation is non-linear with respect to the hydrazine baths (Figure 6.8b) for which the PPD increases initially with concentration from 0.04 mol/L to 0.08 mol/L after which no significant improvement in PPD values is observed. This indicates that an initial $NiSO_4$ concentration of 0.08 mol/L in hydrazine baths is sufficient enough to produce nickel–ceramic composite membranes with PPD values equivalent to those fabricated with 0.16 mol/L using hypophosphite as the reducing agent. Also, the hydrothermal assisted plating case can be observed for hydrazine baths to be ineffective for enhancing PPD at nickel metal solution concentrations greater than 0.12 mol/L. The large variation in the PPD profiles for both reducing agent baths is due to the larger attrition of metal in the hypophosphite bath due to the release of lighter H_2 gas on the membrane surface whose faster release is detrimental for the metal adhesion during the plating process.

6.3 Efficacy of hydrothermal conditions

Figure 6.9 summarizes the optimal values of selective conversion, average nickel layer thickness and PPD for various conditions at the loading of 393 cm^2/L and C_i = 0.16 mol/L. For the case of hypophosphite baths (Figure 6.9a), the maximum selective conversion obtained from hydrothermal condition (45.4%) is almost twice that of the base case and agitation brought forward by membrane stirring at 200 rpm while it is slightly lower than the corresponding value for sonication assisted plating baths. On the other hand, the maximum selective conversion value for the baths under hydrothermal conditions together with sonication (58.8%) is significantly higher than that achieved by sonication alone (50.8%) and hydrothermal conditions assisted plating process (45.42%). Corresponding values of thickness also follow the same trend. The maximum values of PPD achieved by hydrothermal condition (97.3%) as well as hydrothermal with sonication (98.6%) are higher than the PPD obtained in all other cases namely the base case (88.3%), membrane stirring (93%) and sonication (95.5%). This indicates that hypophosphite based electroless nickel plating baths assisted with hydrothermal conditions can achieve highest

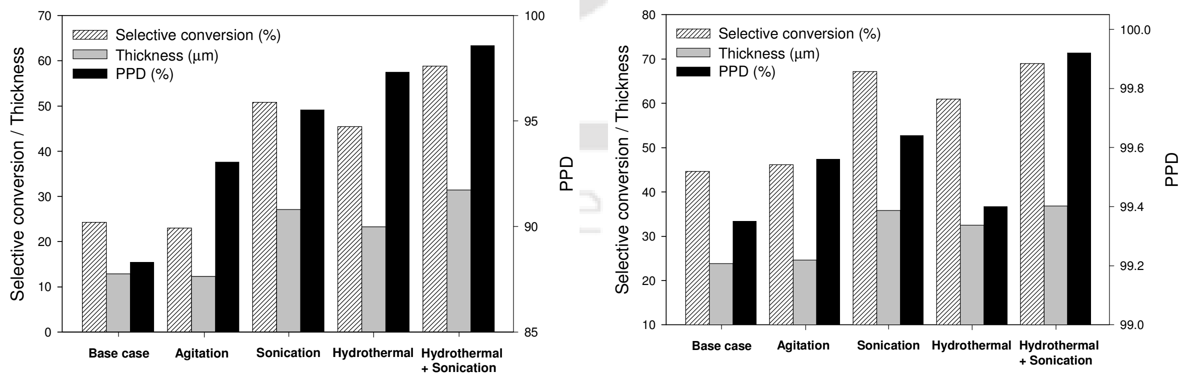

(a) **(b)**

Figure 6.9: Comparison of optimal performance characteristics of electroless plating baths under various process conditions (C_i = 0.16 mol/L; θ = 393 cm^2/L).
(a) hypophosphite baths; (b) hydrazine baths.

PPD values.

Similar trends in selective conversion and thickness are observed with hydrazine baths (Figure 6.9b) as well. The maximum selective conversion corresponds to 68.93% for the HTSO case. However, the maximum PPD value obtained in hydrothermal case (99.4%) is close to that of the base case but slightly lower than the PPD value for membrane stirring and sonication. PPD value as high as 99.92% is achieved by hydrothermal condition together with sonication (HTSO). Therefore, both hydrothermal (HT) and HTSO can be found to be the most efficient mass transfer enhancement techniques in comparison with agitation and sonication and they can be used as the best possible options for 100% pore densification. Also, the exponential increase in membrane thickness for an insignificant enhancement in the PPD is evident in all mass transfer enhancement cases namely sonication, hydrothermal case and HTSO. Such an increase in membrane thickness is not beneficial from membrane perspective, as larger film thickness accounts for lower membrane flux. Therefore, mass transfer enhancement techniques indicate towards support optimization studies so as to obtain membranes with narrow pore size distribution and lower average pore size (to the order of 50–100 nm).

6.4 Summary and conclusions

This work yields many important conclusions. Firstly, the role of hydrothermal and HTSO as potential mass transfer enhancements has been realized. These techniques are observed to be effective to enhance the PPD values significantly close to 100% (Table 6.4). A possible reason for not achieving 100% PPD is the selection of a support with larger pore size distribution and larger average pore size (275 nm). Nonetheless, the obtained results are satisfactory, as mass transfer enhancements are supposed to provide best PPD values for non-optimal support characteristics. Secondly, mass transfer

Table 6.4: Comparison between hypophosphite and hydrazine based electroless plating baths under hydrothermal conditions.

Parameter	**Hypophosphite baths**	**Hydrazine baths**
Conversion (%)	37.5–77.5	40–82
Efficiency (%)	99.1–67.2	99.4–78.0
Pore diameter (nm)	86–33	66–8
PPD (%)	90.2–98.6	94.3–99.9
Porosity of metal layer	0.0013–0.022	0.0024–0.149
Thickness (µm)	4.8–31.4	5.2–36.8
Average mass transfer coefficient, $\bar{k}$ (s^{-1})	251–566	349–984
Optimal concentration (mol/L)	0.08	0.12

enhancements such as hydrothermal conditions do not appear to be satisfactory at higher metal solution concentrations for hydrazine baths, which is not the case for hypophosphite baths. Thirdly, hypophosphite baths enable the realization of membranes with larger average pore size and this is associated to the formation of pin holes, which themselves are surface defects. Fourthly, the efficacy of mass transfer enhancement techniques for metal ceramic membrane fabrication needs to be assessed from selective conversion, pore densification and enhancement in average reaction rate (or metal film thickness). From membrane pore densification perspective, HTSO yields the best possible conditions of nickel metal deposition on the membrane surface and corresponds to a combinatorial performance characteristics of 81.87% conversion, 84.19% plating efficiency, 99.92% PPD for a nickel composite membrane with film thickness of 37 microns prepared using 0.16 mol/L of nickel solution metal concentration (Table 6.4). Finally, from the general understanding of the experimental results together with the previous studies indicate that hydrazine based electroless plating baths are more beneficial than the conventionally used sodium hypophosphite baths for faster and efficient nickel deposition over ceramic substrate.

The autogenous pressure that is generated under hydrothermal conditions has significant impact on the improvement of process as well as membrane characteristics. These observations are indicative of the fact that mass transfer enhancements can play a greater role in the engineering of metal films for metal composite membrane fabrication.

CONCLUSIONS AND FUTURE WORK

This chapter summarizes the inferences drawn from various works presented in this thesis. Also, some suggestions towards the scope for future research are outlined.

7.1 Conclusions

This work deals with the combinatorial performance characteristics of electroless plating baths for the fabrication of nickel–ceramic composite membranes along with the preparation and characterization of inexpensive ceramic membrane support with a nominal pore size of 275 nm which can also be used as a separation medium for microfiltration applications. Few mass transfer enhancement techniques such as stirring, sonication and hydrothermal conditions are also studied.

This work also provides a good number of insights with respect to the mass transfer enhancements for nickel–ceramic composite membrane fabrication. Prior to this work, only a few literatures [41, 51, 62, 69, 96, 105] were reported without systematic investigations due to which, the study of performance characteristics of electroless plating baths for nickel–ceramic membrane fabrication have been considered as the major objective of this work. Based on the obtained results, the conclusions of this work based on various parameters are presented as follows.

a) **Selective conversion:** For hypophosphite electroless plating baths, sonication and hydrothermal conditions appear to be the most competent mass transfer enhancements for nickel–ceramic composite membrane fabrication, as the selective conversions greater than 45% were achieved for these cases only (Table 7.1). For hydrazine based electroless plating baths as well, sonication and hydrothermal mass transfer enhancements brought forward about 50–100% enhancement in selective conversion. Stirring did not suffice to contribute to significantly improved performance characteristics of the electroless plating baths.

b) **Thickness:** For both electroless plating baths (hypophosphite and hydrazine), once again, sonication and hydrothermal mass transfer enhancements only contributed to enhancement in thickness but not stirring.

c) **Porosity:** For both the cases (hypophosphite and hydrazine based electroless plating baths), only sonication provided reduction in porosity than stirring, hydrothermal and HTSO coupling effects. This indicates that membrane densification is effective for only sonication coupled processes.

d) **Pore size and PPD:** For hypophosphite electroless plating baths, mass transfer enhancements contributed to about 10.3–16.5% enhancement in PPD with respect to the base case. On the other hand, for hydrazine electroless plating baths, mass transfer enhancements did not improve PPD to more than 9.4% with respect to the base case. It is also interesting to note that both sonication and HTSO yielded similar nickel film thicknesses but HTSO provided better PPD values than sonication.

Membrane engineering of metal films attempts to target intermediate diffusion layers with variegated characteristics. These include skin layers with the following combinations of parameter choices (pore size, porosity and thickness).

a) Low pore size, low porosity and low thickness
b) Low pore size, high porosity and low thickness
c) High pore size, low porosity and low thickness
d) High pore size, high porosity and low thickness

Table 7.1: Summary of results for various cases (θ = 393 cm^2/L).

Case	**Reducing agent**	**Selective Conversion** (%)	**Thickness** (μm)	**Pore size** (nm)	**Effective Porosity** (%)	**PPD** (%)
Base case	Hypophosphite	11.9–24.2	1.6–12.9	128–94	0.16–1.48	78.3–88.3
	Hydrazine	17.5–44.6	2.3–23.8	94–22	0.28–11.2	88.4–99.4
Stirring	Hypophosphite	13.6–23.0	1.8–12.2	100–72	0.10–1.28	86.7–93.0
	Hydrazine	20.3–46.2	2.7–24.6	81–18	0.15–6.18	91.3–99.6
Sonication	Hypophosphite	31.8–50.8	4.2–27.1	76–58	0.04–0.65	92.4–95.5
	Hydrazine	33.5–67.2	4.5–35.8	58–16	0.08–3.66	95.5–99.6
Hydrothermal	Hypophosphite	36.2–45.4	4.8–23.3	86–45	0.34–2.20	90.2–97.3
	Hydrazine	39.4–61.0	5.2–32.5	66–21	0.83–14.9	94.3–99.4
Hydrothermal + Sonication	Hypophosphite	42.1–58.8	5.6–31.4	63–33	0.13–1.04	94.8–98.6
	Hydrazine	44.7–72.4	6.0–36.8	41–8	0.24–6.47	97.8–99.9

Generally, skin layers with larger metal film thicknesses (>30 μm) are not desired, as the skin layer contributes to the gas permeation resistance. Inferring from Table 7.1, case (a) can be achieved with ultrasonic hydrazine baths, case (b) can be achieved with hydrothermal hydrazine baths, case (c) can be achieved with ultrasonic hypophosphite baths and case (d) can be achieved with hydrothermal hypophosphite baths.

However, if the average porosity is not of primary concern, then membrane engineering of the desired skin layer can be achieved with either of the following two combinations.

a) High pore size and low thickness
b) Low pore size and low thickness

As shown in Figure 7.1, the first case (a) can be achieved with hypophosphite based electroless plating baths while the second (b) can be achieved with the hydrazine based electroless plating baths.

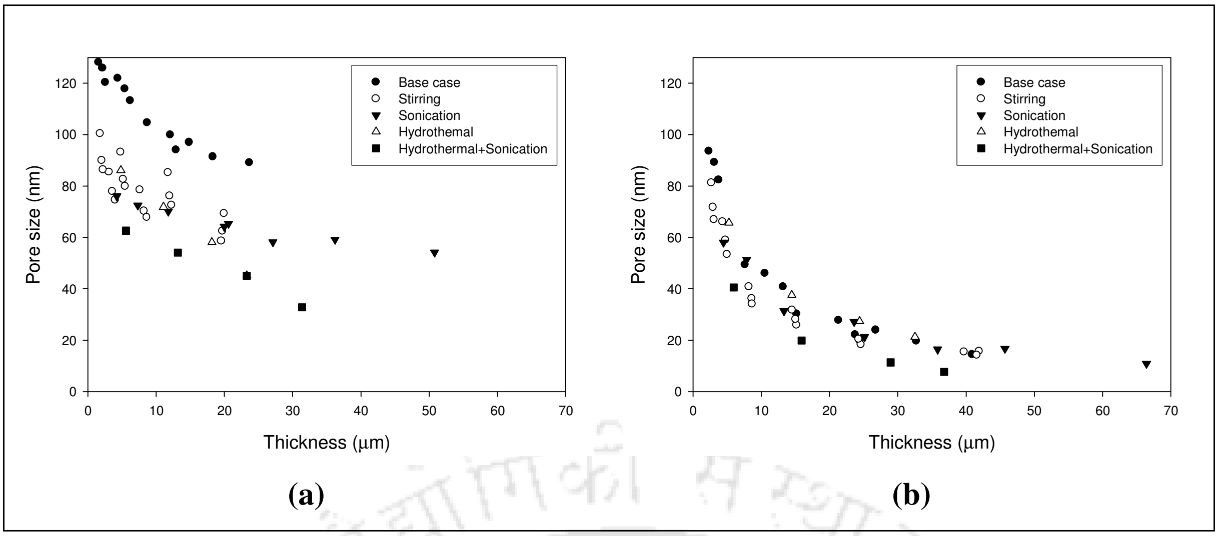

(a) **(b)**

Figure 7.1: Pore size versus thickness data for various cases.
(a) hypophosphite baths; (b) hydrazine baths.

For hydrazine based electroless plating baths (Figure 7.1b), mass transfer enhancements result in a coherent variation of pore size with thickness that can be marginalized with a non-linear correlation, which is not the case with hypophosphite baths (Figure 7.1a).

An important insight that is anticipated to be gained from the comparative assessment of the parameters obtained for membrane fabrication is with respect to the tradeoffs associated with the process. Electroless plating variables for membrane fabrication include process variables (conversion and efficiency), membrane variables (film thickness, average porosity and average pore size) and plating process conditions (concentration, loading ratio and selected mass transfer enhancement). For a simplistic assessment of the plating baths, it is necessary to combine these process variables to the bare minimum possible. Figure 7.2 (a) and (b) represent such an effort where membrane process variables are combinatorially represented as $d_o^2\delta$ and plating process variables are represented in terms of selective conversion. Conceptually, it is anticipated that the plating process must relate to a maximum value of selective conversion and minimal value of $d_o^2\delta$. For instance, for dense palladium membranes, state of the art research could indicate

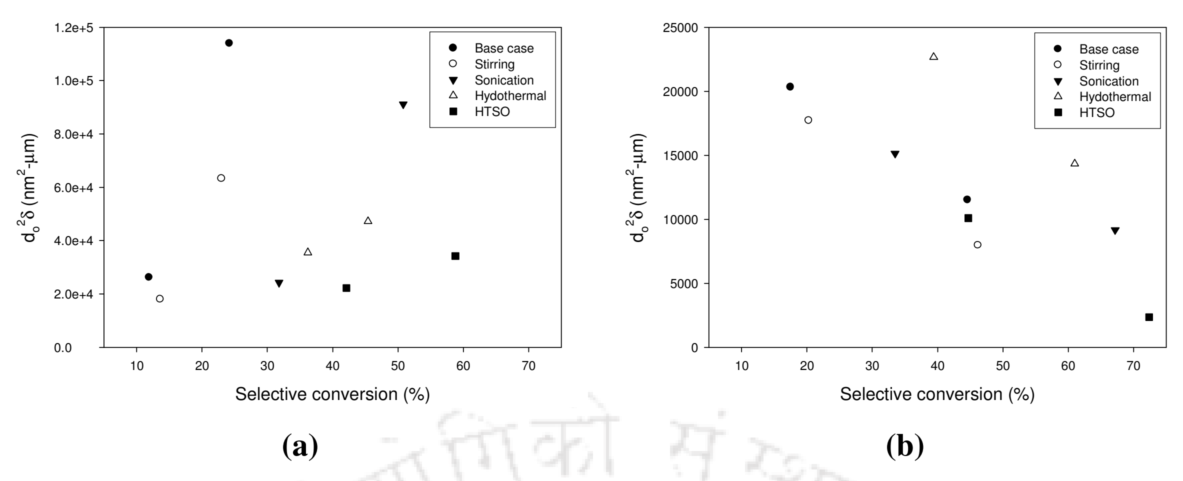

(a) **(b)**

Figure 7.2: $d_o^2\delta$ versus selective conversion for various cases.

(a) hypophosphite baths; (b) hydrazine baths.

achieving a dense palladium membrane with an average pore size of 1–2 nm and a palladium film thickness of 5 microns which refers to a $d_o^2\delta$ value of 20. As presented in the figure, the $d_o^2\delta$ values for hypophosphite baths varied from 18,000–114,000 (nm^2-µm) for a selective conversion variation from 12–59%. On the other hand, hydrazine plating baths referred to a combinatorial combination of 2,350–22,650 for $d_o^2\delta$ and selective conversion of 17.5–72.4%. Based on these plots, it is apparent that the following information can be inferred:

(a) There are many alternate processes that yield the same combinations of $d_o^2\delta$. For instance in Figure 7.2b, it can be observed that sonication and HTSO can yield a similar $d_o^2\delta$ value of 10,000 thereby indicating that in one case, thinner nickel films with larger average pore size can be achieved and in the second case, a thicker nickel film with lower average pore size can be obtained. This critical observation is indicative of the fact that mass transfer enhanced electroless plating processes offer wider flexibilities to achieve nickel membranes with diverse membrane morphological characteristics.

(b) The shown plots can be projected towards optimal tradeoff balance between selective conversion and $d_o^2\delta$ values. In the shown plots, it is always desired to obtain cases that refer to maximum value of x–axis (selective conversion) and minimal value of the y–axis ($d_o^2\delta$). In other words, the concept elaborated in this work is useful to serve as a general guideline for all electroless plating processes used for membrane fabrication research and development.

(c) The scale range of $d_o^2\delta$ for hypophosphite plating baths is 10 times higher than the scale range for hydrazine plating baths.

(d) For dense palladium composite membranes, a ten fold reduction in the y–axis scale range is anticipated with the $d_o^2\delta$ values ranging from 0–200, without much variation in the selective conversion scale range. However, this needs to be experimentally verified.

The observed performance characteristics of electroless plating baths for nickel–ceramic composite membrane fabrication are very promising towards the electroless plating of palladium membranes. This is due to the fact that for Pd, more than 90% conversion is achievable [51] with agitation in 60 minutes at a temperature of 60°C with a solution concentration of 0.016 mol/L and a loading ratio of 250 cm^2/L, which is significantly higher than the nickel conversion observed in this work (<60% for agitated hydrazine baths). Therefore, palladium electroless plating baths are expected to possess higher selective conversion and PPD values in comparison with those obtained for nickel electroless plating baths.

This work did not project towards the possible applications of nickel membranes fabricated by electroless plating with and without mass transfer enhancements. This is due to the fact that a preliminary comparative technical overview on the possible role of mass transfer enhancements in metal composite membranes prior to this work is not available and therefore this work assumed such a research direction. Most importantly, this work enables to realize that sonication or HTSO do not contribute to 100% pore densification for the chosen support, even though they contribute to enhance efficient nickel deposition rate substantially.

The presence of micro-pores in the FESEM images of nickel composite membranes fabricated with hypophosphite baths even at an initial nickel concentration of 0.16 mol/L and 8 sequential depositions is possibly due to the lack of effective pore coverage/densification of the larger pores of the support. If this hypothesis is true, then hypophosphite baths fail to accomplish uniform deposition for the supports with wider pore size distribution characteristics.

7.2 Recommendations for future work

Research findings in this work provided a good number of insights with respect to the performance of electroless plating baths and the fabrication of nickel–ceramic composite membranes. Few research areas for future work are presented as follows.

a) **Time dependent performance characteristics:** In this work, average performance characteristics based on 8 hour sequential deposition have been reported. Time dependent performance characteristics of electroless plating baths for nickel–ceramic composite membrane fabrication is an interesting area of research that could promote further insights in the metal deposition characteristics such as variation in thickness, effective porosity and average pore size with time of deposition. Thereby, process optimization studies can be targeted that feature the minimal number of plating steps required to achieve desired membrane characteristics.

b) **Other mass transfer techniques:** Studies on other alternatives to the mass transfer techniques already presented in this work such as gas sparging, oscillation, vacuum and additives such as surfactants. Preliminary studies using ionic surfactants (SDS and CTAB) were carried out recently [112]. However, there is a scope for extensive research in this area.

c) **Nickel/γ-alumina membranes for hydrogen separation:** In this work, the consideration of a low cost ceramic membrane with high average pore size and higher pore size distribution is regarded to be the primary reason to not achieve dense nickel–ceramic membranes despite considering various mass transfer enhancement techniques and a time frame of 8 h sequential deposition. The performance characteristics of electroless plating baths for the fabrication of dense nickel/γ-alumina membranes is an important area of research that can be explored, as thin dense nickel membranes can be engineered to be alternate technology for the expensive palladium composite membrane technology. Typical applications for such membranes such as hydrogen separation and purification can be also targeted to quantify membrane separation characteristics. Alternatively, the usage of chromia to obtain dense nickel–ceramic membranes is also of particular interest.

d) **Nickel–ceramic membranes as supports for Pd composite membranes:** From the available literatures, nickel powder impregnated membranes possess an average pore size of 33 nm, where as in this work we have been able to obtain nickel composite membranes with an average pore size of 8–20 nm. In other words, research so far in the field of metal–ceramic membrane technology addressed limited options for engineering of the inter-diffusion layer which can be eliminated by targeting film engineering using electroless plating technique. Therefore, we anticipate to further research that ascertain the functional use of nickel films as intermediate diffusion barriers and thereby achieve dense palladium membranes with minimal Pd film thickness. Interesting feature of such research is to examine the compatibility of nickel and palladium films and their stability at high temperature. Performance characteristics of both nickel plating baths and palladium plating baths towards dense palladium–nickel composite membrane fabrication is an important area of research that can be investigated in the near future.

e) **Nickel–ceramic membranes as supports for silver composite membranes:** To date, one publication reports the applicability of silver membranes for bacteriostatic applications [10]. However, in comparison to the dense palladium–nickel composite membranes, the silver membranes need to be porous for maximizing hydraulic permeability of the membrane. Performance characteristics of electroless plating baths for the preparation and application of porous silver–nickel low cost ceramic membranes can be a potential area of research that requires engineering study for both nickel as well as silver films.

f) **Electroplating mass transfer enhancements:** Mass transfer enhancements (bath agitation, vacuum and sonication) for the fabrication of nickel or palladium composite membranes by electroplating on porous stainless steel supports can be also investigated.

g) **Other applications for nickel membranes:** Other low cost applications of nickel composite membranes for waste water treatment, oil–water emulsions, microfiltration/ultrafiltration of fruit juices etc. can as well be explored.

h) **Fuel cell component research:** the fundamentals presented with respect to mass transfer enhanced electroless plating can be targeted towards the materials research of fuel-cell components as reported in some literatures.

i) **Performance characteristics of tubular membranes:** The present work is dovetailed towards disk shaped membranes and engineering studies towards fabrication of tubular nickel ceramic membranes can be also explored in the near future.

j) **Artificial neural network (ANN) modeling:** Based on large sets of data generated from experimental investigations, ANN modeling can be targeted to obtain greater insights into experimental design and achievement of the same, without enhancing the number of experiments for palladium membranes. ANN based modeling to quantify palladium plating performance characteristics based on nickel plating performance characteristics is an important area of research that can be explored in the near future.

The conceptual insights gathered in this work need further refinement and fine tuning towards assessing the role of better quality porous supports in combinatorial performance characteristics of electroless plating baths. Needless to say, an immediate extension of this work is to target similar studies for dense Pd membranes and identify all possible parametric combinations (including mass transfer enhancement techniques) that can realize dense Pd membranes. Such a development would enable researchers as well as corporates to judiciously adopt mass transfer enhancement techniques towards 100% pore densification based on cost analysis.

References

[1] A. Brunetti, S. Simone, F. Scura, G. Barbieri, A. Figoli, E. Drioli, "Hydrogen mixture separation with PEEK-WC asymmetric membranes", Separation and Purification Technology 69 (2009) 195–204.

[2] K.P. Lee, T.C. Arnot, D. Mattia, "A review of reverse osmosis membrane materials for desalination — Development to date and future potential", Journal of Membrane Science 370 (2011) 1–22.

[3] J. Barzin, C. Feng, K.C. Khulbe, T. Matsuura, S.S. Madaeni, H. Mirzadeh, "Characterization of polyethersulfone hemodialysis membrane by ultrafiltration and atomic force microscopy", Journal of Membrane Science 237 (2004) 77–85.

[4] N. Agoudjil, N. Benmouhoub, A. Larbot, "Synthesis and characterization of inorganic membranes and applications", Desalination 184 (2005) 65–69.

[5] J.N. Armor, "Applications of catalytic inorganic membrane reactors to refinery products", Journal of Membrane Science 147 (1998) 217–233.

[6] S. Yun, S.T. Oyama, "Correlations in palladium membranes for hydrogen separation: A review", Journal of Membrane Science 375 (2011) 28–45.

[7] S. Karellas, E. Kakaras, T. Papadopoulos, C. Schäfer, J. Karl, "Hydrogen production from allothermal biomass gasification by means of palladium membranes", Fuel Processing Technology 89 (2008) 582–588.

[8] Y. Chen, Y. Wang, H. Xu, G. Xiong, "Efficient production of hydrogen from natural gas steam reforming in palladium membrane reactor", Applied Catalysis B: Environmental 80 (2008) 283–294.

[9] T. Sato, H. Yokoyama, H. Miki, N. Itoh, "Selective dehydrogenation of unsaturated alcohols and hydrogen separation with a palladium membrane reactor", Journal of Membrane Science 289 (2007) 97–105.

[10] H. Basri, A.F. Ismail, M. Aziz, K. Nagai, T. Matsuura, M.S. Abdullah, B.C. Ng, "Silver-filled polyethersulfone membranes for antibacterial applications — Effect of PVP and TAP addition on silver dispersion", Desalination 261 (2010) 264–271.

[11] Johnson Matthey Gas Purification Technology, USA, The PureGuard™ Palladium Hydrogen Gas Purifiers, Available at: http://pureguard.net/cm/About_Us/About_JM_Gas_Purification_Technology.html (May 2011).

[12] ECN, Netherlands, Energy efficient hydrogen separator, Available at: http://www.ecn.nl/news/newsletter-en/2010/september-2010/energy-efficient hydrogen-separator/ (May 2011).

[13] GE Osmonics Labstore, USA, GE Silver Membranes**,** Available at: http://www.osmolabstore.com/OsmoLabPage.dll?BuildPage&1&1&326 (October 2010).

[14] SPI Supplies, USA, SPI-Pore™ Silver Membrane Media, Available at: http://www.2spi.com/catalog/spec_prep/silver-membrane-filtration-media.html (October 2010).

[15] SKC Inc., USA, SKC Silver Membrane Filters, Available at: http://www.skcinc.com/prod/225-1801.asp (October 2010).

[16] Sterlitech Corporation, USA, Sterlitech™ Silver Membrane Filters, Available at: http://www.sterlitech.com/membrane-disc-filters/silver-membranes/silver-membrane-filters-45330.html (June 2011).

[17] Wacorp Hyundai India Limited, India, Nano silver membrane filter, Available at: http://www.indiamart.com/wacorphyundai/water-filter.html#nano-silver-membrane-filter (May 2011).

[18] Mott Corporation, USA, GasShield® PENTA® Filters, Available at: http://www.mottcorp.com/products/biotechnology-semiconductor/penta.cfm (October 2010).

[19] Mykron, China, Mykrolis™ Nickel Membrane Filters, Available at: http://www.mykrons.com/ProductThree.asp?id=72 (October 2010).

[20] Entegris, USA, Surface Mount Metal Gas Filter, Available at: http://www.entegris.com/ProductLine_catGasFilter_divFiltration_lineGF_Surface_Mount_Metal_Gas_Filter.aspx (October 2010).

[21] N. Itoh, T. Akiha, T. Sato, "Preparation of thin palladium composite membrane tube by a CVD technique and its hydrogen permselectivity", Catalysis Today 104 (2005) 231–237.

[22] C.A. Cooper, Y.S. Lin, "Microstructural and gas separation properties of CVD modified mesoporous γ-alumina membranes", Journal of Membrane Science 195 (2002) 35–50.

[23] H.Y. Ha, S.W. Nam, T.H. Lim, I.-H. Oh, S.-A. Hong, "Properties of the TiO_2 membranes prepared by CVD of titanium tetraisopropoxide", Journal of Membrane Science 111 (1996) 81–92.

[24] S. Gopalakrishnan, J.C.D. Costa, "Hydrogen gas mixture separation by CVD silica membrane", Journal of Membrane Science 323 (2008) 144–147.

[25] Y. Gu, S.T. Oyama, "Permeation properties and hydrothermal stability of silica–titania membranes supported on porous alumina substrates", Journal of Membrane Science 345 (2009) 267–275.

[26] J. Tong, C. Su, K. Kuraoka, H. Suda, Y. Matsumura, "Preparation of thin Pd membrane on CeO_2-modified porous metal by a combined method of electroless plating and chemical vapor deposition", Journal of Membrane Science 269 (2006) 101–108.

[27] Y. Huang, R. Dittmeyer, "Preparation of thin palladium membranes on a porous support with rough surface", Journal of Membrane Science 302 (2007) 160–170.

[28] E. Kikuchi, Y. Nemoto, M. Kajiwara, S. Uemiya, T. Kojima, "Steam reforming of methane in membrane reactors: comparison of electroless-plating and CVD membranes and catalyst packing modes", Catalysis Today 56 (2000) 75–81.

[29] L.-J. Wang, F.C.-N. Hong, "Carbon-based molecular sieve membranes for gas separation by inductively-coupled-plasma chemical vapor deposition", Microporous and Mesoporous Materials 77 (2005) 167–174.

[30] C.-S. Jun, K.-H. Lee, "Palladium and palladium alloy composite membranes prepared by metal-organic chemical vapor deposition method (cold-wall)", Journal of Membrane Science 176 (2000) 121–130.

[31] S.-K. Ryi, J.-S. Park, S.-H. Kim, S.-H. Cho, D.-W. Kim, K.-Y. Um, "Characterization of Pd–Cu–Ni ternary alloy membrane prepared by magnetron

sputtering and Cu-reflow on porous nickel support for hydrogen separation", Separation and Purification Technology 50 (2006) 82–91.

[32] L. Xiong, S. Liu, L. Rong, "Fabrication and characterization of Pd/$Nb_{40}Ti_{30}Ni_{30}$/Pd/porous nickel support composite membrane for hydrogen separation and purification", International Journal of Hydrogen Energy 35 (2010), 1643–1649.

[33] S.-K. Ryi, J.-S. Park, S.-H. Kim, S.-H. Cho, D.-W. Kim, "The effect of support resistance on the hydrogen permeation behavior in Pd–Cu–Ni ternary alloy membrane deposited on a porous nickel support", Journal of Membrane Science 280 (2006) 883–888.

[34] S.-K. Ryi, J.-S. Park, S.-H. Kim, D.-W. Kim, K.-I. Cho, "Formation of a defect-free Pd–Cu–Ni ternary alloy membrane on a polished porous nickel support (PNS)", Journal of Membrane Science 318 (2008) 346–354.

[35] Y. Zhang, T. Ozaki, M. Komaki, C. Nishimura, "Hydrogen permeation characteristics of V-15Ni membrane with Pd/Ag overlayer by sputtering", Journal of Alloys and Compounds 356–357 (2003) 553–556.

[36] R. Checchetto, N. Bazzanella, B. Patton, A. Miotello, "Palladium membranes prepared by r.f. magnetron sputtering for hydrogen purification", Surface and Coatings Technology 177–178 (2004) 73–79.

[37] J. O'Brien, R. Hughes, J. Hisek, "Pd/Ag membranes on porous alumina substrates by unbalanced magnetron sputtering", Surface and Coatings Technology 142–144 (2001) 253–259.

[38] H.-B. Zhao, G.-X. Xiong, G.V. Baron, "Preparation and characterization of palladium-based composite membranes by electroless plating and magnetron sputtering", Catalysis Today 56 (2000) 89–96.

[39] F.C. Gielens, H.D. Tong, C.J.M.V. Rijn, M.A.G. Vorstman, J.T.F. Keurentjes, "High flux palladium-silver membranes fabricated by microsystem technology", Desalination 147 (2002) 417–423.

[40] A.L. Athayde, R.W. Baker, P. Nguyen, "Metal Composite membranes for hydrogen separation", Journal of Membrane Science 94 (1994) 299–311.

[41] S.C. Chen, G.C. Tu, C.C.Y. Hung, C.A. Huang, M.H. Rei, "Preparation of palladium membrane by electroplating on AISI 316L porous stainless steel supports and its use for methanol steam reformer", Journal of Membrane Science 314 (2008) 5–14.

[42] S.-E. Nam, S.-H. Lee, K.-H. Lee, "Preparation of a palladium alloy composite membrane supported in a porous stainless steel by vacuum electrodeposition", Journal of Membrane Science 153 (1999) 163–173.

[43] S.-E. Nam, K.-H. Lee, "A study on the palladium/nickel composite membrane by vacuum electrodeposition", Journal of Membrane Science 170 (2000) 91–99.

[44] K.H. Choi, H.S. Kim, T.H. Lee, "Electrode fabrication for proton exchange membrane fuel cells by pulse electrodeposition", Journal of Power Sources 75 (1998) 230–235.

[45] S.-E. Nam, Y.-K. Seong, J.W. Lee, K.-H. Lee, "Preparation of highly stable palladium alloy composite membranes for hydrogen separation", Desalination 236 (2009) 51–55.

[46] S. Lertviriyapaisan, N. Tantavichet, "Sublayers for Pt catalyst electrodeposition electrodes in PEMFC", International Journal of Hydrogen Energy 35 (2010) 10464–10471.

[47] H. Kim, N.P. Subramanian, B.N. Popov, "Preparation of PEM fuel cell electrodes using pulse electrodeposition", Journal of Power Sources 138 (2004) 14–24.

[48] Q. Wei, X. Ren, J. Du, S. Wei, S. Hu, "Study of the electrodeposition conditions of metallic manganese in an electrolytic membrane reactor", Minerals Engineering 23 (2010) 578–586.

[49] S. Hrapovic, M.-F. Manuel, J.H.T. Luong, S.R. Guiot, B. Tartakovsky, "Electrodeposition of nickel particles on a gas diffusion cathode for hydrogen production in a microbial electrolysis cell", International Journal of Hydrogen Energy 35 (2010) 7313–7320.

[50] J.-H. Lee, Y.-W. Chung, M.-H. Hon, I.-C. Leu, "Fabrication of tunable pore size of nickel membranes by electrodeposition on colloidal monolayer template", Journal of Alloys and Compounds 509 (2011) 6528–6531.

[51] M.E. Ayturk, Y.H. Ma, “Electroless Pd and Ag deposition kinetics of the composite Pd and Pd/Ag membranes synthesized from agitated plating baths”, Journal of Membrane Science 330 (2009) 233–245.

[52] G. Zeng, A. Goldbach, H. Xu, “Defect sealing in Pd membranes via point plating”, Journal of Membrane Science 328 (2009) 6–10.

[53] M. Seshimo, M. Ozawa, M. Sone, M. Sakurai, H. Kameyama, “Fabrication of a novel Pd/γ-alumina graded membrane by electroless plating on nanoporous γ-alumina”, Journal of Membrane Science 324 (2008) 181–187.

[54] S.K. Gade, P.M. Thoen, J.D. Way, “Unsupported palladium alloy foil membranes fabricated by electroless plating”, Journal of Membrane Science 316 (2008) 112–118.

[55] X. Zhang, G. Xiong, W. Yang, “A modified electroless plating technique for thin dense palladium composite membranes with enhanced stability”, Journal of Membrane Science 314 (2008) 226–237.

[56] Z. Ke, G. Huiyuan, R. Zebao, L. Yuesheng, L. Yongdan, “Preparation of Thin Palladium Composite Membranes and Application to Hydrogen/Nitrogen Separation”, Chinese Journal of Chemical Engineering 15(5) (2007) 643-647.

[57] B.K.R. Nair, J. Choi, M.P. Harold, “Electroless plating and permeation features of Pd and Pd/Ag hollow fiber composite membranes”, Journal of Membrane Science 288 (2007) 67–84.

[58] Y. Huang, R. Dittmeyer, “Preparation and characterization of composite palladium membranes on sinter-metal supports with a ceramic barrier against intermetallic diffusion”, Journal of Membrane Science 282 (2006) 296–310.

[59] T. Huang, M. Wei, H. Chen, “Preparation of hydrogen-permselective palladium-silver alloy composite membranes by electroless co-deposition”, Separation and Purification Technology 32 (2003) 239-245.

[60] F. Roa, J.D.Way, R.L. McCormick, S.N. Paglieri, “Preparation and characterization of Pd–Cu composite membranes for hydrogen separation”, Chemical Engineering Journal 93 (2003) 11–22.

[61] Y.S. Cheng, K.L. Yeung, “Effects of electroless plating chemistry on the synthesis of palladium membranes”, Journal of Membrane Science 182 (2001) 195–203.

[62] W. Zheng, L. Wu, "Preparation and pore size shrinkage of palladium–ceramic composite membrane by electroless plating under hydrothermal conditions", Materials Science and Engineering A 283 (2000) 122–125.

[63] H.B. Zhao, G.X. Xiong, G.V. Baron, "Preparation and characterization of palladium-based composite membranes by electroless plating and magnetron sputtering", Catalysis Today 56 (2000) 89–96.

[64] J.N. Keuler, L. Lorenzen, R.D. Sanderson, V. Prozesky, W.J. Przybylowicz, "Characterising palladium-silver and palladium-nickel alloy membranes using SEM, XRD and PIXE", Nuclear Instruments and Methods in Physics Research B 158(1999) 678–682.

[65] A. Li, W. Liang, R. Hughes, "Fabrication of defect-free Pd/α-Al_2O_3 composite membranes for hydrogen separation", Thin Solid Films 350 (1999) 106–112.

[66] K.L. Yeung, S.C. Christiansen, A. Varma, "Palladium composite membranes by electroless plating technique: Relationships between plating kinetics, film microstructure and membrane performance", Journal of Membrane Science 159 (1999) 107–122.

[67] J.N. Keuler, L. Lorenzen, R.D. Sanderson, V. Prozesky, W.J. Przybylowicz, "Characterization of electroless plated palladium-silver alloy membranes", Thin Solid Films 347(1999) 91–98.

[68] H.B. Zhao, K. Pflanz, J.H. Gu, A.W. Li, N. Stroh, H. Brunner, G.X. Xiong, "Preparation of palladium composite membranes by modified electroless plating procedure", Journal of Membrane Science 142 (1998) 147–157.

[69] P. Kathirgamanathan, "Ultrasound-assisted electroless deposition of copper onto and into microporous membranes for electromagnetic shielding", Polymer Communications 35 (1994) 430–432.

[70] E. Kikuchi, S. Uemiya, "Preparation of supported thin palladium-silver alloy membranes and their characteristics for hydrogen separation", Gas Separation & Purification 5 (1991) 261–266.

[71] X. Tang, C. Bi, C. Han, B. Zhang, "A new palladium-free activation process for Ni electroless plating on ABS plastic", Materials Letters 63 (2009) 840–842.

[72] H. Ma, F. Tian, D. Li, Q. Guo, “Study on the nano-composite electroless coating of Ni-P/Ag”, Journal of Alloys and Compounds 474 (2009) 264–267.

[73] H. Zhang, S. Wang, G. Yao, Z. Hua, “Electroless Ni-P plating on Mg-10Li-1Zn alloy”, Journal of Alloys and Compounds 474 (2009) 306–310.

[74] S.S. Mahmoud, “Electroless deposition of nickel and copper on titanium substrates: Characterization and application”, Journal of Alloys and Compounds 472 (2009) 595–601.

[75] P. Sahoo, “Wear behaviour of electroless Ni-P coatings and optimization of process parameters using Taguchi method”, Materials and Design 30 (2009) 1341–1349.

[76] J. Novakovic, P. Vassiliou, “Vacuum thermal treated electroless NiP-TiO_2 composite coatings”, Electrochimica Acta 54 (2009) 2499–2503.

[77] A.A. Aal, M.S. Aly, “Electroless Ni-Cu-P Plating onto Open Cell Stainless Steel Foam”, Applied Surface Science 255 (2009) 6652–6655.

[78] Z. Wu, S. Ge, M. Zhang, W. Li, K. Tao, “Synthesis of nickel nanoparticles supported on metal oxides using electroless plating: Controlling the dispersion and size of nickel nanoparticles”, Journal of Colloid and Interface Science 330 (2009) 359–366.

[79] D. Song, J. Zhou, W. Jiang, X. Zhang, Y. Yan, F. Li, “A novel activation for electroless plating on preparing Ni/PS microspheres”, Materials Letters 63 (2009) 282–284.

[80] W.L. Liu, S.H. Hsieh, W.J. Chen, Y.C. Hsu, “Growth behavior of electroless Ni–Co–P deposits on Fe”, Applied Surface Science 255 (2009) 3880–3883.

[81] Y. Kong, J. Shao, W. Wang, Q. Liu, Z. Chen, “Electroless Sn–Ni alloy plating with high Sn content free of activation pretreatment”, Journal of Alloys and Compounds 477 (2009) 328–332.

[82] A. Shibata, Y. Imamura, M. Sone, C. Ishiyama, Y. Higo, “Pd–Ni–P metallic glass film fabricated by electroless alloy plating”, Thin Solid Films 517 (2009) 1935–1938.

[83] K.K. Kar, D. Sathiyamoorthy, “Influence of process parameters for coating of nickel–phosphorous on carbon fibers”, Journal of Materials Processing Technology 209 (2009) 3022–3029.

[84] M. Yan, H.G. Ying, T.Y. Ma, W. Luo, “Effects of Yb^{3+} on the corrosion resistance and deposition rate of electroless Ni–P deposits”, Applied Surface Science 255 (2008) 2176–2179.

[85] R. Elansezhian, B. Ramamoorthy, P.K. Nair, “Effect of surfactants on the mechanical properties of electroless (Ni–P) coating”, Surface & Coatings Technology 203 (2008) 709–712.

[86] Y. Hazan, D. Werner, M. Z’graggenc, M. Groteklaes, T. Graule, “Homogeneous Ni-P/Al_2O_3 nanocomposite coatings from stable dispersions in electroless nickel baths”, Journal of Colloid and Interface Science 328 (2008) 103–109.

[87] Y. Cheng, Y. Zou, L. Cheng, W. Liu, “Effect of the microstructure on the anti-fouling property of the electroless Ni–P coating”, Materials Letters 62 (2008) 4283–4285.

[88] F.D. Grande, A. Thursfield, I.S. Metcalfe, “Morphological control of electroless plated Ni anodes: Influence on fuel cell performance”, Solid State Ionics 179 (2008) 2042–2046.

[89] H. Liu, N. Li, S. Bi, D. Li, Z. Zou, “Effect of organic additives on the corrosion resistance properties of electroless nickel deposits”, Thin Solid Films 516 (2008) 1883–1889.

[90] Y.S. Huang, F.Z. Cui, “Effect of complexing agent on the morphology and microstructure of electroless deposited Ni–P alloy”, Surface & Coatings Technology 201 (2007) 5416–5418.

[91] X. Changrong, G. Xiaoxia, L. Fanqing, P. Dingkun, M. Guangyao, “Preparation of asymmetric Ni/ceramic composite membrane by electroless plating”, Colloids and Surfaces A: Physicochemical and Engineering Aspects 179 (2001) 229–235.

[92] D. Xue, J. Deng, “Amorphous Ni–B alloy/ceramic composite membrane prepared by an improved electroless plating technique”, Materials Letters 47 (2001) 271–275.

[93] S. Haag, M. Burgard, B. Ernst, “Pure nickel coating on a mesoporous alumina membrane: Preparation by electroless plating and characterization”, Surface & Coatings Technology 201 (2006) 2166–2173.

[94] I.P. Mardilovich, E.E. Engwall, Y.H. Ma “Dependence of hydrogen flux on the pore size and plating surface topology of asymmetric Pd-porous stainless steel membranes”, Desalination 144 (2002) 85–89.

[95] L. Huang, C.S. Chen, Z.D. He, D.K. Peng, G.Y. Meng, “Palladium membranes supported on porous ceramics prepared by chemical vapor deposition”, Thin Solid Films 302 (1997) 98-101.

[96] O. Altinisik, M. Dogan, G. Dogu, “Preparation and characterization of palladium-plated porous glass for hydrogen enrichment”, Catalysis Today 105 (2005) 641–646.

[97] S.-K. Ryi, J.-S. Park, S.-H. Kim, S.-C. Hong, D.-W. Kim, “The study of a new porous nickel support for palladium-based alloy membrane”, Desalination 200 (2006) 216–218.

[98] J.P. Collins, J.D. Way, “Preparation and Characterization of a Composite Palladium–Ceramic Membrane”, Industrial & Engineering Chemistry Research 32 (1993) 3006–3013.

[99] M. Dogan, S. Kilicarslan, “Effects of process parameters on the synthesis of palladium membranes”, Nuclear Instruments and Methods in Physics Research Section B: Beam Interactions with Materials and Atoms 266 (2008) 3458–3466.

[100] S.N. Paglieri, K.Y. Foo, J.D. Way, J.P. Collins, D.L. Harper-Nixon, “A New Preparation Technique for Pd/Alumina Membranes with Enhanced Stability at High Temperatures”, Industrial & Engineering Chemistry Research 38 (1999) 1925–1936.

[101] R. Elansezhian, B. Ramamoorthy, P.K. Nair, “The influence of SDS and CTAB surfactants on the surface morphology and surface topography of electroless Ni–P deposits”, Journal of Materials Processing Technology 209 (2009) 233–240.

[102] L. Li, M. An, “Electroless nickel-phosphorus plating on SiC_p/Al composite from acid bath with nickel activation”, Journal of Alloys and Compounds 461 (2008) 85–91.

[103] H. Bi, K.C. Kou, A.E. Rider, K. Ostrikov, H.W. Wu, Z.C. Wang, “Low-phosporous nickel-coated carbon microcoils: Controlling microstructure through an electroless plating process”, Applied Surface Science 255 (2009) 6888–6893.

[104] J.T.W. Jappes, B. Ramamoorthy, P.K. Nair, “A study on the influence of process parameters on efficiency and crystallinity of electroless Ni–P deposits”, Journal of Materials Processing Technology 169 (2005) 308–313.

[105] J. Jiang, H. Lu, L. Zhang, N. Xu, “Preparation of monodisperse Ni/PS spheres and hollow nickel spheres by ultrasonic electroless plating”, Surface and Coatings Technology 201 (2007) 7174–7179.

[106] S. Vichaphund, D Atong, “Fabrication of Ni-alumina Composite Membrane via Powder and Bulk Impregnation Method for Hydrogen Separation”, Journal of Materials Science & Technology 26 (2010) 589–596.

[107] M.C. Almandoz, J. Marchese, P. Prádanos, L. Palacio, A. Hernández, “Preparation and characterization of non-supported micro-filtration membranes from aluminosilicates”, Journal of Membrane Science 241 (2004) 95–103.

[108] J. Marchese, C.L. Pagliero, “Characterization of asymmetric polysulphone membranes for gas separation”, Gas Separation & Purification, 5 (1991) 215–221.

[109] L. Palacio, P. Prádanos, J.I. Calvo, A. Hernández, “Porosity measurements by a gas penetration method and other techniques applied to membrane characterization”, Thin Solid Films 348 (1999) 22–29.

[110] Y. Lu, “Improvement of copper plating adhesion on silane modified PET film by ultrasonic-assisted electroless deposition”, Applied Surface Science 256 (2010) 3554–3558.

[111] F. Touyeras, J.Y. Hihn, X. Bourgoin, B. Jacques, L. Hallez, V. Branger, “Effects of ultrasonic irradiation on the properties of coatings obtained by electroless plating and electro plating”, Ultrasonics Sonochemistry 12 (2005) 13–19.

[112] V.K. Bulasara, Ch.S.N.M. Babu, R. Uppaluri, “Effect of surfactants on the performance of electroless plating baths for nickel–ceramic composite membrane fabrication”, Surface Engineering, In Press, doi: 10.1179/1743294411Y.0000000035 (2011).

A: Nitrogen permeation test

Equations (2.15)–(2.20) are actually derived for single gases. However, air permeation is carried out as it is relatively inexpensive compared to the N_2 permeation for routine membrane testing. Therefore, to validate the air permeation analysis, single gas permeation tests were conducted. Figure A.1 presents the parity plot of flow rates of nitrogen gas versus air during gas permeations tests using some of the prepared nickel–ceramic composite membranes. From this figure, it can be observed that both these gases (N_2 and air) have very similar permeation properties. Hence it can be inferred that the air permeation experiments are equally valid to the single gas permeability tests using N_2.

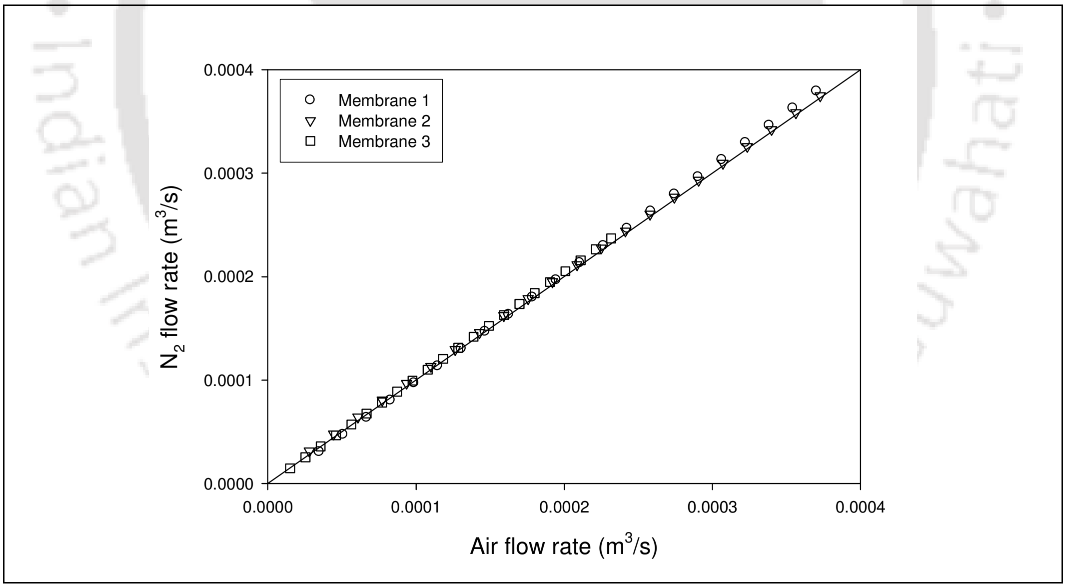

Figure A.1: Comparison of flow rates of N_2 and air during gas permeation tests.

B: Error analysis

For experimental investigations, it is common that some differences exist between the sets of measured values during repetitions. Therefore, based on several experimental runs average values are usually reported. The confidence levels associated with the average values and measured values is often summarized in the form of an error analysis in scientific and technical reports. Error analysis reveals the accuracy of calculations and reliability of the reported experimental data. Broadly, there exist two types of errors namely systematic error and random error. Systematic errors arise due to faulty assumptions and improper experimental measuring techniques. In this work, proper care was taken in eliminating systematic errors by appropriately designing the experiments and adopting well accepted methods for the analysis of data. On the other hand, random errors arise due to variation in the precision of measured parameters. Usually, random errors are contributed by minor variations in successive measurements made by the experimentalist under nearly identical conditions. Therefore, random errors can not be eliminated. The aim of the error analysis section presented here is to quantify the magnitude of the random errors. In many experiments performed in this work, quantities were evaluated by weight gain measured using digital microbalance, titrations. Therefore, significant amount of random error is not anticipated in these measurements.

Error in the measurement of concentration

Concentrations of plating baths before and after deposition were measured using titration analysis. Therefore, the parallax error could be up to a minor calibration of the burette (0.05 ml) containing the standardized solution of EDTA. This may lead to a possible error of 0.1% in the evaluated concentrations which may lead to 0.2% error in the conversion values and reaction rates.

Error in the measurement of weight gain

Dry weights of the membranes before and after nickel deposition were measured using a digital microbalance with four digit precision after the decimal and a minor variation was observed only in the fourth digit during measurements. Therefore, the measurement errors in this case were about 0.01–0.1%. This may lead to a possible error of 0.01–0.1% in the evaluated plating efficiencies and average thickness values.

Error in the measurement of gas flow rates

Air permeation experiments were conducted to evaluate the average pore size and porosity of all the nickel–ceramic composite membranes. The permeate gas flow-rates were measured using a calibrated rotameter. Therefore, the error in the gas flow-rates at each trans-membrane pressure drop could be up to 0.1 LPM (1.67×10^{-6} m^3/s). This may lead to a possible error of 0–2 nm in the estimation of average pore size, 0.001–0.01% in the porosity values and 0–0.0053% in the evaluated PPD values.

Reproducibility of the results

Several experiments were repeated randomly to test for reproducibility of the results reported in the thesis. Similar results as of those reported in the thesis were obtained with negligible errors and were within the ranges discussed above possibly due to the contribution of random errors.

C: Sample calculations

Sample calculations of various parameters for one membrane (base case, C_i = 0.04 mol/L, θ = 196 cm^2/L) are presented here.

C_i = 0.04 mol/L

$$\text{Titration: } N_1 = \frac{N_2 \times V_2}{V_1} = \frac{0.1\times 3.6}{5} = 0.072 \text{ N} = 0.036 \text{ mol/L} \qquad \text{(Eq. (2.14))}$$

C_f = 0.036 mol/L

$$\text{Conversion, } x = \frac{C_i - C_f}{C_i} = \frac{0.04-0.036}{0.04} = 0.1 \quad (= 10\%) \qquad \text{(Eq. (2.9))}$$

$$w_0 = (nV_0C_i)\, M_{Ni} = (8\times 0.1\times 0.04)\, 58.71 = 1.8787 \text{ g} \qquad \text{(Eq. (2.11))}$$

$$\text{Efficiency, } \eta = \frac{w_2 - w_1}{w_0 x} = \frac{12.9706-12.7883}{1.8787\times 0.1} = 0.9703 \quad (=97.03\%) \qquad \text{(Eq. (2.10))}$$

$$\text{Selective conversion} = x\times\eta = 0.1\times 0.9703 = 0.097 \quad (=9.7\%)$$

$$\text{Average deposition rate, } \overline{r}_e = \frac{C_i - C_f}{t}\times\eta = \frac{0.04-0.036}{3600}\times 0.9703 \qquad \text{(Eq. (2.26))}$$

$$= 1.078\times 10^{-6} \text{ mol/L.s}$$

$$\text{Film thickness, } \delta = \frac{w_2 - w_1}{\rho_{Ni} A_m}\times\frac{1}{1-(\varepsilon/q^2)_{film}} \qquad \text{(Eq. (2.12))}$$

$$= \frac{12.9706-12.7883}{8.8\times 80}\times\frac{1}{1-0.0029}$$

$$= 0.000259 \text{ cm} = 2.59\ \mu\text{m}$$

$$\text{Percent pore densification, } PPD = \left(\frac{d_i^2 - d_o^2}{d_i^2}\right)\times 100 \qquad \text{(Eq. (2.13))}$$

$$= \frac{(275)^2 - (120)^2}{(275)^2}\times 100 = 80.87\%.$$

Articles published in international refereed journals

[1] **V.K. Bulasara**, H. Thakuria, R. Uppaluri, M.K. Purkait, "Effect of process parameters on electroless plating and nickel–ceramic composite membrane characteristics", *Desalination*, Vol. 268, p. 195–203 (2011).

[2] **V.K. Bulasara**, H. Thakuria, R. Uppaluri, M.K. Purkait, "Nickel–ceramic composite membranes: Optimization of hydrazine based electroless plating process parameters", *Desalination*, Vol. 275, p. 243–251 (2011).

[3] **V.K. Bulasara**, H. Thakuria, R. Uppaluri, M.K. Purkait, "Combinatorial performance characteristics of agitated nickel hypophosphite electroless plating baths", *Journal of Materials Processing Technology*, Vol. 211, p. 1488–1499 (2011).

[4] **V.K. Bulasara**, R. Uppaluri, M.K. Purkait, "Manufacture of nickel–ceramic composite membranes in agitated electroless plating baths", *Materials and Manufacturing Processes*, Vol. 26, p. 862–867 (2011).

[5] **V.K. Bulasara**, O. Chandrashekar, R. Uppaluri, "Effect of surface roughness and mass transfer enhancement on the performance characteristics of nickel–hypophosphite electroless plating baths for metal–ceramic composite membrane fabrication", *Chemical Engineering Research and Design*, Vol. 89, p. 2485–2494 (2011).

[6] **V.K. Bulasara**, M.S. Abhimanyu, T. Pranav, R. Uppaluri, M.K. Purkait, "Performance characteristics of hydrothermal and sonication assisted electroless plating baths for nickel–ceramic composite membrane fabrication", *Desalination*, Vol. 284, p. 77–85 (2012).

[7] **V.K. Bulasara**, R. Uppaluri, M.K. Purkait, "Effect of ultrasound on the performance of nickel hydrazine electroless plating baths", *Materials and Manufacturing Processes*, In Press, doi: 10.1080/10426914.2011.566663 (2011).

[8] **V.K. Bulasara**, Ch.S.N.M. Babu, R. Uppaluri, "Effect of surfactants on the performance of electroless plating baths for nickel–ceramic composite membrane fabrication", *Surface Engineering*, In Press, doi: 10.1179/1743294411Y.0000000035 (2011).

Article in preparation

[1] **V.K. Bulasara**, R. Uppaluri, M.K. Purkait, "Effect of mass transfer enhancement on the characteristics of nickel–ceramic microfiltration membranes". In Preparation (2012).

National Conference

[1] **V.K. Bulasara**, R. Uppaluri, "Fabrication of nickel–ceramic composite membranes by electroless plating", Presented in the 64th Annual Session of the Indian Chemical Engineering Congress, *CHEMCON–2011*, Bangalore, India, 27th–29th December 2011, Technical Session 9, Paper 34 (2011).